

DISINFECTION BY-PRODUCT FORMATION FROM BIOFILM CHLORINATION IN DRINKING WATER PIPES

Carolina Montoya-Pachongo

Submitted in accordance with the requirements for the degree of

Doctor of Philosophy

University of Leeds

School of Civil Engineering

March 2018

Intellectual property and publication statement

The candidate confirms that the work submitted is her own, except where work which has formed part of jointly authored publications has been included. The contribution of the candidate and the other authors to this work has been explicitly indicated below. The candidate confirms that appropriate credit has been given within the thesis where reference has been made to the work of others.

Chapter 3 refers to the field assessment of bacterial communities and their relationships with engineered factors. The results reported in this chapter were used to generate a jointly authored publication:

*C. Montoya-Pachongo, I. Douterelo, C. Noakes, M.A. Carmargo-Valero, A. Sleight, J.C. Escobar-Rivera, P. Torres-Lozada. Field assessment of bacterial communities and total trihalomethanes: implications for drinking water networks. *Journal Science of the Total Environment*. 616–617, pp. 345–354.*

The candidate is the first author of the publication and her contribution is related to planning and executing the field work, sample processing, literature review, result analysis, writing up the manuscripts, and making corrections for further publication. Other authors' contribution was in the form of advice on field work planning, easing access to laboratory facilities and equipment, laboratory techniques, academic guidance, and writing style.

This copy has been supplied on the understanding that it is copyright material and that no quotation from the thesis maybe published without proper acknowledgment. 2018. The University of Leeds. Carolina Montoya Pachongo.

Acknowledgements

Firstly, I would like to express my sincere gratitude to my supervisors Prof Catherine Noakes, Dr Miller-Alonso Camargo-Valero, and Dr Andrew Sleight for the continuous support of my PhD study and related research, for their guidance and support. My sincere thanks also go to Dr Isabel Douterelo-Soler for her guidance on molecular methods applied to drinking water research.

Secondly, special gratitude with Colciencias for funding the PhD and the Leeds experience. Thanks to the John Fox Award and the School of Civil Engineering for funding my field work in Colombia. I want to thank Universidad del Valle for giving me access to laboratory facilities and field-work equipment. Thanks to staff of EMCALI EICE ESP for granting permission and support on sample collection. In particular, I am grateful with Prof Cristian Picioreanu for introducing me to COMSOL modelling. Special thanks to colleagues in the Faculty of Engineering at the University of Leeds for their guidance and advice on coding and modelling.

Last but not the least, I would like to thank my family: my parents Valentina and Harold, aunts, cousins, and friends for spiritually supporting me throughout the PhD process. Special gratitude goes to Diana and Davidde for supporting me under especial circumstances.

Abstract

Biofilms in drinking water distribution networks (DWDNs) are recognized as potential pathogen reservoirs. Recent experiments have found that biofilm can also act as precursors for the formation of disinfection by-products (DBPs). This project aimed to better understand the impact of the presence of biofilms and improve prediction of DBPs in DWDNs. To study the microbial significance of biofilms in water pipes, bacterial communities in biofilm and bulk water were identified in a DWDN in a tropical climate country. Drinking water and biofilms were characterised by physico-chemical parameters. Relationships between biotic, physico-chemical parameters and engineered factors (i.e., pipe age, material and diameter; and water age) were explored by the application of statistical tests.

Additionally, improvement of DBP prediction in DWDNs was approached by modelling the role of biofilms as DBP precursors. Two models for predicting DBP formation potentials were developed from chlorination of cells and extracellular polymeric substances. The first model corresponded to stagnant conditions and a second more complex model was produced for transitional and turbulent flow. The models were implemented in the software COMSOL Multiphysics 5.2a and sensitivity analysis was carried out to screen the parameters influence on the response variables.

Field-work assessment allowed determining that biofilms are richer habitats than bulk water. Pipe age, pipe material, water age, free chlorine, pH and temperature can be key to the composition of bacterial communities. Model simulations suggested that the important DBP exposure is related to dichloroacetonitrile, stagnant bulk, and slow flow. The microbial and chemical significance of biofilms is important in the context of climate change and developing countries because water managers can face multiple challenges under these conditions. Alterations of raw water properties, increasing occurrence of extreme weather events and poor capacity to mitigate such events may rise the chemical and microbiological risk associated to biofilms in DWDNs in tropical countries.

TABLE OF CONTENT

LIST OF ABBREVIATIONS	XIX
NOMENCLATURE	XXI
1 INTRODUCTION	1
1.1 MOTIVATION	1
1.2 PROBLEM DEFINITION	3
1.3 RESEARCH QUESTIONS, AIM AND OBJECTIVES	7
1.3.1 RESEARCH QUESTIONS	7
1.3.2 AIM	8
1.3.3 OBJECTIVES	8
1.4 GENERAL METHODOLOGY OF THE RESEARCH PROJECT	8
1.4.1 STRUCTURE OF THE THESIS	9
2 LITERATURE REVIEW	11
2.1 INTRODUCTION	11
2.2 PHYSICAL, HYDRAULIC AND WATER QUALITY INTEGRITY OF DRINKING WATER DISTRIBUTION NETWORKS	11
2.2.1 PHYSICAL INTEGRITY OF DWDNS	11
2.2.2 HYDRAULIC INTEGRITY OF DWDNS	13
2.2.3 WATER QUALITY INTEGRITY OF DWDNS	15
2.2.4 PLUMBING SYSTEMS	17
2.3 BASICS OF TRANSPORT PHENOMENA	18
2.3.1 FLUXES AND CONSERVATION OF CHEMICAL SPECIES	18
2.3.2 MASS TRANSFER AND BOUNDARY CONDITIONS AT INTERFACES	19
2.3.2.1 Sherwood number	20
2.3.2.2 Engineering correlations	21
2.4 BIOFILMS IN DRINKING WATER DISTRIBUTION NETWORKS	23
2.4.1 TAXONOMY AND DIVERSITY	24
2.4.2 MICROBIOME IDENTIFICATION IN BULK WATER AND BIOFILMS IN DRINKING WATER NETWORKS	25

2.4.3	BIOFILM MODELLING	33
2.5	WATER DISINFECTION	46
2.5.1	CHLORINE REACTIONS IN WATER	46
2.5.1.1	Hydrolytic reactions	46
2.5.1.2	Redox reactions	47
2.5.2	DISINFECTANT DECAY MODELS	47
2.5.2.1	Wall reaction kinetics	48
2.5.2.2	Mass transfer kinetics	50
2.5.2.3	Overall rate	50
2.6	DBPs IN DRINKING WATER	50
2.6.1	DISINFECTION APPROACHES	50
2.6.2	DBP SPECIES	51
2.6.3	DBP REGULATION	54
2.6.4	DBP PRECURSORS	55
2.6.5	FACTORS INFLUENCING DBP FORMATION	56
2.6.6	DBPs AND PUBLIC HEALTH	58
2.6.7	DISINFECTION BY-PRODUCTS MODELLING	59
2.7	BIOFILMS AS PRECURSORS OF DBPs	74
2.8	FURTHER RESEARCH NEEDED: IMPROVE THE UNDERSTANDING OF THE ROLE OF BIOFILMS AS DBP PRECURSORS	77
3	FIELD ASSESSMENT OF BACTERIAL COMMUNITIES AND THEIR RELATIONSHIPS WITH ENGINEERED FACTORS	81
3.1	INTRODUCTION	81
3.2	METHODOLOGY	81
3.2.1	DATA COLLECTION FROM COLOMBIAN WATER COMPANIES	81
3.2.2	AREA OF STUDY	82
3.2.3	PRELIMINARY ACTIVITIES	85
3.2.4	WATER AGE DATA	85
3.2.5	SAMPLE COLLECTION	87
3.2.6	PHYSICOCHEMICAL ANALYSIS	89

3.2.7	MOLECULAR METHODS _____	90
3.2.8	DATA ANALYSIS _____	91
3.3	RESULTS _____	93
3.3.1	SUSPENSION OF DRINKING WATER SUPPLY IN THE STUDIED NETWORK _____	93
3.3.2	WATER LEVELS IN SERVICE RESERVOIRS IN THE DWDN _____	96
3.3.3	WATER AGE _____	100
3.3.4	PHYSICAL CHARACTERISTICS OF SAMPLED PIPES _____	100
3.3.5	WATER QUALITY AND BIOTIC PARAMETERS _____	101
3.3.6	CHARACTERIZATION OF THE BACTERIAL COMMUNITY STRUCTURE OF BIOFILMS AND BULK WATER ____	104
3.3.7	MICROBIAL RICHNESS AND DIVERSITY _____	107
3.4	DISCUSSION _____	108
3.4.1	BULK WATER QUALITY AND BIOTIC PARAMETERS AND THEIR RELATIONSHIPS WITH ENGINEERED FACTORS _____	108
3.4.2	IDENTIFICATION OF THE BACTERIAL COMMUNITY STRUCTURE OF BIOFILMS AND BULK WATER _____	108
3.4.3	INFLUENCE OF NETWORK CHARACTERISTICS OVER THE BACTERIAL COMMUNITIES AND RICHNESS AND DIVERSITY INDICES IN BIOFILMS AND BULK WATER SAMPLES _____	112
3.5	SIGNIFICANCE AND LIMITATIONS OF THE STUDY _____	115
3.6	CONCLUSIONS _____	116
4	A SIMPLE BIOFILM CHLORINATION MODEL _____	118
4.1	INTRODUCTION _____	118
4.2	MODEL DEVELOPMENT _____	119
4.2.1	MODEL DEFINITION _____	119
4.2.2	MODEL EQUATIONS _____	121
4.2.3	PARAMETERS SELECTION _____	123
4.2.3.1	Biofilm thickness (BT) _____	123
4.2.3.2	Initial volumetric biofilm density (X_0) _____	126
4.2.3.3	Initial concentration of EPS (E_0) _____	129
4.2.3.4	Effective diffusion coefficient of dissolved substances (τ_c and τ_s) _____	130
4.2.3.5	Reaction rates (k_1 and k_2) and yield coefficients (Y_1 and Y_2) _____	130
4.2.3.6	Factors F_x and F_E _____	131

4.2.3.7	Temperature	131
4.2.4	BOUNDARY CONDITIONS	132
4.2.5	GEOMETRY AND MESH	133
4.2.6	ANALYSIS OF MESH DEPENDENCE	133
4.2.7	PROCESSING AND NUMERICAL METHODS	134
4.2.8	MODEL IMPLEMENTATION IN COMSOL MULTIPHYSICS	136
4.2.9	SELECTION OF TIME STEP	136
4.2.10	EXPERIMENTAL STUDY USED AS A REFERENCE	137
4.2.11	DATA ANALYSIS	138
4.3	RESULTS AND DISCUSSION	139
4.3.1	TYPICAL MODEL BEHAVIOUR	139
4.3.2	CHLORINE PENETRATION WITHIN THE BIOFILM	141
4.3.3	SENSITIVITY ANALYSIS	142
4.3.3.1	τ_s , reaction rates k_1 and k_2 , and initial chlorine concentration	143
4.3.3.2	Temperature	147
4.3.3.3	Yield coefficients Y_1 and Y_2 and reactor volume	148
4.3.3.4	Biofilm thickness, initial cell and EPS concentration, fraction of cells and EPS transformed into DBP and biofilm area	149
4.3.3.5	Comparison among parameters	150
4.3.4	FACTORS AFFECTING THE DBP FORMATION	155
4.3.5	COMPARISON BETWEEN MODEL RESULTS AND EXPERIMENTAL DATA	155
4.3.6	SIMULATION OF SCENARIOS: BUILDING PLUMBING SYSTEM SUPPLIED WITH WARM WATER	156
4.3.6.1	Chloroform formation compared with field assessment (Chowdhury, 2016)	157
4.3.6.2	Chloroform formation	159
4.3.6.3	Dichloroacetonitrile formation	161
4.3.6.4	Chlorine demand	162
4.3.6.5	Influence of S/V ratio on DBP formation	163
4.3.6.6	Discussion of DBP formation potentials simulated under stagnation conditions	166
4.4	MODEL APPLICATIONS AND LIMITATIONS	167
4.5	CONCLUSIONS	169

5	MODELLING DBP FORMATION FROM BIOFILM CHLORINATION UNDER HYDRODYNAMIC CONDITIONS	171
5.1	INTRODUCTION	171
5.2	MODEL DEVELOPMENT	171
5.2.1	MODEL DEFINITION	171
5.2.2	MODEL EQUATIONS AND INITIAL AND BOUNDARY CONDITIONS – REACTIONS	173
5.2.3	MODEL EQUATIONS AND INITIAL AND BOUNDARY CONDITIONS – BULK FLOW	179
5.2.4	PRE-PROCESSING	184
5.2.4.1	Geometry and mesh	184
5.2.4.2	Mesh convergence and selection of time step	187
5.2.4.3	Selection of turbulence model	190
5.2.5	IMPLEMENTING THE MODEL IN COMSOL	197
5.2.6	SCENARIOS SIMULATED	198
5.2.7	PARAMETERS SELECTION	198
5.2.8	EFFECTIVE DIFFUSION COEFFICIENT OF DBPs	199
5.2.9	MASS TRANSPORT	201
5.2.10	SENSITIVITY ANALYSIS	201
5.2.10.1	Parameter screening with Morris method	202
5.2.10.2	Higher-order parameter interaction effects	204
5.2.10.3	Implementation of Morris method	204
5.2.11	POST-PROCESSING	205
5.3	RESULTS AND DISCUSSION	205
5.3.1	TYPICAL MODEL BEHAVIOUR	205
5.3.1.1	Flow field	205
5.3.1.2	Concentrations of substances in biofilm and bulk water	208
5.3.1.3	Fluxes of dissolved substances at biofilm surface	212
5.3.1.4	Variation of \bar{Sh} at the biofilm surface	213
5.3.1.5	Concentrations of dissolved substances at the pipe outlet	213
5.3.2	INFLUENCE OF FLOW REGIME ON DBP FORMATION AND TRANSPORT	214
5.3.3	INFLUENCE OF RE ON DBP TRANSPORT	216

5.3.3.1	Chloroform and dichloroacetonitrile formation _____	216
5.3.3.2	Mass transport _____	222
5.3.4	INFLUENCE OF S/V RATIO ON DBP TRANSPORT _____	225
5.3.4.1	Different flow rates and equal Re _____	225
5.3.4.2	Equal flow rates and different Re _____	227
5.3.5	DBP FORMATION UNDER SEVERAL CONDITIONS OF DRINKING WATER QUALITY _____	229
5.3.5.1	Transitional flow _____	229
5.3.5.2	Turbulent flow _____	232
5.3.6	DISCUSSION _____	234
5.3.7	SENSITIVITY ANALYSIS _____	235
5.3.7.1	\bar{Sh} - chlorine _____	235
5.3.7.2	\bar{Sh} - DCAN _____	237
5.3.7.3	Average DCAN _____	238
5.3.7.4	Median DCAN _____	240
5.3.7.5	Summary _____	241
5.4	MODEL APPLICATIONS AND LIMITATIONS _____	242
5.5	CONCLUSIONS _____	244
6	<u>GENERAL DISCUSSION, IMPLICATIONS AND APPLICATIONS</u> _____	246
6.1	GENERAL DISCUSSION _____	246
6.2	BACTERIAL COMMUNITIES AND PUBLIC HEALTH _____	250
6.3	DBPs AND PUBLIC HEALTH _____	252
6.4	IMPLICATIONS _____	258
6.4.1	IMPLICATIONS FOR WATER QUALITY IN CALI'S DWDN IN THE CONTEXT OF EXTREME WEATHER EVENTS _____	258
6.4.2	IMPLICATIONS FOR O&M ACTIVITIES IN DWDN _____	260
6.5	APPLICABILITY OF THE CURRENT RESEARCH PROJECT _____	261
7	<u>KEY FINDINGS, CONCLUSION AND FUTURE RESEARCH</u> _____	263
7.1	GENERAL CONCLUSION _____	263
7.2	KEY FINDINGS _____	263

7.2.1	BACTERIAL COMMUNITIES IN A TROPICAL-CLIMATE DWDN _____	263
7.2.2	RELATIONSHIPS BETWEEN ABIOTIC AND BIOTIC PARAMETERS IN A TROPICAL-WEATHER DWDN _____	264
7.2.3	DBP FORMATION POTENTIALS FROM BIOFILM CHLORINATION UNDER STAGNATION CONDITIONS _____	264
7.2.4	DBP FORMATION POTENTIALS FROM BIOFILM CHLORINATION UNDER HYDRODYNAMIC CONDITIONS _	265
7.2.5	PRACTICAL RECOMMENDATIONS ON BIOFILM AND DISINFECTION BY-PRODUCTS CONTROL IN DRINKING WATER NETWORKS _____	265
7.3	FUTURE RESEARCH _____	266
8	REFERENCES _____	268
9	APPENDICES _____	290

LIST OF TABLES

<i>Table 2-1. Characteristics of plumbing systems</i>	17
<i>Table 2-2. Summary of bacterial composition in DWDNs supplied by surface water sources</i>	28
<i>Table 2-3. Summary of studies on biofilm modelling</i>	34
<i>Table 2-4. Disinfectant decay constants reported in experimental studies</i>	48
<i>Table 2-5. Distinctive functional groups of chlorination DBPs</i>	51
<i>Table 2-6. Regulation of concentration limits of DBPs in drinking water</i>	55
<i>Table 2-7. Models for DBP formation</i>	61
<i>Table 2-8. Main features of the interaction between disinfectant and drinking water biofilms according to experimental studies</i>	75
<i>Table 3-1. Water sources and treatment description of the water supply system of the city of Cali</i>	84
<i>Table 3-2. Description of the code used to classify the type of suspension of drinking water supply in Colombia</i>	93
<i>Table 3-3. Hydraulic conditions of the sub-network 4 during sampling campaign</i>	99
<i>Table 3-4. Network characteristics in sampling points</i>	101
<i>Table 3-5. Water quality, biotic parameters and descriptive statistics</i>	102
<i>Table 3-6. Spearman correlation coefficients for bulk water parameters</i>	103
<i>Table 3-7. Spearman correlation coefficients for biofilm parameters</i>	103
<i>Table 3-8. ANOSIM test for RA of species</i>	106
<i>Table 3-9. Medians and means of richness and diversity indices</i>	107
<i>Table 4-1. Model equations in biofilm</i>	122
<i>Table 4-2. Review of biofilm thickness data reported by drinking-water-related studies</i>	124
<i>Table 4-3. Descriptive statistics of biofilm thickness reported in Table 4-2</i>	126
<i>Table 4-4. Review of cell density data in drinking water biofilm reported by other researchers</i>	127
<i>Table 4-5. Descriptive statistics of cell density in drinking water biofilm reported by other researchers</i> ...	129
<i>Table 4-6. Values of reaction rates (k_1 and k_2) and yield coefficients (Y_1 and Y_2)</i>	131
<i>Table 4-7. Initial and boundary conditions in 1D model</i>	132
<i>Table 4-8. Number of elements of every type of mesh</i>	134
<i>Table 4-9. Main features for model implementation in COMSOL Multiphysics 5.2a</i>	136

Table 4-10. Experimental conditions and results of tests developed by Wang et al. (2013a)	138
Table 4-11. Base parameters used in the sensitivity analysis	142
Table 4-12. Percentage of change of parameters and the respective chloroform concentrations in bulk water	152
Table 4-13. Percentage of change of parameters and the respective chloroform concentrations in bulk water	153
Table 4-14. Parameters used to simulate DBP formation in plumbing systems	157
Table 4-15. TTHMs and free chlorine concentrations measured in plumbing systems (Chowdhury, 2016)	158
Table 4-16. Chlorine demand on plumbing system scenarios	163
Table 5-1. Mass balance equations and initial conditions in 2D model – Cylindrical pipes	175
Table 5-2. Boundary conditions for transport of dissolved substances in 2D model – Cylindrical pipes ...	178
Table 5-3. Navier-Stokes equations for incompressible flow	179
Table 5-4. Boundary conditions for flow field in 2D model – Cylindrical pipes	180
Table 5-5. Navier-Stokes equations for turbulent incompressible flow	181
Table 5-6. Equations of the turbulent model SST	183
Table 5-7. Geometry configurations tested in the current model	184
Table 5-8. Characteristics of the mapped mesh for pipe diameter of 10 inches	186
Table 5-9. Characteristics of the mapped mesh for pipe diameter of 6 inches	187
Table 5-10. Characteristics of the mapped mesh for pipe diameter of 3 inches	187
Table 5-11. Description of five turbulence models included in COMSOL Multiphysics 5.2a	191
Table 5-12. Percentage of difference between pairs of turbulence model – Maximal velocity	193
Table 5-13. Percentage of difference between pairs of turbulence model – Median velocity	193
Table 5-14. Percentage of difference between pairs of turbulence model – Average velocity	193
Table 5-15. Percentage of difference between COMSOL and Fluent for the same turbulence model – Maximum velocity	195
Table 5-16. Percentage of difference between COMSOL and Fluent for the same turbulence model – Median velocity	196
Table 5-17. Percentage of difference between COMSOL and Fluent for the same turbulence model – Average velocity	196
Table 5-18. \overline{Sh} for different turbulent models	196
Table 5-19. Main features for model implementation in COMSOL Multiphysics 5.2a	197

Table 5-20. Parameters used in the 2D model simulations	199
Table 5-21. Ranges of parameters considered for sensitivity analysis	205
Table 5-22. \bar{S}_h and k_f for dissolved substances for two scenarios of drinking water quality – Transitional flow.....	230
Table 5-23. \bar{S}_h and k_f for dissolved substances for two scenarios of drinking water quality – Turbulent flow.....	233
Table 5-24. Median and standard deviation of EEs on response variable \bar{S}_h - Chlorine	236
Table 5-25. Median and standard deviation of EEs on response variable \bar{S}_h - DCAN	237
Table 5-26. Median and standard deviation of EEs on response variable average DCAN.....	239
Table 5-27. Median and standard deviation of EEs on response variable median DCAN.....	240
Table 5-28. Ranking of parameters according to their influence on response variables.....	242
Table 6-1. Potential pathogenic bacteria identified in Cali's DWDN and their corresponding risk area defined by Pérez-Vidal et al. (2012)	251
Table 6-2. Main results of 1D model of potential of DBP formation from biofilm chlorination	253
Table 6-3. Main results of 2D model of potential of DBP formation from biofilm chlorination	255

LIST OF FIGURES

<i>Figure 1-1. Chemical and biological processes occurring in water pipes</i>	<i>3</i>
<i>Figure 1-2. Issues arising in DWDNs</i>	<i>5</i>
<i>Figure 1-3. Methodological approach of the current research project.....</i>	<i>9</i>
<i>Figure 2-1. Schematic representation of mass flux at a surface with a unit normal n and arbitrary orientation</i>	<i>19</i>
<i>Figure 3-1. Location of the study area</i>	<i>83</i>
<i>Figure 3-2. Fractions of pipe materials in the DWDN of the city of Cali</i>	<i>84</i>
<i>Figure 3-3. Water age ranges for the sampling sub-network.....</i>	<i>86</i>
<i>Figure 3-4. Procedure for collection of water and biofilm samples.....</i>	<i>87</i>
<i>Figure 3-5. Location of sampling points in the city of Cali.....</i>	<i>88</i>
<i>Figure 3-6. Inner walls of cast iron pipeline of sampling point 2.....</i>	<i>90</i>
<i>Figure 3-7. Stages in the multivariate analysis based on similarity coefficients</i>	<i>92</i>
<i>Figure 3-8. Characterization of events of suspension of drinking water supply in the DWDN of the city of Cali</i>	<i>94</i>
<i>Figure 3-9. Evolution of events of suspension of WTP operation in the period 2000-2016.....</i>	<i>95</i>
<i>Figure 3-10. Water levels in service reservoirs during sampling activities (a) La Campiña (b) Normal (c) Siloé (d) Nápoles (e) Ciudad Jardín</i>	<i>97</i>
<i>Figure 3-11. Water age of sampling points</i>	<i>100</i>
<i>Figure 3-12. RA of bacterial groups to (a) phylum level and (b) genus level in water samples.....</i>	<i>104</i>
<i>Figure 3-13. RA of bacterial groups to (a) phylum level and (b) genus level in biofilm samples.....</i>	<i>105</i>
<i>Figure 3-14. Non-metric MDS analysis of bacterial RA. Factors (a) Habitat and (b) and pipe material - biofilm samples</i>	<i>106</i>
<i>Figure 4-1. Schematic representation of the 1D model.....</i>	<i>120</i>
<i>Figure 4-2. 1D mass balance equations for soluble and particulate components in biofilm and biofilm surface.....</i>	<i>122</i>
<i>Figure 4-3. Box plot biofilm thickness data</i>	<i>126</i>
<i>Figure 4-4. Box plot cell density data</i>	<i>129</i>
<i>Figure 4-5. Linear correlation between biofilm thickness and EPS concentration (Celmer et al., 2008) ...</i>	<i>130</i>
<i>Figure 4-6. Representation of the 1D model mesh</i>	<i>133</i>
<i>Figure 4-7. Influence of grid size on simulation results</i>	<i>134</i>

Figure 4-8. Time step comparison among chloroform concentrations in bulk water	137
Figure 4-9. Dissolved substances within biofilm (a) Chlorine (b) Chloroform	139
Figure 4-10. Dissolved substances in bulk water after 3 hours	140
Figure 4-11. Decay of particulate substances (a) Cells (b) EPS.....	140
Figure 4-12. Comparison of chlorine penetration within biofilm (a) Chen and Stewart (1996): experimental vs model data (b) Experimental data from Chen and Stewart (1996) vs simulated data from current model	142
Figure 4-13. Influence of τ_S on chloroform concentration in bulk water (a) Chloroform concentrations in bulk water at different values of τ_S after $t = 3$ h (b) Temporal variation of chloroform concentrations in bulk water for three values of τ_S	144
Figure 4-14. Influence of reaction rate k_1 on chloroform concentration in bulk water (a) Chloroform concentrations in bulk water at different values of k_1 after $t = 3$ h (b) Temporal variation of chloroform concentrations in bulk water for several values of k_1	145
Figure 4-15. Influence of reaction rate k_2 on chloroform concentration in bulk water (a) Chloroform concentrations in bulk water at different values of k_2 after $t = 3$ h (b) Temporal variation of chloroform concentrations in bulk water for several values of k_2	146
Figure 4-16. Influence of initial chlorine concentration on chloroform concentration in bulk water (a) Comparison between C_{lo} and minimum cell concentration (b) Comparison between C_{lo} and minimum EPS concentration.....	147
Figure 4-17. Temperature influence on chloroform concentration in bulk water (a) Chloroform concentrations in bulk water at different temperatures after $t = 3$ h (b) Temporal variation of chloroform concentrations in bulk water at the temperature range 5-25 °C	148
Figure 4-18. Influence of (a) Y_1 , (b) Y_2 , and (c) reactor volume on chloroform concentration in bulk water after $t = 3$ h	149
Figure 4-19. Parameters with linear influence on chloroform concentration in bulk water (a) Biofilm thickness (b) Initial cell concentration (c) Initial EPS concentration (d) F_X (e) F_E (f) Biofilm area	150
Figure 4-20. Comparison of influence on chloroform concentration in bulk water among parameters (a) 14 parameters tested (b) 12 parameters tested excluding V and Y_1	151
Figure 4-21. (a) Chloroform and (b) DCAN concentrations according to results of Wang et al. (2013a)..	156
Figure 4-22. Chloroform concentrations in bulk water for different pipe diameter	158
Figure 4-23. Chloroform concentrations in bulk water for several scenarios of initial chlorine and cell concentration (a) $BT = 7 \mu m$ (b) $BT = 102 \mu m$	159
Figure 4-24. DCAN concentrations in bulk water for several scenarios of initial chlorine and cell concentration (a) $BT = 7 \mu m$ (b) $BT = 102 \mu m$	162
Figure 4-25. Chlorine concentrations in bulk water, under several scenarios of initial chlorine and cell concentration (a) $BT = 7 \mu m$ (b) $BT = 102 \mu m$	163
Figure 4-26. Influence of S/V ratio on DBP concentrations in bulk water (a) Chloroform (b) DCAN.....	164

Figure 4-27. DBP concentrations in bulk water and regulation limits / guidelines (a) Chloroform, Clo = 1.66 mg/L, Xo = 4.44x10 ⁻³ mg/cm ² (b) DCAN, Clo = 1.66 mg/L, Xo = 1.28x10 ⁻⁴ mg/cm ²	165
Figure 4-28. Cell concentration according to pipe diameter	166
Figure 5-1. Schematic representation of the 2D model.....	171
Figure 5-2. Process for building a flow-coupled model to predict DBP formation potentials from chlorination of biofilms	172
Figure 5-3. 2D mass balance equations for soluble and particulate components in biofilm, biofilm surface, and bulk water.....	174
Figure 5-4. Geometry of the water pipe	185
Figure 5-5. Mesh details of the water pipe.....	185
Figure 5-6. Comparison of velocity and \overline{Sh} between mesh 1 and 2 (a) Velocity monitored in the centre of bulk water domain along r axis (b) \overline{Sh} for chlorine (c) \overline{Sh} for chloroform.....	189
Figure 5-7. Comparison of \overline{Sh} (a) and average chloroform concentration at the pipe outlet (b) in mesh 1	190
Figure 5-8. Regimes of the turbulent flow near to a flat wall.....	191
Figure 5-9. Comparison of five turbulence models included in COMSOL Multiphysics 5.2a (a) Velocity monitored at the middle of bulk water domain (b) Average chloroform concentrations at the pipe outlet .	193
Figure 5-10. Comparison of velocity monitored at the middle of bulk water domain between software COMSOL and Fluent (a) Laminar and SST (b) SST.....	195
Figure 5-11. Influence of τ_s on (a) chloroform concentrations in bulk water at the pipe outlet and (b) \overline{Sh}	200
Figure 5-12. Influence of τ_s on (a) DCAN concentrations in bulk water at the pipe outlet and (b) \overline{Sh}	201
Figure 5-13. Pressure (Pa) surface plot – Inlet: left; Outlet: right (a) Laminar flow (b) Transitional flow (c) Turbulent flow	206
Figure 5-14. Velocity profiles (a) Laminar flow (b) Transitional flow (c) Turbulent flow	207
Figure 5-15. Sketch of the non-scaled geometry.....	208
Figure 5-16. Contour plots of substance concentrations in biofilm – BT = 102 μ m, Clo = 1.66 mg/L, Xo = 2.33 mg/L , Re = 2774, ϕ = 3”	210
Figure 5-17. Contour plots of concentrations of dissolved substances in bulk water - BT = 102 μ m, Clo = 1.66 mg/L, Xo = 2.33 mg/L , Re = 2774, ϕ = 3”	211
Figure 5-18. Flux of dissolved substances at the biofilm surface (a) DCAN (b) Chlorine	212
Figure 5-19. Variation of \overline{Sh} at the pipe outlet	213
Figure 5-20. Average concentration of chlorine and DCAN at the pipe outlet.....	213
Figure 5-21. Average concentration of chloroform at the pipe outlet according to flow regime (a) Chloroform (b) DCAN	214

Figure 5-22. Variation of local Sh according to flow regime (a) DBPs (b) Chlorine	214
Figure 5-23. Average chloroform concentration at the pipe outlet for several Re – Transitional flow (a) $BT = 7 \mu m$ (b) $BT = 102 \mu m$	216
Figure 5-24. Average DCAN concentration at the pipe outlet for several Re – Transitional flow (a) $BT = 7 \mu m$ (b) $BT = 102 \mu m$	217
Figure 5-25. Average chlorine concentration at the pipe outlet for several Re – Transitional flow (a) $BT = 7 \mu m$ (b) $BT = 102 \mu m$	218
Figure 5-26. Average chloroform concentration at the pipe outlet for several Re – Turbulent flow (a) $BT = 7 \mu m$ (b) $BT = 102 \mu m$	218
Figure 5-27. Average DCAN concentration at the pipe outlet for several Re – Turbulent flow (a) $BT = 7 \mu m$ (b) $BT = 102 \mu m$	219
Figure 5-28. Average chlorine concentration at the pipe outlet for several Re – Turbulent flow (a) $BT = 7 \mu m$ (b) $BT = 102 \mu m$	220
Figure 5-29. \bar{Sh} (a) and mass transfer rate (b) of chloroform for several Re – Transitional flow	222
Figure 5-30. \bar{Sh} (a) and mass transfer rate (b) of chloroform for several Re – Turbulent flow	222
Figure 5-31. \bar{Sh} (a) and mass transfer rate (b) of DCAN for several Re – Transitional flow	223
Figure 5-32. \bar{Sh} (a) and mass transfer rate (b) of DCAN for several Re – Turbulent flow	223
Figure 5-33. \bar{Sh} (a) and mass transfer rate (b) of chlorine for several Re – Transitional flow	223
Figure 5-34. \bar{Sh} (a) and mass transfer rate (b) of chlorine for several Re – Turbulent flow	224
Figure 5-35. Average chloroform (a) and DCAN (b) concentrations at the pipe outlet for several pipe diameters – Transitional flow.....	226
Figure 5-36. Average chlorine concentrations at the pipe outlet for several pipe diameters – Transitional flow.....	226
Figure 5-37. Average \bar{Sh} for DBPs (a) and Chlorine (b) for several pipe diameters – Transitional flow ...	227
Figure 5-38. Average chloroform (a) and DCAN (b) concentrations at the pipe outlet for several pipe diameters – Turbulent flow	228
Figure 5-39. Average chlorine concentrations at the pipe outlet for several pipe diameters – Turbulent flow	228
Figure 5-40. Average \bar{Sh} for DBPs (a) and Chlorine (b) for several pipe diameters – Turbulent flow.....	228
Figure 5-41. Average concentrations of (a) chloroform and (b) DCAN at the pipe outlet for two scenarios of drinking water quality – Transitional flow.....	229
Figure 5-42. Flux of DCAN at the biofilm surface for two scenarios of drinking water quality (a) Least critical scenario (b) Most critical scenario.....	231
Figure 5-43. Flux of chlorine at the biofilm surface for two scenarios of drinking water quality – Transitional flow (a) Least critical scenario (b) Most critical scenario	232

Figure 5-44. Average concentrations of (a) chloroform and (b) DCAN at the pipe outlet for two scenarios of drinking water quality – Turbulent flow	233
Figure 5-45. EEs on response variable \bar{S}_h - Chlorine (a) Median vs Standard deviation (b) Median vs Standard deviation including upper and lower bounds	237
Figure 5-46. EEs on response variable \bar{S}_h - DCAN (a) Median vs Standard deviation (b) Median vs Standard deviation including upper and lower bounds	238
Figure 5-47. EEs on response variable average DCAN (a) Median vs Standard deviation (b) Median vs Standard deviation including upper and lower bounds	239
Figure 5-48. EEs on response variable median DCAN (a) Median vs Standard deviation (b) Median vs Standard deviation including upper and lower bounds	241
Figure 6-1. Dual role of biofilms studied in the current research project.....	246
Figure 6-2. Two approaches to study the microbial and chemical significance of biofilms in drinking water	247
Figure 9-1. Water age for subnetwork 4 at the DWDN of the city of Cali - Colombia	290
Figure 9-2. Bray Curtis similarities of the relative abundance percentage of species in biofilm samples – Water species	295
Figure 9-3. Bray Curtis similarities of the relative abundance percentage of species in biofilm samples – Biofilm species.....	298
Figure 9-4. Bray Curtis similarities of the relative abundance percentage of species in biofilm samples – Water and biofilm species together	300

LIST OF APPENDICES

Appendix 9-A. Water age map.....	290
Appendix 9-B. Normality tests of correlated parameters	291
Appendix 9-C. Two-dimensional plots of the Multi-Dimensional Scaling (MDS) analysis and dendrograms for visualization of Bray Curtis similarity index.....	292

LIST OF ABBREVIATIONS

1D	One dimension
2D	Two dimensions
AMD	Advanced micro devices
ANOSIM	Analysis of similarities
CCP	Concrete cylinder pipe
CDC	Centres for disease control and prevention
CPU	Central processing unit
CV	Coefficient of variation
DBP	Disinfection by-product
DCAN	Dichloroacetonitrile
DICL	Ductile iron cement-lined
DNA	Desoxyribose nucleic acid
DPD	N,N diethyl-p-phenylene diamine
DWDN	Drinking water distribution network
EE	Elementary effects
EPS	Extracellular polymeric substances
GPU	Graphics processing unit
HAA	Haloacetic acid
HOCl	Hypochlorous acid
HPC	Heterotrophic plate count
IRB	Iron-reducing bacteria
MDPE	Medium density polyethylene
MDS	Multidimensional scaling
NOM	Natural organic matter
NTU	Nephelometric turbidity units

O&M	Operation and maintenance
OTU	Operational taxonomic unit
PCR	Polymerase chain reaction
PE	Polyethylene
PVC	Polyvinyl chloride
Q1	Quartile 1
Q3	Quartile 3
QAC	Quaternary ammonium chloride
R	Hydrocarbon
R2	Different chemical combinations
RA	Relative abundance
RAM	Random access memory
RNA	Ribose nucleic acid
S/V	Pipe surface area to volume ratio
Sh	Local Sherwood number
SRB	Sulphate-reducing bacteria
SST	Shear stress transport
SUVA	Specific ultraviolet absorbance
THM	Trihalomethane
TOC	Total organic carbon
TTHM	Total trihalomethanes
UK	United Kingdom
USA	United States of America
UV ₂₅₄	Ultraviolet absorbance
WTP	Water treatment plant

NOMENCLATURE

A	Parameter empirically determined
A_b	Biofilm area (cm^2) (m^2)
B	Parameter empirically determined
BT	Biofilm thickness (μm)
C	Chlorine concentration (mg/L)
C_0 Cl_0	Initial concentration of chlorine (mg/L)
d	Length scale
D_{C-B}	Molecular diffusion coefficient of chlorine in biofilm (m^2/sec)
D_{S-B}	Diffusion coefficient of chloroform/DCAN in in biofilm (m^2/sec)
E	EPS concentration (mg/L)
E_0	Initial EPS concentration (mg/L)
F_E	Fraction of EPS transformed into chloroform (dimensionless)
F_X	Fraction of cells transformed into chloroform (dimensionless)
k	Thermal conductivity Chlorine decay constant
k_1	Disinfectant decay rate – cells disinfection ($\text{m}^3/\text{g-sec}$)
k_2	Disinfectant decay rate – EPS oxidation ($\text{m}^3/\text{g-sec}$)
k_b	Reaction coefficient in bulk water
k_f	Mass transfer rate
$\overline{k_f}$	Global mass transfer rate
k_w	Reaction coefficient at pipe walls
M	Parameter empirically determined
M_R	Molecular mass of DBP (g/mol)
n	Parameter empirically determined
Q	Flow rate
Re	Reynolds number
r_h	Hydraulic radius

S	Chloroform/DCAN concentration ($\mu\text{g/L}$)
Sc	Schmidt number
Sh	Sherwood number
\bar{Sh}	Global Sherwood number
T	Temperature ($^{\circ}\text{C}$)
t	Time
Uo	Velocity magnitude
\vec{u}	Velocity vector
V	Reactor volume (mL) (m^3)
X	Cells concentration (mg/L)
Xo	Initial cell concentration (mg/L)
Y ₁	Cell-chlorine yield coefficient (g/g)
Y ₂	EPS-chlorine yield coefficient (g/g)
ϕ	Pipe diameter
τ_c	Biofilm-bulk water diffusion coefficient ratio of chlorine (dimensionless)
τ_s	Biofilm-bulk water diffusion coefficient ratio of DBP (dimensionless)

Subscripts

b	Biofilm
Bs	Biofilm surface
C	Chlorine
E	EPS
L	Bulk liquid
S	DBP
w	Wall
X	Cells

1.1 MOTIVATION

The supply of water and sanitation services is one of the most effective strategies for reducing poverty around the world. The Sustainable Development Goals from the United Nations Organization include in the goal number 6: “*Ensure availability and sustainable management of water and sanitation for all*” (United Nations, 2015). However, preserving drinking water to consumers represents a challenge for water utilities, since technical and economic resources, appropriate knowledge and training, and adequate operation and maintenance (O&M) programmes are required to achieve this purpose. To respond to this challenge in the drinking water distribution networks (DWDNs) is an enormous task because several phenomena occur in the pipes such as biofilm growth, disinfection by-products (DBPs) formation, sedimentation, corrosion, discolouration, among others. Therefore, efforts must be addressed to minimize such phenomena and to find the balance between acute and chronic risk in drinking water supply.

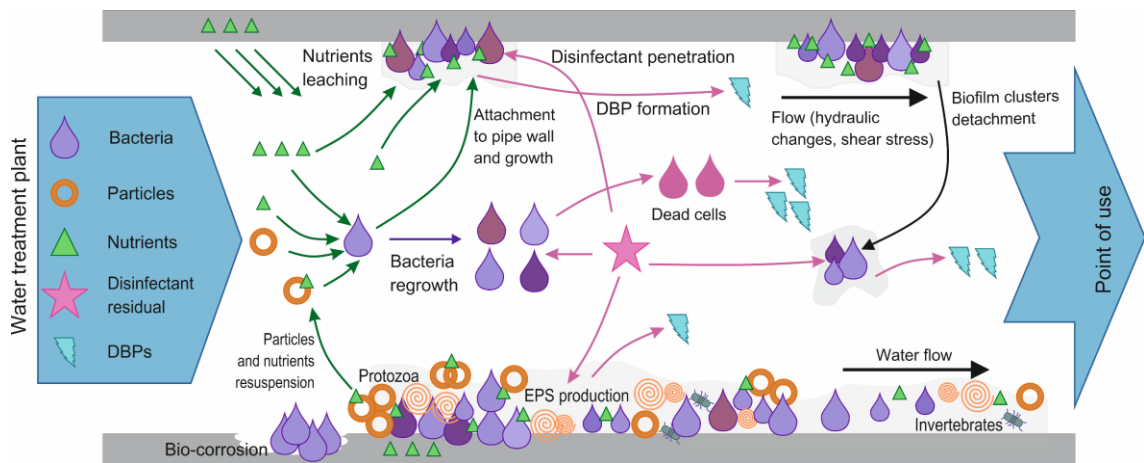
Once raw water is treated in water treatment plants (WTPs) for human consumption, DWDNs are used to transport drinking water to consumers. DWDNs are mainly composed by pipes, fittings, storage facilities, and back-flow prevention devices (NRCNA, 2006). In drinking water systems, treated water at the outlet of the WTPs is not sterile and still contains cells and organic matter. Then, microorganisms develop biofilms as a strategy to survive in DWDNs. Biofilms are habitats fixed to wet surfaces where live bacteria, archaea, fungi, and protozoa. The ability of some microorganisms to produce Extracellular Polymeric Substances (EPS) enables their attachment to surfaces in hostile environments (e.g., low nutrient concentrations, bulk flow, and presence of disinfectant). Other organisms can also adhere to the biofilm once this started forming (Wang et al., 2014; Fish et al., 2015; Srivastava and Bhargava, 2015). DBPs are the result of the reaction between disinfectants and natural organic matter (NOM), biofilms, anthropogenic contaminants, bromide, and iodide during the production and/or distribution of drinking water. Such reaction is driven by several factors such as pH, temperature, type and concentration of precursor and disinfectant, and contact time (Chowdhury et al., 2009).

Biofilm and DBP formation has become a major concern in the operation of DWDNs since they can cause acute and chronic effects on human health. Biofilms can lead to corrosion, discoloured waters and odours; host pathogens which may be released to bulk water; detach and recolonize clean surfaces; act as precursors for the formation of DBPs, and consequently, contribute to disinfectant decay (NRCNA, 2006). In this line, biofilm modelling has shown a further development

in order to better understand phenomena which allow attachment, growing, detachment, and survival of cells, considering hydraulic and molecular conditions (Wang and Zhang, 2010a).

On the other hand, it is widely accepted that DBPs have negative effects on human health as they have been identified as carcinogenic, teratogenic and mutagenic substances (WHO, 2008). The multiple factors involved in reactions between disinfectants and organic matter and the diverse nature of precursors has resulted in numerous DBP species; to date, 600 species have been identified (Hrudey, 2009). From those, chloroform and dichloroacetonitrile (DCAN) are approached in this project because the first DBP is the most abundant substance in the group trihalomethanes (THMs), which is one of the few DBP groups regulated around the world (Richardson et al., 2007). The second DBP is the most abundant substance in the group haloacetonitriles (HANs), which has not regulated yet and experimental tests on mice has shown that they are more toxic than regulated DBPs such as haloacetic acids (HAAs) (Muellner et al., 2007). In this line, DBP formation modelling has been developed to predict their concentrations by empirical models according to different environmental, hydraulic and chemical variables such as pH, temperature, residence time, disinfectant and bromide concentrations, and type and amount of precursors (Chowdhury et al., 2009).

Biological and chemical processes related to biofilms in drinking water pipes are described in Figure 1-1. Recently, DBP formation in DWDNs has also been attributed to the reaction of disinfectants with biofilm matrix, which is mainly composed by intracellular organic matter, EPS, and other biomolecules (Wang et al., 2012c; Wang et al., 2013a; Xue et al., 2014). Therefore, recent experimental studies have focussed on the formation of DBPs from pure cells and heterogeneous biofilms, planktonic cells, and extracted EPS (Hong et al., 2008; Fang et al., 2010a; Fang et al., 2010b; Wang et al., 2012c; Wang et al., 2013a; Wang et al., 2013b). Considering that biofilms act as DBP precursors and that most of the empirical models developed to date do not include the contribution of biomass to the bulk water concentrations of these substances, further research is required to define the role of drinking water biofilms into the formation of DBPs in distribution networks. The capacity of biofilms to act as both pathogen reservoir and DBP precursor was the driver behind this research.



Adapted from Prest et al. (2016)

Figure 1-1. Chemical and biological processes occurring in water pipes

1.2 PROBLEM DEFINITION

Tropical climate is characterised by average temperatures higher than 18 °C, high precipitation, and then high humidity. In contrast to temperate weather, there are not seasons in tropical climate regions but periods of higher or lower precipitation (The British Geographer, 2017). Tropical climate region is located between the Tropic of Cancer and the Tropic of Capricorn (The British Geographer, 2017); it means Latino American, African and Pacific Ocean countries are located in this region. Furthermore, climate change has significantly impacted water availability, since extreme events as droughts and floods are more frequent and more severe in different regions of the world (Delpla et al., 2009). Then, it is important to highlight that less developed countries are more vulnerable to the consequences of extreme weather events but developed regions are also susceptible to them (Cann et al., 2012; Rataj et al., 2016). Thus, water supply in the developing world may represent a challenge under extreme weather conditions and economical limitations. Several factors can or may affect drinking water quality; the following describes some of them.

According to Delpla et al. (2009), surface water quality has been especially affected due to temperature increase and the alteration of almost all physico-chemical equilibriums and biological reactions; therefore, rise of organic and inorganic micro-pollutants, dissolved organic matter, nutrients and pathogens is expected. Climate change could impact drinking water quality because of the rise of DBP concentrations with increasing water temperature; and elevated levels of turbidity and organic matter found in river waters during rainy seasons in tropical countries may deteriorate treatment performance, demanding more sophisticated technologies and, therefore, more

economical resources (Dearmont et al., 1998; Yorkshire Water, 2013; Hutton and Varughese, 2016).

In particular, inefficient performance of water treatment processes could lead to solids accumulation and biofilm and DBP formation in areas of DWDNs where flow velocity is low (end zones and storage/distribution tanks). Wen et al. (2014) showed that improving coagulation can restrict microbial regrowth in tap water by phosphate elimination in water treatment. This was concluded by testing conventional treatment with three different coagulants and enumerating microbes by flow cytometry. Microbial regrowth potential was identified by inoculation of bottled mineral water of filtered de-chlorinated water and addition of nutrients such as phosphate and carbon. Their results showed that coagulation was the crucial step for decreasing the microbial re-growth potential and producing phosphorous-limited water. Indeed, it is known that limiting nutrient content in treated water contributes to achieve bio-stability of the water. This procedure is used to limit carbon concentrations in mid-northern Europe (Hammes et al., 2010) and phosphate concentrations in northern Europe (Miettinen et al., 1997).

In addition, events which compromise hydraulic and physical integrity of networks like water supply interruption, leakages repairs, and infrastructure replacements also promote solid accumulation and increase of nutrient concentrations (Propato and Uber, 2004; NRCNA, 2006; Vreeburg and Boxall, 2007). Although some authors argue that limiting particle accumulation and reducing assimilable organic carbon are the best way to preserve drinking water quality in DWDNs (Brettar and Höfle, 2008; Liu et al., 2013), other considerations like high variability of quality of surface water sources, improved performance of WTPs, loss of the physical integrity of DWDNs, and the ability of bacteria to grow in oligotrophic environments (Simões and Simões, 2013) should be recognized in planning and O&M of drinking water supply systems.

Water treatment, including disinfection, is not completely effective to remove all biomass present in raw water and, as a result, treated water still contains viable microorganisms. Low velocities, low residual disinfectant concentrations, presence of nutrients, and biofilm-former microorganisms in bulk water together promote biofilm formation in all the components of a DWDN. Biofilm represents the large fraction of total biomass in drinking water (Abe et al., 2012). Figure 1-2 shows the existing relationships between factors that can lead to acute and chronic risk for consumers. Such risk is associated with bacterial re-growth and DBP formation. In addition, customer complaints to water utilities and regulatory agencies can occur due to changes in aesthetic characteristics and intermittence in the service (e.g., discoloured water, broken pipes). In summary, drinking water quality can deteriorate when the physical barrier (physical integrity) of the DWDNs is broken,

hydraulic changes occurs (hydraulic integrity), and physico-chemical and biological processes occur within the water pipes (water quality integrity).

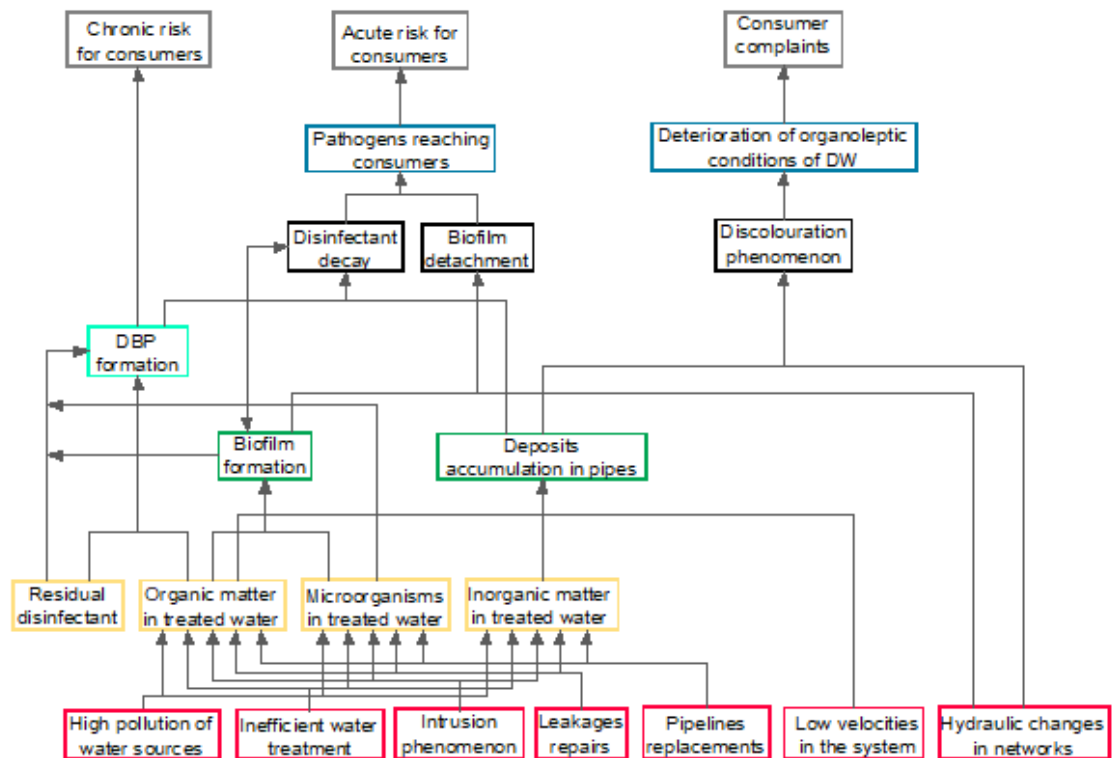


Figure 1-2. Issues arising in DWDNs

Precisely, biofilms are a concern because they can promote corrosion of pipes, discoloured waters and odours; host pathogens which may be released to bulk water; detach and recolonize clean surfaces; be precursors of DBPs and, consequently, causing disinfectant decay (Lehtola et al., 2004; Berry et al., 2006; Wang et al., 2012a; Pu et al., 2013; Wang et al., 2013a; Sun et al., 2014; Xue et al., 2014). Biofilm control has been oriented toward application of disinfection strategies (Berry et al., 2006; Simões and Simões, 2013) due to its role as pathogen reservoir (Wingender and Flemming, 2011). Several studies have investigated the effects of disinfectants on the structure of biofilms and survival of cells (Codony et al., 2005; Gagnon et al., 2005; Roeder et al., 2010). Even though there is evidence of DBP formation from the disinfection of biofilms and that EPS exert a protection barrier against disinfectants, recent studies still recommend to adjust operation parameters for disinfection considering appropriate doses of disinfectant in order to inactivate efficiently both biofilm and detached clusters (Xue et al., 2012; Xue et al., 2014; Prest et al., 2016).

Drinking water quality in distribution networks is frequently threatened by several factors such as sudden variations of raw water quality, inefficient treatment, intrusion phenomenon, and routine maintenance practices (Figure 1-2). In order to preserve drinking water quality in the DWDNs, water

operators carry out regular practices such as flushing and pipeline cleaning, which are known as the simplest and most cost effective ways of reducing the risk of discolouration (Vreeburg and Boxall, 2007). The objective of flushing pipes is to remove, in a controlled way, soft deposits from a sector of distribution network; flushing can be effective in soft deposit removal in cast iron pipes (Lehtola et al., 2004; Vreeburg et al., 2008) but relatively ineffective in achieving biofilms detachment (Abe et al., 2012; Fish et al., 2012).

DBP formation is another concern in the control of water quality in DWDNs because they have a negative effect on human health as they have been identified as potential carcinogenic, teratogenic and mutagenic substances (WHO, 2008). DBPs are the result of the reaction between oxidant substances, halogens and organic matter. There are more than 600 species identified to date (Hrudey, 2009), and they are commonly classified into two groups: carbonaceous and nitrogenous DBPs. The highest occurrence of DBPs is for chlorate, followed by chloroform, dichloroacetic acid, dibromoacetic acid, trichloroacetic acid, bromate, and chlorite (Richardson et al., 2007).

Despite of the wide variety of DBP species, only THMs and HAAs (carbonaceous DBPs) are the regulated groups around the world (Richardson et al., 2007). DBP formation starts, under the presence of disinfectants, in water treatment and continues during distribution and storage, increasing with water age. This principle applies for THMs but not for unstable DBPs such as HAAs, since some species of this group are biodegradable and their concentrations can be lower at points where biological activity is high within DWDNs, such as areas with high residence time and low chlorine residuals (Tung and Xie, 2009). Similarly, DCAN is an unstable DBP species, which degrades under certain conditions of free chlorine and pH. DCAN degrades in the absence of chlorine above pH 7 and below pH 6.5. In the presence of free chlorine, DCAN degradation can be much faster in the condition of a pH of about 6–8.5 under low to moderate chlorine residuals (Reckhow et al., 2001).

Considering that biofilms are present in every component of DWDNs and are DBP precursors; a particular interest has grown in the recent years in relation to DBP formation from disinfection of pure cells and heterogeneous biofilms, planktonic cells, and extracted EPS from pure cells. For example, studies of disinfection of microbial biomass from cyanobacteria and green microalgae (i.e., highly relevant in tropical climate countries) were undertaken to determine the yield of THMs and HAAs (Hong et al., 2008; Fang et al., 2010a; Fang et al., 2010b; Pu et al., 2013; Xie et al., 2013), focusing on disinfection of surface water from reservoirs and water in pools and cooling towers.

In addition, EPS from planktonic pure cells, biofilm pure cells, and isolated drinking water biofilms have been tested after disinfection with chlorine and/or chloramines to quantify carbonaceous and nitrogenous DBPs (Wang et al., 2012c; Wang et al., 2013a; Wang et al., 2013b). Another focus of research has been developed by Yang et al. (2010) and Huang et al. (2012) towards quantification of nitrogenous DBPs from nitrogenous organic compounds since these DBPs are considered more toxic than carbonaceous DBPs (Muellner et al., 2007; Plewa et al., 2008). Doederer et al. (2014) also investigated this topic on disinfection of treated wastewater.

These studies were based on laboratory tests and their results demonstrate that biofilms contribute significantly to the DBP formation in disinfection processes. However, more information is still required to determine parameters which allow mathematical simulation of this phenomenon in order to apply it to experiment design and DWDN operation. It is recognized that modelling could represent a less expensive tool when compared to experimental/field work and it allows testing different scenarios to predict and optimize processes. Finally, it is worth noting that biofilm and DBP modelling has been approached separately, resulting in the need for improving the development of DBP models that take into account the role of biofilms as DBP precursors.

1.3 RESEARCH QUESTIONS, AIM AND OBJECTIVES

Following the above discussion, the current document corresponds to a research project aimed to improve the understanding of biofilms presence in drinking water pipes by conducting a field work in a tropical climate country and developing a flow-coupled mathematical model to predict the contribution of biofilms to the DBP concentration in bulk water. This project addressed the gaps in knowledge related to (i) the type of bacterial communities present in real scale DWDNs, especially in tropical climates, and (ii) limited previous models that couples biofilms and DBPs together, principally under transitional and turbulent flow conditions.

1.3.1 Research questions

- Is there any correlation between hydraulic factors, water quality, biofilm properties, bacterial communities and total THMs concentrations in a tropical-climate DWDN?
- What are the bacterial communities present in bulk water and biofilms of a tropical-climate DWDN?
- What are the main parameters influencing the formation of DBPs under stagnation conditions?

- Can the interaction between these parameters be quantified?
- How flow regime and pipe surface/volume ratio and biofilm characteristics affect the DBP formation in drinking water pipes?
- Which are the practical recommendations for O&M of DWDNs in order to reduce the formation of DBPs, related to biofilms?

1.3.2 Aim

The aim of this project is to better understand the impacts on water quality from the presence of biofilms in DWDNs in tropical climate countries, with particular emphasis on their dual role as pathogen reservoirs and DBPs precursors, under transitional and turbulent flow conditions.

1.3.3 Objectives

1. To understand the current knowledge on drinking water quality associated with biofilms and DBPs, microbiological methods, and modelling.
2. To identify the bacterial communities existing in biofilm and bulk water of a tropical-climate DWDN.
3. To identify the interrelationship between hydraulic, physical, chemical and biological factors in a tropical-climate DWDN.
4. To build a simple biofilm model in order to understand the basis of modelling the chlorination of biofilms, and the chloroform and DCAN formation potentials, under stagnation conditions.
5. To develop a flow-coupled model to predict chloroform and DCAN formation from chlorination of biofilms in drinking water pipes.
6. To provide practical recommendations on biofilm and DBPs control in drinking water networks, with a particular focus on tropical climate.

1.4 GENERAL METHODOLOGY OF THE RESEARCH PROJECT

The general methodological approach of the current research project is described in Figure 1-3. The starting point of this study was an extensive literature review to identify the gap on the study of biofilms and DBPs in drinking water. Then, the problem, research questions, aim, and objectives were established. In order to achieve such objectives, a field work and the development of one-dimensional (1D) and two-dimensional (2D) models were carried out. The results of such work were

analysed and discussed in order to improve the understanding of the impact of the presence of biofilms and prediction of DBPs in DWDNs.

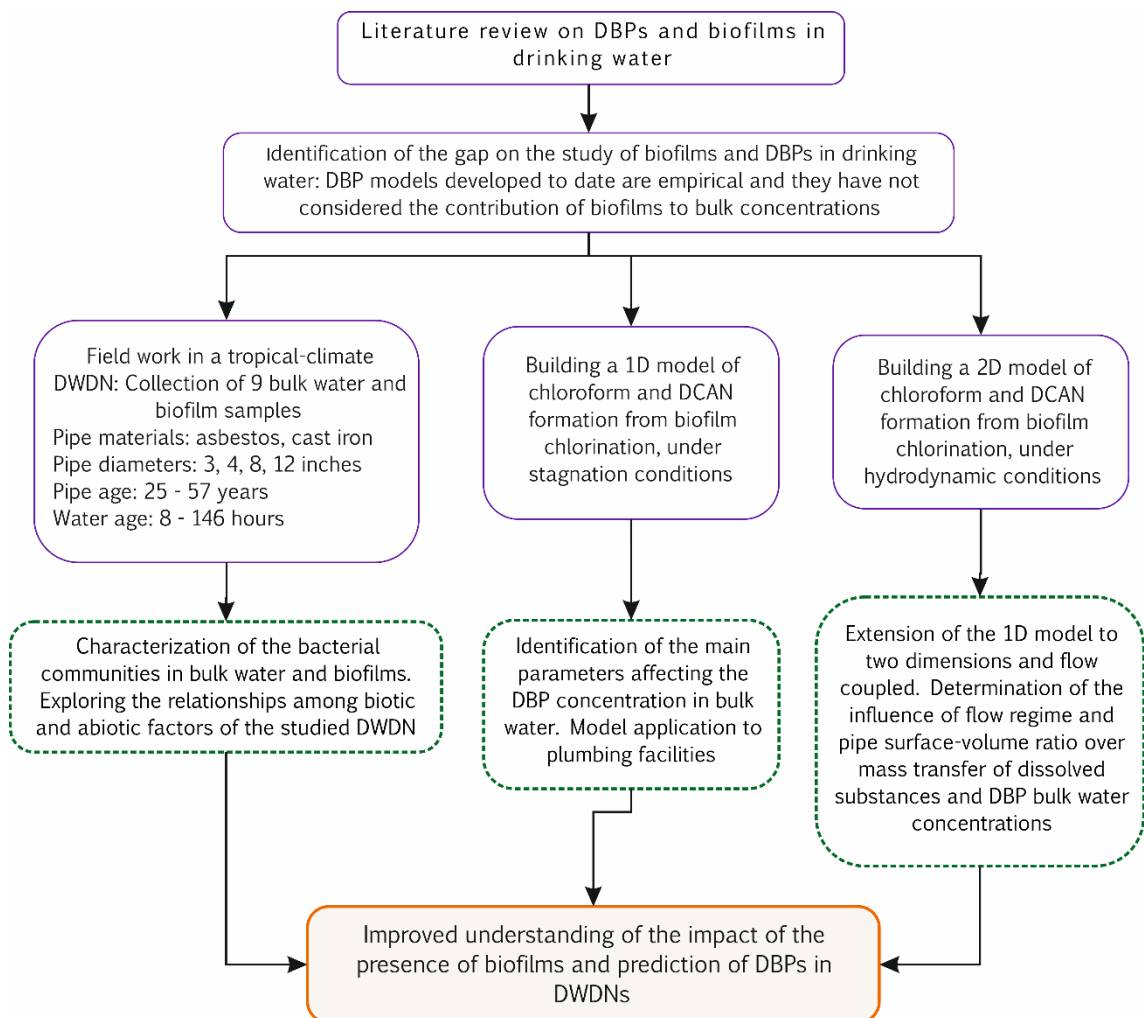


Figure 1-3. Methodological approach of the current research project

1.4.1 Structure of the thesis

The current thesis is structured as it follows:

- **Chapter 2: Literature review.** This chapter explains the basic concepts related to this study such as physical, hydraulic, and water quality integrity in DWDNs; water disinfection, biofilms, and DBPs. The literature review shows the evolution of research on biofilms and DBPs and focuses on the relationship between these two elements. Finally, this chapter presents the current gap related to such relationship and explains how this project intends to fill it.
- **Chapter 3: Field assessment of bacterial communities and their relationships with engineered factors.** Here the identification of bacterial communities in bulk water and biofilms is presented. The relationships among biotic and abiotic properties of a tropical-climate DWDN

are defined by statistical tests, and the relationship between methylotrophic bacteria and total THMs concentrations is also explored.

- **Chapter 4: A simple biofilm disinfection model.** This chapter presents the basics for developing a 1D model of biofilm chlorination, under stagnation conditions, and the consequent chloroform and DCAN formation. The parameter influence on the bulk concentration of these substances is also assessed, and the model is applied to plumbing building conditions.
- **Chapter 5: Modelling DBP formation from biofilm chlorination under hydrodynamic conditions.** The simple biofilm model built in Chapter 4 forms the basis for the extended 2D model, flow-coupled developed here. This chapter evaluates the influence of parameters such as Re , flow regime, pipe surface to volume ratio (S/V), and water quality on the mass transfer of dissolved substances through the biofilm surface.
- **Chapter 6: General discussion, implications and applications.** Here the results obtained in Chapters 3, 4, and 5 are discussed together and their implications are reported in the context of climate change and human health. Special focus is brought into the practicalities of the results in the water industry.
- **Chapter 7: Key findings, conclusion and future research.** This final chapter summarize the main findings of the current research project, presents a general conclusion linked to the aim and mentions potential areas for further investigation.

2.1 INTRODUCTION

The current research project was described in the previous chapter, including the problem identification and objectives. In order to identify the research gaps in current knowledge on biofilm and DBP research, the current chapter outlines a conceptual framework to physico-chemical and biological processes occurring in DWDNs, with special focus on biofilms, DBPs, and modelling.

2.2 PHYSICAL, HYDRAULIC AND WATER QUALITY INTEGRITY OF DRINKING WATER DISTRIBUTION NETWORKS

The preservation of water quality for the consumers is a major challenge for utilities, and the origin of substantial changes in the DWDN must be understood in order to reach a suitable performance in O&M. Those changes can be associated with different events which affect the physical, hydraulic, and water quality integrity such as cross-connections, leakages, metal leaching, pipe corrosion, residual disinfectant loss, formation of DBPs, bacterial regrowth, turbidity fluctuations, inadequate network construction, and maintenance and repairs (Kirmeyer et al., 2001).

As a result, water contamination sources in DWDNs are generally studied to identify potential health risks and strategies for future investments and operation and maintenance activities. Because of this, the USA National Research Council established that maintaining the physical, hydraulic, and water quality integrity in DWDNs is necessary to preserve water quality, considering that the networks can be less vulnerable to contamination than contamination of surface water sources (NRCNA, 2006), but reducing risks could be more difficult if they became contaminated (Stevens et al., 2004).

2.2.1 Physical integrity of DWDNs

Physical integrity of DWDNs applies to the primary physical barriers used to avoid the entry of external contaminants to the distribution network resulting in poor water quality. Those barriers comprises mains, services lines, and premise plumbing; fittings (crosses, tees, ells, hydrants, valves, and meters); storage facilities (service reservoirs and storage tanks); and back-flow prevention devices (NRCNA, 2006). The loss of physical integrity is related to corrosion (Kettler and Goulter, 1985; Ahmadi et al., 2013); biodegradation (Wang et al., 2011); missing cover of

storage facilities (USEPA, 2002b); unsanitary activity during construction, replacement, or repair of pipes and fittings (RSPH et al., 2017); among others (NRCNA, 2006). According to the NRCNA (2006), the loss of physical integrity is mainly due to material failure as a result of its alteration, and absence and improper installation of the barrier. Material modification can be related to chemical interactions between the materials and the surrounding environment, eventually leading to holes, leaks, and other breaches. Material collapse can be accelerated by high water pressure and stress on pipes, and during natural disasters (NRCNA, 2006).

Losing the physical integrity of the system affects the water quality by the introduction of microbial and chemical contaminants, debris, and particulate matter into the distribution system, sometimes accompanied by changes in aesthetic characteristics (i.e., water colour, turbidity, taste, and odour). However, aesthetic changes do not always represent a direct health impact (NRCNA, 2006). Strategies such as monitoring, prediction and prevention of failures; disinfection of new pipes; design and implementation of protocols for leakage repairs and accessories and pipeline replacements, and inspections are recommended to maintain the physical integrity of DWDNs (RSPH et al., 2017). In addition, maintenance activities such as proper material selection, corrosion control, avoiding permeation, cleaning and inspection of storage facilities, and cross-connection control should also be implemented (NRCNA, 2006).

Water supply interruption and environmental damage due to wasting water are the immediate repercussions of leakages. They can impact customers' perception on water companies and their own water saving strategies (CCWater, 2013). The Consumer Council for Water in the United Kingdom (UK) promotes the reduction of leaks in DWDNs in order to keep high levels of customer satisfaction and reduce negative environmental impacts. The latest report for water companies in England and Wales "Diving into Water 2011-12 to 2015-16" informed about the change of trend: industry-wide leakage levels were rising since 2011-12 but more recently it was found a reduction of 1.4% in leakage levels for 2015-16 (CCWater, 2013).

Despite of the immediate consequences of leakages, the most serious effect is the negative impact on water quality. Therefore, strategies to reduce their number include setting leakage targets; replacement of pipelines with cast iron and stainless steel pipes (Farley, 2015); however, others recommend plastic materials over metal considering biological aspects of drinking water quality (Fish et al., 2016). Additionally, changing water management by installing water meters and controlling losses; reducing pressure transients and stress in the pipe network by setting valve operations, pumping routines and pressure management to operate at the optimum level (pressure districts); real time monitoring; smart asset management by identifying leaks as soon as they

propagate; integrated data management by handling “big data”; and researching to reduce the risk of failure of plastic pipes (polyethylene) (Farley, 2015).

2.2.2 Hydraulic integrity of DWDNs

Hydraulic integrity refers to the maintenance required to keep a desirable water flow, water pressure, and water age, taking both potable water and fire flow provision into account. Generally, big cities have centralised drinking water supply systems and continuous service provision. However, extreme weather events such as droughts and heavy rain are impacting the normal operation of WTPs and, therefore, impacting drinking water quality (Khan et al., 2015). Such impacts can lead to water interruption supply in developing countries as reported by Montoya et al. (2011) in Colombia, but in industrialised countries like the USA and Australia main concerns are more related to changes in the quality of water sources and subsequent formation of DBPs (Water Research Foundation, 2014; Raseman et al., 2017). Similarly, water scarce areas have drinking water supply systems which must be operated intermittently (Kumpel and Nelson, 2016). This irregular operation of DWDNs can cause pressure transients, changes in flow regime, and backflow (NRCNA, 2006; Kumpel and Nelson, 2016), which can lead to water quality deterioration.

Water demand is the driving force for the operation of DWDNs. Due to its stochastic nature, operation of DWDNs requires an understanding of the amount of water being used, where it is being used, and the temporal variation of water consumption (NRCNA, 2006). For instance, water age is a factor related to the hydraulic design of the system and directly influences water quality (USEPA, 2002a). One of the most commonly acknowledged effects of increasing water age is the decay of disinfectant residuals such as chlorine and chloramines. DWDN operators are commonly committed to keep residual concentrations of disinfectants in the networks, but very often none or very low concentrations of disinfectant can be found in locations at the farthest distances from the actual WTP, along with an increment of DBP concentrations such as THMs (USEPA, 2002a).

Low flow velocities in pipes create long travel times, resulting in pipe sections where sediments can accumulate and microorganisms can form biofilms (USEPA, 2002a). Long detention times can also greatly reduce corrosion control effectiveness by reversing blended metha- and poly-phosphates to orthophosphates with time (i.e., as they tend to hydrolyse) and increasing their concentration in bulk water; orthophosphates are less effective as corrosion inhibitors (USEPA, 2002a). The need for pH control is another consequence of high water age, since the interaction between water and cement linings significantly increases pH; unstable, soft, low-mineralized waters can revert to

untreated water pH conditions by the time the water reaches the point-of-use tap (USEPA, 2002a). Thus, reducing water age is important to maintain the hydraulic integrity of the system (USEPA, 2002a; NRCNA, 2006).

Factors causing loss of hydraulic integrity include pipe deterioration, pressure transients and changes in flow regime, hydraulic changes during maintenance and emergencies, tuberculation and scale, inadequate operational control of DWDNs related to the lack of focus on water-quality-related issues. Several procedures can be applied to maintain and/or recover the hydraulic integrity of DWDNs such as providing alternative water sources, managing pressure zones, using devices for surge protection, flushing water mains, maintaining sufficient mixing and turnover rates in storage facilities, and cleaning pipes (NRCNA, 2006).

For instance, it is advisable to divide a new or existing DWDN into pressure zones when pressure differentials in relation to minimal and maximal values are outside of their desirable values (NRCNA, 2006). Pressure zones are created by installation of closed valves, and pressure-regulating valves are placed between the zones to improve reliability and stretches of new pipe are used to eliminate dead ends (NRCNA, 2006). Adequate pressure zones will reduce leaks by properly controlling pressure fluctuations, breaks, and pumping costs; improving reservoir turnover rates; and avoiding over-pressured systems (NRCNA, 2006), which can lead to reduce pipe leakages. However, pressure districts or sectorization can also lead to deterioration of drinking water quality since they reduce the network redundancy, increase the probabilities of sediment resuspension, and promote the deterioration of drinking water quality due to the increase of number of dead zones and water age (Grayman et al., 2009; Di Nardo et al., 2013; Wright et al., 2014) .

Pipe flushing is considered a maintenance activity aimed to eliminate loose deposits and poor-quality water accumulated mainly in dead ends. This procedure can be conducted by conventional or unidirectional flushing. Conventional flushing consists simply in opening one or more hydrant valves to let sediments be washed out of the distribution network. In unidirectional flushing water flow is increased in a specific “dirty” pipe by cutting off flows in other segments of the network and increasing scouring velocities (to 1.5 – 3.0 m/s), with the resulting effect of flushing out sediments, biofilms, corrosion products, and tuberculation (Antoun et al., 1999). Although, unidirectional flushing requires more labour, equipment, data collection, and appropriate measures to dispose disinfected water, it is more efficient and uses on average 40 percent less water than conventional flushing (Barbeau et al., 2005).

Storage tanks or service reservoirs are used in the DWDNs to provide disinfectant contact time, water reserve, and pressure regulation. Poor design and/or operation of storage facilities can

promote insufficient mixing and consequently increase water age, which promotes DBP formation, losing disinfectant residual, microbial regrowth, organoleptic alterations and water recontamination in the network (USEPA, 2002b). Montoya et al. (2012) and Montoya-Pachongo et al. (2016) recommended to promote mixing times in service reservoirs to be higher than the duration of filling times, reduce minimum water levels, avoid thermal stratification, increase turnover rates, and change inlet configuration in order to increase jet momentum to impact positively water quality stored in service reservoirs.

2.2.3 Water quality integrity of DWDNs

Water quality integrity refers to the maintenance of finished water quality via prevention of internally derived contamination. It was already explained how issues with physical and hydraulic integrity may result in deterioration of water quality; however, this can also occur even in the absence of external contamination events due to transformations which take place within pipes, tanks, and premises plumbing (NRCNA, 2006). The factors that affect water quality integrity include biofilm growth (Srivastava and Bhargava, 2015), nitrification (Lipponen et al., 2002), leaching substances from network materials (WHO, 2008), internal corrosion (WHO, 2008), scale formation and dissolution (Peng et al., 2010), disinfectant loss (WHO, 2008), and DBP formation (WHO, 2008). The core focus of the research work reported herein is on biofilms and DBP formation; therefore, these subjects will be discussed in depth in the following sections.

Biological nitrification is a process in which nitrifying bacteria oxidize reduced nitrogen compounds (e.g., ammonia) to nitrite and then nitrate (Lipponen et al., 2002). It is associated with long retention times in distribution systems practicing chloramination (NRCNA, 2006). However, nitrification potential has also been identified in chlorinated and non-disinfected DWDNs, but no correlations between retention times and occurrence of nitrifying bacteria has been identified, as reported in a study conducted in Finland covering 15 DWDNs from eight towns (Lipponen et al., 2002). One of the most important problems exacerbated by nitrification is loss of the chloramine disinfectant residual (NRCNA, 2006). In addition, all materials in the DWDN leach substances into the water, which can alter the taste and odour of drinking water. For instance, leaching lead from lead-pipes can represent a substantial health risk (NRCNA, 2006; WHO, 2008).

Internal corrosion manifests as the destruction of metal pipe interiors by both uniform and pitting corrosion, which can lead to accumulation of scales. The latter one can also be formed by the precipitation of some metals dissolved in bulk water as a consequence of changes in water pH and

redox potential. Corrosion and scaling in pipes offer higher surface area for biofilm growth, which can be detached changing the organoleptic characteristics of bulk water (NRCNA, 2006). To preserve drinking water quality, it is necessary to monitor it and carry out adequate O&M to prevent or solve any case of water quality integrity loss (WHO, 2005). Monitoring water quality can include the installation of on-line monitoring devices for conductivity, chlorine, pH, turbidity, and temperature; and surveillance of biological quality indicators in both biofilms and bulk water with emphasis on opportunistic and pathogenic organisms and other microorganisms associated with them (e.g., amoebas, *Cryptosporidium*, *Staphylococcus*, etc.) (NRCNA, 2006).

In addition, the NRCNA (2006) stated that drinking water can serve as a transmission vehicle for a variety of hazardous agents such as enteric microbial pathogens from human or animal faecal contamination (e.g., noroviruses, *E. coli* O157:H7, *Cryptosporidium*, fungi like moulds and yeasts), aquatic microorganisms that can cause harmful infections in humans (e.g., nontuberculous mycobacteria, *Legionella*), and toxins from aquatic microorganisms such as cyanobacteria (Fan, 2012; Badar et al., 2015). In addition, some aquatic invertebrates have organoleptic and clinical importance because can alter the turbidity of drinking water and serve as transport hosts for pathogenic bacteria (e.g., free living amoeba and bacteria *Legionella*) (Lau and Ashbolt, 2009). Such organisms have been found in bulk water from WTPs, main pipelines (Wolmarans et al., 2005), and premise plumbing (Buse et al., 2013).

According to WHO (2005), monitoring can be defined as “*the act of conducting a planned series of observations or measurements of operational and/or critical limits to assess whether the components of the water supply are operating properly.*” This kind of monitoring involves design and application of corrective actions in order to amend the deviation and maintain water quality in the short and long term (WHO, 2005). The drinking water surveillance could be achieved by traditional methods (water sampling by fixed stations) (Montoya et al., 2009) or computational applications (real-time operation) (Perelman and Ostfeld, 2013); however, both methods may be based on new technologies of both software and hardware. Although their application seems to be sophisticated, these could be applied in large cities of developing countries if adequate knowledge, training and funding are provided. However, developing countries still need to deal with providing treatment facilities and increasing coverage of water supply in rural areas and small towns; therefore, in the meantime, real-time monitoring of drinking water quality may be mainly affordable for large DWDNs.

Procedures such as reduction of organic matter content and nutrients in WTPs; cleaning pipes by flushing; controlling corrosion by appropriate selection of materials and maintaining suitable

chemical conditions of water; and keeping appropriate concentrations of residual disinfectant, taking into consideration a balance between acute and chronic health risk, can be carried out to directly control water quality (NRCNA, 2006). In summary, physical, hydraulic, and water quality integrity are closely interrelated, which reflects the complexity of DWDNs and their O&M. The main purpose of a water company is to deliver drinking water to the consumers with appropriate amount and quality. This firstly requires to know in detail the distribution system itself (infrastructure and operation), to monitor the most influencing factors on water quality, and to apply simultaneously procedures to preserve it (NRCNA, 2006). This demands adequate technical and administrative structure of the water company, where the different departments sustain fluent communication channels for planning, decision making, and supporting to each other.

2.2.4 Plumbing systems

The last component of the water supply chain is the plumbing systems. Plumbing premises comprise health and education institutions, private housing, commercial buildings, among others; and it is in there where actual water consumption occurs (Chowdhury, 2016). However, regulation and monitoring by agencies and water utilities take place in the distribution networks (NRCNA, 2006). The same physical, chemical, and biological processes occurring in a full scale DWDN take place in plumbing systems, but these may be exacerbated by being located at the end of the network, and poorer water quality can be found. Table 2-1 briefly explain the main characteristics of plumbing buildings.

Table 2-1. Characteristics of plumbing systems

Characteristic	Description
High surface area to volume ratio (S/V)	One of the most prominent characteristics of plumbing premises is the high S/V ratio because they are lengthy sections and small-diameter tubing (NRCNA, 2006). S/V is inversely proportional to pipe diameter ($4/\phi$). According to Hallam et al. (2002), the higher S/V, the larger the surface across which mass transfer can occur and the greater the number of reactive sites available for each unit volume of water passing through the pipe. While the public infrastructure can have S/V of 0.26 cm ² /mL, private infrastructure can have S/V of 2.1 cm ² /mL (NRCNA, 2006). This represents that wall effects on bulk water are more important in these systems as it will be explained later.
High water age	In plumbing systems, water flow is more dependent on household consumption patterns. These systems are characterized for stagnation conditions since the buildings can remain unoccupied for several hours, days or weeks in houses, commercial buildings or schools, respectively. It should be noted that the negative effects of water age are exacerbated if the biological stability of the water in the DWDN is poor (NRCNA, 2006).
Presence of different materials	Several materials can be found in plumbing premises such as copper, plastics, brass, lead, galvanized iron, and stainless steel. Such variety is not usually found in

Characteristic	Description
	public DWDNs. The type of pipe material influences the interaction with disinfectants and microorganisms (NRCNA, 2006).
Extreme temperatures	Interior of buildings are naturally warmer than outdoors, especially in geographic regions with temperate weather, which use heating systems during cold season. This is reflected in warmer water temperatures in plumbing facilities. In addition, the domestic hot-water distribution systems also transfer heat to adjacent pipes.
Low or no disinfectant residual	The reaction of disinfectants with pipe materials, organic and inorganic matter, and biofilms promotes the disinfectant decay. If the disinfectant concentrations are already low in the service lines, it is expected total disappearance of this under stagnation conditions in building facilities (Lu et al., 1999; Buamah et al., 2014; Lee et al., 2014).
Potential bacterial regrowth and biofilm formation	Type of pipe material (Song et al., 2015), high S/V, warm water, and low concentration of disinfectant promote the bacterial regrowth and biofilm formation or survival. This increases the risk by potential survival and exposure to pathogenic microorganisms (NRCNA, 2006).
Highly variable velocities	Plumbing premises are characterized by start-stop flow patterns. This induces a high variation of flow velocities, which can lead to biofilm detachment and potential consumption of pathogenic microorganisms by the consumers, if these were released to the bulk water (NRCNA, 2006).
Exposure to vapours and bioaerosols	Showering is an important exposure route to bioaerosols with hygienic importance such as <i>Mycobacterium avium</i> and <i>Legionella</i> (Whiley et al., 2015) and volatile DBPs such as THMs (Cantor et al., 2010; Chowdhury, 2016).
Proximity to service lines	According to NRCNA (2006), service lines are the connection between the distribution main and the premise plumbing. The potential contamination of these by water leaks and repairs can affect individual consumers due to the proximity of plumbing premises to service lines.
Prevalence of cross-connections	Maintenance activities of plumbing systems are developed by the household or by plumbers, who are not trained and licensed in all the cases. Thus, the risk of cross-connections may increase leading to backflow and contamination of the drinking water within the facilities (NRCNA, 2006).

2.3 BASICS OF TRANSPORT PHENOMENA

Transport phenomena occurs when a perturbation of the equilibrium occurs in a physical system. Such perturbation can correspond to gradients of temperature, substance concentrations, and velocity. Energy, matter and momentum tend to move from regions of higher to lower concentration. The central aspects of the analysis of transport phenomena is the establishment of suitable constitutive equations to relate the fluxes of energy, matter, and momentum to local material properties.

2.3.1 Fluxes and conservation of chemical species

The fluxes of energy, matter, and momentum are composed by convective transport, which is related to bulk motion, and molecular or diffusive transport, which is related to small-scale molecular displacements. For the case of heat conduction, the Fourier's law is used as the

constitutive equation to describe the heat fluxes; Equation (2-1) represents the heat flux \mathbf{q} (energy flow per unit cross-sectional area). A schematic representation of the heat flux vector is presented in Figure 2-1 for an imaginary surface, which is perpendicular to a vector \mathbf{n} of unit magnitude. Equation (2-2) expresses the heat flux q_n normal to the surface. Here k is the thermal conductivity, ∇ is the gradient operator, and T is temperature.

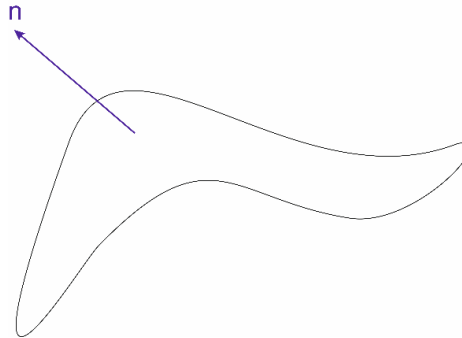


Figure 2-1. Schematic representation of mass flux at a surface with a unit normal \mathbf{n} and arbitrary orientation

$$\mathbf{q} = -k\nabla T \quad (2-1)$$

$$q_n = \mathbf{n} \cdot \mathbf{q} = -k(\mathbf{n} \cdot \nabla T) \quad (2-2)$$

A similar analysis can be done for a given species in a mixture, which results from a gradient in a concentration of that species; in this case, the Fick's law is used as the constitutive equation to describe the fluxes. The total flux (\mathbf{N}_i) is given by Equation (2-3).

$$\mathbf{N}_i = C_i \mathbf{u} + \mathbf{J}_i \quad (2-3)$$

Here, $C_i \mathbf{u}$ is the convective flux (C_i : concentration, \mathbf{u} : mass-average velocity) and \mathbf{J}_i is the molar flux of the species i . For liquid solutions, the molar flux is given by Equation (2-4), where D_i is the diffusion coefficient of the substance.

$$\mathbf{J}_i = -D_i \nabla C_i \quad (2-4)$$

2.3.2 Mass transfer and boundary conditions at interfaces

The analysis of conservation equations for interfaces found in Deen (1998) defined an interfacial balance valid at any instant in time given by the flux relative to the interface between two phases. Such interfacial source creates a difference in the normal components of the fluxes relative to the

interface. In general, all of the quantities involved are functions of position on the interface, so that the balance changes from point to point. This interfacial balance is a key result, because it is the basis for many of the boundary conditions in mass transfer problems. Further simplification of such interfacial balances led to the boundary condition flux continuity, which is commonly used in biofilm modelling (Equation (2-5)) (IWA Task Group on Biofilm Modeling et al., 2006; Taherzadeh et al., 2012). Here flux in the phase biofilm (B) at the biofilm surface (Bs) is equal to the flux in liquid (L) at the same point.

$$D_B \frac{dC}{dn} \Big|_B = D_L \frac{dC}{dn} \Big|_L \quad (2-5)$$

In the case of bulk motion, convection boundary condition at the biofilm surface is defined in the Equation (2-6) (Deen, 1998). Here k_f is the mass transfer rate specific to the substance since it depends in part on its diffusivity, so it is different for each component of a mixture. C_{L-Bs} is the concentration of the substance i in liquid at the biofilm surface. C_o is the concentration in the bulk far away from the biofilm surface, concentration at the reactor inlet is usually used as C_o (Taherzadeh et al., 2012). According to Deen (1998), when mass transfer is accompanied by bulk flow normal to the interface, the boundary condition shown in Equation (2-6) is best preserved if the mass transfer coefficient continues to refer only to the diffusive part of the solute flux (i.e., \mathbf{J}_{Bs} rather than \mathbf{N}_{Bs}). This is because this analogy has been adapted from the analysis of heat transfer; then heat transfer coefficients have been defined to represent only the conduction heat flux and not energy transfer by bulk flow (Deen, 1998).

$$\mathbf{J}_{Bs} = k_{f-i}(C_{i-L-Bs} - C_o) \quad (2-6)$$

2.3.2.1 Sherwood number

Despite of the simplicity of Equation (2-6), the parameter k_f and variable C_{L-Bs} are not always available. In biofilm analysis, k_f can be calculated from experimental tests of penetration of a specific substance and monitoring its concentration in the bulk and within the biofilm by micro-sensors. More details of this can be found in Chen and Stewart (1996) and Guimerà et al. (2016). By combining Equations (2-4) and (2-6), k_f is given by Equation (2-7); where δ_c represent the thickness of the stagnant film in the fluid next to the wall; δ_c is also known as boundary layer thickness.

$$k_f = \frac{D_L}{\delta_c} \quad (2-7)$$

In some cases, δ_c is not available; therefore, the Sherwood number (Sh) is used mainly for modelling purposes (IWA Task Group on Biofilm Modeling et al., 2006; Tosun, 2007). Since δ_c depends on the convection just outside the interface, Sh gives a measurement of the convective and diffusive fluxes to such interface. Sh is a dimensionless form of k_f and is represented by the Equation (2-8). Here L_{ch} is the characteristic length which can be assumed as pipe diameter or radius, width of a channel, or radius of the bubble for the case of transport around a gas bubble in a liquid (COMSOL, 2017). For instance, Taherzadeh et al. (2012) used the biofilm head diameter as L_{ch} for studying the fluid dynamics and mass transfer of biofilm streamers with a small immobile base attached to the support and a flexible tail elongated in the flow direction, which can vibrate in fast flows.

$$Sh_i = \frac{k_{f-i} L_{ch}}{D_i} \quad (2-8)$$

By combining the Equations (2-4), (2-6) and (2-8), an expression for Sh based on concentration gradient at the biofilm surface (Equation (2-9)) is obtained, which leads to the calculation of local Sh; then the global Sh (\overline{Sh}) can be determined by a surface integration and averaging (Equation (2-11)). This allows comparing Sh for different system configurations and obtaining the global mass transfer ($\overline{k_f}$) in biofilm modelling (Equation (2-12)). For instance, this approach was used by Taherzadeh et al. (2012). Here ds refers to differential of biofilm surface. In the case of biofilm attached to the pipe wall, ds represents the differential of pipe surface.

$$Sh_i = \frac{k_{f-i} L_{ch}}{D_i} = \frac{L_{ch} \frac{dC}{dn} |_{Bs}}{C_{i-Bs} - C_{i-o}} \quad (2-9)$$

$$\frac{dC_i}{dn} |_{Bs} = \frac{J_i}{-D_i} \quad (2-10)$$

$$\overline{Sh}_i = \frac{\int_{Bs} Sh_i ds}{\int_{Bs} ds} = \frac{\overline{k_{f-i}} L_{ch}}{D_i} \quad (2-11)$$

$$\overline{k_{f-i}} = \frac{\overline{Sh}_i D_i}{L_{ch}} \quad (2-12)$$

2.3.2.2 Engineering correlations

According to Tosun (2007), most engineering problems do not have theoretical solutions, then a large portion of engineering analysis is concerned with experimental information, which is usually

expressed in terms of engineering correlations. In the case of mass transfer between bulk liquid and biofilm, calculation of Sh becomes important in order to obtain the values of k_f for each substance of interest. According to Guimerà et al. (2016) and IWA Task Group on Biofilm Modeling et al. (2006), Sh is often expressed as a function of the non-dimensional Reynolds number (Re – Equation (2-13)) and Schmidt number (Sc – Equation (2-14)): $Sh=f(Re, Sc)$. Sh is usually represented by a power function $Sh=A+B\cdot Re^m\cdot Sc^n$. The parameters A , B , m , and n are, in most cases, determined empirically from experimental data for a specific system.

$$Re = \frac{uL}{\nu} \quad (2-13)$$

$$Sc = \frac{\nu}{D_i} \quad (2-14)$$

Where ν is the kinematic viscosity of the fluid (m^2/s), u is the velocity of the fluid with respect to the object (m/s), L is a characteristic linear dimension (m), and D is the mass diffusivity (m^2/s) of species i . In relation to Sh , Equation (2-15) reported by Horn and Lackner (2014; cited by (Guimerà et al., 2016)) is used for turbulent models and Equation (2-16) is applied to laminar flow (Zhang and Bishop, 1994). Experimental data from Guimerà et al. (2016), who characterized external and internal mass transport of dissolved oxygen in an heterotrophic biofilm, fitted very well with the Equation (2-16).

$$Sh = 0.239 \cdot Re^{0.8} \cdot Sc^{0.33} \quad (2-15) \quad \text{Turbulent flow}$$

$$Sh = 0.369 \cdot Re^{0.5} \cdot Sc^{0.33} \quad (2-16) \quad \text{Laminar flow}$$

Due to the empirical origin of expressions to calculate Sh , their application to biofilm modelling must be cautious since parameters depend on the geometry of the biofilm support medium, the type of substance, and are valid only for a defined range of Re and Sc . Extrapolating from these conditions can yield erroneous results (IWA Task Group on Biofilm Modeling et al., 2006). Additionally, most correlations for Sh were derived for rigid particles, but the elastic and heterogeneous nature of the biofilm can influence external mass transfer (IWA Task Group on Biofilm Modeling et al., 2006). Despite of the mentioned cautions, engineering correlations can be useful to correlate experimental data to simplified models; which in turn can represent an acceptable physical process. However, with the further and accelerated development of numerical methods, computational techniques,

software, and hardware, applying theoretical concepts to physical process in drinking water industry is more feasible every day, the more reliable results can be obtained from modelling approaches.

2.4 BIOFILMS IN DRINKING WATER DISTRIBUTION NETWORKS

Biofilms can be understood as a biological strategy of microorganisms to survive in hostile environments. From a microscale point of view, biofilms are a group of microorganisms, mainly bacteria but archaea, fungi and protozoa are also important (Wang et al., 2014; Fish et al., 2015), living as a consortium, attached to a surface as a result of the secretion of EPS (Srivastava and Bhargava, 2015). Biofilms are successful due to the protective effect of EPS to cells against oxidant substances, grant cells attachment to surfaces under certain hydraulic conditions, and improve availability of nutrients as a result of organic matter retention. With regards to hydraulic forces, flushing water pipes has been proved as a proper technique to remove soft sediments and biological material but inefficient to completely detach biofilms (Abe et al., 2012; Douterelo et al., 2013). From a macroscale point of view, biofilms can be conceived as reservoirs of organic matter due to the presence of lipids, proteins, carbohydrates, DNA, and organic matter particles (Wang et al., 2012b; Fish et al., 2015).

Biofilms are naturally found in most of the solid/liquid interfaces such as showers, pools, teeth, food industry facilities, wastewater treatment plants, water supply systems, among others. In water systems for human consumption, biofilms grow in the walls of reactors of WTPs, pipes, valves, tanks, pumps and all the fittings of the system. In this case, drinking water biofilms are a major concern because they can lead to corrosion, discoloured waters and odours; host pathogens which may be released to bulk water; detach and recolonize clean surfaces; act as precursors for the formation of DBPs, and consequently, contribute to disinfectant decay (NRCNA, 2006).

Biofilm formation starts with the adhesion or incorporation of microorganisms depending on their ability to produce EPS, salivary pellicle or if the cell structure includes components such as flagella (Song et al., 2015). Material properties like surface charge, surface energy, roughness, topography, surfaces with topographic patterns, and stiffness influence the adhesion of microorganisms. Some bacteria like *P. aeruginosa* use the surface sensing ability to probably modify cell surfaces to better attach to negatively charged surfaces (Song et al., 2015). The organisms may attach to surfaces as primary colonizers and actively establish biofilms alone or in combination with other microorganisms. However, they can also become integrated in pre-existing biofilms as secondary

colonizers. Bacteria such as *Pseudomonas*, *Staphylococcus*, and *Methylobacterium* are known as biofilm formers (Simões et al., 2007; Simões et al., 2010; Douterelo et al., 2014c).

In a second step, incorporation of other organisms such as virus, fungi, and invertebrates occurs. In this stage, heterotrophic bacteria, free-living protozoa and fungi can multiply and persist if they have adapted to the oligotrophic conditions characteristic of engineered water systems (Wingender and Flemming, 2011). Given suitable laboratory conditions, all relevant water-related pathogenic bacterial species have actually been shown to be able to adhere to solid surfaces and/or to form mono-species biofilms, indicating their potential as biofilm organisms (Wingender and Flemming, 2011). However, enteric viruses and parasitic protozoa are obligate parasites and dependent on multiplication in animal or human hosts. Such organisms can only be expected to attach to and persist in biofilms without being able to proliferate (Wingender and Flemming, 2011). Finally, chlorine effects and shear stress can cause the detachment of the biofilm (Xue and Seo, 2013), releasing the organisms, which can reach the customers, colonize new surfaces, or be incorporated in other biofilms downstream.

2.4.1 Taxonomy and diversity

Population genetics and taxonomy fields are two very different aspects of biology and necessitate very different assumptions, theories and methods, but they overlap at some degree (Wheeler, 2008). First, taxonomy refers to naming, describing and classifying organisms and includes all plants, animals and microorganisms discovered in nature. This branch of biology is being transformed according to the technical and technological progress made in the access of electronic publications, molecular analysis, and bioinformatics (Wheeler, 2008). Then, the taxonomic rank allows allocating an organism in a certain group defined by the kingdom, phylum, class, order, family, genus, and species. In the environment, ecosystems are an assemblage of populations, plants, animals, bacteria, fungi (Whittaker, 1975), and the recent-defined archaea, that live in an environment and interact with one another, forming together a distinctive living system with its own composition, structure, environment relations, development, and function (Whittaker, 1975).

Natural ecosystems are forests, lagoons, mangroves, etc. DWDNs can be considered engineered ecosystems since all the characteristics previously mentioned are present in there, with the difference that they have been designed, constructed, operated and maintained by humans. Therefore, it can be inferred that most of the variables influencing the behaviour of such systems can be modified according to the needs of the managers and drinking water consumers. In order

to study living systems in their environmental contexts, ecology arises as the area of the biology concerning to it.

Whittaker (1975), by studying the communities in redwood forests, analysed the species diversity by the application of indices, according to the alpha (within community); beta (between communities; and gamma diversity (between regions) (Whittaker, 1975; Sepkoski, 1988). Examples of alpha-diversity metrics are Margalef and Chao1 richness estimators, and Simpson and Shannon diversity estimators (Whittaker, 1975; Gamito, 2010; Douterelo et al., 2013). According to the scope of this project, calculation of Shannon (H) and Margalef (d) indices to calculate alpha diversity are explained in this section (Equations (2-17), (2-18) and (2-19)). Here S is the number of species, N is the total number of individuals in the sample, p_i is the relative importance values for these same species.

$$d = \frac{S - 1}{\ln N} \quad (2-17)$$

$$H' = - \sum_{i=1}^S p_i \log p_i \quad (2-18)$$

$$S = \exp(H') \quad (2-19)$$

2.4.2 Microbiome identification in bulk water and biofilms in drinking water networks

Culture-dependent methods, routinely used by water utilities to assess the microbiological quality of drinking water, present shortcomings such as underestimation of the amount and diversity of the microbial community (Theron and Cloete, 2000). Heterotrophic bacterial counts only represent a limited fraction of the whole microbial community (Douterelo et al., 2014a; Ren et al., 2015), when used to estimate bacterial loads in water samples. Moreover only less than 5% of the biomass is present in the water phase and 95% is living in the biofilm phase (Flemming et al., 2002). Current drinking water quality standards rely on culture-dependent techniques to quantify specific pathogenic organisms (e.g., *E. coli*, *Enterococci*, Coliform bacteria) (UK Parliament, 2000; Ministerio de la Protección Social and Ministerio de Ambiente Vivienda y Desarrollo Territorial, 2007) and heterotrophic bacteria in bulk water. Then, biofilms are only explored for research purposes and, to date, they have not been included in routine operative and regulatory plans by drinking water operators and agencies, respectively.

Recently, water microbiology research is focused on developing and applying culture-independent practices in order to improve the diagnostic of microbiological quality of water. Therefore, molecular analysis is being used for studying the microbial community in bulk water and biofilms. According to Douterelo et al. (2014a), studying microorganisms in a DWDN allows improving knowledge about how abundant they are, which types of microorganisms are present, how their activities shape the environment or influence other organisms, including any possible effects on human health, and how the environment influences the structure and functions of the microorganisms present. Douterelo et al. (2014a) also described the classification of microbiological techniques used to study microbial communities according to their purpose and nature: culture-based methods, microscopy, polymerase chain reaction (PCR), molecular techniques, and quantification of metabolism by-products. In particular, molecular techniques include cloning and sequencing, metagenomics, and next generation sequencing. The molecular techniques are applied to study the microbial community composition and involve the extraction of nucleic acid, followed by PCR amplification of “marker genes” to obtain taxonomic information. The most commonly used marker gene in microbiological research is the ribosomal RNA (rRNA) gene, 16S rRNA for prokaryotes and 18S rRNA for eukaryotes (Douterelo et al., 2014a).

According to Douterelo et al. (2014a), cloning and sequencing is the conventional and more widespread genomic approach used when detailed and accurate phylogenetic information from environmental samples is required. After DNA extraction and amplification of the rRNA gene with suitable primers, clone libraries using sequencing vectors must be constructed (Rondon et al., 2000). Selected clones are then sequenced (Sangerbased) (Sanger et al., 1977) and the nucleotide sequence of the rRNA gene retrieved, allowing estimates of the microbial diversity in the samples by comparison with sequences available in databases (e.g., GenBank, EMBL and Silva). The generation of DNA clone libraries followed by sequencing has being extensively applied in drinking water microbiology. The need to analyse the extensive amount of data related to sequence reads from environmental samples led to the development of the bioinformatics field, which involves software and analysis tools (Douterelo et al., 2014a).

Understanding of microorganisms in DWDNs has been developed by sampling water and biofilms. In relation to water sampling, guidelines from environmental and regulatory agencies exist for sampling methods and interpretation of results of traditional and well-known laboratory parameters. For instance, there are several International Organization for Standardization (ISO) standards for detection and enumeration of faecal indicator organisms in water, which are listed in WHO (2017). The environmental agency of the United States has designed a guide for sampling biological contaminants in bulk water (USEPA, 2016b). In the European territory, the standard ISO 19458 is

recommended for compliance samples for microbiological parameters (European Union, 2015). Locally, the UK Environment Agency also offers guidelines for sampling drinking water to test microbiological parameters (Environment Agency, 2010).

However, if molecular analysis and/or proteomics/metabolomics-based approaches are desired, there is not enough guidance about the minimal representative sampling volume required to capture the complete microbiome in a DWDN. Therefore, comparisons are difficult to make. In relation to biofilm sampling, two approaches have been used to study biofilms in DWDNs such as scrapping attached biofilm from cut-out pipes or directly from devices inserted into the pipes. Both methods can be used for sampling in real-scale or laboratory DWDNs (Douterelo et al., 2014a).

Pipe cut-out sampling are labour-intensive, then it is common to take advantage of the leakage repairs or pipe replacement activities to collect pipe samples. Due to the random nature of leakages location, the arbitrary selection of sampling points according to the scope of the study is limited. Therefore, the sampling campaign may last several months in order to cope with all the selected criteria. Otherwise, the study must be based on few variables in order to find the balance time-scope. On the other hand, excavation and cutting processes often lead to concerns with contamination and representative sampling and preservation of the physical integrity of the sample (Douterelo et al., 2014a). The use of devices, commonly coupons, that can be deployed repeatedly either within a pilot-scale test facility or in an operational DWDN, allows the study of biofilm dynamics over time in relation to changing abiotic and biotic factors *in situ*. According to Douterelo et al. (2014a), commonly the main limitation of some of these devices is that they distort hydraulic conditions in pipes and, in most cases, shear stress and turbulence regimes are different from those expected in real pipes, artificially influencing the way biofilms develop.

Recent studies applying molecular analysis in DWDNs supplied by surface water, either simulated or real-scale DWDNs, are summarized in Table 2-2. These studies were developed mainly in temperate-climate areas; with water treated by different treatment processes, including chlorine and chloramines as disinfectants. Samples were collected from several pipe materials such as polyvinyl chloride (PVC), HDPE, ductile and cast iron, cement, copper. Pipe material was the variable more frequently tested among these studies. Results reported in every investigation found *Proteobacteria* as the predominant phylum in biofilm and bulk water samples. Particularly, research in USA indicates that other phyla also dominating include *Cyanobacteria* and *Actinobacteria* (Holinger et al., 2014; Kelly et al., 2014). By comparison, bacterial class, family and genera exhibit more variety of the microbial communities in the studied samples.

Table 2-2. Summary of bacterial composition in DWDNs supplied by surface water sources

Reference and study country	Type of system	Water treatment	Sampling point	Type of sample	Pipe material	Pipe age (Years) / Biofilm age	Composition of bacterial communities in pipelines (dominant communities and relative abundance -RA-)		
							Phyla	Class	Genera
Gomez-Alvarez et al. (2012) USA	Simulated DWDN	FLOC, SEDIM, pH adj., SFILT, GAC, and chlorine disinfection	Tap	Water	PVC	NS	Proteobacteria	<i>Alphaproteobacteria</i> (35%)	<i>Mycobacterium</i> , <i>Acidovorax</i> , <i>Burkholderia</i> , <i>Pseudomonas</i> , <i>Dechloromonas</i>
		chloramine disinfection					Proteobacteria Actinobacteria	<i>Alphaproteobacteria</i> (22%) <i>Actinobacteria</i> (28%) <i>Betaproteobacteria</i> (24%)	<i>Caulobacter</i> , <i>Rhodopseudomonas</i> , <i>Synechococcus</i> , <i>Bradyrhizobium</i> , <i>Pseudomonas</i> (chloraminated system)
Henne et al. (2012) Germany	Full scale DWDN	FLOC, COAG, SFILT, chlorination	Pipe	Biofilm	NS	NS	Proteobacteria (9-62%)	<i>Alphaproteobacteria</i> (2-30%) <i>Chlorofexi</i> (7-65%) <i>Betaproteobacteria</i> (1-20%) <i>Actinobacteria</i> (6-19%)	NS
			Tap	Water			Proteobacteria (27-41%)	<i>Alphaproteobacteria</i> (17-28%) <i>Actinobacter</i> (16-25%) <i>Bacteroidetes</i> (14-25%)	NS
Douterelo et al. (2013) UK	Simulated DWDN	NS	Flushing points in the network	Biofilm	HDPE	NS	Proteobacteria	<i>Gammaproteobacteria</i> (6-87%) <i>Betaproteobacteria</i> (4-60 %)	<i>Pseudomonas</i> (20-65%)
				Water				<i>Alphaproteobacteria</i> (59-88 %)	<i>Methylocistis</i> (20-40%) <i>Methylocella</i> (10-20%)
Henne et al. (2013)	Full scale DWDN	FLOC, COAG, SFILT, chlorination	Tap	Cold water	NS	NS	<i>Proteobacteria</i> (15-72%) <i>Bacteroidetes</i>	<i>Alphaproteobacteria</i> (7-28%) <i>Betaproteobacteria</i> (6-28%) <i>Gammaproteobacteria</i> (2-16%)	NS

Reference and study country	Type of system	Water treatment	Sampling point	Type of sample	Pipe material	Pipe age (Years) / Biofilm age	Composition of bacterial communities in pipelines (dominant communities and relative abundance -RA-)		
							Phyla	Class	Genera
Germany							(17-36%) <i>Actinobacteria</i> (8-30%)		
Holinger et al. (2014) USA	Full scale DWDNs	NS Disinfection with chloramine : 2 sampling points Disinfection with chlorine : 7 sampling points	Taps of buildings	Water	NS	NS	<i>Cyanobacteria</i> <i>Actinobacteria</i> <i>Proteobacteria</i>	<i>Chloroplast</i> (24-91%) <i>Sphingomomadales</i> (45%) Other (29%)	<i>Mycobacterium</i> (43-52%)
Kelly et al. (2014) USA	Full scale DWDN	CLAR, OZON, BAF, and chlorine disinfection	Pipelines	Biofilm	Ductile iron	40-45	<i>Proteobacteria</i> <i>Actinobacteria</i>	<i>Gammaproteobacteria</i>	<i>Methylomonas</i> (95.5%) <i>Mycobacterium</i> (59.1%) Unclassified <i>Xanthomonadaceae</i> (50.4%) <i>Acinetobacter</i> (74.2%)
Shaw et al. (2014) Australia	NS	COAG, MIEX, MIEX + COAG + GAC, MF	Pipelines	Biofilm	NS	Biofilm age: 28 months	<i>Proteobacteria</i>	<i>Alphaproteobacteria</i>	NS
Sun et al. (2014) China	Full scale DWDNs	COAG, SEDIM, FILT, GACAd, and chlorine disinfection	Pipelines	Biofilm	Cl	≈ 20	<i>Proteobacteria</i> (40-60%)	<i>Bacilli</i> (30-35%) <i>Betaproteobacteria</i> (25-30%)	<i>Raistoria</i> <i>Burkholderia</i> <i>Delftia</i> <i>Bacillus</i>

Reference and study country	Type of system	Water treatment	Sampling point	Type of sample	Pipe material	Pipe age (Years) / Biofilm age	Composition of bacterial communities in pipelines (dominant communities and relative abundance -RA-)		
							Phyla	Class	Genera
									<i>Mycobacterium</i> (RA closest to max. value: 42.21%)
Wang et al. (2014) USA	Simulated DWDN	4.0 mg/L chlorine 4.8 mg/L chloramine	Ports located in pipelines	Biofilm	Cement, iron and PVC	Biofilm age: 6 months	<i>Proteobacteria</i> (66-98%)	<i>Alphaproteobacteria</i> (25-96%) <i>Betaproteobacteria</i> (1.2-69%)	NS
El-Chakhtoura et al. (2015) The Netherlands	Full scale DWDN	COAG, FLOC, SEDIM, OZON, DMF, GACAd, and chlorine dioxide disinfection (no residual disinfectant)	Effluent of treatment facility Pipeline in water network	Water	Cemented steal and PVC	NS	<i>Proteobacteria</i> (58.6%)	<i>Gammaproteobacteria</i> (34.0%)	NS
Lührig et al. (2015) Sweden	Full scale DWDN	NS	Water meters	Biofilm	Brass and plastic	4-10	<i>Proteobacteria</i> (45-87 %)	<i>Alphaproteobacteria</i> (70-85 %)	NS
			Pipelines		Cast iron	45-103	<i>Proteobacteria</i> (58-86 %)	<i>Gammaproteobacteria</i> (60-65%) <i>Betaproteobacteria</i> (35%) <i>Alphaproteobacteria</i> (35 %)	NS
Mahapatra et al. (2015) India	Full scale DWDN	NS	Commercial water purifier systems and pipelines	Water	PVC	Commercial water purifier systems: 27 months Pipelines: NS	<i>Proteobacteria</i>	<i>Gammaproteobacteria</i>	<i>Acinetobacter</i> (24.7%) <i>Pseudomonas</i> (20.8%) <i>Klebsiella</i> (18.5%)
Ji et al. (2015) USA	Full scale DWDNs	Conventional treatment, chlorine/chloramine disinfection (5 WTP)	Building plumbing rigs	Biofilm	CU, CPVC, CU/Lead	Pipe age: NS Biofilm age: 1 year	<i>Proteobacteria</i> (50-90%)	<i>Alphaproteobacteria</i> <i>Betaproteobacteria</i> <i>Gammaproteobacteria</i> <i>Actinobacteria</i>	<i>Staphylococcus</i>

Reference and study country	Type of system	Water treatment	Sampling point	Type of sample	Pipe material	Pipe age (Years) / Biofilm age	Composition of bacterial communities in pipelines (dominant communities and relative abundance -RA-)		
							Phyla	Class	Genera
Ren et al. (2015) China	Full scale DWDN	FLOC, SFILT, and chlorine disinfection	Pipelines: ends of the DWDS	Biofilm	DCIP, GCIP, GSP, SSCP, PVC	11-13	<i>Proteobacteria</i> (71-99%)	<i>Alphaproteobacteria</i> (68%, 83%) <i>Betaproteobacteria</i> (41%) <i>Gammaproteobacteria</i> (45%, 73%)	<i>Hypromicrobium</i> (28%) <i>Desulfovibrio</i> (17%) <i>Pseudomonas</i> (43%, 63%) <i>Sphingomonas</i> (72%)
Revetta et al. (2016) USA	Full scale DWDN	GAC, chlorine disinfection	Coupons incubated within biofilm annular reactors and glass bead baskets	Biofilm	Polycarbonate	Biofilm age: 3-18 months	<i>Proteobacteria</i> <i>Actinobacteria</i>	<i>Alphaproteobacteria</i> (34%) <i>Actinobacteria</i> (24%) <i>Betaproteobacteria</i> (20%) <i>Gammaproteobacteria</i> (12%)	<i>Mycobacterium</i> (23%) <i>Limnobacter</i> (11%)
					Glass	Biofilm age: 6-11 months			
Bautista-de los Santos et al. (2016) UK	Full scale DWDN	COAG, rapid gravity filtration, chlorine disinfection , and orthophosphate dosing (another WTP included air flotation after coagulation)	Faucets	Water	NS	NS	<i>Proteobacteria</i> (> 98%)	<i>Betaproteobacteria</i> (92.2%) <i>Alphaproteobacteria</i> (76.6%)	<i>Comamonadaceae</i> ^(a) (64.9%) <i>Sphingomonadaceae</i> (2.22%)
Zhang et al. (2017) China	Full scale laboratory DWDN	NS	Coupons	Biofilm	PE	3 years	<i>Proteobacteria</i> <i>Actinobacteria</i>	<i>Alphaproteobacteria</i> (32.58%) <i>Bacilli</i> (15.65%) <i>Gammaproteobacteria</i> (15.63%) <i>Betaproteobacteria</i> (14.30%) <i>Actinobacteria</i> (10.44%)	<i>Sphingomonas</i> (25.25%) <i>Streptococcus</i> (7.64%)

Reference and study country	Type of system	Water treatment	Sampling point	Type of sample	Pipe material	Pipe age (Years) / Biofilm age	Composition of bacterial communities in pipelines (dominant communities and relative abundance -RA-)		
							Phyla	Class	Genera
					Ductile iron			<i>Enhydrobacter</i> (33.84%) <i>Propionibacterium</i> (8.08%) <i>Acinetobacter</i> (5.59%)	
					SS			<i>Betaproteobacteria</i> (27.53%) <i>Flavobacteria</i> (25.15%) <i>Verrumicrobiae</i> (13.4%) <i>Cytophagia</i> (12.04%) <i>Flavobacterium</i> (24.76%) <i>Arcicella</i> (12.03%) <i>Acidovorax</i> (8.98%)	
				Water	--	--	<i>Proteobacteria</i>	<i>Betaproteobacteria</i> (95.5%) <i>Methylophilus</i> (95.41%)	

(a): The authors reported these organisms as classified at the family/genus level | BAF: biologically active filtration | CI: cast iron | CLAR: clarification | COAG: coagulation | CPVC: polyvinyl chloride with brass fitting | CU: copper | DCI: ductile cast iron | DMF: dual medium filtration | FILT: filtration | FLOC: flocculation | GAC: granular activated carbon | GACAd: granular activated carbon adsorption | GCI: grey cast iron | GS: galvanized steel | HDPE: High-density polyethylene | MIEX: magnetic ion exchange contact | MF: membrane filtration | NS: not specified | OZON: ozonation | PB: polybutylene (PB) | PE: polyethylene | PVC: polyvinyl chloride | SEDIM: sedimentation | SFILT: sand filtration | SS: stainless steel | SSC: stainless steel clad | ST: steel coated with zinc |

2.4.3 Biofilm modelling

As previously explained, biofilms in drinking water pipes are heterogeneous and includes multiple bacteria species such as aerobic, anaerobic, heterotrophic, and autotrophic bacteria. Substances like EPS, biomolecules and other microorganisms such as fungi, archae, and invertebrates are also present. In addition, hydraulics affect the biofilm physical structure by the influence of shear stress, which can cause detachment, and nutrients transport. Disinfectant in drinking water also affect the biofilm by killing cells and oxidizing biomolecules, which can translate into genetic adaptation or physical resistance and DBP formation. Drinking water is an oligotrophic environment and, according to nutrient concentrations, carbon, and nitrogen or phosphorous can be the growth-limiting nutrient.

Multiple factors affect the growth of biofilms in drinking water pipes. Table 2-3 reports 31 studies conducted on biofilm modelling between 1994 and 2017 in order to better explain the different approaches applied by researchers to represent biofilm dynamics. As it can be observed in Table 2-3, biofilm models have been low-dimensional continuum models (Stewart, 1994; Stewart and Raquepas, 1995; Eberl and Demaret, 2007; D'Acunto and Frunzo, 2011; Clarelli et al., 2013; D'Acunto et al., 2015), discrete-continuum/cellular automaton models (Picioreanu et al., 1998a; Picioreanu et al., 1998b; Xavier et al., 2005a; Xavier et al., 2005b; Jayathilake et al., 2017), multidimensional biofilm models with biomass and flow coupling under laminar regime (Eberl et al., 2000; Picioreanu et al., 2000a; Xavier et al., 2005a; Eberl and Sudarsan, 2008; Zhang et al., 2008; Duddu et al., 2009; Lindley et al., 2012; Taherzadeh et al., 2012; Zhang, 2012; Coroneo et al., 2014; Tierra et al., 2015; Zhao et al., 2016) and other multidimensional biofilm models (Eberl et al., 2001; Eberl and Efendiev, 2003; Duddu et al., 2008; Cogan, 2010; Cumsille et al., 2014).

Most of the models have focused on biofilm structure as a result of biofilm growth and spreading, and substrate transport and consumption. However, other models have evolved to consider external flow and effects of antimicrobial agents to simulate the antimicrobial penetration barrier, persistent cells, and viscoelastic properties of biofilm. Due to the important role played by EPS in initial formation, growth, and survival of biofilms; 15 of 31 reviewed studies included EPS production in the biofilm models (Kommedal et al., 2001; Xavier et al., 2005a; Xavier et al., 2005b; Duddu et al., 2008; Zhang et al., 2008; Duddu et al., 2009; Cogan, 2010; Cogan, 2011; Lindley et al., 2012; Clarelli et al., 2013; Ghosh et al., 2013; Macias-Díaz, 2015; Tierra et al., 2015; Zhao et al., 2016; Jayathilake et al., 2017).

Table 2-3. Summary of studies on biofilm modelling

Reference	Type of model	System / Domain dimensions	Model components						Flow regime and Re	Max. BT (μm) and Time of growth	Computer and computational time	Observations	
			Spatial character. of biofilm	Bacteria species	Biomass detachment	Substrate	EPS production	Biocide effect					
Stewart (1994)	1D - continuum	Length: 1.4 and 87 μm	Not simulated	Active and inert cells	Simulated	Dissolved oxygen	Not simulated	Simulated Type of antibiotic not specified	Not specified	Not specified	Not specified	Disinfection modelling was simulated up to 8 hours	
Stewart and Raquepas (1995)	1D - continuum	Not apply	Not simulated	Active and inert cells	Not simulated	Not apply	Not simulated	Simulated Type of antibiotic not specified	Not specified	Not specified	Not specified	Model assessed the decay of active cells by action of antibiotics	
Picioreanu et al. (1998a)	2D - Discrete	Length: 600 μm ; Depth: 600 μm	Simulated Spatial structure of colonies	<i>Nitrosomonas</i> and <i>Nitrobacter</i>	Not simulated	Dissolved oxygen	Not simulated	Not simulated	Not specified	No apply	Common personal computers Comp. time not specified	Spatial characteristics of colonies are described qualitatively. Growth was simulated up to 20 days	
	3D - Discrete	Length: 120 μm ; Depth: 120 μm ; Height: 120 μm			Simulated								
Picioreanu et al. (1998b)	2D - Discrete	Length: 2000 μm ; Depth: 400 μm	Simulated Finger- and mushroom-like shape	<i>Nitrosomonas</i> and <i>Nitrobacter</i>	Not simulated	Dissolved oxygen	Not simulated	Not simulated	Not simulated	Not simulated	300 5 days	Not specified	BT varied according to the biomass growth rate: compact biofilms
											300 7 days		
											300 11 days		
											300 18 days		
											350 31 days		
												BT varied according to the	

Reference	Type of model	System / Domain dimensions	Model components						Flow regime and Re	Max. BT (μm) and Time of growth	Computer and computational time	Observations
			Spatial character. of biofilm	Bacteria species	Biomass detachment	Substrate	EPS production	Biocide effect				
	3D - Discrete	Length: 800 μm ; Depth: 320 μm ; Height: 400 μm								350 71 days 350 141 days 250 50 days	biomass growth rate: mushroom shape biofilm -	
Eberl et al. (2000)	3D - continuum	1.6 mm	Simulated Mushroom shape: pores, cavities, channels	Single species	Not simulated	Constant - not specified	Not simulated	Not simulated	Laminar Re 4.1 32.6	12.5-137.5 Time of growth not specified	High perf. comp. Comp. time not specified	
Piciooreanu et al. (2000a)	2D - continuum	Height: 500 μm ; Length: 2000 μm	Simulated Mushroom shape	Single species	Not simulated	Dissolved oxygen	Not simulated	Not simulated	Laminar Re 0.8 6.7	15 4 days 20 18 days 50 5 days 120 38 days 150 6 days 200 80 days	8 or on 16 processors from a Cray T3E parallel machine with 128 processors at 400 MHz Comp. time 1 day	BT values corresponded to two Re values

Reference	Type of model	System / Domain dimensions	Model components						Flow regime and Re	Max. BT (μm) and Time of growth	Computer and computational time	Observations
			Spatial character. of biofilm	Bacteria species	Biomass detachment	Substrate	EPS production	Biocide effect				
Eberl et al. (2001)	3D - continuum	Length: 121 μm ; Depth: 121 μm	Simulated Wavy and mushroom shapes	Single species	Not simulated	Not specified	Not simulated	Not simulated	Static	121 643 hours	Not specified	-
Kommedal et al. (2001)	1D - continuum	No apply	Not simulated	<i>P. aeruginosa</i>	Not simulated	Glucose	Simulated	Not simulated	Static	No apply	Not specified	-
Eberl and Efendiev (2003)	3D - continuum	Not specified	Simulated	Inert and active cells	Not simulated	Dissolved oxygen	Not simulated	Simulated - Disinfectant not specified	Static	-	Not specified	Decay or growth of active cells according to initial values of BT and disinfectant concentrations at $t = 1.6-90$ days
Xavier et al. (2005a)	2D - Discrete	Length: 4000 μm ; Depth: 31 μm	Simulated Mushroom shape	Heterotrophic bacteria	Simulated	Dissolved oxygen and	Simulated	Not simulated	Laminar Re not specified	75 40 days	Not specified	CFD was applied for solving the flow

Reference	Type of model	System / Domain dimensions	Model components						Flow regime and Re	Max. BT (μm) and Time of growth	Computer and computational time	Observations
			Spatial character. of biofilm	Bacteria species	Biomass detachment	Substrate	EPS production	Biocide effect				
	3D - Discrete	Length: 500 μm ; Depth: 500 μm				organic carbon				300 30 days		
Xavier et al. (2005b)	2D and 3D - Discrete	Length: 1000 μm ; Depth: 1000 μm	Simulated Mushroom shape	Active and inert cells	Not simulated	Dissolved oxygen and organic carbon	Simulated	Not simulated	Not specified	400 20 days	Not specified	-
Eberl and Demaret (2007)	1D - continuum	Length: 500 μm ; Depth: 500 μm	Simulated Moving interface: mushroom shape	Not specified	Not simulated	One/two substrates (oxygen and nutrients)	Not simulated	Not simulated	Not specified	Not specified	Not specified	Irregular morphology was observed at t=19.12 days. Channels and clusters appeared at t=159.13 days
Duddu et al. (2008)	2D - continuum	Length: 200/500 μm ; Depth: 10/500 μm	Simulated	Not specified	Not simulated	Dissolved oxygen	Simulated	Not simulated	Not specified	100 7.3 days 300 31 days 250 28.6 days 400 44 days	Not specified	Variation of BT corresponded to different type of seeds (semi-circular and slab biofilm)

Reference	Type of model	System / Domain dimensions	Model components						Flow regime and Re	Max. BT (μm) and Time of growth	Computer and computational time	Observations
			Spatial character. of biofilm	Bacteria species	Biomass detachment	Substrate	EPS production	Biocide effect				
Eberl and Sudarsan (2008)	2D - continuum	Not specified	Simulated Colonies	Single species	Not simulated	Dissolved oxygen	Not simulated	Simulated - Disinfectant not specified	Laminar Re 0.32x10-5 1x10-5 0.32x10-4 1x10-4 0.32x10-3 1x10-3 0.32x10-2 1x10-2	No apply	Shared environment on the SGI Altix 330 with 16 processors (4 processors for each simultaneous run), 1.5 GHz and 32 GB main memory, 4 MB cache Comp. time 20-60 min	Colonies formation occurs in 1.1 days
Zhang et al. (2008)	2D - continuum	Not specified	Simulated	Single species	Simulated	Not specified	Simulated	Not simulated	Laminar Re 9.98x10-4	Not specified	Not specified	BT was reported as fractions. Biofilm growth was reported at t=3.5, 4.7 and 10.5 days, according to different type of seeds (single hump, mushroom shape, compact biofilm)
Duddu et al. (2009)	2D - continuum	Length: 1000/2000	Simulated Mushroom shape	Single species	Simulated	Dissolved oxygen	Simulated	Not simulated	Laminar Re 0.8 - 10	200 120 days	Not specified	This study tested several previous models,

Chapter 2. Literature review

Disinfection by-product formation from biofilm chlorination in drinking water pipes
 Carolina Montoya Pachongo. School of Civil Engineering

Reference	Type of model	System / Domain dimensions	Model components						Flow regime and Re	Max. BT (μm) and Time of growth	Computer and computational time	Observations
			Spatial character. of biofilm	Bacteria species	Biomass detachment	Substrate	EPS production	Biocide effect				
Taherzadeh et al. (2012)	2D	Length: 12,000 μm ; Height: 3,000 μm	No apply	Single cell with moving tail	No apply	Dissolved oxygen	Not simulated	Not simulated	Laminar Re 33-150	No apply	AMD Opteron 3174 Processors (48 cores) and 256 GB RAM Comp. time: 6 days using 4 cores of code running	-
Zhang, 2012	2D - continuum	Length: 1000 μm ; Height: 1000 μm	Not simulated	Active and inert cells	Not simulated	Not simulated	Not simulated	Simulated Biocides: Hypochlorous acid, glutaraldehyde, QAC, Nisin	Laminar Re 20	No apply	Not specified Comp. time 60 min	This study did not consider biofilm growth because there was not substrate after rinsing biocide in experimental tests
Lindley et al. (2012)	2D - continuum	Length: 1000 μm ; Height: 1000 μm	Simulated Hump shape and effect of shear stress	Single species	Simulated	Dissolved oxygen	Simulated	Not simulated	Laminar Re 1×10^{-3} 1	Not specified Time of growth 3.5 days	Not specified	-
Clarelli et al. (2013)	1D, 2D and 3D - continuum	Length: 1 cm	Simulated Hump biofilm	Autotrophs: active and inert <i>Cyanobacteria</i> cells	Not simulated	Light	Simulated	Not simulated	Not specified	200 60 days	Standard laptops Comp. time 1D: 3.25 min 2D: 40 min 3D: 1.84 hours	-

Reference	Type of model	System / Domain dimensions	Model components						Flow regime and Re	Max. BT (μm) and Time of growth	Computer and computational time	Observations
			Spatial character. of biofilm	Bacteria species	Biomass detachment	Substrate	EPS production	Biocide effect				
Ghosh et al. (2013)	2D - continuum	Not specified	Simulated Colonies	<i>Bacillus subtilis</i> : Active and inert cells	Not simulated	Not specified	Simulated	Not simulated	Not simulated	No apply	Not specified	Colonies formation was simulated up to 24 hours
Cumsille et al. (2014)	2D - continuum	Length: 119 μm ; Height: 179 μm	Simulated Finger- and mushroom-like shape	Single species	Not simulated	Dissolved oxygen Glucose	Not simulated	Not simulated	Re Negligible	63 1.3 hours	Intel Core Duo CPU P9600 machine at 2.67 GHz Comp. time: Several hours (e.g., 1440 iterations took 25 min for the finest grid)	Biofilm and flow were fluids with two different viscosity and both of them satisfied the Hele-Shaw equations. BT corresponded to several biofilm shapes: compact, mushroom, finger, semi-circular biofilms
		900 1.8 hours										
		1000 13.7 hours										
		1100 17.6 hours										
Coroneo et al. (2014)	2D - continuum	Length: 600 μm ; Depth: 300 μm ; Height: 10 μm	Simulated Circular and finger shape	Not specified	Not simulated	Dissolved oxygen	Not simulated	Not simulated	Laminar Re not specified	Not specified	Not specified	8 days were required to reach finger-like shape of biofilm
D'Acunto et al. (2015)	1D and 3D - continuum	Length: 2000 μm	Not simulated	Multi-species: autotrophs, heterotrophs, inert cells	Simulated	Dissolved oxygen Organic carbon Ammonia	Not simulated	Not simulated	Not specified	Not specified	Not specified	Biofilm growth was simulated up to 5 days

Reference	Type of model	System / Domain dimensions	Model components						Flow regime and Re	Max. BT (μm) and Time of growth	Computer and computational time	Observations
			Spatial character. of biofilm	Bacteria species	Biomass detachment	Substrate	EPS production	Biocide effect				
Macías-Díaz (2015)	2D - continuum	Not specified	Simulated Mushroom shape	Active and inert cells	Not simulated	Not specified	Simulated	Not simulated	Not specified	Not specified	Not specified	-
Tierra et al. (2015)	2D - continuum	Length: 1000 μm ; Height: 1000 μm	Simulated Finger-like shape	No apply	Simulated	No apply	Simulated	Not simulated	Laminar Re 5.6 27.8 111.1	No apply	Not specified	Biofilm growth was not included: time scale deformation and detachment vs biofilm growth (seconds vs hours)
Zhao et al. (2016)	3D - continuum	Length: 1000 μm ; Depth: 2000 μm	Simulated Mushroom shape	Persister and susceptible bacteria	Not simulated	Dissolved oxygen	Simulated	Simulated Antimicrobial agent not specified	Laminar Re not specified	Not specified	CPU-GPU hybrid environm. High perf. comp.	Biofilm growth was reported for 1, 10, 55, 27.8 hours
Jayathilake et al. (2017)	3D - Discrete	Length: 100 μm ; Dept: 400 μm ; Height: 100 μm	Simulated Mushroom shape	Multi-species: aerobic, anaerobic, anoxic growth	Simulated: deformation and erosion	Organic substrate: oxygen, nitrates, nitrites	Simulated	Not simulated	Simulated Flow regime not specified	48 4.6 days	Not specified	-

In general, modelling evolves according to the interests and needs of researchers and consultants, advance on numerical methods and development of software and hardware. It can be observed in Table 2-3 that such research have followed a cyclic pattern on time. Models start with great simplifications such as ignoring the spatial characteristics of biofilm in order to evaluate the effects of substances like disinfectants on certain populations of bacteria. Particularly, biofilm modelling reported in the early 90's corresponded to one-dimension models of biofilm disinfection, and the spatial characteristics of the biofilm were not considered (Stewart, 1994; Stewart and Raquepas, 1995). Then, other features were included in the models as progress on numerical methods, software and hardware is being done. Colonies, finger-like, and mushroom shape biofilms are then modelled in 2D and 3D. Models also become more sophisticated by including several species in the biofilm according to their metabolism and resistance to biocides. Similarly, EPS production has also been included in these models, especially when they were aimed to assess the viscoelastic properties of biofilms and effects of shear stress. In the last case, biofilm detachment has also been simulated. Despite of the evident evolution of biofilm modelling, mass transport by coupled flow-biofilm is limited to laminar flow with low Re .

Biofilm modelling is computationally expensive, depending on the characteristics to be included. Ideal models in drinking water pipes should include biofilm growth, multi-species, detachment, EPS production, multi-substrates, disinfection, DBP formation, and mass transport under turbulent flow. However, including all those characteristics in one model might not be feasible in reasonable times for practical applications. Therefore, simplifications must be done. For instance, less than 60 min of computational time have been reported for 1D and 2D models of disinfectant effects on colonies growth (Eberl and Sudarsan, 2008), antibiotic impact on initial concentration of biomass (spatial characteristics of biofilm were not simulated) (Zhang, 2012), growth of humps of autotrophic bacteria (Clarelli et al., 2013), and growth of finger-like and mushroom shape of biofilms

Other 2D model of disinfection of persister and susceptible bacteria, hump-shaped biofilm, lasted nine hours, using a 21-node cluster of GPU. More expensive computations were run for 2D models of mushroom-shaped biofilm under laminar flow and $Re < 7$, with eight or 16 processors from a parallel machine; simulations lasted one day (Picioreanu et al., 2000a). Similarly, Taherzadeh et al. (2012) used CFD to solve the flow field under laminar regime and $Re = 33-150$ and calculate the mass transport between bulk and an spherical cell with a moving tale. 48 processors and 6 days were required for those simulations (Taherzadeh et al., 2012).

Regarding the effects of flow on biofilm dynamics, Lehtola et al. (2006) stated that it is commonly believed that increasing water flow velocity can increase the bacterial numbers in biofilms due to

better mass-transfer of growth-limiting nutrients at the higher flow velocity of water, but there are conflicting results about this matter. The studies developed by Donland and Pipe (1988) and Ragazzo (2002) (cited by Lehtola et al. (2006)) have reported that the number of bacteria in biofilms correlated negatively with water flow rate; shear stress appeared to have no interaction on biofilm formation and no significant effects of flow rate were identified on biofilm thickness. As a result, Lehtola et al. (2006) studied the changes in water quality and the formation of biofilms in copper and plastic pilot systems in response to gradual increase of water flow (0.2-1.5 L/min) and velocity (0.04-0.28 m/s). Pilot systems were composed by 2 parallel loops (ϕ 50 mm), each one connected to two parallel copper-loops (ϕ 10 mm) and plastic-loops (ϕ 12 mm), respectively. Water and biofilm samples were taken, the latter one by using collectors made of pieces of pipes of each material. Biofilm was characterized by heterotrophic plate count (HPC) and total bacteria measurements using culture and dyeing methods. This study reported that increasing flow rate did not significantly affect HPC in biofilms in copper pipes, but this parameter increased in plastic pipes.

Therefore, this confirmed that number of bacteria in biofilm increased with higher flow rate, resulting from better mass-transfer of growth-limiting nutrients. This result is attributable to velocity changes and not to nutrients concentrations and dilution changes since the experiments considered water recirculation. However, it is necessary to examine the methods for characterizing biofilm growth since bacteria culture has recognized limitations regarding the ability to generate accurate results. In addition, HPC count only represent a limited fraction of the whole microbial community (Douterelo et al., 2014a; Ren et al., 2015), when used to estimate bacterial loads in water samples. Consequently, this study might have included non-realistic estimation of bacteria count in biofilm and water (Lehtola et al., 2006). This study also found that biofilms detachment occurred in copper pipes during the experiments. A recent work by Abokifa et al. (2016a), who built and validated a model to predict THM concentrations in DWDNs including the contribution of biomass, found that the flow velocity significantly affects the THM formation from biomass as it controls bacterial regrowth by enhancement of mass transfer of solutes across the bulk/biofilm interface caused by higher velocity.

In relation to the effects of antimicrobial agent on biofilms, Cogan (2008) developed a two-dimension continuum model of biofilm disinfection, including coupled motion, external fluid, and viscoelastic properties of the biofilm by considering this as a fluid with viscosity notably higher than viscosity of bulk water. To determine the various model components for each time-step, the researchers determined the fluid and biofilm velocities by solving incompressible Stokes equations; computed the advection, diffusion and reaction of the chemical substances; and the chemical concentrations were assumed to be at quasi-steady-state, since these equilibrate rapidly. One of

the key aspects of modelling two fluids is to define the interface between them and solving the respective equations. Cogan (2008) used the boundary integral method (BIM) which consists of transforming the equation governing both materials in each subdomain into a single integral equation, whose solution is the velocity at each point in the domain. Cogan (2008) compared the disinfection curves for varying biofilm viscosity and they found that flow regimes and high viscosity of biofilm have very little difference in disinfection using a dynamic interface as compared to the fixed simulations considered by Cogan (2006). Therefore, assuming a fixed interface may be a reasonable simplification for a range of flow regimes.

It has been identified that biofilms have physiological protection, which consists of spatially dependent nutrient consumption leading to regions of lowered biocide effectiveness. Because of this, typical antimicrobial agents and antibiotics are most effective at killing respiring bacteria (Costerton et al., 1995). Therefore, disinfection rate must be dependent directly on the nutrient availability by assuming that disinfection rate is proportional to the bacterial growth rate. This delays the action of an antimicrobial within the biofilm since the bacteria near the fluid interface consume the nutrient leading to nutrient-depleted regions. These regions will not be susceptible to antimicrobial agents since they have zero growth rate. This makes the process transient where cells near to interface are also more susceptible to disinfection and they are killed quickly, nutrients can penetrate further into the biofilm reducing the nutrient depleted zones inducing susceptibility (Cogan, 2008).

The previous explanation agrees with the experiments run by Xue et al. (2014) with pure cells of *P. aeruginosa* and *P. putida* in order to study reactivity between EPS and monochloramine. They found that reactivity between protein-EPS and monochloramine is eight times higher than polysaccharides-EPS. High reaction rate reduced monochloramine concentrations at the biofilm surface and lower concentrations were found in deeper layers of biofilm. According to the nutrient and oxygen gradients, cells enclosed in the interior of a biofilm may be in a dormant state (Xue et al., 2014). According to the research of Cogan (2008) and Xue et al. (2014), modelling biofilm disinfection considering physiological tolerance is a good approach to study resistance mechanisms of bacteria. However, modelling DBP formation from biofilm disinfection should also include the transformation of dead bacteria into DBPs since they are still organic matter which reacts with disinfectant. Similarly, the biomolecules embedded in EPS reacts with disinfectant, forming DBPs, which may contribute to increase its concentrations in bulk water. In this line, disinfection rate may not be fully dependent of bacteria growth rate, which may lead to a simplification of the model.

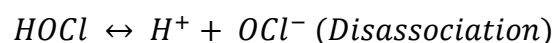
2.5 WATER DISINFECTION

Water supply history started with the access to safe water. Due to increasing contamination of water sources, the efforts were then addressed to improve treatment processes. Chlorine was introduced to urban drinking water supply systems for first time in the USA at the beginning of the 20th century and it has been used to control pathogenic bacteria in drinking water around the world (Nieuwenhuijsen et al., 2000). As a result of the discovery of DBP formation from oxidation of organic matter by chlorine and extensive research, other chemical disinfectants such as chloramine, chlorine dioxide, ozone, and ultraviolet light (UV) have raised as alternatives to chlorine. However the first three previous disinfectants also lead to DBP formation (Chowdhury et al., 2009) and the last two disinfectants only work at point-of-use since they do not produce residual concentrations in the DWDNs (Betancourt and Rose, 2004). Since a “perfect” disinfectant has not been discovered yet, chlorine is still used widely by virtue of it is easy to use, low cost, and especially for its residual effect, which is an important factor to protect drinking water against any potential microbial contamination in the distribution networks (WHO, 2005). Chlorine is an oxidizing substance and it is relatively unstable in water; therefore, chlorine decays in DWDNs since it reacts with particulate and dissolved substances in bulk water, biofilms, materials of the components of the network, incrustations, and sediments (Al-Jasser, 2007).

2.5.1 Chlorine reactions in water

2.5.1.1 Hydrolytic reactions

When chlorine gas (Cl_2) is added to water, hypochlorous acid (HOCl) and hypochlorite ion are formed (OCl^-). These compounds are known as free residual chlorine and they are produced in two phases:



The ratio HOCl: OCl^- depends directly on pH. When dissolved free chlorine is considered, the predominant chlorine species present in the pH 1-3 region is chlorine (Cl_2), whereas HOCl predominates in the pH 5-7 region and the hypochlorite ion is the major species present above pH 8 (Gordon and Tachiyashiki, 1991). This indicates that pH is an important variable in disinfection processes since HOCl is a more powerful disinfectant while hypochlorite ion is weaker (Scarpino et al., 1972).

2.5.1.2 Redox reactions

Chlorine can react with either organic or inorganic substances present in water, especially with those containing nitrogen. Chloramines are produced rapidly when chlorine reacts with ammonium; other non-disinfectant chlorinated substances are formed when chlorine reacts with organic nitrogen and other substances. These reactions are slow and can last days or even weeks (Arboleda, 2000).

2.5.2 Disinfectant decay models

Disinfectant decay is probably the process most commonly simulated in DWDNs due to its direct relationship with other important parameters such as bacteria regrowth, cells inactivation, and DBP formation. Water quality models including disinfectant, coupled with network hydraulics (dead/low velocities zones, water age), are regarded as a proxy model for this inactivation and are used to identify bacteria regrowth episodes; explain water quality complaints; select water quality monitoring points, among others (Clark, 2015). To model the disinfection decay process, parameters such as decay coefficients in bulk water and at pipe walls have been calculated from experimental data and represented by first and second order kinetic equations.

Chlorine decay in DWDNs is influenced by several factors such as corrosion processes, chlorine mass transport between bulk water and pipe walls, and reactions with both organic and inorganic substances in bulk water and with biofilms attached to the wall of pipes, tanks, and accessories of the system (Vasconcelos et al., 1997). A general first-order expression can be used to describe the variation of chlorine at different residence times in the distribution network (Equation (2-20)).

$$\frac{\partial C}{\partial t} = -kC \quad (2-20)$$

Here C is the chlorine concentration and k is the first-order decay constant of chlorine. Integrating Equation (2-20) and defining $C = C_0$ at $t=0$, Equation (2-21) is obtained to describe chlorine decay.

$$C = C_0 e^{-kt} \quad (2-21)$$

According to Vasconcelos et al. (1997), k reflects the factors mentioned previously and, as consequence, it is site-specific and must be verified by field measurements. Therefore, chlorine

decay constant is including simultaneously the reactions in bulk water and pipes walls (Equation (2-22)).

$$k = k_w + k_b \quad (2-22)$$

Here k_b is the reaction coefficient in bulk water and k_w is the reaction coefficient at pipe walls. Chlorine can quickly oxidize certain substances such as sulphides, ferrous iron, manganese, and humic material (Vasconcelos et al., 1997). The reaction rate of the remaining chlorine is frequently well-characterized as a simple first-order decay process or, in some cases, a second-order rate process (Clark, 1998). Pipe materials and biofilms play an important role in the quantification of k_w . The two-steps experimental test is usually used to determine k_b and k_w ; k_b is determined by testing chlorine decay in water stored in glass flasks while overall k is calculated by testing chlorine decay in aged pipes. The difference between k and k_b results in k_w (Vasconcelos et al., 1997).

2.5.2.1 Wall reaction kinetics

In relation to wall reaction kinetics, chlorine is transported from bulk water to the wall reacting according to either first-order or zero-order kinetics. According to Vasconcelos et al. (1997), first-order wall reaction is more appropriate when chlorine is the limiting reactant, as might be the case with reactions involving biomolecules and EPS inside of biofilms (see more details in Section 2.7). Zero-order wall reactions can be used to represent the case in which chlorine oxidizes immediately some reductant as ferrous compounds and the rate is dependent on how fast the reductant is produced by the pipe; this representation would be more likely applied to corrosion-induced reactions. Several studies have identified the chlorine wall decay by laboratory or in-situ tests, analysing the demand exerted by either only biofilms or all the components of pipe walls (sediments, corrosion by-products, biofilms, loose deposits, etc.); Table 2-4 summarises such values of k_w .

Table 2-4. Disinfectant decay constants reported in experimental studies

Reference	Description	Chlorine wall decay constant	
		(m ³ /g-day)	(1/day)
Lu et al. (1999)	Growth of biofilm (7 months) in polystyrene beads with sand filtered water, ozonated water and finished water. Temperature was maintained at 18 °C ±1 (reference water). Tests were run with finished water (reference water was also used and decay rates are much lower).	5.10	5.00
		6.29	6.16
		2.48	5.11
		2.19	4.52
		(¹)	Cl: 0.72 – 39.36

Reference	Description	Chlorine wall decay constant	
		(m ³ /g-day)	(1/day)
Hallam et al. (2002)	Determination of chlorine wall decay by in-situ and laboratory experiments. In-situ tests: measurements of chlorine decay between two points, considering residence time, uniform pipe material and diameter. Laboratory tests: measurements carried out in PVC instrument, including new pipe sections, new pipes installed in the DWDN for three weeks to allow biofilm growth, and pipe sections belonging originally to the DWDN.		DICL: 3.12 ⁽²⁾
			PVC: 2.16 ⁽²⁾
			MDPE: 1.20 ⁽²⁾
Buamah et al. (2014)	Chlorine decay in bulk water and overall decay were tested in PVC, asbestos and cast iron aged pipes. $\phi = 152$ mm. Modelled drinking water was used in the tests. Wall decay was calculated by the difference between overall and bulk water decay constant. Clo = 0.74 / 1.44 mg/L (Water temperature = 26-30 °C; pH = 6.5-8.5).	5.50	6.00
		4.18	4.56
		8.37	9.12
Lee et al. (2014)	Growth of biofilm (10 days) in PVC reactors, $\phi = 77, 98, 145$ mm, reclaimed water, disinfection with chlorine (Clo = 1, 2, 4 mg/L) (pH = 6.84-6.93).	2.30	4.59
		1.63	3.27
		1.04	2.07

⁽¹⁾ Specific initial concentrations of chlorine were not reported | ⁽²⁾ Average | CI: Cast iron | DICL: cement-lined ductile iron | MDPE: medium density polyethylene

Disinfectant decay constant in pipe walls has been attributed to reactions with the pipe material, biofilms and deposits (Lu et al., 1999; Buamah et al., 2014). This demonstrates that biofilms and deposits represent an important source of disinfectant decay, especially in smaller diameter pipes (Lu et al., 1999; Buamah et al., 2014; Lee et al., 2014) as the interactions between the wall and bulk water are more significant when the diameter is small. For instance, Lu et al. (1999) studied the influence of biofilms on chlorine demand by growing biomass in polystyrene beads and analysing S/V^1 ratios. These researchers found that diameters smaller than 40 mm (≈ 1.5 inches) and biodegradable dissolved organic carbon higher than 0.6 mg/L are more relevant for chlorine decay. Such pipe dimensions correspond to that used in building plumbing systems. On the other hand, Buamah et al. (2014), by testing and simulating PVC, cast iron, and asbestos aged pipes, found that diameters of three and six inches influenced more the wall chlorine decay in comparison to nine inches. In contrast, Lee et al. (2014) tested reclaimed treated wastewater by growing biofilms in PVC reactors. By assessment of the S/V ratios, they found that wall chlorine decay in $\phi=77$ mm (≈ 3 inches) is about 4–5 times larger than $\phi=145$ mm (≈ 6 inches).

¹ Pipe inner wall surface area per unit volume of pipe

2.5.2.2 Mass transfer kinetics

Based on the transport process described in Section 2.3, Rossman et al. (1994) represented chlorine reaction with pipe walls by a film-resistant model of mass transfer, along the pipe. The rate at which chlorine is hydrodynamically transported to the wall is proportional to the difference between the bulk concentration and the concentration at the wall (Equation (2-23)).

$$\frac{dC}{dt} | \text{mass transfer} = \frac{k_f}{r_h} (C - C_w) \quad (2-23)$$

Here r_h is the hydraulic radius and k_f is the mass transfer coefficient, which is usually expressed in terms of Sh (Equation (2-8)).

2.5.2.3 Overall rate

Disinfectant decay is the primary water quality parameter monitored by water operators and effective efforts have been done to represent this process by mathematical models, which can be used in the routine operation of the DWDNs. The overall rate of chlorine loss in a pipe is the key kinetic variable for models of DWDNs containing this disinfectant; it combines the effects of bulk reaction, wall reaction, and mass transfer. Equations (2-24) and (2-25) show the expressions for first-order and zero-order wall reactions, respectively (Vasconcelos et al., 1997).

$$\frac{\partial C}{\partial t} = - \left(k_b + \frac{k_{w,1} k_f}{k_{w,1} + k_f} \right) C \quad (2-24)$$

$$\frac{\partial C}{\partial t} = -k_b C - \min \left(\frac{k_{w,0}}{r_h}, \frac{k_f C}{r_h} \right) \quad (2-25)$$

2.6 DBPs IN DRINKING WATER

2.6.1 Disinfection approaches

DBPs are the result of the reaction between disinfectants (chlorine, chlorine dioxide, chloramines, and ozone) and NOM, biofilms, anthropogenic contaminants, bromide, and iodide, during the production and/or distribution of drinking water. According to Hrudey (2009), the publication by Rook (1974) on the discovery of THMs in drinking water changed the perspective that water safety was only related to waterborne diseases. Since then, extensive research has been conducted to determine the mechanisms of DBP formation, characterize their precursors, identify different types

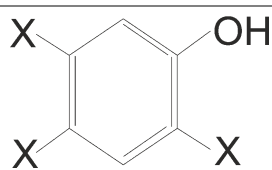
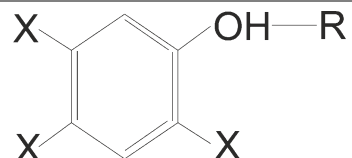
of DBPs formed according to several variables and evaluate exposure routes and the effects on human health. In addition, the applicability of chlorine as the main water disinfectant has been questioned because of DBP formation, its inefficiency for inactivation of *Giardia lamblia* and *Cryptosporidium* (Roccaro et al., 2013), the inability to prevent biofilm formation (Wang et al., 2014), and the incapacity to fully penetrate biofilms in order to deactivate bacteria embedded in the EPS. As a result, other disinfectants such as chloramine, ozone, chlorine dioxide, and ultraviolet light (UV) have been proposed but other DBPs, such as haloquinones, can be formed, which can be even more dangerous than THMs (Chowdhury et al., 2009).

2.6.2 DBP species

NOM, precursor of DBPs, is highly complex in drinking water; as a consequence, the multiple products of any chemical reaction with NOM are largely unknown (Weinberg, 2009). As a consequence of the diverse nature of DBP precursors, fewer than half of the halogenated by-products resulting from the chlorination of drinking water has been identified, and even less is known about the by-products in water treated with other disinfectants (Weinberg, 2009). According to Hrudey (2009), over 600 DBP species have currently been identified in chlorinated drinking waters; they are grouped as THMs, HAAs, haloacetonitriles (HANs), haloketones, chloropicrin, chloral hydrate, cyanogen halides, halonitromethanes, oxyhalides, bromate, aldehydes, aldoketoacids, carboxylic acids, maleic acids, chlorophenoles, chloroanisoles, haloacids, haloacetates, halonitromethanes, iodoacids, iodo-THMs, halo-ketones, halo-aldehydes, haloamides, halopyrrole, halofuranones, nitrosamines, carbonyls, volatile organic compounds, methyl DBPs, and other halomethanes. Table 2-5 presents a summary of the chlorination DBP groups and their distinctive functional group.

Table 2-5. Distinctive functional groups of chlorination DBPs

DBP group	Distinctive functional group	DBP group	Distinctive functional group
1. THMs	$\begin{array}{c} \text{X} \\ \diagdown \\ \text{CH} \\ \diagup \\ \text{X}'' \end{array}$	2. Haloacetates	$\begin{array}{c} \text{X}' \quad \text{O} \\ \quad \\ \text{X}-\text{C}-\text{C}-\text{OH} \\ \\ \text{R} \end{array}$
3. HAAs	$\begin{array}{c} \text{X}' \quad \text{O} \\ \quad \\ \text{X}-\text{R}-\text{C}-\text{OH} \\ \\ \text{X}'' \end{array}$	4. Halonitromethanes	$\begin{array}{c} \text{X}' \quad \text{O} \\ \quad \\ \text{X}-\text{R}-\text{N}_+ - \text{O} \\ \\ \text{X} \end{array}$

DBP group	Distinctive functional group	DBP group	Distinctive functional group
5. Haloacetonitriles	$\begin{array}{c} X' \\ \\ X-CH-C\equiv N \end{array}$	6. Iodoacids	$\begin{array}{c} O \\ \\ X \\ \\ I \\ \\ R-C-OH \end{array}$
7. Haloketones	$\begin{array}{c} X' \quad O \\ \quad \\ X-CH-C-R \end{array}$	8. Iodo-THMs	$\begin{array}{c} I \\ \\ CH-X \\ \\ X' \end{array}$
9. Miscellaneous chlorinated organics (Chloropicrin and Chloral hydrate)	$\begin{array}{c} X' \\ \\ X-C-R_2 \\ \\ X'' \end{array}$	10. Halo-ketones	$\begin{array}{c} X \quad O \\ \quad \\ X-R-C-R \\ \\ X \end{array}$
11. Cyanogen halides	$X-C\equiv N$	12. Haloacids	$\begin{array}{c} O \quad X \quad O \\ \quad \quad \\ R-C-C-R-C-OH \\ \\ X \end{array}$
13. Oxyhalides	$\begin{array}{c} O \\ // \\ X-O^- \\ // \\ O \end{array}$	14. Halo-aldehydes	$\begin{array}{c} O \\ \\ X \\ \\ R-CH \\ \\ X' \end{array}$
15. Aldehydes	$\begin{array}{c} O \\ \\ H-C-R \end{array}$	16. Haloamides	$\begin{array}{c} X \quad O \\ \quad \\ X-R-C-NH_2 \\ \\ X \end{array}$
17. Aldoketoacids	$\begin{array}{c} O \quad O \\ \quad \\ R-C-C-OH \end{array}$	18. Halopyrrole	$\begin{array}{c} NH \\ / \quad \backslash \\ X \quad \quad X \\ \quad \quad \\ X \quad \quad \end{array}$
19. Carboxylic acids	$\begin{array}{c} O \\ \\ R-C-OH \end{array}$	20. Halofuranones	$\begin{array}{c} O \quad R \quad O \\ \quad \quad \\ CH-C-C-C-OH \\ \\ X \end{array}$
21. Maleic acids	$\begin{array}{c} O \quad O \\ \quad \\ OH-C-R-C-OH \end{array}$	22. Nitrosamines	$R-N-N=O$
23. Chlorophenoles		24. Carbonyls	$\begin{array}{c} O \\ \\ R-CH \end{array}$
25. Chloroanisoles		26. Volatile organic compounds and methyl DBPs	

DBP group	Distinctive functional group	DBP group	Distinctive functional group
27. Other halomethanes	$\begin{array}{c} \text{X} \\ \diagup \\ \text{CH}_2 \\ \diagdown \\ \text{X}' \end{array}$		$\begin{array}{c} \text{X}' \\ \\ \text{X}-\text{C}-\text{CH} \\ \quad \diagdown \\ \text{X} \quad \text{X} \\ \quad \quad \diagdown \\ \quad \quad \quad \text{X}' \end{array}$

Adapted from Hrudey (2009) | X, X', X'': halogen atom (chlorine -Cl-, bromine -Br-, and iodine -I-) | R: hydrocarbon | R2: different chemical combinations

Despite that diversity, only a small number has been assessed either in quantitative occurrence or health-effects studies. The most studied DBPs are those derived from halogens such as THMs, HAAs, HANs, and haloketones (Karanfil et al., 2008). According to Richardson et al. (2007) and Roccaro et al. (2013), the highest occurrence among regulated and non-regulated DBPs is for chlorate (high $\mu\text{g/L}$ levels), followed by chloroform, chlorite, dichloroacetic acid, dibromoacetic acid, and trichloroacetic acid (low-to mid- $\mu\text{g/L}$ levels). In relation to nitrogenous and unregulated DBPs, HAN occurrence corresponds to sub- to low- $\mu\text{g/L}$ levels. These DBPs can include chlorine and bromine atoms or both of them and brominated species result more toxic and carcinogenic than chlorinated species (Roccaro et al., 2013; Bond et al., 2014). The current research project is focused on chloroform and DCAN, which belongs to the groups THMs and HANs, respectively, in order to cover regulatory and toxicity aspects of DBPs.

▪ Chloroform

Chloroform is also known as trichloromethane, methane trichloride, trichloroform, methyl trichloride, and formyl trichloride. Its molecular formula is CHCl_3 , and its relative molecular mass is 119.37 g/mol. At room temperature, chloroform is a clear, colourless, volatile liquid with a pleasant etheric odour. Sources of chloroform in the air can be natural and anthropogenic such as algae and fungi production in marine and soil environments, respectively (WHO, 2004). Anthropogenic sources include industrial production and as a result of its formation from other substances such as chlorination of paper pulp and water for human consumption and swimming pools (WHO, 2004). Other sources include hazardous waste sites, and sanitary landfills. Due to the volatility properties of chloroform, inhalation is an important exposure route.

The major effect from acute (short-term) inhalation exposure to chloroform is central nervous system depression. Chronic (long-term) exposure to chloroform by inhalation in humans has resulted in effects on the liver, including hepatitis and jaundice, and central nervous system effects, such as depression and irritability (USEPA, 2000). Chloroform has been shown to be carcinogenic

in animals after oral exposure, resulting in an increase in kidney and liver tumours (USEPA, 2000). Chloroform is generally considered to be a no genotoxic carcinogen whose mechanism of action involves cytotoxicity and regenerative cell proliferation (IARC, 1999). EPA has classified chloroform into the Group B2, as a substance possibly carcinogenic to humans. The reference dose for chronic oral exposure of chloroform is 0.01 mg/Kg-day (USEPA, 2016a).

▪ Dichloroacetonitrile

DCAN belongs to the HAN group, which includes seven species: bromoacetonitrile, dibromoacetonitrile, bromochloroacetonitrile, chloroacetonitrile, DCAN, trichloroacetonitrile, and iodoacetonitrile. According to WHO (2017), DCAN is by far the most predominant halogenated acetonitrile species detected in drinking-water. Similarly, this species has also been identified as predominant in biomass disinfection tests (Wang et al., 2012c). It has also been reported that DCAN degrades over a period of hours or days, depending on pH and chlorine concentration (Reckhow et al., 2001). In order to reduce the occurrence of chlorinated DBPs, water managers are switching from chlorine to chloramine disinfection (Muellner et al., 2007), but this disinfectant increases the nitrogenous DBPs, including HANs. In addition, HANs are also formed when disinfectants such as chlorine, chloramine, chlorine dioxide, or ozone disinfection are applied in the WTPs (McGuire et al., 2002). In a review work, researchers found that every HAN species induced DNA damage in mammalian cells of Chinese hamster ovary (Richardson et al., 2007). By cell assays, Muellner et al. (2007) tested the cytotoxicity and genotoxicity of HANs. In descending order of cytotoxicity dibromoacetonitrile (2.8 μ M) > iodoacetonitrile \approx bromoacetonitrile > bromochloroacetonitrile > DCAN > chloroacetonitrile > trichloroacetonitrile (0.16 mM). Genotoxicity potency, associated with DNA damage, resulted in descending order highest for iodoacetonitrile (37 μ M) > bromoacetonitrile \approx dibromoacetonitrile > bromochloroacetonitrile > chloroacetonitrile > trichloroacetonitrile > DCAN (2.7 mM).

2.6.3 DBP regulation

Even though a wide variety of DBPs exists, regulation or guidance values of these substances in drinking water has been applied mainly to few DBP species of the groups THMs, HAAs and HANs (see Table 2-6). In addition, maintaining residual disinfectant in DWDNs is required to protect drinking water against microbiological contamination. Accordingly, the Water Health Organization recommends residual disinfectant concentrations between 0.2-1.0 mg/L (WHO, 2008) and

Colombian regulation establishes 0.3-2.0 mg/L range (Ministerio de la Protección Social and Ministerio de Ambiente Vivienda y Desarrollo Territorial, 2007); USEPA (1998) regulates 0.8-4.0 mg/L in the United States (depending on the type of secondary disinfectant), and European Union, England and Wales do not establish specific values for residual disinfectant (European Union, 1998; UK Parliament, 2000). However, biofilm research has proved that pathogenic bacteria grow within biofilms, have active metabolism and are protected against disinfectants since EPS exerts a demand, thus reducing the effective disinfectant concentration to inactivate the cells (Gomez-Alvarez et al., 2012; Xue et al., 2013).

Table 2-6. Regulation of concentration limits of DBPs in drinking water

Main Group	Compounds	Regulations (µg/L)				
		WHO (WHO, 2017)	European Union ⁽³⁾	UK ⁽⁴⁾	USA (USEPA, 2006)	Colombia ⁽⁵⁾
THM	Chloroform	300	-	-	-	-
	Bromodichloromethane (BDCM)	60	-	-	-	-
	Bromoform (TBM)	100	-	-	-	-
	Dibromochloromethane (DBCM)	100	-	-	-	-
Total THMs		⁽²⁾	100	100	80	200
HAAs	Dichloroacetic acid (DCAA)	50	-	-	-	-
	Chloroacetic acid (CAA)	20	-	-	-	-
HAA5 ⁽¹⁾		-	-	-	60	-
Haloacetonitriles (HANs)	Dibromoacetonitrile (DBAN)	70	-	-	-	-
	(DCAN)	20	-	-	-	-

Source: Adapted from Chowdhury et al. (2009)

⁽¹⁾ HAA5 (sum of monochloroacetic acid, dichloroacetic acid, trichloroacetic acid, monobromoacetic acid, and dibromoacetic acid).

⁽²⁾ The sum of the ratio of the concentration of each to its respective guideline value should not exceed 1.

⁽³⁾ European Union (1998)

⁽⁴⁾ UK Parliament (2000)

⁽⁵⁾ Ministerio de la Protección Social and Ministerio de Ambiente Vivienda y Desarrollo Territorial (2007)

2.6.4 DBP precursors

NOM, e.g., humic substances, is present at various degrees in all water supply systems and constitute the major component of the total organic carbon (TOC) concentration in most waters and it has been identified as the principal precursor in the formation of THMs and HAAs (Liang and Singer, 2003). NOM contains both hydrophobic and hydrophilic fractions; the hydrophobic fractions are generally composed of the higher molecular weight NOM with activated aromatic rings, phenolic hydroxyl groups and conjugated double bonds, and are considered the major precursors of THMs and HAAs; the hydrophilic fractions are typically composed of the lower molecular weight NOM with

aliphatic ketones and alcohols (Liang and Singer, 2003). The hydrophobic fractions of NOM exhibit higher ultraviolet absorbance (UV_{254})² and higher specific ultraviolet absorbance (SUVA), defined as $100 UV_{254}/DOC$ ³. Hydrophobic fractions tend to be more reactive with chlorine than bromine, while the hydrophilic fractions of NOM exhibit lower UV_{254} and lower SUVA, and are generally more reactive with bromine than chlorine (Liang and Singer, 2003).

The presence of bromide ions (Br^-) represents further challenges to the control of DBP formation (Barrett et al., 2000). Waters without Br^- mainly form chlorinated THMs (e.g, chloroform) due to reactions between HOCl and the hydrophobic fractions of NOM. As such, a significant fraction of the hydrophilic NOM may be left unreacted in these waters. Conversely, in waters with Br^- , the hydrophilic fractions of NOM form brominated THMs through reactions with hypobromous acid (HOBr), while these brominated THMs may not be adequately characterized by the low SUVA or low UV_{254} values (Chowdhury et al., 2009). The removal of hydrophilic NOM through coagulation processes is often difficult because of their low molecular weights. As such, hydrophilic NOM tends to remain in finished waters. As a result, formation of brominated THMs in finished water in the presence of bromide ions is more likely to occur (Chowdhury et al., 2009). Additionally, experimental evidence from chlorine disinfection of single-species biofilm suspensions has shown that these can also be important DBP precursors resulting from the oxidation of EPS and lead to the formation of carbonaceous DBPs and nitrogenous DBPs (Wang et al., 2012c).

2.6.5 Factors influencing DBP formation

During disinfection of drinking waters, most of the chlorine demand is exhausted by reactions with NOM. Chlorine also reacts with various inorganic compounds in the WTPs and distribution systems (e.g., ammonia, Fe^{+2} , Mn^{+2} , S^{-2} , Br, pipe materials, biofilms) (Chowdhury et al., 2009). It has been shown that increasing pH, within the range 6-8, can increase THM formation (Chowdhury and Champagne, 2008) but reducing pH can lead to an increase in HAA formation, within the same range (Liang and Singer, 2003). Considering that pH is also an operational variable to control dominant chlorine species, the determination of the optimum pH range for disinfection is often necessary during the operation of water supply systems in order to balance the microbiological and

² Ultraviolet light at the 254 nm wavelength is passed through a quartz cell containing the sample water and it provides an indication of the concentration of organic matter, specifically those that contain aromatic rings or unsaturated bonds (double and triple) in their molecular structures. (<http://realtechwater.com/uv254/>)

³ SUVA is defined as the UV absorbance of a water sample at a given wavelength normalized for dissolved organic carbon (DOC) concentration. Weishaar, J.L. et al. 2003.

chemical safety of the water. Increase in contact time has also been noted to increase THM formation; on the other hand, reduction of HAA concentrations has been found with higher retention times (Tung and Xie, 2009). This has been associated with the biodegradation of dichloroacetic acid by methylotroph bacteria such as *Methylobacterium* and *Delftia* (Hozalski et al., 2008; Zhang et al., 2009). However, controlling contact time in DWDNs is often a challenge due to variable hydraulic conditions and water demands imposed in distribution systems.

Temperature and seasonal variability has also been reported to affect THM formation, where the formation of THMs in warmer waters or during summer seasons has been reported to be higher than colder waters or winter months (Rodriguez and Sérodes, 2001; Wei et al., 2010; Parvez et al., 2011). However, other studies have reported no seasonal influence on variations of THM concentrations (Charisiadis et al., 2015). Wei et al. (2010) also analysed the temporal variation of other DBP species, finding that HAAs, HANs, and haloketones presented the highest concentrations in winter, while chloral hydrate were observed in autumn, and chloropicrin concentrations were the highest in summer. This represents that control of DBP formation is highly complex since every species seems to have a particular relationship with environmental and operational variables.

Because organic/inorganic substances act as DBP precursors, their removal prior to disinfection has proven to be an effective approach for reducing DBP formation potential. Treatments prior to chlorination can partially remove NOM, which can be reinforced by using granular activated carbon, enhanced coagulation and membrane filtration; but these may significantly increase O&M costs (Chowdhury et al., 2007). Formation of DBPs can also be reduced by introducing alternative disinfectants or a combination of disinfectants, including chloramine, ozone, chlorine dioxide and ultraviolet radiation followed by post chlorination to protect water quality against microbiological recontamination in bulk phase. However, the use of these alternative disinfectants can still lead to the formation of the more toxic DBPs. For instance, Muellner et al. (2007) compared the toxicity index among four DBP groups and found that genotoxicity and cytotoxicity indices were of magnitude order of 2×10^4 and 1×10^5 for HANs, respectively, while those indices were of magnitude order of 1×10^3 and 6×10^2 for HAA5, respectively. Higher toxicity index indicates higher toxic effects.

Taking into account that biofilms are formed in chlorinated and chloraminated distribution systems (Gomez-Alvarez et al., 2012; Wang et al., 2014; Mi et al., 2015) and that they can potentially be DBP precursors as well, it is necessary to develop a decision-making scheme for each water supply system in order to balance the microbiological and chemical safety of drinking water. For instance, Raseman et al. (2017) recommended improved decision support systems for adaptation of WTPs

to extreme weather events. Such tool may be expanded to O&M of DWDNs under normal and climate change conditions. Protecting water sources and improving water treatment processes to minimize the content of NOM and nutrients in drinking water seems to be the first and most urgent procedure to be applied by water managers, since it is well known that they are the primary source for DBP and biofilm formation, respectively. As a consequence, governmental institutions, water companies and community in general should be prepared for increasing costs if better drinking water quality is desired (Dearmont et al., 1998; Yorkshire Water, 2013; Hutton and Varughese, 2016). In addition, proper O&M of DWDNs is also required to avoid that external substances enter to the system, directly or indirectly leading to increase in the content of TOC and nutrients in the distribution system, then losing the effort made by the water operators in the WTP.

2.6.6 DBPs and public health

The DBP exposure routes of humans include inhalation, dermal contact, and ingestion by showering, bathing, and cooking. The study developed by Chowdhury (2016) found that ingestion route was the highest contributor of risk from THMs and HAAs; in addition, due to the volatile properties of chloroform, inhalation while showering represents an important exposure pathway (Villanueva et al., 2007). It is widely accepted that DBPs have negative effects on human health as they have been identified as potential carcinogenic, teratogenic and mutagenic substances (WHO, 2008). Carcinogenic properties of DBPs refer to the ability to produce cancer tumours and can be by either cytotoxicity or genotoxicity, which are related to cell or genetic material damage, respectively (Humpage, 2012; Kristiana et al., 2012). Teratogenicity is related to disruption of the development of the embryo or foetus, causing birth defects. Mutagenicity is a subtype of genotoxicity in which single DNA bases are substituted or deleted, changing the “code” contained in the DNA (Humpage, 2012).

In line with that, DBP control in water treatment works has improved considerably, particularly in developed countries, but many concerns still remain with regard to the formation of DBP within DWDNs, due to the multiple operational variables involved in the system. Despite the great variety of DBP species, only THMs and HAAs are regulated by most of the water authorities worldwide since they are the most abundant species in drinking water (Chowdhury et al., 2009; Hrudey, 2009; Bull et al., 2011). In contrast, THMs and HAAs are now considered as largely unrelated to public health risk and are currently considered as primarily surrogates or indicators for other DBPs rather than being a likely causal agent for the adverse health outcomes suggested by some epidemiological studies (Hrudey, 2009; Bull et al., 2011).

The maximum permissible limits regulated for THMs and HAAs have been established following precautionary considerations; however, epidemiological evidence found to date is not conclusive yet to link a specific DBP species to certain type of cancer (Hrudey, 2009; Hrudey et al., 2015a). To date, the epidemiological studies by Villanueva et al. (2007) and Cantor et al. (2010) offer the most substantive evidence for significant association between THM exposure and bladder cancer risk, but the causative DBP agent has not been identified yet (Hrudey et al., 2015a). Therefore, more research efforts still must be done in order to clarify the wide spectrum of negative health effects of DBPs.

Similarly, emerging DBPs have been increased with the changes of disinfection process and some of them are substantially more toxic than the THMs. In this line, Hrudey (2009) states that the risk management associated with the control of DBP formation should be addressed to reduce the precursors of these substances, which may reduce other conceivable DBP formation and consequently should not create an alternative DBP risk.

2.6.7 Disinfection by-products modelling

Modelling is an important tool used in hydraulic and water quality assessment in water industry. Chowdhury et al. (2009) presented a chronological review of models for prediction of DBP formation in drinking water, in the period 1983-2009. Table 2-7 presents the review of the models reported by this author and was updated to the year 2017. According to this review, there are 52 studies reporting 179 models. Few models included kinetic rates (16%) and most of them are empirical models based either on laboratory or field data, which make them site-specific. Due to the high complexity of the process of DBP formation, a general model to predict their concentrations for every type of raw/drinking water, treatment, and climate has not been created yet, to the author's knowledge. The most simulated DBP group or species are those related to THMs and chlorine as disinfectant followed by HAAs since these are the regulated DBPs, so there is interest on developing tools to manage regulation compliance. Sixteen models were built for other disinfectants such as ozone, chloramine, and chloride dioxide (see Table 2-7).

The models were constructed using commercial humic/fulvic acids and raw waters; despite of this, the researchers applied them to predict DBP concentrations in drinking water (outlet of the WTP or in distribution network). Only 12 models were based on drinking water concentrations, therefore making them applicable to distribution networks. Most of the models reported in Table 2-7 consider the main influencing factors such as contact time, pH, temperature, precursor indicator, and

chlorine dose. However, any of the models included neither the contribution of biofilms to DBP concentrations in bulk water nor conditions of building systems, despite of the experimental evidence on biological material leading to DBP formation (more details are described in Section 2.7). However, four models developed by Sung et al. (2000) included the variable algae. This can be considered the first attempt to acknowledge the contribution of biological substances to DBP formation in drinking water. After, Golfinopoulos and Arhonditsis (2002a) included chlorophyll-a as indicator of algae presence in four empirical models.

In addition, a recent version of the popular hydraulic and water quality model EPANET named EPANET multi-species extension (USEPA, 2008) includes the contribution of biofilms and pipes wall to disinfectant decay caused by the demand exerted by the biofilm matrix and corrosion scales, respectively. Then, it can be noted that the interest on contribution to DBP formation from disinfection of biological substances in drinking water systems is gradually increasing.

Table 2-7. Models for DBP formation

Reference	Number of models	DBPs modelled	Precursors / Water sources	Disinfectant	Model description					Applicability **	Observations
					Scale	Type of model	Variables	Verification	R ²		
Minear and Morrow (1983) cited by Chowdhury et al. (2009)	1	THMs	River raw water + commercial humic acid	Chlorine	Laboratory	Multi regression model	Br Cl pH T NVTOC	Data obtained from field-sampling data	> 0.90	Treatment: prechlorination	--
Urano et al. (1983)	1	THMs	Humic acid extracted from river raw water and commercial product	Chlorine	Laboratory	Empirical model	k pH TOC Cl t	River and lake waters using historical data and laboratory experiments	NR	Treatment: prechlorination	--
Engerholm and Amy (1983) cited by Chowdhury et al. (2009)	1	Chloroform	Synthetic water: commercial humic acid + deionized water	Chlorine	Laboratory	NS	k1a k2a TOC Cl t	NS	NR	Treatment: prechlorination	--
Morrow and Minear (1987)	4	THMs	River raw water	Chlorine	Laboratory	Nonlinear regression models	Br Cl pH T NVTOC	Data of river raw water and finished water supply systems	NR	Inlet and outlet of the treatment	Model based on Minear and Morrow (1983)
Amy et al. (1987) cited by Chowdhury et al. (2009)	1	THMs	River raw waters	Chlorine	Database from laboratory experiments	Linear and nonlinear regression models	UV ₂₅₄ TOC Cl t T pH Br	NS	0.90	Treatment: prechlorination	--
Adin et al. (1991)	1	THMs	Fulvic and humic acids extracted from lake sediment	Chlorine	Laboratory	Mechanistic model	Ao Cl t K1a K2a K3a K4a	Field survey of humic and bromide	0.90 (model and	Treatment: prechlorination	K1a, K2a, K3a, and K4a: kinetic rate constants obtained by

Reference	Number of models	DBPs modelled	Precursors / Water sources	Disinfectant	Model description					Applicability **	Observations
					Scale	Type of model	Variables	Verification	R ²		
								concentrations in lake water	field data)		curve fitting to the experimental results
Harrington et al. (1992)	1	THMs	River raw waters	Chlorine	Database from laboratory experiments	Linear and nonlinear regression models	UV ₂₅₄ TOC Cl t T pH Br	Simulated total trihalomethanes (TTHMs) were compared with observed values in a limited database or water utilities	NR	Treatment: prechlorination	Model based on Amy et al. (1987). Extensive data base was used to predict TTHM formation, removal of NOM, and alkalinity and pH changes
Malcolm Pirnie Inc. (1992) cited by Chowdhury et al. (2009)	3	BDCM, chloroform, DBCM	Drinking water	Chlorine	Laboratory	Empirical model	TOC UV ₂₅₄ Cl t Br T pH	NS	NR	Distribution system	Model for individual species
Malcolm Pirnie Inc. (1993) cited by Chowdhury et al. (2009)	5	THMs, BDCM, chloroform, DBCM, bromoform	Drinking water	Chlorine	Laboratory	Empirical model	TOC UV ₂₅₄ Cl NH ₃ -N t Br T pH	NS	NR	Distribution system	Model for individual species
Montgomery Watson (1993) cited by	11	Chloroform	Raw water	Chlorine	Three laboratory data base	Empirical models	TOC UV ₂₅₄ Br pH Cl t T	Validation using independent database	0.88	Treatment: prechlorination	Database included the

Reference	Number of models	DBPs modelled	Precursors / Water sources	Disinfectant	Model description					Applicability **	Observations
					Scale	Type of model	Variables	Verification	R ²		
Chowdhury et al. (2009)		BDCM					Br pH Cl t T		0.8 (for Cl/Br < 75)	work of Amy et al. (1987)	
		BDCM					TOC Br Cl t T		0.92 (for Cl/Br > 75)		
		DBCM					TOC Br Cl t T		0.82 (for Cl/Br < 50)		
		DBCM					UV ₂₅₄ TOC Br pH Cl t T		0.83 (for Cl/Br > 50)		
		Bromoform					TOC Br pH Cl t		0.86		
		MCAA					TOC Br pH Cl t		0.82		
		DCAA					TOC UV ₂₅₄ Br Cl t T		0.97		
		TCAA					TOC UV ₂₅₄ Br pH Cl t T		0.98		
		MBAA					TOC UV ₂₅₄ Br pH t T		0.80		
		DBAA					TOC UV ₂₅₄ Br Cl t T		0.95		

Reference	Number of models	DBPs modelled	Precursors / Water sources	Disinfectant	Model description					Applicability **	Observations
					Scale	Type of model	Variables	Verification	R ²		
Lou and Chiang (1994) cited by Chowdhury et al. (2009)	1	THMs	River raw water	Chlorine	Laboratory	Regression model	THMo pH NVTOC t Cl	Observed data were within 10.9% of the simulated results	NR	Treatment: prechlorination	--
Ibarluzea et al. (1994)	1	Chloroform	Treatment plant and distribution network	Chlorine	Field	Multiple regression model	Flu pH T Cl	NR	0.82	Treatment: prechlorination and distribution network	--
Ozekin (1994) cited by Chowdhury et al. (2009)	1	Bromate	NS	Ozone	Laboratory	Empirical models	DOC pH O ₃ Br t (for T < 20 °C) ABR O ₃ B20 T (for T > 20 °C)	NR	NR	NS	--
Siddiqui and Amy (1994)	6	Bromoform	River and groundwater	Ozone	Bench - laboratory	Empirical models	DOC pH O ₃ Br t	Comparison with values reported in the literature	0.78	Treatment: prechlorination	--
		TOBr					DOC pH O ₃ Br T (time = 24 h)		0.95		
		Bromate					DOC pH O ₃ Br Toz		0.88		
		Bromate					DOC pH Br		0.64		
		Bromate					DOC pH Cl O ₃ t Br (0 < t < 1 h)		0.68		
Song et al. (1996)	1	Bromate	NOM isolated from several water sources	Ozone	Batch - laboratory	Multiple regression model	DOC NH ₃ -N pH O ₃ Br IC t	Laboratory-scaled and literature-published data	0.93	Treatment	--

Chapter 2. Literature review

Disinfection by-product formation from biofilm chlorination in drinking water pipes
 Carolina Montoya Pachongo. School of Civil Engineering

Reference	Number of models	DBPs modelled	Precursors / Water sources	Disinfectant	Model description					Applicability **	Observations
					Scale	Type of model	Variables	Verification	R ²		
Rathbun (1996b)	4	Chloroform	River raw water	Chlorine	Laboratory	Multiple regression model	pH Cl DOC Br	Comparison with experimental concentrations	0.97	Treatment: prechlorination	--
		BDCM							0.86		
		DBCM							0.94		
		Bromoform							0.78		
Rathbun (1996a)	2	THMs	River raw water	Chlorine	Laboratory	Multiple regression model	pH Cl UV ₂₅₄ t	Comparison with experimental concentrations	0.98	Treatment: prechlorination	Model based on Rathbun (1996b)
		NPTOX							0.96		
Chang et al. (1996) cited by Chowdhury et al. (2009)	3	THMs	River raw water and WTPs	Chlorine	Laboratory	Multiple regression model	TOC t Cl	NS	0.94	Treatment	--
							TOC t UV ₂₅₄ Cl		0.97		
							t UV ₂₅₄ Cl		0.95		
Garcia-Villanova et al. (1997a)	1	Chloroform	WTPs	Chlorine	Field	Multiple regression model	T pH	Comparison with observed values	0.65	Treatment	--
Garcia-Villanova et al. (1997b)	1	Chloroform	Drinking water	Chlorine	Field	Multiple regression model	T pH	Comparison with observed values	0.86	Distribution system	Continued from Garcia-Villanova et al. (1997a)
Huixian et al. (1997)	2	POX	Fulvic acid extracted from lake water	Chlorine	Laboratory	Nonlinear regression models	t TOC Cl pH T	Comparison with measured values	0.94	Treatment: prechlorination	--
		NPOX							0.92		
Clark and Sivaganesan (1998)	1	THMs	Commercial humic acid	Chlorine	Bench - laboratory	2nd order kinetic model	Cl u TOC pH T	Validation using data from two field studies performed in the past	0.71	Treatment: prechlorination	Variable u includes kinetic rate

Reference	Number of models	DBPs modelled	Precursors / Water sources	Disinfectant	Model description					Applicability **	Observations
					Scale	Type of model	Variables	Verification	R ²		
Golfinopoulos et al. (1998)	1	THMs	WTP	Chlorine	Field	Multi regression model	Chla pH Br T Cl	82% of predicted values were found to be within $\pm 20\%$ of the measured values	0.98	Outlet of the WTP	--
Amy et al. (1998) cited by Chowdhury et al. (2009)	1	THMs	River raw water	Chlorine	Laboratory	Empirical model	DOC Cl Br T pH t	NS	NR	Treatment: prechlorination	--
Nokes et al. (1999)	4	THMs intermediates	Distribution system	Chlorine	Laboratory	Kinetic models	12 kinetic rates Concentrations of HOBr and HOCl Chlorine or Bromine atom	NR	NR	--	The fundamental premise of this model is the kinetic-controlled process of the THM formation
Rodriguez et al. (2000)	2	THMs	River raw waters	Chlorine	Database from laboratory experiments	Empirical models	DOC t pH Cl T DOC pH T	Validation using field-database from small water utilities in Quebec (Canada)	0.90 0.34	Treatment: prechlorination	Models based on data from Amy et al. (1987), Rathbun (1996a,b) and Montgomery (1993)

Reference	Number of models	DBPs modelled	Precursors / Water sources	Disinfectant	Model description					Applicability **	Observations
					Scale	Type of model	Variables	Verification	R ²		
Milot et al. (2000)	1	Prediction of probabilities of exceeding specified values of THMs	Distribution networks	Chlorine	Database from Quebec's Ministry of the Environment	Empirical model	Type of treatment Geographical region in Quebec Season Water source	None	--	Prediction of possible carcinogenic and non-carcinogenic effects to human as well as to perform epidemiological studies	--
Sung et al. (2000)	4	THMs	River raw water	Chlorine	Field	Semi-mechanistic models	OH ⁻ Cl k UV ₂₅₄ algae	Validated with monitoring data	NR	Treatment: prechlorination	These models incorporate chlorine decay kinetics (k)
		Chloroform							0.93		
		HAA5							0.74		
		TCAA							0.87		
Westerhoff et al. (2000)	1	THMs	River raw water	Chlorine	Databases from WTPs. Laboratory tests	Regression model	DOC Cl Br T pH t	None	NR	Treatment: prechlorination	--
Elshorbagy et al. (2000)	1	THMs	Drinking water	Chlorine	--	Nonlinear optimization in a full dynamic DWDN	THMs-t Cl	Application to a portion of a real DWDN	NR	Distribution system	Development of the model involves a kinetic approach for THM formation
Clark et al. (2001)	12	Three species of THMs and nine species of HAAs	Commercial humic acid	Chlorine	Laboratory	2nd order kinetic model	Cl u pH Br pH	Comparison with experimental concentrations	0.5280-0.9980	Treatment: prechlorination	Variable u includes kinetic rate

Reference	Number of models	DBPs modelled	Precursors / Water sources	Disinfectant	Model description					Applicability **	Observations
					Scale	Type of model	Variables	Verification	R ²		
Golfinopoulos and Arhonditsis (2002a)	3	THMs	WTP	Chlorine	Field	Multiple regression models	Chla pH Br T Cl	Comparison with measured values	0.52	Outlet of the WTP	--
		Chloroform					Chla pH T Cl		0.51		
		BDCM					Chla pH Br T Cl		0.62		
Golfinopoulos and Arhonditsis (2002b)	1	THMs	Lakes and treatment plants	Chlorine	Field	Kinetic model based on differential equations	k TOC Halogen concentration Q	Comparison with measured values	--	Outlet of the WTP	--
Korn et al. (2002)	1	Chlorite	Ground and surface sources	Chlorine dioxide	Bench - laboratory	Linear regressions	pH T t NPOC UV ₂₅₄	Internal and external validations. The last one using independent experimental results	0.95	Treatment	--
Gang et al. (2002)	2	THMs	River and lake raw water followed by jar tests	Chlorine	Laboratory	Kinetic model	DBP yield coefficient Cl k t	None	NR	Treatment	--
		HAAs									
Sérodes et al. (2003)	12	HAAs	Treated waters prior to disinfection	Chlorine	Bench - laboratory	Regression models	TOC Cl t	None	0.89	Outlet of the WTP	--
							TOC Cl t T		0.92		
							TOC Cl t T		0.80		
		THMo TOC Cl t					0.78				
		THMo TOC Cl t					0.89				
		Cl t					0.56				
4	THMs		Chlorine	Laboratory		pH t	None	0.53		--	

Chapter 2. Literature review

Disinfection by-product formation from biofilm chlorination in drinking water pipes
 Carolina Montoya Pachongo. School of Civil Engineering

Reference	Number of models	DBPs modelled	Precursors / Water sources	Disinfectant	Model description					Applicability **	Observations
					Scale	Type of model	Variables	Verification	R ²		
Nikolaou et al. (2004)		HAAs	River raw waters			Multiple regression models	pH Cl		0.58	Treatment: prechlorination	
							pH t Cl		0.38		
							pH Cl		0.28		
Al-Omari et al. (2004)	1	THMs	Raw and clarified water	Chlorine	Laboratory	Regression model	t Cl TOC Br pH	Comparison with field data collected in the DWDN	NR	Treatment	--
Boyalla (2004)	3	THMs	Raw and drinking water	Chlorine	Laboratory	Regression models	Cl pH TOC t	Comparison with measured values	0.77	Treatment	--
		DCAN					Cl pH RCl t		0.69		
		TCP					Cl pH t		0.68		
Lekkas and Nikolaou (2004)	2	THMs	River raw water	Chlorine	Bench - laboratory	Regression models	pH t Cl	Comparison with measured values	0.87	Treatment: prechlorination	--
		HAAs					pH Br t Cl		0.51		
Sohn et al. (2004)	16	THMs	Raw and coagulated waters	Chlorine	Database from bench-scale experiments	Multiple regression models	DOC Cl Br T pH t	Validation using data from two studies performed in the past	0.90	Treatment	Models developed based on Amy et al. (1987, 1998) and Montgomery (1991)
							UV ₂₅₄ Cl Br T pH t		0.7		
							DOC UV ₂₅₄ Cl Br T pH t		0.81		
							DOC Cl Br t		0.87		
							UV ₂₅₄ Cl Br t		0.90		
							DOC UV ₂₅₄ Cl Br t		0.92		

Reference	Number of models	DBPs modelled	Precursors / Water sources	Disinfectant	Model description					Applicability **	Observations
					Scale	Type of model	Variables	Verification	R ²		
		HAA6					THM (pH=7.5, T=20°C) pH T		0.92		
							DOC Cl Br T pH t		0.87		
							UV ₂₅₄ Cl Br T pH t		0.80		
							DOC UV ₂₅₄ Cl Br T pH t		0.85		
							DOC Cl Br t		0.92		
							UV ₂₅₄ Cl Br t		0.92		
							DOC UV ₂₅₄ Cl Br t		0.94		
							HAA6 (pH=7.5, T=20°C) pH T		0.85		
		TOBr					Br DOC O ₃ pH TIC NH ₃ -N H ₂ O ₂		0.98		
							Br DOC O ₃ pH T		0.95		
Uyak et al. (2005)	1	THMs	Lake raw, finished, and drinking water	Chlorine	Field	Multiple regression model	TOC pH Cl T	Validation with data collected from a different WTP	0.98	Treatment: prechlorination	--

Reference	Number of models	DBPs modelled	Precursors / Water sources	Disinfectant	Model description					Applicability **	Observations
					Scale	Type of model	Variables	Verification	R ²		
Toroz and Uyak (2005)	1	THMs	Lake raw, finished, and drinking water	Chlorine	Field	Regression model	TOC T Cl	Comparison with measured values	0.83	Treatment and distribution system	--
Tyrovola and Diamadopoulou (2005)	1	Bromate	Groundwater	Ozone	Laboratory	Multiple regression model	Br pH O ₃ t	None	0.80	Treatment: preozonation	--
Rodrigues et al. (2007)	5	THMs	Synthetic water prepared with hydrophobic fraction of fulvic acid, isolated from a dam	Chlorine	Laboratory	Regression models	FA Cl T	None	NR	Treatment: prechlorination	--
		Chloroform									
		BDCM									
		DBCM									
Uyak and Toroz (2007)	7	Chloroform	Lake raw water	Chlorine	Laboratory	Probabilistic model of THM and HAA speciation	Concentrations of HOBr and HOCl	None	NR	Treatment: prechlorination	--
		DCBM									
		DBCM									
		Bromoform									
		DCAA									
		BCAA									
		DBAA									
Hong et al. (2007)	3	THMs	River raw water	Chlorine	Laboratory	Multiple regression models	t Cl DOC pH T Br	Comparison with measured values	0.87	Treatment: prechlorination	--
		Chloroform					t pH T Br		0.86		
		BDCM							0.87		
Semerjian et al. (2009)	3	THMs	River raw and drinking water	Chlorine	Laboratory and field	Multivariate regression models	Cl SUVA Cl UV ₂₅₄	None	0.39	Treatment and distribution system	--
							Cl UV ₂₅₄		0.33		
							t Br Cl		0.31		

Reference	Number of models	DBPs modelled	Precursors / Water sources	Disinfectant	Model description					Applicability **	Observations
					Scale	Type of model	Variables	Verification	R ²		
Chen and Westerhoff (2010)	23	THMs	Raw water from five sources not specified	Chlorine and chloramine	Laboratory	Regression models: weight- and molar-based models for DBP potential formation prediction	DOC UV ₂₅₄ Br	Comparison with an independent data source: jar-tested wastewater effluents	0.87	Treatment	--
		Chloroform							0.88		
		BDCM							0.69		
		HAA9							0.84		
		Four species of HAAs							0.81 - 0.85		
		DCAN					0.62				
		HAN4					0.62 - 0.63				
		NDMA					0.77				
		HAN4					0.64 - 0.66				
		NDMA					0.77 - 0.80				
Di Cristo et al. (2013)	1	THMs	Drinking water	Chlorine	Field	Kinetic model	Ka Kb Cl t	Comparison with measured values in field	NR	Distribution system	Ka: global chlorine decay rate. Kb: kinetic constant of THMs formation
Mukundan and Van Dreason (2014)	1	THMs	Drinking water	Chlorine	Fied	Empirical model	TOC pH t T	None	0.75	Distribution system	--
Babaei et al. (2015)	8	THMs	Drinking water	Chlorine	Field	Multiple regression models	T SUVA Cl	None	0.34 - 0.37	Distribution system	--
							T Cl		0.32		
							SUVA Br RCl Cl		0.45 - 0.54		
							T RCl Cl		0.52		

*Adapted and updated from Chowdhury et al. (2009) | ** Applicability was defined according to the current study author's criteria and considering the precursors/water sources used in the experimental tests.*

Ao: humic acid concentration | BDCM: bromodichloromethane | Br: bromide concentration | Chla: Chlorophyll-a | Cl: chlorine dose | DBCM: Dibromochloromethane | DBAA: Dibromoacetic acid | DCAA: Dichloroacetic acid | DCAN: Dichloroacetonitrile | DOC: Dissolved organic carbon | DON: Dissolved organic nitrogen | FA: Fulvic acid | Flu: Fluorescence | HAA5: group of five species of haloacetic acids (MCAA+DCAA+TCAA+MBAA+DBAA) | HAA6: HAA5 + BCAA | HAN4: Group of four species of haloacetonitriles | IC: Inorganic carbon | MCAA: Monochloroacetic acid | MBAA: Monobromoacetic acid | N: Ammonia, nitrite, nitrate, and DON | NDMA: N-nitrosodimethylamine | NPTOX: Non-purgeable organic halide | NS: not specified | NR: not reported | NVTOC: Non-volatile TOC | POX: Purgeable organic halide | Q: inflow/outflow flow rate | O₃: Ozone dose | RCl: residual free chlorine | SUVA: Specific ultraviolet absorption | T: temperature | TCAA: Trichloroacetic acid | TCP: 1,1,1-trichloropropanone | t: time (contact time / water age) | THMs: Trihalomethanes | TIC: Total inorganic carbon | TOBr: Total organic bromide | TOC: Total organic carbon | UV₂₅₄: Ultraviolet absorption at 254 nm wavelength

In relation to correlation coefficients, approximately 45% of the models reported R^2 values higher than 0.90, 22% did not report the coefficients, and 33% had R^2 values lower than 0.90. Inclusion of DBP contribution of pipe walls as a consequence of biofilm disinfection may improve the correlation coefficients of empirical models, especially in smaller pipe diameters, where wall reactions become more relevant. To improve DBP prediction may help to better assess the exposure to these substances, which is an important input in epidemiological studies, as mentioned in Section 2.6.6.

Despite of the important efforts made to develop tools for easily predicting DBP concentrations in the treatment and distribution of drinking water, it is unknown if the water utilities actually have used any of the models reported in Table 2-7. Thus, this is an opportunity to bring the convenience of using DBP predictive models to the attention of water managers and operators as a decision-making tool to better control the formation of such substances during the treatment processes and along the distribution networks to identify the worst scenarios in terms of possible health risks. For researchers, it is also important to create and maintain communication channels with the water industry in order to offer, explain, and adapt such tools to apply them to real cases and effectively contribute to the improvement of drinking water quality delivered to customers.

2.7 BIOFILMS AS PRECURSORS OF DBPs

Biofilm formation and control have been studied by medical, dental, food and water sciences. Flemming and Wingender (2010) pointed out that biofilm matrix is composed by microorganisms (5%) and extracellular materials (95%), although the study developed by Fish et al. (2012) found that 28-day old biofilms from a full scale experimental distribution system was composed by 34% of EPS. Biofilms in DWDNs have mainly been studied from the point of view of serving as shelters of pathogenic microorganisms (Wingender and Flemming, 2011; Simões and Simões, 2013; Fish et al., 2016), which may be released to bulk water and reach the consumers. With regards to EPS, these includes polysaccharides, nucleic acids, surfactants, lipids, proteins (Flemming and Wingender, 2010), and humic acids (Fang et al., 2014); most of which can be the result of microbial metabolism, known as soluble microbial products (Wang and Zhang, 2010b).

Then, the biofilm role as precursors of DBPs have recently been studied. Table 2-8 shows the main features identified in experimental studies on interaction between disinfectants and biofilms, biofilm clusters, planktonic cells and bacterial EPS. Such findings are evidencing the role of biofilms as DBP precursors.

Table 2-8. Main features of the interaction between disinfectant and drinking water biofilms according to experimental studies

Study	Features
Wang et al. (2012c)	Disinfection of suspended culture of <i>P. putida</i> yielded higher concentrations of chloroform than <i>P. aeruginosa</i> . Nitrogen-based EPS secreted by <i>P. putida</i> may contain more aromatic structures than polysaccharides-based EPS secreted by <i>P. aeruginosa</i> . Aromatic structures are known as the main THM precursors.
Xue et al. (2012)	EPS secreted by <i>P. aeruginosa</i> may be related to selective removal of dissolved organic matter molecules with hydroxyl, carboxyl, and ester groups. The presence of EPS reduced chlorine transport in biofilm. Results of viability ratio of cells suggest biofilm can be represented by a mushroom shape: viability ratio was lower at surface and bottom of the biofilm and higher in the middle. Lower biomass density at the bottom generates void spaces, then promoting disinfectant transport and inactivation efficiency.
Wang et al. (2013a)	THM formation potentials are higher in disinfection of planktonic cells of <i>E. coli</i> than <i>P. aeruginosa</i> biofilms.
Xue et al. (2013)	The role of alginate-based EPS secreted by <i>P. aeruginosa</i> in chlorine disinfection is related to increasing disinfectant demand and then reducing the concentration for effective cells inactivation.
Wang et al. (2013b)	Amino acid Tyrosine yielded higher concentrations of chloroform, suggesting this substance may constitute an important THM precursor.
Xue et al. (2014)	The action of typical antibiotics depends on the growth rate: disinfection of bacteria is proportional to the product of nutrient consumption and the bacterial concentration. Thus, bacteria that are exposed to higher nutrient levels are more susceptible to the antimicrobial agent.
Shen et al. (2016)	Increase of stiffness and decrease of biofilms outer layer thickness may be related to consumption of EPS by disinfectants in the outer layer and the lack of EPS production by the inactivated cells near to such layer. Such EPS layer was refilled after three months, under disinfection conditions. Higher biofilms stiffness may be due to higher fraction of EPS protein. No voids or channels were observed in the studied biofilms, which were one-year old and were continuously disinfected with chlorine and chloramine for three months.
Lemus Pérez and Rodríguez Susa (2017)	Characterization of EPS extracted from drinking water biofilms, which were incubated for 20 months and disinfected for four months with high and low chlorine concentrations, indicated that EPS were conformed principally of aromatic proteins, fulvic acid-like substances, soluble microbial proteins, and humic acid-like substances. Such composition was determined by chlorine concentration; biofilm disinfected with high chlorine concentration (B1) produced more aromatic proteins in comparison with biofilms disinfected with low chlorine concentration (B2). DBP formation potential tests indicated that HAA were higher followed by THM and emergent DBP (1,1-dichloro-2-propanone, 1,1,1-trichloro-2-propanone, chloropicrin, DCAN, dibromoacetonitrile, and bromochloroacetonitrile). DBP formation potential of HAA and chloroform were higher in B1 than B2. Authors suggest that B2 would have profited from the low biocide effect of chlorine to adsorb more organic matter and iron.

Xue et al. (2014) investigated the influence of monochloramine reactivity with different EPS components on the viability of biofilm and detached clusters using pure cells of *P. putida* and *P. aeruginosa*. The authors found that reactivity between EPS and monochloramine is minimal, while protein-based EPS reacted rapidly with this disinfectant. Disinfection of *P. putida* (protein-based EPS) presented higher consumption of monochloramine because it reacted with the biofilm surface while the middle and deeper layers were protected from disinfectant (Xue et al., 2014). However,

this study did not measure DBPs resulting from this reaction. In contrast, Wang et al. (2012c) studied the carbonaceous DBPs and nitrogenous DBP formation from disinfection of extracted EPS from *P. aeruginosa* and *P. putida* variants, testing five different chlorine dosages, two pH values, six water age values, and bromide influence on DBP yields. These authors found that THM and HAA yields were higher from chlorine disinfection of extracted EPS from *P. putida* compared to *P. aeruginosa*. This was associated with the content of more aromatic structures in protein-based EPS in contrast with polysaccharide-based EPS from these two strains respectively (Wang et al., 2012c).

Wang et al. (2013b) evaluated the influence of the major biomolecules in EPS and their chemical compositions on DBP formation and speciation. These authors experimented with the chlorine disinfection of extracted EPS from *P. aeruginosa*, *P. putida*, mixed species of biofilm samples isolated from a water utility, and EPS surrogate. Their results indicated that the composition of polysaccharide monomers in the bacterial EPS were different, since bacteria species and bacteria growth condition may significantly affect chemical composition of EPS. They also found similar results from Wang et al. (2012c) in relation to carbonaceous DBPs from disinfection of protein-based EPS, identifying extremely high formation of DCAN and 1,1-dichloro-2-propanone from isolated EPS from drinking water biofilms, likely associated with nitrogenous DBP precursors.

Additionally, Wang et al. (2013a) explored the effects of bacteria phenotype and type of materials of drinking water pipes on DBP formation from cellular organic matter, using *E. coli* K-12 as planktonic cells and *Pseudomonas aeruginosa* PAO1 as biofilms grown in PVC and galvanized zinc. *E. coli* cells reacted for one hour with chlorine or chloramine, while *Pseudomonas aeruginosa* grew on chips and reacted with sodium hypochlorite solution. Results showed that THM concentrations were higher in bulk-cell experiment than in biofilm experiment; the opposite occurred in HAN concentrations, which may be related to a higher content of nitrogen-based compounds in the biofilm matrix. There were not differences of DBP concentrations between pipe materials (Wang et al., 2013a).

In particular, considering the high content of organic nitrogen in wastewaters and biofilms of DWDNs and the current trend of changing disinfectant from chlorine to chloramines, Yang et al. (2010) assessed the formation of organic chloramines, nitrogenous DBPs, and intermediates during reactions between monochloramine and organic-nitrogen compounds. This study found that higher reaction times produced higher concentrations of nitrogenous DBPs, and that these by-products also originate from organic chloramines and organic-nitrogen compounds. The authors concluded that using chloramines in order to reduce THM and HAA formation should only be

attempted with carefully consideration since organic chloramines can contribute to nitrogenous DBPs which are of great concern to public health.

Recently, Lemus Pérez and Rodríguez Susa (2017) studied in detail the characteristics of EPS extracted from drinking water biofilms. Such biofilms were stabilized for 20 months, then were chlorinated for four months under high (B1: 2.6 mg/L) and low concentrations (B2: 0.7 mg/L) conditions to emulate the proximity and most remote locations in a DWDN in relation to the WTP location. The researchers found that chlorination conditions affected the EPS composition of biofilms, then influencing the type and amount of DBP formed. Results indicated that B1-EPS were composed by aromatic proteins and B2-EPS were composed by humic substances. The authors hypothesized that EPS played a protective role for B1 and were nutrient reservoirs for B2. The results of Lemus Pérez and Rodríguez Susa (2017) are consistent with those from Shen et al. (2016); both studies found that EPS decreased in biofilms disinfected with high chlorine concentrations (7.5 mg/L). In addition, Lemus Pérez and Rodríguez Susa (2017) found that B1-EPS had greater aromaticity due to proteins, which exert a protective role to cells. This agrees with results of Xue et al. (2013), who identified that proteins reacted with both chlorine and chloramines, while carbohydrates only reacted with chlorine.

Applying disinfectants to wastewater as part of the treatment process has also been a concern for researchers due to the DBP formation as a result of the presence of dissolved organic nitrogen, synthetic organic compounds, and soluble microbial products (Huang et al., 2012; Doederer et al., 2014; Liu et al., 2017). The results of these investigations indicated that haloacetamides, THMs and HAAs can impact water sources and arrays of chloraminating utilities for recycled water, negatively affecting water quality for human consumption.

2.8 FURTHER RESEARCH NEEDED: IMPROVE THE UNDERSTANDING OF THE ROLE OF BIOFILMS AS DBP PRECURSORS

Most of the research on microbial communities in real scale DWDNs have been focused mainly on either bulk water (Henne et al., 2013; Holinger et al., 2014; El-Chakhtoura et al., 2015; Mahapatra et al., 2015) or biofilms habitat (Kelly et al., 2014; Sun et al., 2014; Ji et al., 2015; Lührig et al., 2015; Ren et al., 2015; Revetta et al., 2016). Few studies have simultaneously analysed the microbiome on both habitats (Henne et al., 2012). Additionally the majority of the studies have been conducted in temperate climate geographic regions where different pipes materials and ages were considered (Holinger et al., 2014; Kelly et al., 2014; Sun et al., 2014; Wang et al., 2014; Ren et al.,

2015). Up to date, there are only two research works reported in a tropical country on this topic (Mahapatra et al., 2015; Ren et al., 2015) ⁴.

On the other hand, in agreement with Hrudehy (2009), who claims that DBP control should be approached from minimization of precursors concentrations, several studies have evaluated, by laboratory tests, the DBP formation from the disinfection of single-species culture and heterogeneous biofilms, planktonic cells, and extracted EPS (Fang et al., 2010a; Fang et al., 2010b; Wang et al., 2012c; Pu et al., 2013; Wang et al., 2013a; Wang et al., 2013b; Xie et al., 2013; Lemus Pérez and Rodríguez Susa, 2017). Such experiments were carried out under different conditions of pH, chlorine doses, and contact time to evaluate the influence of those variables on concentrations and yields of carbonaceous DBPs and nitrogenous DBPs. Concentrations of carbonaceous DBPs from disinfection of cellular material have been reported in the range of 2-150 µg/L and 0.1-5.0 µg/L for nitrogenous DBPs (Fang et al., 2010a; Fang et al., 2010b; Wang et al., 2012c; Wang et al., 2013a); and carbonaceous DBPs yields have been reported in the range of 0.53-105 µg/mg C and 0.1-5.0 µg/mg C for nitrogenous DBPs (Hong et al., 2008; Wang et al., 2012c; Wang et al., 2013a; Wang et al., 2013b). It is important to highlight that the UK and Colombian regulations establish 100 µg/L and 200 µg/L, respectively as the maximum concentrations of total THMs in drinking water (UK Parliament, 2000; Ministerio de la Protección Social and Ministerio de Ambiente Vivienda y Desarrollo Territorial, 2007), which represents that disinfection of cellular materials may result in concentrations of THMs higher than the regulated limit.

In summary, biofilms in DWDNs have mainly been studied from the point of view of serving as shelters of pathogenic microorganisms (Wingender and Flemming, 2011; Simões and Simões, 2013; Fish et al., 2016), which can be released to bulk water and reach the consumers, if the proper hydraulic conditions occurred. Investigating the role of EPS in the biofilm formation and development has also been a crucial step to understand the growth, attachment, protection, and detachment processes of the biofilm matrix (Tsuneda et al., 2003; Wang et al., 2012b; Xue et al., 2012; Xue et al., 2013; Shen et al., 2016). Disinfectant demand by biofilms and the consequent by-products have been recently studied (THMs, HAAs, and HANs), and the reactive components of the biofilms matrix (cells and biomolecules) with disinfectant have also been identified (Wang et al., 2013b).

⁴ Research of Mahapatra et al. (2015) applied culture methods by incubation in tubes and subcultures in MaConkey agar.

DWDNs are complex systems where multiple biological, chemical, physical, and hydraulic interactions may occur simultaneously. Thus, further research is required to define the role of biofilms into the formation of DBPs in DWDNs. This is especially important if it is noticed that epidemiological studies have not produced conclusive results on the relationship between DBPs and negative effects on human health (Hrudey, 2009; Bull et al., 2011). The most substantive evidence was offered for bladder cancer risk and THM exposure (Villanueva et al., 2007; Cantor et al., 2010) but it is not strong enough to classify these DBPs as causal agents. Additionally, there are many uncertainties in medical and genetic aspects of human bladder, which make difficult to study such associations (Hrudey et al., 2015a). On the other hand, exposure assessment is another limitation of epidemiological studies, since they are usually based on historical data of water utilities, which only includes routine monitoring of regulated DBPs.

Considering that linking bladder cancer and THMs have been studied but there are not conclusive results yet, it is logically expected that the information of association between other types of cancer and other DBP species (among over 600 species) is very limited. Due to the study of DBP effects on human health is very complex and involves several disciplines like medicine, genetics, epidemiology, and water engineering, several knowledge gaps still remain and must be addressed to elucidate the real causal DBP agents of negative effects on human health. This may require an important investment of time and money (Hrudey et al., 2015b). In this line, biofilms must be studied from the point of view of its role as DBP precursors and, obviously, from the acute risk they represent for being potential reservoir of pathogens. In general, the most distinguished characteristic of the biofilms is that their presence in DWDNs is undesirable and effective mechanisms to minimize their growth and/or to remove them are still required.

With regards to mathematical modelling, biofilm growth, detachment, and disinfectant penetration have been simulated in drinking water in order to find the strategies to minimize its presence in water systems. In this case, the modelling includes the transport of dissolved substances (disinfectant, substrate, and nutrients) from bulk water towards biofilm matrix, and some of them included EPS production by cells. In relation to DBP modelling, most of the models developed to date are empirical, few of them include kinetic parameters, and are site-specific. It is unknown if such models are or were actually used by water utilities. Furthermore, DBP and biofilm modelling approaches have been clearly addressed separately. In this line, the current research project intends to close the gap existing in the understanding of the role of biofilms as DBP precursors in drinking water, according to biofilm, flow, and water quality characteristics. Furthermore, the role of pathogen reservoir in a real-scale DWDN located in a tropical-climate country was also studied.

This was done by characterizing the bacterial communities in bulk and biofilms in a tropical-climate DWDN, characteristics which have been scarcely explored together; exploring the relationship between methylotrophic bacteria and THM concentrations in bulk water; and developing a numerical model based on the physics of the system by the hydraulic, chemical, microbiological and transport processes (biofilm (cells and EPS) ↔ bulk water) occurring in drinking water pipes. Such model may represent a progress on the predictive tools, which may improve the exposure assessments of DBPs and highlight the role of biofilms as DBP precursors and the need to minimize its growth in DWDNs. The model may also enable to water operators and managers to take practical decisions to reduce DBP concentrations and to appropriately control biofilm formation.

3 FIELD ASSESSMENT OF BACTERIAL COMMUNITIES AND THEIR RELATIONSHIPS WITH ENGINEERED FACTORS

3.1 INTRODUCTION

The previous chapter explained the terms physical, hydraulic and water quality integrity in DWDNs and their interrelations. A summary of recent studies applying molecular analysis to DWDNs supplied with treated surface water was presented as well. The recent approach of molecular methods applied to study microbial communities in drinking water systems was also described. A review of empirical models for DBP prediction in drinking water and their main characteristics were also discussed in Chapter 2. The current chapter presents the field assessment of bacterial communities of biofilm and bulk water from a real-scale DWDN located in a tropical-climate city; characteristics that have scarcely explored together. Water and pieces of pipes were collected in nine sampling points; biofilm samples were scrapped from the internal walls of the pipes; and DNA were extracted from bulk water and biofilms. Additionally, drinking water was characterised by physico-chemical parameters such as temperature, pH, chlorine, total organic carbon (TOC), and total trihalomethanes (TTHMs).

This chapter also presents the analysis of statistical correlations between microbiological [unit dry biomass, TOC, relative abundance (RA) of bacterial communities, and diversity and richness indices], physical (pipe age and material), hydraulic (water age), and water quality parameters (pH, temperature, free chlorine, and TTHMs); and explores the relationships between bacteria and TTHMs. The results reported by previous published investigations are also discussed and compared in the current chapter. This study aimed to characterise the physical properties, water chemistry and microbial communities of the DWDN to explore the relationships between biotic and abiotic factors, and to further understand the involvement of microorganisms in processes such as DBP formation. This new knowledge is needed to inform operational strategies and to ultimately protect public health.

3.2 METHODOLOGY

3.2.1 Data collection from Colombian water companies

Initially, in order to identify the O&M framework of DWDNs in Colombia, this study intended to apply a survey to Colombian water companies. A questionnaire was created and sent to 22 companies,

which supply drinking water to the capitals of provinces in the country and to 12 companies corresponding to the second largest cities of the provinces. However, only two of these water companies completed the questionnaire, which are named WC1 and WC2 in this document. Due to the low response of the Colombian water utilities, the current study was focused on data collection from the DWDN of the city of Cali. The main findings of the completed questionnaires are presented below.

Both water companies are considered large utilities since they have more than 2,500 customers, according to the Colombian Superintendence of Public Services (Superintendencia de Servicios Públicos Domiciliarios, 2013). The water sources are rivers for both WC1 and WC2, which continuously supply potable water to their respective city. In relation to disinfection, both utilities apply chlorine secondary disinfection and only one of them uses gaseous chlorine for primary disinfection. In relation to the distribution network, both networks are operated by gravity and one of them also combines it with pumping. The water consumption is measured by micrometres and none of the networks include re-disinfection stations. PVC is the most common pipe material in both networks and asbestos is also present. Both water companies are building a validated hydraulic model, therefore such models are not used yet for simulating water quality.

In relation to drinking water quality, the maximal, minimal and average of the parameters of sanitary interest of year 2014 reported by WC1 and WC2 were compared to the Colombian regulation (Ministerio de la Protección Social and Ministerio de Ambiente Vivienda y Desarrollo Territorial, 2007). Maximal values of free residual chlorine, turbidity, nitrites, and total iron exceeded the upper permissible limit established by the Colombian standards. Only WC1 reported monitored concentrations of THMs, being the maximal values equal to 200 µg/L. Finally, with regards to O&M of the distribution networks, few data was reported by both water companies. The indicator of approximately 0.8 leakage repairs per Km of network was found for both WC1 and WC2 for the year 2014.

3.2.2 Area of study

The present study was carried out in a DWDN in Colombia (see Figure 3-1), in the city of Cali, located in the province Valle del Cauca, at 995 meters above sea level, with an annual average

temperature of 24.5 °C (23.8-25.1 °C⁵) and an average annual precipitation of 1425 mm (1048.8-1742.7 mm⁶) (IDEAM, 2017). The water supply system is operated by one utility and is composed of four sub-networks originated from four surface water sources and five WTPs, which are described in Table 3-1. These sub-networks operate by gravity, pumping, or by a combination of both. In total, the distribution network comprises 2977 Km of pipelines (SUI, 2017), 10 service reservoirs, 28 storage tanks, and 19 pumping stations in order to deliver potable water to 2,400,653 people⁷ (CCC et al., 2016; DANE, 2017).

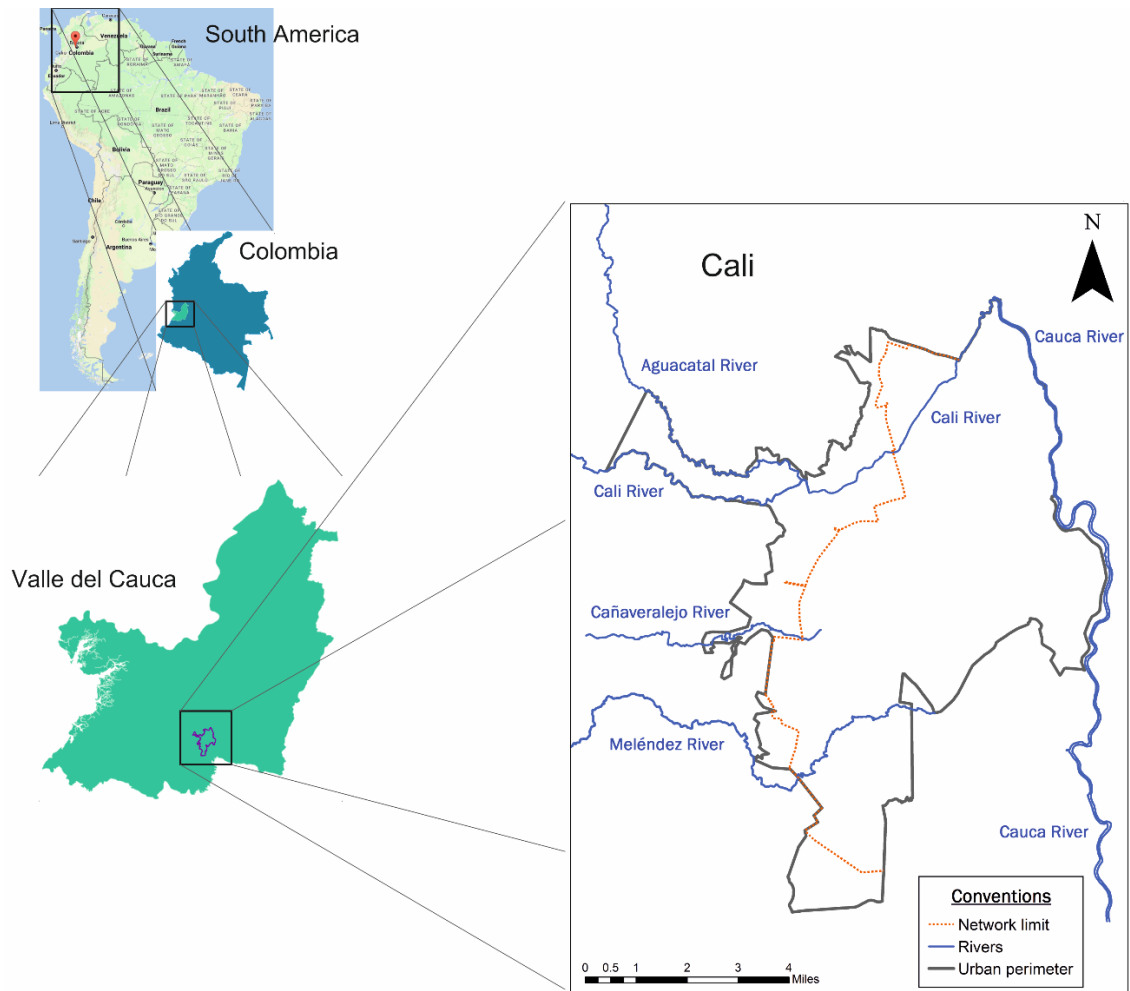


Figure 3-1. Location of the study area

⁵ Period 1981-2010

⁶ Period 1981-2010

⁷ Calculated from a coverage of drinking water supply of 99.2% for 2015 (CCC, C.d.C.d.C. et al. 2016. *Cali cómo vamos. Informe de Calidad de Vida en Cali 2015*. Santiago de Cali.) and projected population for Cali in 2017 of 2,420,013 people (DANE. 2017. *Proyecciones de población*. [Online]. [Accessed 24th April]. Available from: www.dane.gov.co)

Table 3-1. Water sources and treatment description of the water supply system of the city of Cali

Sub-network	Source water	WTP	Treatment description
1	Pance River	La Ribera	Filtration in multiple phases
2	Meléndez River	La Reforma	Conventional treatment, including the option of direct filtration for raw water with low turbidity.
3	Cali River	Río Cali	Conventional treatment
4	Cauca River	Río Cauca	Conventional treatment and additional specific processes such as activated carbon adsorption.
		Puerto Mallarino	

Figure 3-2 shows the fraction of the total length of the network corresponding to each pipe material⁸. The DWDN of the city of Cali has mainly been made by PVC (53.3%) and asbestos cement (30.4%), which represents an important fraction considering that asbestos cement becomes deteriorated under prolonged exposure to aggressive water due to its ion content such as chloride and sulphates and bio-deterioration due to biofilm growth (Wang et al., 2011). This may lead to structural failures of pipes (WHO, 2008), which then increases the leakage rate, therefore raising the vulnerability of the DWDS. Other pipe materials found in the Cali DWDN are cast iron (9.5%) and, in less proportion, ductile iron, CCP (concrete cylinder pipe), plastic and carbon steel (6.8% all together).

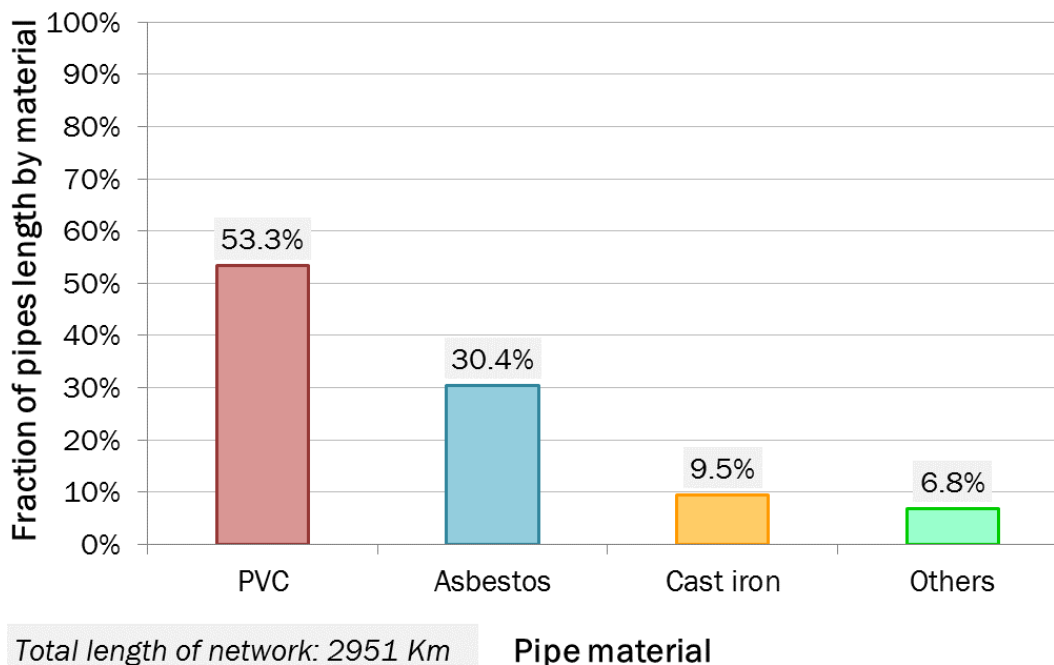


Figure 3-2. Fractions of pipe materials in the DWDN of the city of Cali

⁸ EMCALI EICE ESP, 2014, personal communication, 10th December

Sampling was carried out in the sub-network 4, which is the largest one and supplied with treated water from the second biggest Colombian river by conventional processes including activated carbon adsorption, primary chlorine disinfection, coagulation, sedimentation, filtration, and secondary chlorine disinfection. The main treatment facility of this sub-network has two open-air clarified-water reservoirs to be used as a contingency for supplying drinking water (DW) when turbidity of raw water is higher than 1,000 NTU. When surface water exceeds such turbidity limit, the facility work must close the water intake and operate with the reservoirs up to 9 hours. If raw water does not reach turbidity levels lower than 1,000 NTU after this time, water supply is interrupted for almost 80% of the served population. The same situation occurs when dissolved oxygen of raw water in the source drops below 3.0 mg O₂/L and a decreasing tendency of this parameter has been previously identified in comparison to the normal concentrations in a range of time of hours. More details about this and other events when water supply is suspended in the studied network is presented in Section 3.3.1.

3.2.3 Preliminary activities

First, water age and water level data in service reservoirs were collected, processed and analysed. Raw water age data was delivered by the local water utility in Excel format and was processed in the software ArcMap® 10.2.2, as it is described in the next section. Database of water levels in five service reservoirs was also in Excel format, provided by the local water company, corresponding to the months February and March 2015. The sampling campaign was carried out during this period of time. Water level in service reservoirs allowed determination of how the DWDN operated during sampling activities, since if the services reservoirs are empty, the network is supplied entirely by the WTPs. Otherwise, if the service reservoirs still have water, they are supplying certain sectors of the network and water age can be higher.

3.2.4 Water age data

Water age was determined from a hydraulic model of the sub-network and provided by the local water company. This model was mainly implemented in the software Infowater 11.5 and EPANET 2.00.12 is sometimes used. Currently, the subnetwork 4 is being divided by pressure zones in order to proper manage pressure fluctuations and reduce leakages rate and water loss. The Colombian standards for DWDNs establishes 147 KPa as minimum pressure at the household connections

(Universidad de los Andes, 2010). Therefore, the water company expects to maintain this pressure level in the network by the physical modifications they are currently carrying out. The model was calibrated in the year 2007 and a new calibration is planned since several operative changes have occurred since then⁹.

In order to allocate a water age value to every sampling point, Thiessen polygons were built by using the software ArcMap® 10.2.2; water age map is included in the Appendix 9-A. This method has the unique property that each polygon contains only one input point, and any location within a polygon is closer to its associated point than to the point of any other polygon. The line between two points is located in the middle of the distance between them. Therefore, each sampling point is located inside of a polygon, so respective water age value is well defined. According to the histogram of the water age data (see Figure 3-3), these were classified in four intervals as it follows:

1. Low water age: 0 – 8.5 hours
2. Medium water age: 8.5 – 13 hours
3. High water age: 13 – 68 hours
4. Very high water age: 68 – 437 hours

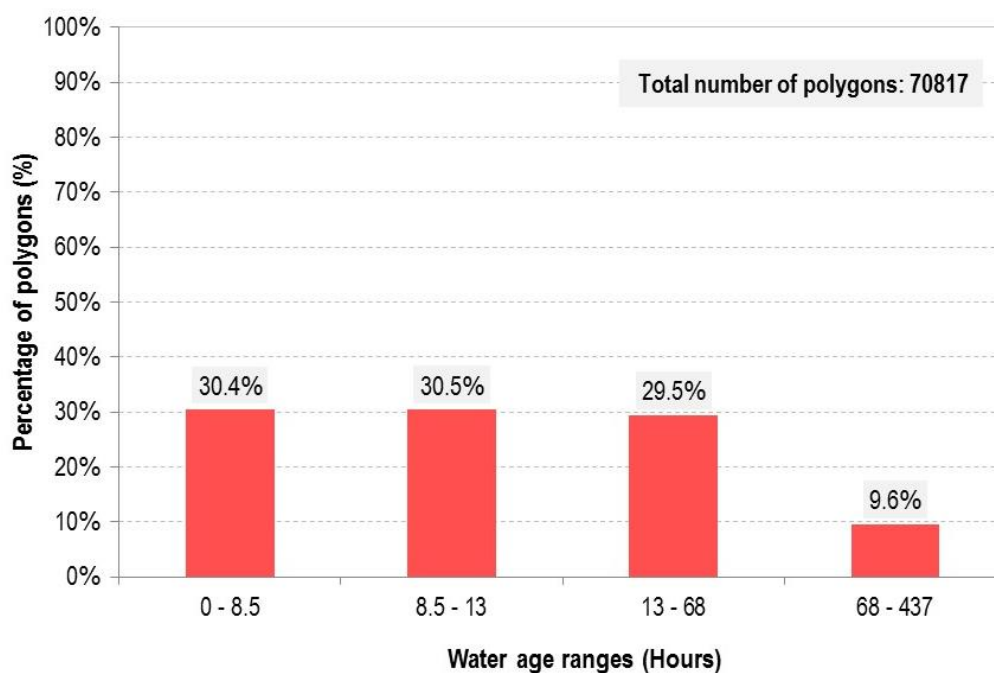


Figure 3-3. Water age ranges for the sampling sub-network

⁹ Rojas Ramírez, 2017, personal communication, 28th March. E-mail: jurojas@emcali.com.co

3.2.5 Sample collection

Sample collection procedure is illustrated in Figure 3-4. Samples were taken from nine sites over a 3-weeks period and their location is included in Figure 3-5. In each case, pipe sections were collected during leakage repairs because the normal operation of the DWDN cannot be interrupted for this kind of activities. This approach for taking biofilm samples is dominated by randomness due to O&M staff must prioritize the daily scheduled repairs according to the size and type of affected population (e.g., big neighbourhoods, areas with hospitals and education institutions). In the case that researchers want to evaluate more strictly engineered variables such as water age, pipe age, pipe materials, type of network component (pipelines, valves, water meters), among others, sampling campaigns must be carried out in a long term. According to the researcher criteria, nine samples of both bulk water and biofilms was an acceptable amount to characterize the bacterial communities in both habitats and their relationships with other engineered and physico-chemical variables. Additionally, field assessment like the current one described here also allows suggesting practical recommendations to the water operators to preserve the drinking water quality to the point of use.



Figure 3-4. Procedure for collection of water and biofilm samples

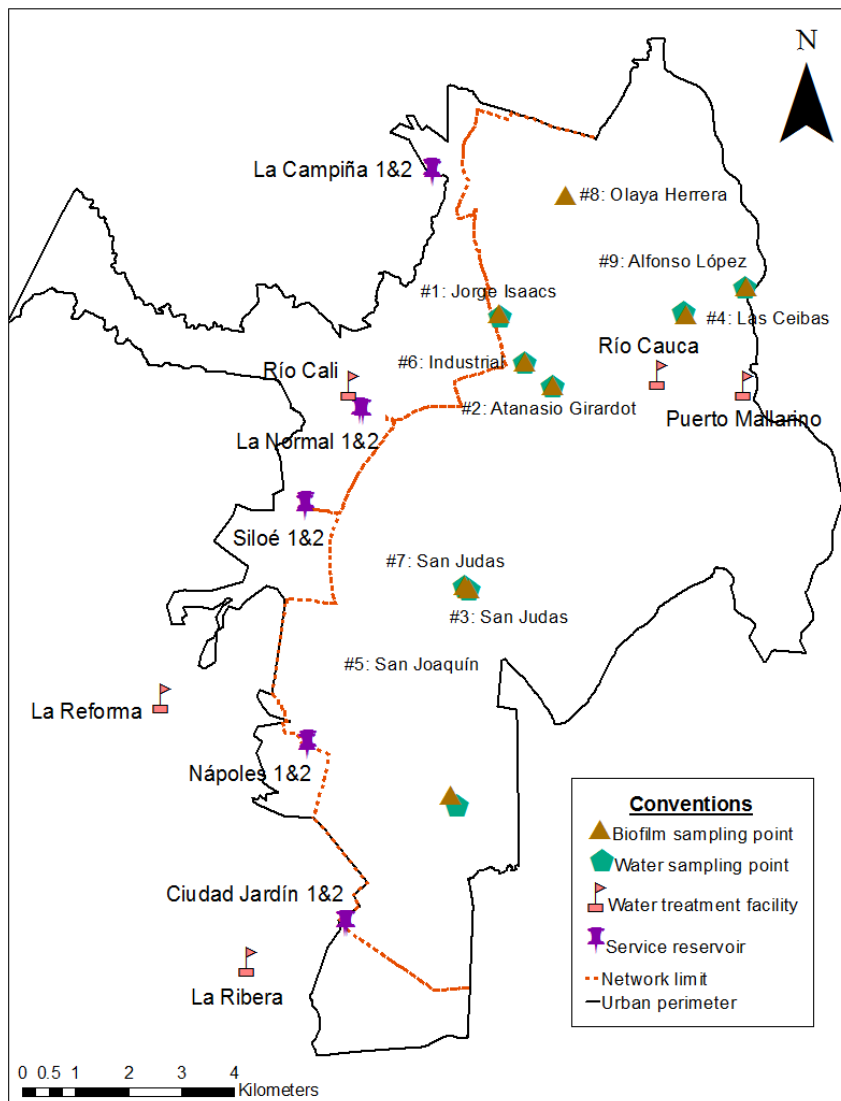


Figure 3-5. Location of sampling points in the city of Cali

First, bulk water samples were taken in the appropriate bottles according to the physico-chemical analysis of interest (step 1); 6 L of DW were collected in sterile plastic bottles for DNA extraction. Water samples were collected in the nearest household; the taps were flushed for 5 min before storage in the respective bottles. Then in-situ parameters were measured (step 2). After this, water supply was interrupted by closing valves in order to isolate and empty that part of the network; this allows to remove the broken piece of pipe and install the new pipe section (step 3). The broken pieces of pipe were washed with sterile water to remove portions of soil attached to pipes sections (step 4). The internal surfaces of pipes were also washed with sterile water to remove loose particles. The pipe sections were wrapped in polythene to be transported at 4 °C to the laboratory (step 5) for subsequent biofilm removal and DNA isolation (step 6). Each sampling point was characterized by water age and pipe characteristics (material, age, and diameter).

3.2.6 Physicochemical analysis

In-situ water parameters were measured as follows: (a) Temperature was measured by a bulb thermometer; (b) pH by portable meter kit (HQ40d HACH Cat. No. HQ40D53000000, Loveland, CO) coupled to a pH electrode; and (c) total and free chlorine by the DPD method using a HACH colorimeter II (Cat. No. 58700-00, Loveland, CO). Quantification of Total Organic Carbon (TOC) and total THMs (TTHMs) in bulk water was carried out by an accredited laboratory following standard methods (5310B and 6232B, respectively) (Eaton et al., 2005). Equipment for TOC and TTHMs analysis were total carbon analyser (Shimadzu TOC 5050A, article number 3750 K3-2, Columbia, MD) and gas chromatograph (HP 5890, Wilmington, DE and Agilent Technologies 7890B, Santa Clara, CA.), respectively.

The standard method 5310B for TOC measurement is based on high-temperature combustion in a total carbon analyser. The water sample is homogenized and diluted and a micro-portion is injected into a heated reaction chamber packed with an oxidative catalyst. The water is vaporized and the organic carbon is oxidized to CO₂ and H₂O. The CO₂ from oxidation of organic and inorganic carbon is transported and measured in the carrier-gas streams. Since total carbon is measured, inorganic carbon must be removed by acidification and sparging or measured separately and TOC is obtained by difference (Eaton et al., 2005).

The standard method 6232B for TTHM measurement is based on liquid-liquid extraction in a gas chromatograph; and it is applicable for measuring chloroform, bromodichloromethane, dibromochloromethane, and bromoform in drinking water. The sample is extracted once with pentane and the extract is injected into the gas chromatograph equipped with a linearized electron detector for separation and analysis. In this equipment, the sample is carried by a gas stream to a separation tube known as the "column" (Eaton et al., 2005).

TOC and dry-biomass content were measured in biofilm samples by scrapping a defined area on the pipe surface of 75 cm² in triplicate, in order to obtain enough biomass for both parameters and for being able to apply descriptive statistics in the case of dry-biomass parameter. For TOC measurement in biofilms, scrapped biofilms were resuspended in 250 mL of deionized water. For dry biomass, scrapped samples were dried at 105 °C, for 24 hours and unit dry biomass was calculated by dividing dry biomass by the scrapped area. Due to the presence of a high amount of tubercles in the cast iron pipe of sample point 2, unit dry biomass was not calculated since the scrapped area could not be determined (see Figure 3-6).



Figure 3-6. Inner walls of cast iron pipeline of sampling point 2

3.2.7 Molecular methods

Previous of taken the biofilm samples from pipe walls, the inner walls were washed again with sterile water to remove any extra loose particles. Biofilm samples were collected by scrapping in triplicate using a sterile frame with area equal to 25 cm² and a sterile spatula. Triplicates allowed to calculate median value of RA of species. DNA isolation was carried out immediately using the Power Biofilm DNA Kit (MoBio Laboratories, Carlsbad, CA) according to the manufacturer's instructions. In total 6 L of DW were filtered for every sampling point (2 L for each triplicate) through nitrocellulose filters (0.22 μm pore-size); filters were further processed for DNA extraction using the Power Water DNA Kit (MoBio Laboratories, Carlsbad, CA) according to the manufacturer's instructions.

Sequencing refers to the determination of the sequence of the nucleobases (adenosine, guanine, adenine and thymine), which compose the RNA and DNA of any cells. Sequencing of DNA extracted from biofilm and water samples was performed by Illumina MiSeq Technology using the Illumina PE MySeq reagent Kit v3 according to the manufacturer's guidelines (Illumina, USA) and performed by the Molecular Research DNA Lab (Shallowater, TX, USA). 2-5 ng/μL of DNA per sample (n=53) was used for amplification (no replicates per sample were generated) and the V4 variable region of the 16S rRNA gene was amplified using primers 515F/806R (Caporaso et al., 2011). Sequence data were processed using Mr DNA analysis pipeline (www.mrdnlab.com, MR DNA, Shallowater, TX). In summary, sequences were merged, depleted of barcodes and primers, sequences < 150 bp and with ambiguous base calls were removed from further analysis. Sequences were denoised and chimeras removed. Operational Taxonomic Units (OTUs) were

defined by clustering at 3% divergence (97% similarity) and were taxonomically classified using BLASTn against a curated database derived from Greengenes, RDP II and NCBI (DeSantis et al., 2006) (<http://www.ncbi.nlm.nih.gov/>, <http://rdp.cme.msu.edu>).

The total number of reads generated per sample ranged between 7780-304912 and between 13759-238406, for biofilm and bulk water samples, respectively. The number of reads that passed quality scores ranged between 7240-256972 for biofilm and between 10257-101379 for bulk water samples. The data set (number of reads per sample) was not normalised or rarefacted to assess alpha-diversity, in order to avoid losing information from potential important sequences (McMurdie and Holmes, 2014).

3.2.8 Data analysis

Physico-chemical data was processed and analysed by descriptive statistics such as minimum, maximum, average, median, quartiles, coefficient of variation (CV), and number of data. The alpha-diversity of the samples at 97% sequence similarity cut off was analysed by Margalef and Shannon community richness and diversity indices, respectively, which were calculated with Primer6 software (PRIMER-E, Plymouth, UK). The alpha diversity was selected because the samples were collected in the same locality, which is supplied by the same surface water source, which is treated by two WTPs. The medians and means of such indices were statistically compared by t-test and Mann Whitney U test using the software IBM SPSS Statistics 21. The associations of RA at species level (considered at 97% sequence similarity cut of) with environmental factors and characteristics of the sampling points were determined by multidimensional scaling (MDS), by means of Bray-Curtis similarity metrics, and analysis of similarities (ANOSIM) using Primer6 software. Spearman correlations were applied to determine the relationships between biofilm parameters and bulk water physicochemical factors; Shapiro-Wilk tests were run in IBM SPSS Statistics 21 to determine normal distribution of variables; results of normality tests are presented in Appendix 9-B. All statistical results were contrasted with significance level equal to 0.05.

With regard to the analysis of bacterial communities in biofilm and water samples, it was based on the analysis of similarities using the Bray-Curtis coefficient (S), followed by hierarchical clustering and ordination of samples by MDS, and finally testing for differences between groups of samples by ANOSIM test. Figure 3-7 shows the stages in the multivariate analysis based on similarity coefficients (Clarke and Warwick, 2001).

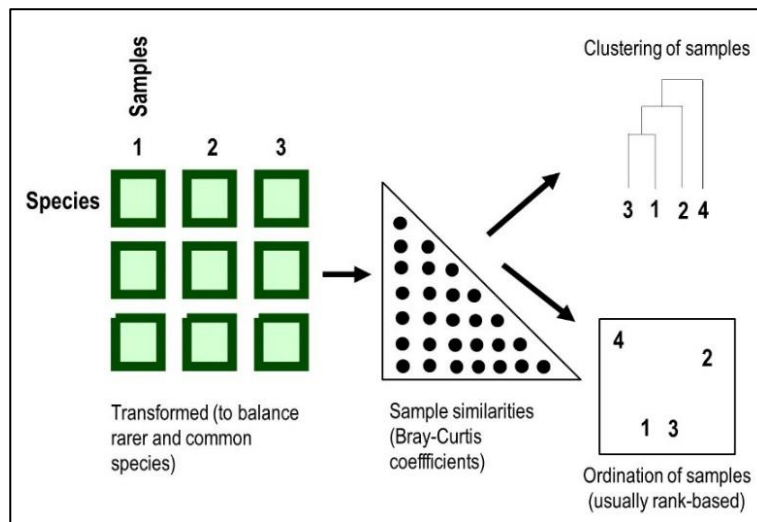


Figure 3-7. Stages in the multivariate analysis based on similarity coefficients

- Similarities between samples: percentage of RA of species identified in every sample were transformed by square root method in order to build a triangular matrix of the similarities coefficients of Bray-Curtis, so these can be ordered (ranked) for further analysis. Calculation of the expression $(100-S)$ allows obtaining the dissimilarities matrix (Clarke and Warwick, 2001).
- Hierarchical clustering: similarities matrix is the start point for building a dendrogram, followed by successively fuse the samples into groups and the groups into larger clusters with the highest mutual similarities and the gradually lowering the similarity level at which groups are formed (Clarke and Warwick, 2001).
- MDS: cluster analysis is often best used in conjunction with ordination methods since agreement between the two representations strengthens reliability of adequacy of both. A MDS graph represents the configuration of the samples, in a specific number of dimensions, which attempts to satisfy all the conditions imposed by the rank of the (dis)similarity matrix. The construction of a MDS involves a numerical algorithm to produce a sample map whose inter-point distances have the same rank order as the corresponding dissimilarities between samples (Clarke and Warwick, 2001).
- ANOSIM: it is a multivariate test for the null hypothesis (H_0) "there are not differences in community composition at the sampling sites" which is based on the statistical parameter R ($-1 < R < 1$) whose calculation is based on the rank of similarities. If $R=1$, all replicates within sites are more similar to each other than any replicates from different sites. If $R=0$, the null hypothesis

is true, so that similarities between and within sites will be the same on average. To test the statistical significance of R, it was verified that the probability that Ho is true was less than 5% (p-value) (Clarke and Warwick, 2001).

3.3 RESULTS

3.3.1 Suspension of drinking water supply in the studied network

The Colombian regulation (Superintendencia de Servicios Públicos, 2006) established the obligation to report, by the utilities, information related to drinking water supply, sewage, and cleaning services to SUI (Sistema Único de Información for its Spanish abbreviation) (SUI, 2017). A piece of the information required by the SUI is the suspension of the drinking water supply, which must be described by type of event, number of customers affected by each event, and duration in hours of the event. The description of the code used to classify the type of event is shown in Table 3-2 and Figure 3-8 presents the characterization of these events. Unfortunately, the description of the type of event does not allow identifying which ones correspond to leakage repairs, operation interruption of the WTPs, pipeline replacements, among others.

Table 3-2. Description of the code used to classify the type of suspension of drinking water supply in Colombia

Code	Code meaning
1	Suspension of potable water supply due to maintenance with previous notification to customers
2	Suspension of potable water supply due to repairs with previous notification to customers
3	Suspension of potable water supply due to operative rationing with previous notification to customers or non-controllable rationing
4	Suspensions of potable water supply without previous notification to customers

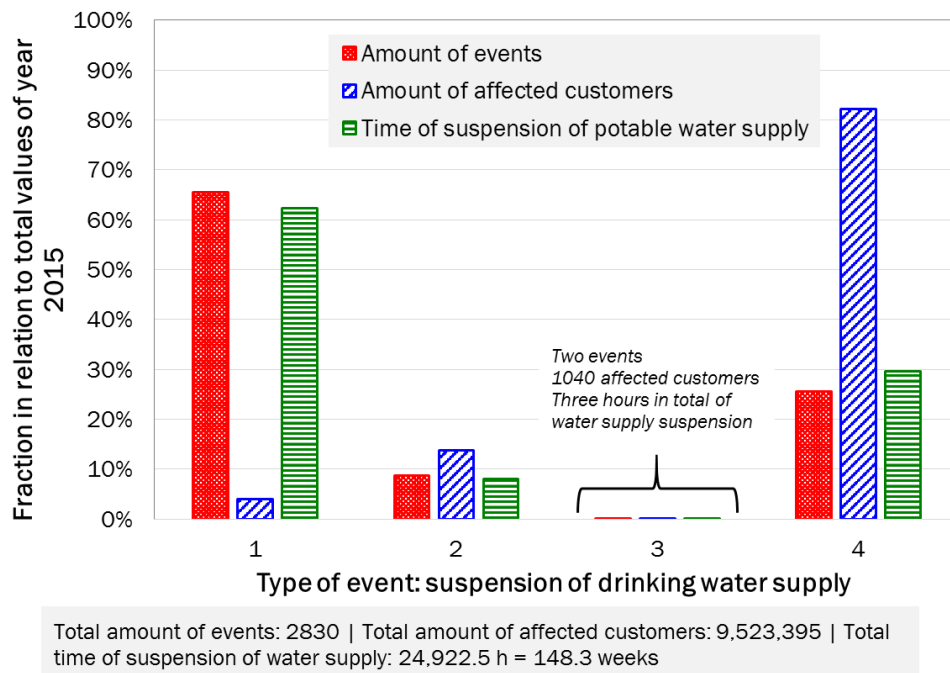


Figure 3-8. Characterization of events of suspension of drinking water supply in the DWDN of the city of Cali

The first three types of events of potable water suspension are related to maintenance, repairs and operative activities with previous notification to customers. The type of event No 1 is the most common one (65.6%) and its influence is more notably on the total duration of the water supply suspension (62.3%) rather than on the amount of affected customers (3.9%). The type of event No 2 is associated with repairs but the code description does not specify what kind of repairs. In general, this event was not frequent (8.8%), affected few customers (13.8%) and the total time of water supply suspension was also short (8.1%). The type of event No 3 is related to operative and non-controllable rationing and its occurrence was very low (0.07%); therefore its impacts on affected customers and total duration of events are also low (0.01% for both criteria). The type of event No 4 refers to suspensions of potable water supply without previous notification to customers. This impacted a high amount of customers (82.3%) but the amount of events (25.6%) and the total time of suspension of potable water supply (29.6%) were relatively low.

By grouping the first three types of events, which include previous notification to customers, most of the events (74.4%) and the highest total time of suspension of potable water supply (70.4%) are linked to this group; the highest amount of affected customers (82.3%) is due to suspension of potable water supply without notification to customers. This is important if it is considered that previous notification to customers can lead to increase the water storage at households as a contingency, then water demand increases, and velocity and shear stress may raise suddenly and

being higher than the values found under normal operation of the DWDN. Such hydraulic changes may lead to biofilm detachment; the consequences of this were already discussed in Chapter 2.

In particular, suspension of drinking water supply associated with deterioration of raw water (high turbidity and low dissolved oxygen) are specially important due to its relation to extreme weather events and climate change (Montoya et al., 2011; Khan et al., 2015). The latest management report of the local water company of the city of Cali (EMCALI EICE ESP, 2016) described the evolution of the events related to decrease of dissolved oxygen in raw water, between 1st January 2000 and 25th September 2016, and the impact of the clarified water reservoirs built in the main water treatment of the system. The data is presented in Figure 3-9; the local water company has named this type of event as “high contaminant load” due to this causes decrease of dissolved oxygen.

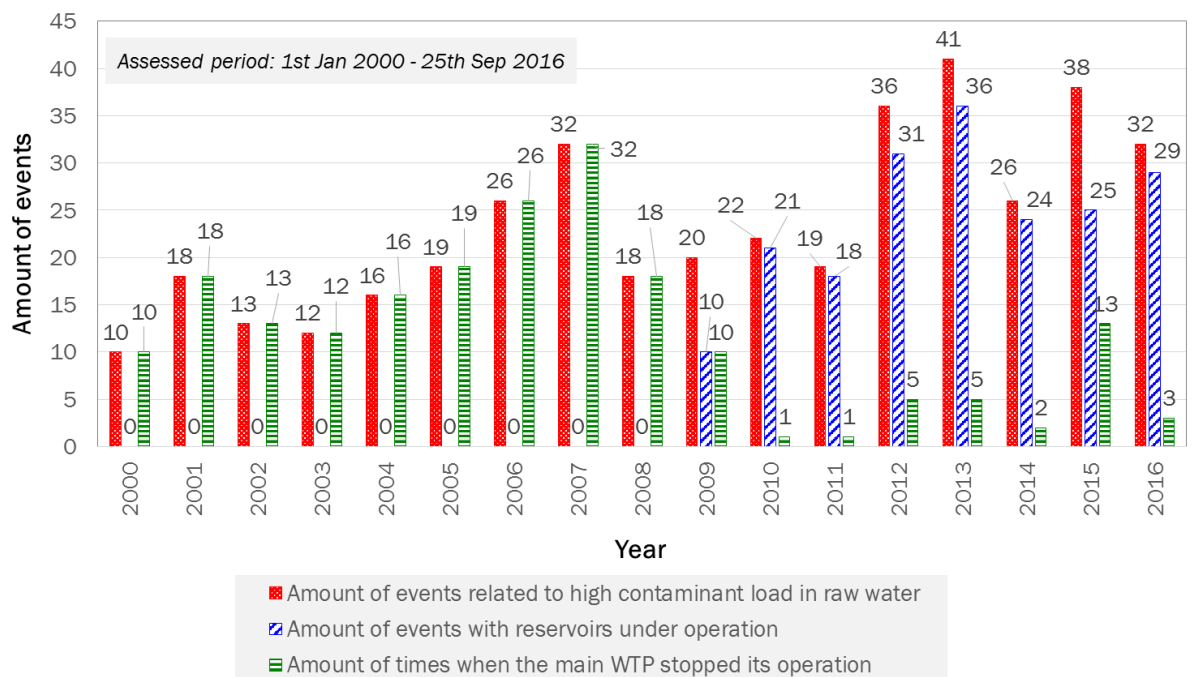


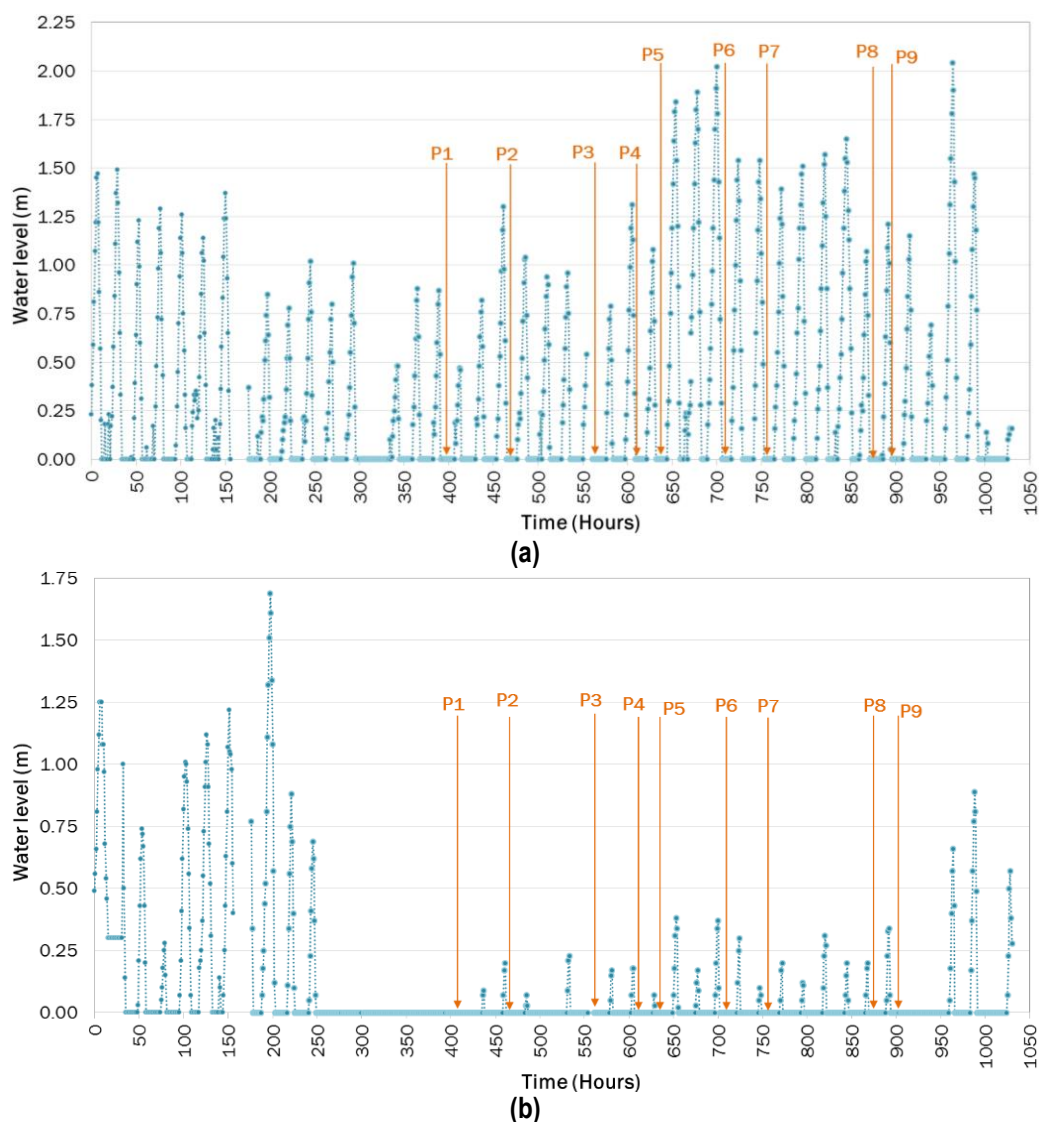
Figure 3-9. Evolution of events of suspension of WTP operation in the period 2000-2016

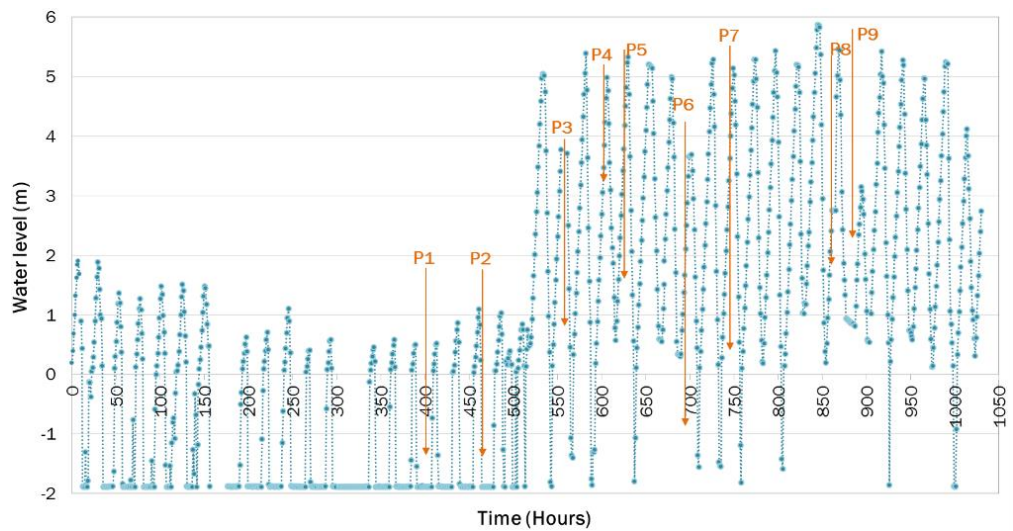
Before the clarified water reservoirs were built and operated in 2009, all the events of high contaminant load in raw water caused suspension of operation of the WTP from year 2000; therefore, customers did not have access to drinking water and hydraulic integrity of the network was lost during these events. From 2009, the WTP was able to operate by using such stored water, guaranteeing the supply of potable water to customers. Although the reservoirs are an acceptable contingency practice, it can be noted in Figure 3-9 that, from year 2012, the number of events causing suspension of WTP operation has increased from once until a maximum of 13 times in 2015. This allows inferring that the duration of the events of high contaminant load is raising since

the reservoirs are designed to operate for up to 9 hours. This again is causing suspension of drinking water supply to customers and loss of the hydraulic integrity of the DWDN. The amount of events has also increased from a minimum of 10 events in 2000 until a maximum of 41 in 2013, with fluctuations between these numbers in the assessed period (Figure 3-9).

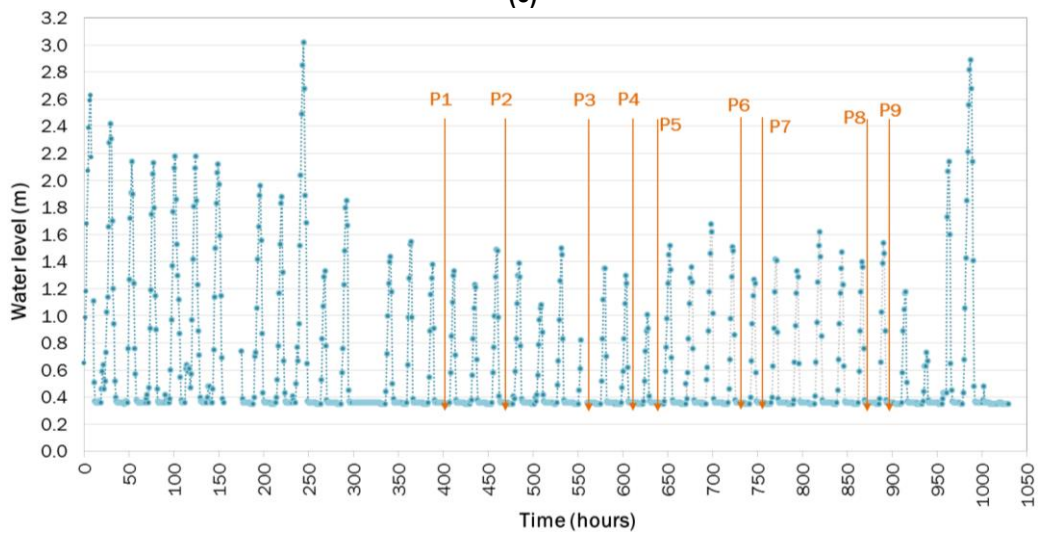
3.3.2 Water levels in service reservoirs in the DWDN

The sub-network 4 has four pairs of service reservoirs and one single reservoir located in strategic points of the city (higher topographic areas) to compensate the pressure in the network (see Figure 3-5); therefore, the network can be supplied partially by both the WTPs and the reservoirs during high-water demand times. Figure 3-10 shows the variation of water levels in the service reservoirs of the sub-network 4 and Table 3-3 presents the operational hydraulic conditions of the sub-network 4 during sampling activities.

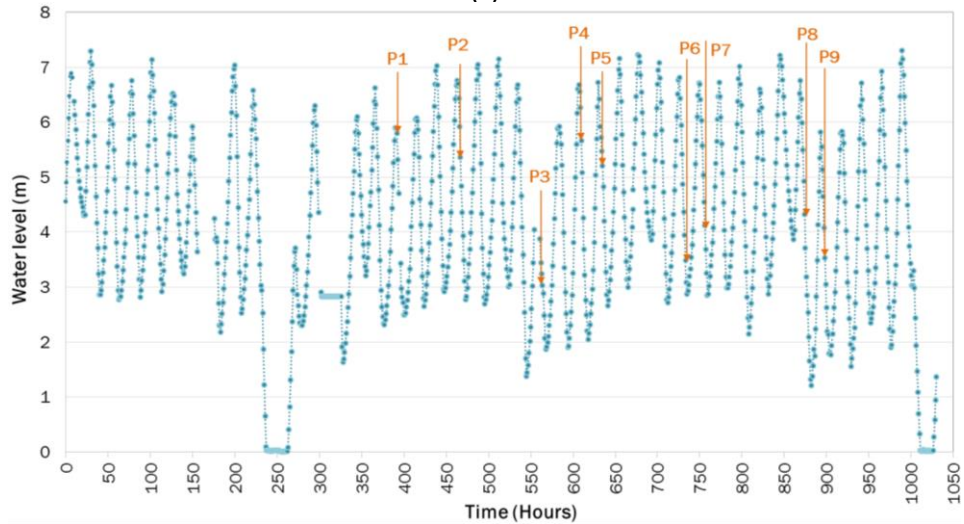




(c)



(d)



(e)

Figure 3-10. Water levels in service reservoirs during sampling activities (a) La Campiña (b) Normal (c) Siloé (d) Nápoles (e) Ciudad Jardín

Table 3-3 presents the hydraulic conditions of the studied subnetwork during the sampling campaign. Four pairs of service reservoirs were empty during most of the sampling activities; Siloé reservoir was supplying its respective area during six sampling journeys but just two of the nine sampling points are probably located in that area (points 3 and 7 - San Judas); in addition, the supply region of service reservoir Siloé is not well defined, according to water company information. Moreover, Ciudad Jardín reservoir was supplying its respective area during the entire sampling campaign but none of the sampling points were located on it; sample location was dependent on where leakages occurred in the network during the experimental collection period. According to the aforementioned, the sub-network 4 was mostly supplied by the WTPs during most of the sampling journeys. As a result, water age was processed according to that condition through Thiessen polygons as explained in Section 3.2.4.

Table 3-3. Hydraulic conditions of the sub-network 4 during sampling campaign

Sampling point	Neighbourhood	Operation of service reservoirs during sampling					Water age of sampling point / Filling cycle of service reservoirs			
							Water		Biofilm	
		La Campiña	La Normal	Siloé	Nápoles	Ciudad Jardín	Value (hours)	Classification	Value (hours)	Classification
1	Jorge Isaacs	WTP working	WTP working	WTP working	WTP working	Draining cycle	13,95	High	13,99	High
2	Atanasio Girardot	WTP working	WTP working	WTP working	WTP working	Draining cycle	9,71	Medium	9,71	Medium
3	San Judas	WTP working	WTP working	Draining cycle	WTP working	Draining cycle	12,37	Medium	12,37	Medium
4	Las Ceibas	WTP working	WTP working	Draining cycle	WTP working	Draining cycle	146,01	Very high	8,12	Low
5	San Joaquín	WTP working	WTP working	Draining cycle	WTP working	Draining cycle	14,41	High	15,59	High
6	Industrial	WTP working	WTP working	WTP working	WTP working	Draining cycle	10,06	Medium	10,06	Medium
7	San Judas	WTP working	WTP working	Draining cycle	WTP working	Draining cycle	11,71	Medium	11,47	Medium
8	Olaya Herrera	WTP working	WTP working	Draining cycle	WTP working	Draining cycle	13,23	High	13,23	High
9	Alfonso López	WTP working	WTP working	Draining cycle	WTP working	Draining cycle	8,00	Low	8,26	Low

3.3.3 Water age

The water age corresponding to every sampling point for both biofilm and water samples is included in Table 3-3 and Figure 3-11. Thus, there are four pairs of samples water-biofilm with medium water age, three pairs of samples with high water age and one pair of samples with different classification of water age; the biofilm sample at point 4 had very high water age and water sample had low water age. The water age at Point 4 differs because water sample had to be taken two streets away from the biofilm sampling point and, despite their geographical proximity, the respective areas had notably different water age values. It can be hypothesised that such notable high water age value may be related to the presence of a recirculation dead-end point in the DWDN.

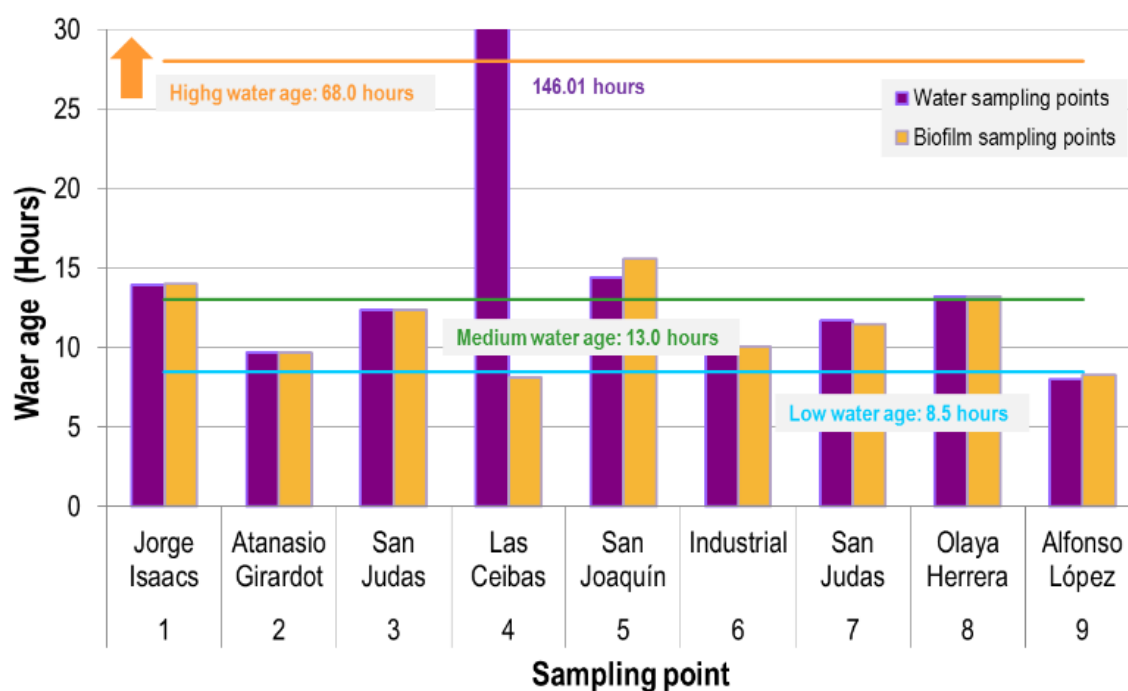


Figure 3-11. Water age of sampling points

3.3.4 Physical characteristics of sampled pipes

Materials, diameters and age of collected pipes for biofilm sampling are described in Table 3-4. The predominant material of sampled pipelines is asbestos cement. One biofilm sample was collected from a cast iron pipeline. Pipe diameters were predominantly 4" and three biofilm samples were taken from 3", 8" and 12" pipelines. The oldest pipeline was installed in February 1958 and the newest one in August 1990. Therefore, the range of pipe age is 25-57 years at the time of sampling.

Table 3-4. Network characteristics in sampling points

Sampling point	Neighbourhood	Pipe material	Pipe diameter (Inches)	Installation date of pipe
1	Jorge Isaacs	Asbestos	4	21/09/1958
2	Atanasio Girardot	Cast iron	4	03/02/1958
3	San Judas	Asbestos	3	18/04/1981
4	Las Ceibas	Asbestos	4	11/12/1979
5	San Joaquín	Asbestos	4	18/08/1990
6	Industrial	Asbestos	8	20/05/1972
7	San Judas	Asbestos	12	04/06/1981
8	Olaya Herrera	Asbestos	4	17/05/1962
9	Alfonso López	Asbestos	4	06/04/1964

3.3.5 Water quality and biotic parameters

Water quality and biotic parameters and descriptive statistics are presented in Table 3-5. Water quality characteristics including temperature, pH, free residual chlorine and TTHMs were within the expected ranges, except for the lowest concentration of chlorine (0.12 mg/L), which was measured at sampling point 4, which corresponded to the highest water age (146 h). Such concentration of free residual chlorine is considered very low according to the recommended values set for drinking water quality standards by local regulators (0.3-2.0 mg/L) (Ministerio de la Protección Social, 2007). TOC measured in biofilm samples presents a lower variation (CV=105.6%) compared to the variation in biofilm mass (CV=321.5%). All concentrations of TOC in DW were reported as lower than the detection limit (<0.8 mg/L). Regarding TTHMs, concentrations in all water samples were lower than 40 µg/L, which falls below the maximum concentration of TTHMs allowed in drinking water according to UK and Colombian regulation (100 and 200 µg/L, respectively).

In relation to biotic factors, unit dry biomass presents the highest variation among all the variables analysed in this study (CV=329.09%; Table 3-5). Although calculation of the unit dry biomass in the cast iron pipe sample (sampling point 2) was not possible, the second highest content of dry biomass in the biofilm (233.7 - 3,664.8 mg) and highest TOC in the water sample (10.10 mg/L; Table 3-5) were found in this point. This result can be related to a significant amount of biofilm and sediments attached to the pipe walls when compared with other sampling sites.

Table 3-5. Water quality, biotic parameters and descriptive statistics

Sampling point	Water quality					Biofilm characteristics		
	Temperature (°C)	pH (Units)	Free res. chlorine (mg/L)	Total res. chlorine (mg/L)	TTHMs (mg/L)	TOC (mg/L)	Unit dry biomass (mg/cm ²) *	
1	26	7,32	1,20	1,35	30,3	0,819	1,41	
2	25	7,16	1,66	1,76	28,9	10,104	-	
3	25	7,35	1,28	1,43	23,5	1,210	1,45	
4	-	7,04	0,12	1,61	36,7	1,453	0,29	
5	25	6,76	1,30	1,45	28,3	1,527	0,38	
6	26	7,01	1,12	1,33	35,5	1,739	3,23	
7	28	7,02	1,15	1,21	30,8	2,139	0,23	
8	26	6,86	0,86	1,02	38,6	1,849	2,09	
9	27	6,62	1,31	1,57	33,3	2,157	3,34	
Descriptive statistics	Minimum	25	6,62	0,12	1,02	23,45	0,819	0,23
	Median	26	7,02	1,20	1,43	30,80	1,74	1,43
	Mean	26	7,02	1,11	1,41	31,76	2,56	1,55
	Maximum	28	7,35	1,66	1,76	38,6	10,10	3,34
	Standard deviation	1	0,23	0,40	0,21	4,47	2,70	1,28
	CV	3,85%	3,26%	36,25%	14,76%	14,09%	105,64%	82,70%
Colombian standards (a)		--	6.5-9.0	0.3-2.0	--	200	--	--

* Median of replicates | Descriptive statistics of all data of unit dry biomass (including replicates - mg/cm²): Min=0.11; Median=1.41; Mean=5.20; Max=81.45; Stand. Dev.=17.11; CV=329.09% | AC: asbestos cement | Cl: cast iron
(a) Ministerio de la Protección Social and Ministerio de Ambiente Vivienda y Desarrollo Territorial (2007)

Several physicochemical characteristics of bulk water were correlated to identify the dynamics present in the studied network; results are presented in Table 3-6. Significant negative correlations were found between total residual chlorine and temperature ($p=0.019$), free residual chlorine and water age ($p=0.004$) and free residual chlorine and TTHMs ($p=0.017$). Weak negative correlations were identified between temperature and free residual chlorine ($p=0.052$, slightly higher than the level of significance) and between pH and TTHMs ($p=0.042$). A positive correlation was observed between temperature and TTHMs ($p=0.003$).

With regards to biofilms, correlations presented in Table 3-7 indicated that there is a strong positive relationship between unit dry biomass and pipe age ($p=0.008$). Additionally, water age was

negatively correlated with TOC in biofilms but the p-value was slightly higher than the level of significance ($p=0.063$) and no association was identified between water age and unit dry biomass, possibly related to the influence of pipe age/material over the later variable.

Table 3-6. Spearman correlation coefficients for bulk water parameters

Variables ↓→	Richness index (Margalef)	Diversity index (Shannon)	Water age	pH	Temper.	Total residual chlorine	Free residual chlorine	TTHMs
Richness index (Margalef)	-							
Diversity index (Shannon)	<i>C.N.T</i>	-						
Water age	0.277	0.315	-					
pH	0.365 ***	0.414 *	<i>C.N.T</i>	-				
Temperature	-0.355 ***	-0.238	<i>C.N.T</i>	<i>C.N.T</i>	-			
Total residual chlorine	0.074	0.149	-0.067	0.117	-0.476 *	-		
Free residual chlorine	-0.251	-0.273	-0.533 **	-0.033	-0.401 ***	<i>C.N.T</i>	-	
TTHMs	-0.259	0.049	0.060	-0.594 *	0.802 **	<i>C.N.T</i>	-0.671 *	-

Correlation is significant at the 0.05* / 0.01** level (2-tailed)

*** Correlation coefficient slightly higher than 0.05 → 0.052 < p-value < 0.089

Table 3-7. Spearman correlation coefficients for biofilm parameters

Variables ↓→	Richness index (Margalef)	Diversity index (Shannon)	Water age	Pipe age	Unit dry biomass	TOC - biofilm
Richness index (Margalef)	-					
Diversity index (Shannon)	<i>C.N.T</i>	-				
Water age	0.364 ***	0.375 ***	-			
Pipe age	-0.404 *	-0.512 **	<i>C.N.T</i>	-		
Unit dry biomass	-0.582 **	-0.733 **	-0.196	0.559 **	-	
TOC - biofilm	-0.294	-0.357	-0.552 ***	0.334	0.259	-

Correlation is significant at the 0.05* / 0.01** level (2-tailed)

*** Correlation coefficient slightly higher than 0.05 → 0.059 < p-value < 0.068

3.3.6 Characterization of the bacterial community structure of biofilms and bulk water

The RA to phylum and genera level for water and biofilm samples can be observed in Figure 3-12 and Figure 3-13, respectively; groups with RA lower than 10% were grouped in the category “Others”. Water samples were dominated mainly by *Proteobacteria* phyla (43-98%), followed by *Cyanobacteria* (0.05-41%), and *Firmicutes* (0.84–34%). With regard to biofilm samples, the predominant phyla were *Proteobacteria* (26-72%), followed by *Firmicutes* (3–30%), and *Actinobacteria* (8-19%). Different genera were dominant in each bulk water sample and those with higher RA were *Bacillus*, *Brucella*, *Cyanothece*, *Methylobacterium*, and *Phyllobacterium* (17.47-95.91%). With regard to biofilm samples, different genera were dominating each sample and those with higher RA were *Acinetobacter*, *Alcaligenes*, *Alcanivorax*, *Bacillus*, *Deinococcus*, *Holophaga*, and *Thermoflavimicrobium* (4.34–43.92%).

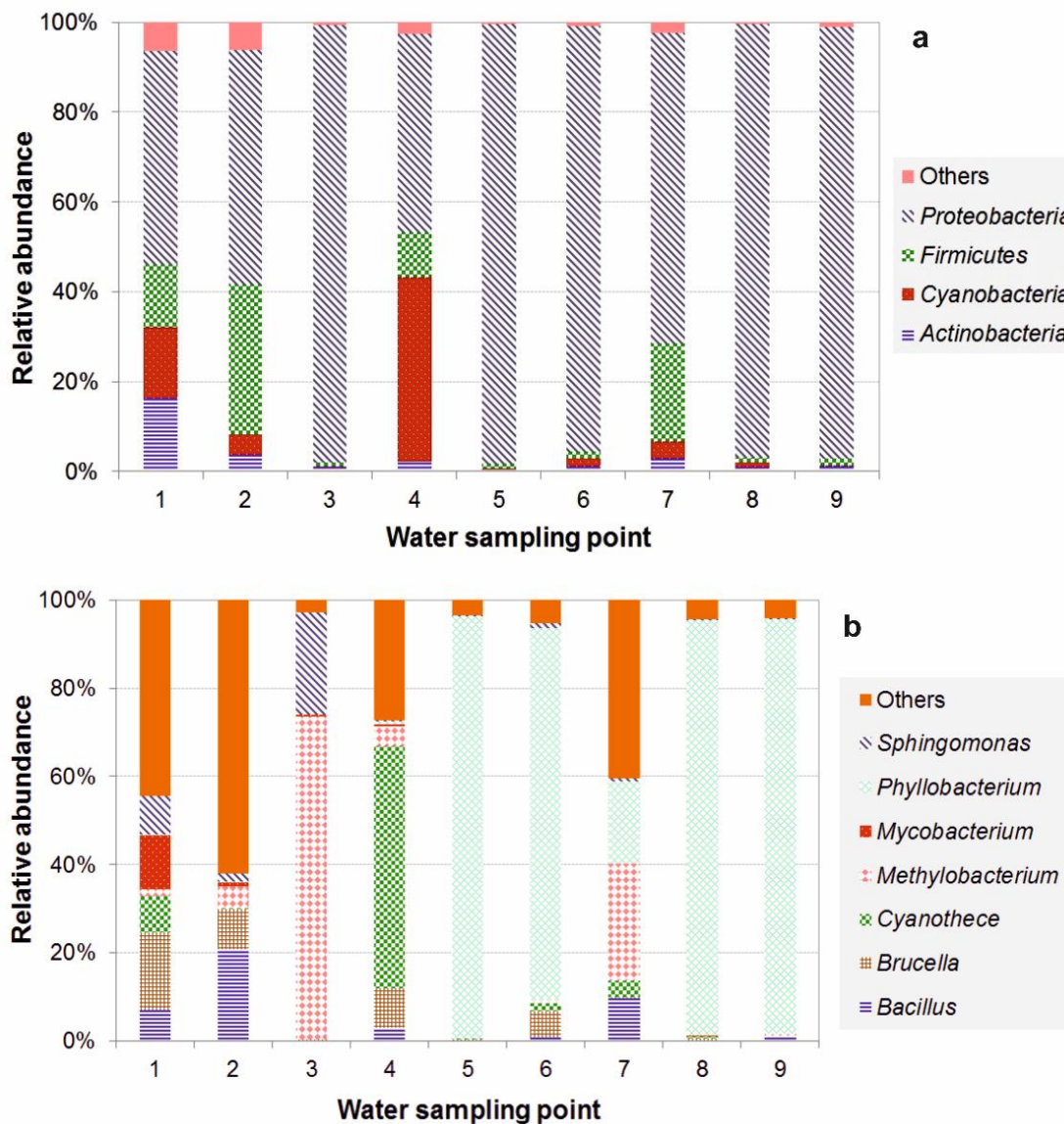


Figure 3-12. RA of bacterial groups to (a) phylum level and (b) genus level in water samples

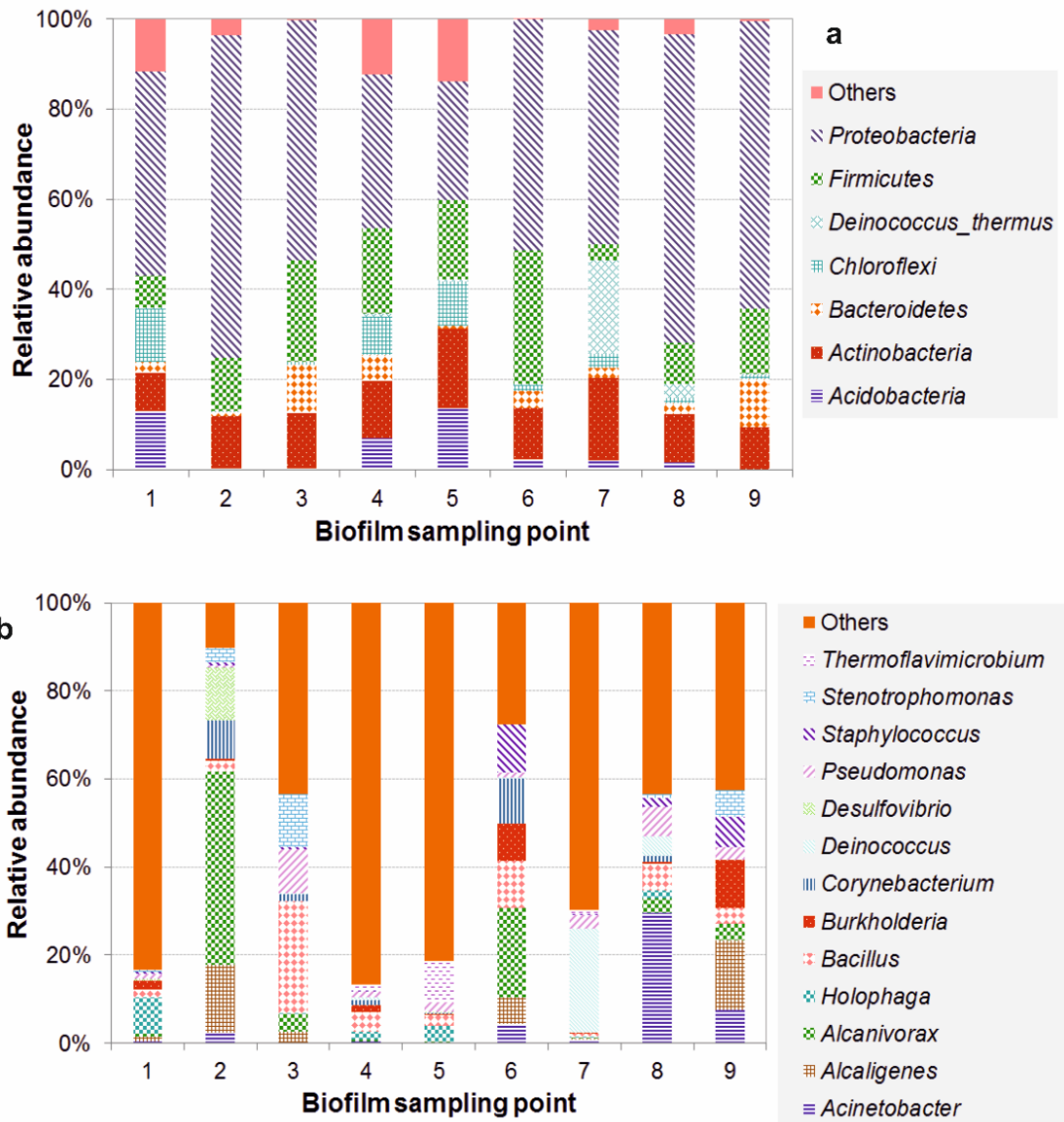


Figure 3-13. RA of bacterial groups to (a) phylum level and (b) genus level in biofilm samples

ANOSIM test was applied to assess the relationships between species RA and engineered factors (global R and p-value; Table 3-8). With regards to water samples, relationships between species RA and factors water age, free chlorine, pH, and free chlorine and water age combined were statistically significant. In relation to biofilm samples, ANOSIM test resulted statistically significant for the factors pipe age, and water age, and unit dry biomass and pipe age combined. Factor “Pipe material” was not included in the statistic tests due to only one sample was collected from CI pipeline, then comparison between CI and asbestos cement would not be statistically strong. Habitat was also a factor influencing the RA of species. MDS analysis also revealed that habitat and pipe material were the factors which clustered bacterial species (Figure 3-14a and Figure

3-14b, respectively). The two-dimensional plots of the MDS analysis and dendrograms for visualization of Bray Curtis similarity index for every parameter considered in this study are included in the Appendix 9-C.

Importantly, other methanotrophic organisms were observed in biofilm samples such as *Methylobacterium* (RA=1.16%) and *Methylosinus* (RA=3.34%). In bulk water, Spearman correlations with TTHMs were statistically significant for the genus *Methylobacter* ($\rho=0.437$; p-value=0.023) and *Methylobacterium* ($\rho=-0.417$; p-value=0.030).

Table 3-8. ANOSIM test for RA of species

Habitat	Factor	ANOSIM		Habitat	Factor	ANOSIM	
		Global R	p-value			Global R	p-value
Bulk water	Water age	0,441	0.002*	Biofilm	Pipe age	0,601	0.001*
	Temperature	0,002	0.430		Pipe diameter	0,122	0,113
	Free chlorine	0,441	0.001*		Water age	0,601	0.001*
	pH	0,441	0.001*		Unit dry biomass	0,127	0,268
	Free chlorine – Water age	0,441	0.001*		Unit dry biomass – Pipe age	0,690	0.013*
Biofilm – Bulk water	Habitat	0,446	0.001*				
	Water age	0,304	0.001*				
	Water age – Habitat	0,666	0.001*				

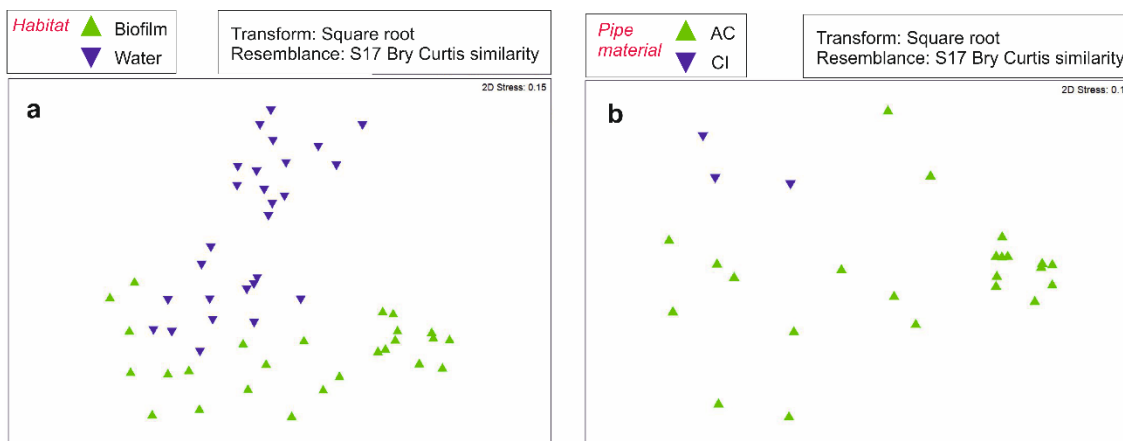


Figure 3-14. Non-metric MDS analysis of bacterial RA. Factors (a) Habitat and (b) and pipe material - biofilm samples

3.3.7 Microbial richness and diversity

Richness and diversity indices were calculated (Table 3-9) according to factors such as habitat and water age. t-test indicated that the means of richness and diversity indices of biofilm samples are higher than those of water samples. Spearman correlations were applied to test the relationships between indices and engineered factors, for both water (Table 3-6) and biofilm (Table 3-7) samples. Negative correlations were found between biofilm indices and pipe age and unit dry biomass. Pipe material is also a factor which is influencing the diversity of species in biofilm samples since median of diversity index from asbestos pipes was higher than those from cast iron pipes. Results of comparisons of medians indicated that median of richness and diversity indices of biofilm samples with high water age was higher than those with medium water age. In water samples, richness index with very high water age was higher than those with low water age; and median of richness index with medium water age was higher than those with low water age. Positive correlations between water age and richness and diversity indices were only found in biofilm samples but the p-values were slightly higher than the significance level.

Table 3-9. Medians and means of richness and diversity indices

Index →	Margalef richness								
Habitat →	Habitat		Bulk water				Biofilm		
Factor →	Habitat		Water age				Water age		
Descriptive statistics ↓	Biofilm	Water	Low	Medium	High	Very high	Low	Medium	High
Median	253,5	272,0	272,0	271,0	253,0	319,0	251,0	185,5	594,0
Mean	417,1	279,7	229,3	276,5	284,4	328,7	449,6	303,3	550,7
Standard deviation	276,68	85,80	74,77	195,60	86,24	50,20	365,30	237,16	234,59
N	26	27	3	12	9	3	5	12	9
p-value	0.022 (a) *		Low - Very high water age 0.050 (b) *				Medium - High water age 0.019 (b) *		
Index →	Shannon diversity								
Habitat →	Habitat		Bulk water				Biofilm		
Factor →	Habitat		Water age				Water age		
Descriptive statistics ↓	Biofilm	Water	Low	Medium	High	Very high	Low	Medium	High
Median	4,978	4,647	4,422	4,611	4,647	4,876	4,696	4,442	5,648
Mean	5,129	4,622	4,440	4,581	4,662	4,842	5,172	4,759	5,598
Standard deviation	0,76	0,30	0,26	0,27	0,36	0,09	0,92	0,73	0,46
N	26	27	3	12	9	3	5	12	9
p-value	0.003 (a) **		-				Medium - High water age 0.013 (b) *		

Means / Medians comparisons: (a): t-test; (b): Mann-Whitney test

Correlation is significant at the 0.05* / 0.01** level. Only significant tests are shown

3.4 DISCUSSION

3.4.1 Bulk water quality and biotic parameters and their relationships with engineered factors

As discussed in Chapter 2, DBP formation is known to be influenced by operational parameters such as pH, temperature, TOC, chlorine dosage, water age, and type and concentration of precursors. The interactions observed between parameters such as water age, temperature, pH, free residual chlorine, and TTHMs confirm the dynamics occurring in a DWDN in relation to THMs formation: increasing water age promotes loss of free residual chlorine because the disinfectant is volatile and reacts with organic and inorganic matter, likewise the concentrations of THMs were increasing. Nescerecka et al. (2014) and Wang et al. (2014) also identified depletion of disinfectant with higher water age in a real scale and simulated DWDNs, respectively.

THM formation is highly directly influenced by pH and temperature (Liang and Singer, 2003). Such relationship is evidenced by the current results, which show a strong correlation between TTHMs and temperature. However a negative relationship between TTHMs and pH was found in the current study, which may be related to the narrow range of pH data (6.62-7.35; CV=3.26%; see Table 3-5); higher concentrations of THMs have been identified with higher pH in a range of 5-8 units in laboratory experiments (Liang and Singer, 2003; Wang et al., 2012c). Positive and negative correlations between pH and THMs in the distribution system have also been reported by Rodriguez and Sérodes (2001) in three DWDNs located in Canada. With regards to unit dry biomass, values found in the current study (0.11-81.45 mg/cm²) were similar to data reported by Ren et al. (2015) in a real scale DWDN (1.96-140.79 mg/cm²), located in a subtropical area in China, which had operated for 11 years at the time of sampling, and included PVC, steel, and cast iron pipes.

3.4.2 Identification of the bacterial community structure of biofilms and bulk water

Comparing phylotypes detected in bulk water and biofilm, biofilm samples seem to be more diverse than water samples (7 vs 4 groups, respectively); this was corroborated by the diversity and richness indices (417,1 vs 279,7 and 5.1 vs 4.6, respectively), as discussed below. Phylum *Actinobacteria*, *Firmicutes*, and *Proteobacteria* were the common phylotypes in the two habitats, with the later community being the dominant group in the entire set of samples. Recent studies from other geographic regions have reported that both water and biofilm samples were dominated

by *Proteobacteria* phyla (Douterelo et al., 2013; Holinger et al., 2014; Kelly et al., 2014; Sun et al., 2014; Wang et al., 2014; Mahapatra et al., 2015; Ren et al., 2015). Particularly, the study of Ren et al. (2015) was developed in the city of Shaoxing, located at the east of China. This city is characterized for a subtropical monsoon climate; the annual average low temperature oscillates between 3-25°C and the annual average high temperature varies between 8-33°C (TravelChinaGuide, 2017). Other important phylotypes in both habitats were *Firmicutes* and *Actinobacteria*, which have also been observed in other real scale DWDNs (Ren et al., 2015; Bautista-de los Santos et al., 2016).

The phylum *Cyanobacteria* was present in all the water samples and it belongs to a diverse group of photosynthetic microorganisms, widespread in aquatic and terrestrial ecosystems; representative genus of this phyla is *Cyanothece*, which was highly abundant in four water samples and has been little studied (Dechatiwongse, 2015) and are not cytotoxin producers (Jakubowska and Szelaż-Wasielewska, 2015). The source for the high presence of these organisms in the analysed samples is likely to be from one of the reservoirs of clarified water located at one of the WTP of the studied sub-network. Revetta et al. (2011), by analyzing 16S rRNA gene clone libraries derived from DNA extracts of 12 samples and comparing to clone libraries previously generated using RNA extracts from the same samples, found that these bacteria may be active in chlorinated drinking water. Since drinking water pipes are dark environments, how *Cyanobacteria* survive in these is not clear yet. However, it is hypothesised that due to the limited action that chlorine has for the inactivation of cyanobacterial planktonic cells (Fan, 2012), cell material could have been transported within the distribution network and ultimately detected by DNA extraction.

At class level, *Alphaproteobacteria* are known for their potential higher resistance to chlorine (Gomez-Alvarez et al., 2012), which explains their dominance in bulk water from seven sampling locations. On the other hand, *Gammaproteobacteria* includes the faecal indicator *E. coli* and genus *Salmonella*, *Yersinia*, *Vibrio*, and *Pseudomonas* (Williams et al., 2010). With regards to bacteria genera, *Bacillus* was the unique common genus present in both habitats; it was present mainly in biofilms but was also detected in bulk water. Members of this group are ubiquitous in the environment, they can form spores that are advantageous as a survival strategy under environmental and nutritional stresses (e.g., disinfectant presence). Species of the genus *Bacillus* are also known for their ability to form a biofilm in different environments (Checinska et al., 2015).

Another example of adaptive-response strategies is the genus *Deinococcus*, which was mainly present in biofilm samples and shows high resistance to ionizing-radiation (gamma and/or UV radiation) (Rainey et al., 2005). This ability may not be related to environmental adaptation since

natural sources of this type of radiation on Earth does not reach the resistant levels showed by these bacteria; compensation of desiccation has been suggested as an explanation for radio-tolerance ability (Rainey et al., 2005). Its presence in biofilm samples may also be a strategy to survive in a hostile environment such as DW pipes.

The water source of the studied DWDN is a river, and its basin supports a diverse range of domestic and industrial activities, which have led to concerning water quality issues (Ocampo-Duque et al., 2013). In addition, soil surrounding the DWDN entering to the network during repair activities and fittings and pipelines replacement may also affect the microbial communities in DWDNs. For example, genera including *Thermoflavimicrobium* and *Phyllobacterium* were highly abundant in bulk water samples at several sampling points. These organisms have been previously reported in soil-related habitats (Rojas et al., 2001; Yoon et al., 2005). Then their presence may be explained by the characteristics of raw water source. Bacteria with anaerobic metabolism were detected only in biofilm samples. *Holophaga* genus includes only one validly described species: *H. foetida*, which was isolated from a dilution series in liquid media inoculated with black anoxic freshwater mud from a ditch in Germany (Itoh et al., 2011). The origin of this microorganism may be the water source which belong to a water basin highly contaminated due to domestic and industrial activities (Ocampo-Duque et al., 2013).

Genus *Desulfovibrio* was only present in point 2 (11.89%), which corresponds to a cast iron pipe sample. These organisms are sulphate-reducing bacteria (SRB), related to iron corrosion. *Desulfovibrio* finds a favourable environment in this kind of pipes, most likely promoting its corrosion and potentially leading to failure. Tubercles found in the sampled piece of pipe (Figure 3-6) may create limited oxygen environment for the growth of these bacteria (Douterelo et al., 2014b). Similar high abundance of this genus was detected by Ren et al. (2015) in 11-years old cast iron pipes (16.90%); however Sun et al. (2014) reported low abundance of *Desulfovibrio* (0.01-0.19%) in 20-years old cast iron pipes. This may be related to the temperatures associated to the sampling campaign; while Ren et al. (2015) carried out their field work between January and September, which are characterized for temperatures between 3-33 °C (TravelChinaGuide, 2017), Sun et al. (2014) measured temperatures between 9-20 °C for the seven water supply systems considered in their study. Temperature indirectly affects pipe corrosion because parameters such as biological activity, dissolved oxygen solubility, solution properties (e.g., viscosity), ferrous iron oxidation rate, and thermodynamic properties of iron scale vary with temperature. Such parameters directly influence corrosion of iron pipes (McNeill and Edwards, 2002). Corrosion of metallic pipes in

DWDNs is inconvenient because tubercles reduce the hydraulic capacity of the pipes due to the scales formation and the accumulation of iron and manganese particles (Douterelo et al., 2014b).

Methylotrophic bacteria were detected in five bulk water samples. *Methylobacterium* genus includes methylotrophic organisms (Leisinger et al., 1994), which are ubiquitous in different environments including soil, freshwater, drinking water, lake sediments, leaf surfaces, and root nodules (Leisinger et al., 1994). This genus is able to degrade DBPs such as HAAs (particularly dichloroacetic acid) (Zhang et al., 2009), and they are biofilm formers with high resistance to sodium hypochlorite disinfection in single-species biofilm (Simões et al., 2010). Importantly, *Methylobacterium* has not been found yet in non-chlorinated DWDNs (Martiny et al., 2005; Liu et al., 2014). Therefore, the presence of these microorganisms in DWDNs should be considered as a potential indicator of DBP presence, despite of *Methylobacterium* presents facultative metabolism and it is able to use a wide range of organic compounds as sources of carbon and oxygen (Gallego et al., 2005). Therefore, the presence of methanotrophs in biofilm samples may indicate the presence of anoxic layers within the biofilms, as discussed previously for the genus *Desulfovibrio*. Such anoxic environment inside of the biofilms leads to the formation of methane by methanogenic organisms, which can be consumed by methanotrophic organisms living inside of the biofilm and bulk water if methane was transported to this habitat. On the other hand, it has also been identified utilization of chloroform in co-metabolic processes by *Methylobacterium* (Patel et al., 1982) and *Methylosinus* (Park et al., 1991). The negative association identified between TTHMs and *Methylobacterium* may be related to an inverse relationship between THMs and HAAs, since reduction of HAAs concentrations has been found with higher retention times (Tung and Xie, 2009).

Pseudomonas was common in most of the biofilm samples (8 of 9 points) but was not the dominant genus. While *Pseudomonas* was present as the dominant group in the initial process of biofilm formation in 28-days-old biofilms (Douterelo et al., 2014c), Henne et al. (2012) found that biofilm communities sampled at nearby points were similar, then the authors hypothesised that during several years physically related biofilm communities will show similar community structures. In contrast, the current study found that dominant bacterial communities of the studied DWDN (25-57 years old) were different in each sampling point; therefore, the present results show that biofilms do not present properties of either young or old biofilms. This may be related to the unstable hydraulic conditions of this water network, which may partially remove biofilm components, then altering the structure of bacterial communities. Similarly, in a laboratory-based full scale DWDN, high flow variations indicated the promotion of young biofilms with more cells and less EPS, by the potential cyclic removal of the first layers of the biofilms (Fish et al., 2017).

Bacteria groups, which include pathogenic and opportunistic organisms, were also observed in biofilm and bulk water samples. *Acinetobacter* was detected in four biofilm samples; members of this genus are ubiquitous in the environment, biofilm formers, and have been found in wastewater treatment reactors, in infected patients, and contaminated clinical devices (Carr et al., 2003; Lin et al., 2003). In bulk water, *Brucella* was also found in four samples; this genus comprises 11 species and 10 of them are associated with human infections (Scholz et al., 2010; Xavier et al., 2010).

Results of this study indicated the presence of genus *Staphylococcus* in bulk water (RA = 0.04-7.07%) and biofilm samples (RA = 0.08-10.91%). Ji et al. (2015) also found this organism in water samples collected from a building plumbing system. Due to this genus constitute a major component of the human microflora (Heilmann et al., 1996), Ji and collaborators discarded the hypothesis of samples contamination since these bacteria were absent in the blanks (Ji et al., 2015). In the present study, Illumina sequencing was not run in blanks but this genus has been isolated from a model-laboratory DWDN and cultured in dual biofilms, being classified as a moderate biofilm former (Simões et al., 2007); this ability is used to colonize hospital devices. In addition, *Staphylococcus aureus* was also detected in bulk water from a rural DW system (Lechevallier and Seidler, 1980). It can be hypothesised that the source of this opportunistic pathogen could be the surface raw water, since the river basin is highly contaminated due to human and industrial activities (Ocampo-Duque et al., 2013).

3.4.3 Influence of network characteristics over the bacterial communities and richness and diversity indices in biofilms and bulk water samples

The higher richness and diversity in biofilms than in bulk water samples can be related to the favourable conditions offered by this microenvironment for bacteria survival such as protection against disinfectant and higher availability of nutrients. Douterelo et al. (2013) also found in 28-days old biofilms higher diversity and richness in biofilms in a chlorinated DWDN, indicating that only certain bacteria in bulk water have the ability to produce EPS and attach to pipe walls. For instance, *Bacillus* was the only common genus detected in the two habitats. *Bacillus* can form spores that protect them from disinfection in bulk water and allow them to attach to biofilms, then when the environmental conditions are favourable they start developing as active cells (Checinska et al., 2015). Conversely, Henne et al. (2012), based on 16S r RNA fingerprints of extracted DNA and RNA, found that richness of microbial communities was higher in bulk water than biofilms from a 20-year-old DWDN. The authors argue that only those bacteria that can actively contribute to the

succession of the biofilm were successful in colonizing biofilms, while bacteria that cannot fill perfectly the narrow niches in biofilms vanished over time.

Relationship between pipe age and unit dry biomass may be related to the detachment of some asbestos fibres which was observed during biofilm scrapping from the sampled pipes and is representative of the potential wear of the pipe material in time, due to the biological activity. The influence of removal of such fibres was described by Wang et al. (2011), who tested the biological activity in 53-54 years-old sections of asbestos pipes. By establishing microbial activity of iron-reducing bacteria (IRB), SRB and biofilm-former bacteria in the patina layer (porous layer, mainly composed of microbial biomass along with interwoven asbestos fibres) of those pipes sections, they established that such microbial activity leads to deterioration of asbestos pipes and potential leakages (Wang et al., 2011). In this study, IRB were observed in biofilm samples, corresponding to 24-56 years-old pipe sections, such as genus *Geobacter* (RA: 1.96-4.51%) and family *Rhodobacteraceae* (RA: 3.74-8.87%); SRB such as genus *Desulforegula* (RA=1.15%), *Syntrophobacter* (RA=1.08%), and *Clostridium* (RA=1.00-3.74%) were also detected.

Although these microbial groups were present with low RA, this fact may indicate the presence of an anoxic layer in asbestos pipes, which promotes the acidification of the media due to the production of organic acids from anaerobic metabolism, leading to local pH decrease. This facilitates the weathering and dissolution of the acid-receptive minerals in hydrated cement matrix, thus, creating pitting and voids within a pipe wall. In the long term, this process continuously caused by biological activity can be considered as biodegradation of asbestos material in water pipes (Wang et al., 2011).

The influence of pipe material on the bacteriological composition of biofilm samples is reflected on the presence of SRB such as *Desulfovibrio*, which was present exclusively in CI pipes. *Desulfovibrio* finds a favourable environment in this type of pipes, most likely promoting its corrosion and potentially leading to failure. Similar high abundance of this genus was detected by Ren et al. (2015) in 11-year old CI pipes however, Sun et al. (2014) reported low abundance of *Desulfovibrio* (0.01-0.19%) in 20-year old cast iron pipes. The tubercles found in the sampled piece of pipe (Figure 3-6) may create a favourable environment for the growth of these bacteria. Additionally, such tubercles can reduce the hydraulic capacity of the pipes due to the formation of scales and the accumulation of iron and manganese particles (Douterelo et al., 2014b). Several studies have confirmed the impact of pipe material over the structure of microbial communities in biofilm samples collected from simulated DWDNs (Wang et al., 2014), bench-scale pipe section reactors (Mi et al., 2015), and real-scale DWDNs (Ren et al., 2015). Although there is not an

absolute consensus about the best material to minimize biofilm growth, in general, plastics appear to be advisable over metals and cements (Fish et al., 2016).

With regards to water age (8-16 hours), the effect of this factor on the biofilms bacterial communities may be associated with the relationship between this parameter and physicochemical characteristics of DW, which was previously discussed. In addition, chlorine low concentrations, stagnation and low velocities conditions associated with high water age lead to increase the cells count in bulk water (Nescerecka et al., 2014) and favour biofilm formation (Fish et al., 2016). Water age is considered as a factor influencing the biological stability of DW (Prest et al., 2016). This was corroborated by Wang et al. (2014) who established in simulated-DWDN biofilm samples that water age (2.3 and 5.7 days), disinfectant, and pipe material interact with each other to create distinct physicochemical conditions and ecological niches, in which various microbes can be selected and enriched in DW systems. Results of Ji et al. (2015) also confirmed that water age (3, 4.5 and 6.5 days) can influence the shifts in microbial communities in building plumbing and obviously affected free chlorine, and selectively influenced lead, copper, and zinc concentrations for certain pipe materials.

In this line, the main purpose to maintain residual disinfectant in a DWDN is to minimise any potential microbiological contamination, taking advantage of its fast oxidation ability, resulting in microorganisms' inactivation, despite the protective effect caused by EPS in the biofilm matrix (Xue et al., 2013). Spearman's correlations showed no associations between indices and concentrations of free chlorine. Due to continuous variation of free chlorine in bulk water, hourly monitoring of this variable assisted by online devices in the network is recommended in order to test further correlations. Points with potential high water age are suggested to monitor residual disinfectant such as extreme points of the DWDN, service reservoirs, storage tanks, and dead-end sections (Montoya et al., 2009).

ANOSIM indicated statistical significant differences among species for the factor pH, which was also correlated positively with both richness and diversity indices. Due to the relationship between pH and alkalinity and the governance of this factor over the relative proportions of hypochlorous and hypochlorite, which present different disinfection efficacies, pH is impacting the variability in the water bacterial community as found by Sun et al. (2014); Ji et al. (2015) also determined higher individual association of pH with the bacteria and archaea organisms in water samples.

Temperature and richness index were negatively correlated; similar results were found by Henne et al. (2013) by comparing microbial communities of cold and hot water ($\Delta T=41$ °C approximately);

cold water presented higher community diversity and high stability over time. This study considered $\Delta T=3$ °C, which corresponds to typical temperature values for tropical cities with hot weather. Deeper analysis should be done in relation to the influence of temperature variation in DWDNs in tropical weather.

3.5 SIGNIFICANCE AND LIMITATIONS OF THE STUDY

The current study collected samples, one sample in time, of bulk water and biofilm in nine points of a DWDN located in a tropical-climate city, where warm temperatures dominate. The bacterial communities were assessed in both habitats, and other physico-chemical parameters were used to characterise them, with special focus on THMs. It is important to acknowledge that size of data is small and temporal variation was not included in this study. It is important to highlight that the p-value of some correlations was slightly higher than the level of significance, which may be associated with the limited number of data collected in this study. The current procedures for attention of leakage repairs also represents a challenge on developing demanding field work studies like the current one, considering that the normal operation cannot be interrupted for sampling activities, consequently, then randomness governs a sampling plan. O&M staff must prioritize the repairs according to the size and type of affected population (e.g., big neighbourhoods, areas with hospitals and education institutions); therefore sampling activities must be carried out in a long term if the scope included the evaluation of more strictly engineered variables such as water age, pipe age, pipe materials, type of network component (pipelines, valves, water meters), among others.

The field assessment approach presented here represents a progress in the study of the bacterial composition in Cali's DWDN, which exhibits several O&M challenges in relation to the loss of hydraulic integrity. To the author knowledge, this is the first time molecular analysis are applied to study, at full scale, the microbiological drinking water quality in this water network. This allowed to correlate biotic parameters with engineered characteristics, then some O&M recommendations were produced, which may be useful to the water utility. The author is aware that some communication mean must be identified in order to present and explain the findings of this study to the water managers of the studied water network.

The bacterial composition of habitats bulk water and biofilm in the studied DWDN was identified by DNA extraction, which only allows indicating the presence of particular bacteria, but it is not possible

to determine when they entered to the system, for how long they have been there, what the exact source is, and if they were metabolically active, viable and/or cultivable. As economical, technical, and trained human resources improves in developing countries such as Colombia, the research and knowledge transfer with regards to biofilms and their interactions with other variables in DWDNs can be promoted. For instance, the recent work by Lemus Pérez and Rodríguez Susa (2017) used biofilms grown with drinking water treated by a WTP in Bogotá (Colombia) to quantitatively assess the influence of the type of EPS in the potential formation of several species of DBPs.

Further studies should incorporate the analysis of RNA and active genes in order to improve the characterization of the role played by microorganisms and their interaction with engineered factors of DWDNs. Additionally, the temporal variation of bacterial communities in DWDNs can also be assessed; Bautista-de los Santos et al. (2016) found that bacterial community composition is significantly different across sampling sites for time-periods during which there are typically rapid changes in water use, which suggests hydraulic changes (driven by changes in water demand) contribute to shaping the bacterial community in bulk drinking water over diurnal time-scales. In relation to hydraulic changes, monitoring turbidity also contributes to identify the relationship between this parameter and the presence of particles, cells, and biofilm detached clusters in bulk water (Douterelo et al., 2013; Douterelo et al., 2014b).

3.6 CONCLUSIONS

The application of sequencing analysis represents a step forward in the study of microbiological aspects of DWDNs in tropical-climate countries. The key findings from the study are:

- Most of the bacterial communities identified in this work have also been found in temperate-weather water systems. This may indicate that some drinking water bacteria are ubiquitous and that treatment and engineered environments shape the bacterial communities in a specific way.
- Similarly to temperate-climate DWDNs, bacterial communities in sampled biofilms are different from those in bulk water, with the former more diverse and richer.
- Pipe age, pipe material, water age, free chlorine, pH and temperature were associated with microbiological parameters indicating that these are key to the composition of bacterial communities. Deeper analysis should be done in terms of the influence of temperature variation in DWDNs in tropical climates.

- Pipe material influences the microbial ecology of DWDNs. *Desulfovibrio* was identified exclusively in the CI pipe.
- Methylophilic bacteria were found in biofilms and bulk water; these microorganisms are known to be able to degrade DBPs as HAAs.
- Significant correlation was found between RA of *Methylobacter* and *Methylobacterium* and TTHM concentrations in bulk water.
- Design and O&M of DWDNs should consider all the possible procedures to minimise biofilm growth to manage both biological and chemical stability of drinking water

4 A SIMPLE BIOFILM CHLORINATION MODEL

4.1 INTRODUCTION

Modelling is an increasingly important tool for O&M activities in the drinking water industry. It is an especial useful tool to help cope with the complexity of DWDNs. Modelling in this context can be classified in two major groups: hydraulic and water quality modelling, with the later one dependent on the first one. Modelling offers useful information using relatively few resources, however it presents challenges mostly related to obtaining reliable primary information (inputs) and validation. In addition, qualified personnel are required to use the model depending on the software and its level of elaboration, and interpret results.

As was discussed in Chapter 2, chlorine decay and DBP formation are the most common targets for water network operators, while biofilm modelling has been addressed mainly for research purposes. Recent laboratory studies have determined that components of the biofilm matrix such as cells, EPS, trapped organic matter, and biomolecules act like DBP precursors (Hong et al., 2008; Fang et al., 2010a; Fang et al., 2010b; Wang et al., 2012c; Wang et al., 2013a; Wang et al., 2013b; Lemus Pérez and Rodríguez Susa, 2017). Despite this, the contribution of biofilms to DBP formation has scarcely been considered in DWDNs models. To the author's knowledge, there is only one study published that includes the contribution of planktonic cells, biofilms, and detached biofilm clusters in the THM formation in main trunk pipes and dead-end zones (Abokifa et al., 2016a).

The literature review of Chapter 2 indicates that DBP and biofilm modelling have been developed separately. Empirical DBP models have been proposed to predict DBP concentrations in drinking water considering the main influencing factors such as time, pH, temperature, precursors, disinfectant dose, and bromide concentration. In relation to precursors, variables such as TOC, DOC, algae, chlorophyll, UV_{254} , and SUVA have been used. The last two have been applied as precursor indicators, but biofilms have not been included yet in empirical models. These models are site-specific since they include the peculiar conditions of each studied DWDN such as seasonal variations, water quality parameters and type of water treatment process or technology.

DBP models have been mainly developed to offer water quality information in the DWDNs, while drinking water biofilm models have been aimed at avoiding, minimizing and/or controlling biofilm growth. Considering the important role played by EPS in initial formation, growth, and survival of biofilms; several models have included the EPS production by bacteria (Kommedal et al., 2001;

Xavier et al., 2005a; Xavier et al., 2005b; Duddu et al., 2008; Zhang et al., 2008; Duddu et al., 2009; Cogan, 2010; Cogan, 2011; Lindley et al., 2012; Clarelli et al., 2013; Ghosh et al., 2013; Macías-Díaz, 2015; Tierra et al., 2015; Zhao et al., 2016).

The model proposed here aims to improve the DBP prediction in water systems by better comprehension of the role of biofilms as DPB precursors in plumbing systems, where stagnation conditions are predominant and DBP exposure occurs. The model predicts the DBP formation potential in one-dimension and involves chlorine as disinfectant and chloroform and DCAN as DBPs. Chloroform and DACN were selected because the first is the most abundant and predominant DBP in drinking water and the second is the most predominant haloacetonitrile species detected in drinking water (WHO, 2017) and in biomass disinfection tests (Wang et al., 2012c), and it has been recognized as a more toxic substance than HAAs (Muellner et al., 2007).

To the author's knowledge, models representing the contribution of the biofilms to the bulk water have been developed only for particulate substances such as biofilm erosion or detachment, but not for dissolved substances. Following this line, the current model represents an original approach in biofilm and DBP modelling by considering the biofilm matrix as an organic matter reservoir penetrated by chlorine, which oxidizes EPS and cells, then transforming a fraction of them into chloroform and DCAN, separately, which are then transported by diffusion from the biofilm to the bulk water. The influence of pertinent parameters on bulk water concentrations is discussed, and the model applications and limitations are also explained.

4.2 MODEL DEVELOPMENT

4.2.1 Model definition

According to Vannecke et al. (2015), it is likely a general rule that increased complexity concerning microbial diversity and/or meso-scale aggregate architecture will be more useful when the focus is on understanding fundamental micro-scale outputs. When the focus is on macro-scale outputs (e.g., substrate removal rates, optimal bulk condition), this complexity is clearly not always necessary. However, under some conditions, such additional model features can be critically informative for bulk reactor behaviour prediction or understanding.

The main purpose of the model developed in this chapter is to represent the formation potentials of chloroform and DCAN by the oxidation of the biofilm matrix with HOCl. As the diffusion processes of simulated substances occur in minutes, biofilm growth, decay and detachment and EPS

formation occur in hours (Picioreanu et al., 2000a), initial constant concentration of cells and EPS and their decay due to the reaction with chlorine within the biofilm were considered. A 1D model was produced to initially represent the experimental results from Wang et al. (2013a), and then the model was extrapolated to plumbing pipes under conditions where stagnation prevails. A schematic representation of the model is presented in Figure 4-1.

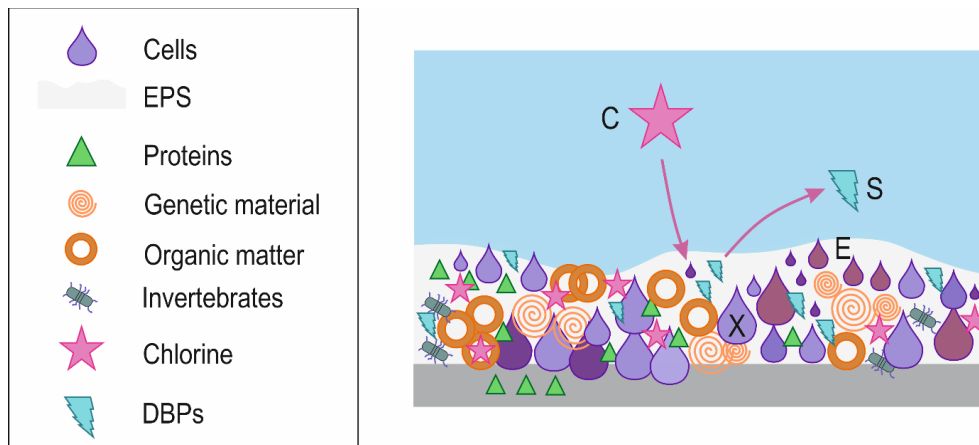


Figure 4-1. Schematic representation of the 1D model

The main assumptions made when developing the current model are:

- Closed system: Glass vessels used in laboratory experiments and drinking water pipes under normal operation can be considered closed systems, where there is not an exchange of materials with the surrounding environment. Therefore, the model presented here also represents a closed system.
- Stagnant fluid: During the evenings, stagnation conditions can be present in DWDNs, especially in residential areas. In plumbing systems, water can be stagnant during periods of no consumption of water such as the evenings, weekends, or holiday seasons.
- Flat biofilm: A biofilm can be compact or present voids and channels within itself. Compact biofilms are the result of systems limited by the biomass growth rate. Finger-like and mushroom-like biofilms are generated in systems limited by the substrate transport (Picioreanu et al., 1998b). Biofilms with irregular surfaces gradually shift to compact biofilms with smooth surface when nutrient availability increases due to higher flow velocities (Picioreanu et al., 2000a). Therefore, it is expected that, under static flow conditions, biofilm should develop with channels, voids, and rough surface. However, biofilms in drinking water pipes of plumbing systems are exposed to both turbulent flow and stagnant conditions but there is not yet evidence on the morphology characteristics of biofilms growing under these conditions. Considering that numerical simulation of complex morphologies of biofilms such as mushroom-like shape is

computationally expensive, flat biofilms were assumed here to reduce the complexity of the calculations.

- Biofilm is a continuous medium; cells and EPS are homogeneously mixed in biofilm matrix: The biofilm is treated here as a homogeneous system. Voids and channels as part of the morphology of the biofilm and the protective role of EPS against cell disinfection are not simulated in the current model to reduce geometric elaboration complexity, which would introduce further solution complexity. Since this model simulates the DBP formation potentials, this assumption means that chlorine reacts at the same time with both cells and EPS.
- Constant biofilm thickness: As described in Table 2-3, Table 2-8, and Table 4-2, biofilm growth can take several hours or days. Consequently, the computational time required to simulate biofilm growth can be in the order of hours, days or weeks, which is subject to the computational resources available. This also implies that internal boundary represented by biofilm surface is fixed, i.e., it does not change as cells and EPS are being transformed into DBPs.
- Fixed initial concentration of cells (X) and EPS (E): This was assumed as the current model simulates the DBP formation potentials and it does not include the biofilm growth.
- Bulk water is a complete mixed reactor: Laboratory experiments of biofilm disinfection have been carried out in small glass vials (40 mL, 65 mL) (Wang et al., 2012c; Wang et al., 2013a). Therefore, it is reasonable to assume this type of reactor, given the small volumes. However, plumbing systems can represent volumes of the order of litres (e.g., 6.3 L for $\phi = \frac{1}{2}$ inches and L = 50 m) and the flow is usually represented by plug flow. Such simplification must be carefully considered for risk assessment since DBP exposure at the point of use depends on which tap is first opened.
- Chloroform (S) and DCAN (S) are modelled separately according to fraction of cells and EPS converted into the respective DBP: The current model was developed to simulate individual species of DBPs in order to make it flexible. The amount of DBP species formed relies on the fraction of cells (F_x) and EPS (F_e) transformed into DBPs; then, as the experimental data are available, it is relatively easy to predict concentrations of individual DBP species from biofilm chlorination.

4.2.2 Model equations

Figure 4-2 sketches the 1D-stagnation model and the corresponding equations are included in Table 4-1. The diffusion of two dissolved substances, chlorine and DBP, through the biofilm matrix was simulated, considering cells and EPS decay. The formation of chloroform and DCAN is

expressed in terms of yield coefficients from disinfection of cells and EPS and their fraction transformed into DBP. Chloroform and DCAN were simulated separately according to each liquid diffusion coefficient and the fraction of cells and EPS transformed into the respective DBP. Bulk water concentrations of dissolved substances are defined by the boundary condition in the biofilm surface, assuming that bulk water is a complete mixed reactor (Equations (4-8) and (4-14)). Under stagnation conditions, diffusion processes are dominating the substance transport; therefore Fick's law is applied in the biofilm and source/sink terms are also included.

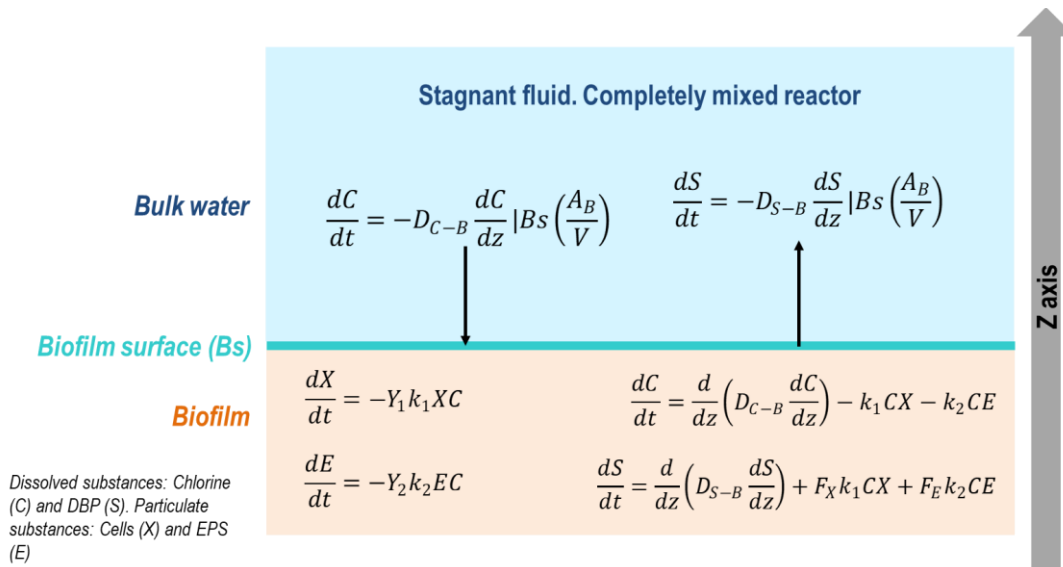


Figure 4-2. 1D mass balance equations for soluble and particulate components in biofilm and biofilm surface

Table 4-1. Model equations in biofilm

Equation	Description of variables	Subscripts
$\frac{dC}{dt} = \frac{d}{dz} \left(D_{C-B} \frac{dC}{dz} \right) - k_1 C X - k_2 C E$ <p style="text-align: center;">(4-1)</p>	C: Disinfectant concentration X: Cell concentration E: EPS concentration k ₁ : Disinfectant decay rate – cells disinfection k ₂ : Disinfectant decay rate – EPS oxidation D _{C-B} : Molecular diffusion coefficient of chlorine in biofilm A _b : Biofilm area V: reactor volume t: Time	C: Chlorine S: DBP X: Cells E: EPS B: Biofilm L: Bulk liquid Bs: Biofilm surface

Equation	Description of variables	Subscripts
$\frac{dX}{dt} = -Y_1 k_1 X C$ <p style="text-align: center;">(4-2)</p>	X: Cell concentration k ₁ : Disinfectant decay rate – cell disinfection Y ₁ : Cell-chlorine yield coefficient	
$\frac{dE}{dt} = -Y_2 k_2 E C$ <p style="text-align: center;">(4-3)</p>	E: EPS concentration k ₂ : Disinfectant decay rate – EPS oxidation Y ₂ : EPS-chlorine yield coefficient	
$\frac{dS}{dt} = \frac{d}{dz} \left(D_{S-B} \frac{dS}{dz} \right) + F_X k_1 C X + F_E k_2 C E$ <p style="text-align: center;">(4-4)</p>	S: DBP concentration D _{S-B} : Diffusion coefficient of chloroform/DCAN in biofilm X: Cell concentration E: EPS concentration F _X : Fraction of cells transformed into DBP F _E : Fraction of cells transformed into DBP	

4.2.3 Parameters selection

4.2.3.1 Biofilm thickness (BT)

Considering that the current model does not include bacteria growth, biofilm thickness (BT) arises as an important input parameter, since it defines the domain size and other parameters such as initial concentration of EPS (E₀). In order to define appropriate values of BT, several drinking-water-related studies were reviewed to identify the reports of this parameter. BT values and the experimental conditions of these studies are described in Table 4-2. It should be noted here that conditions such as inoculum, incubation time, method of BT measurement are diverse and it is also not possible to identify any correlation between biofilm and thickness and biofilm age (see Table 4-2).

Table 4-2. Review of biofilm thickness data reported by drinking-water-related studies

Study	Tests description					Biofilm thickness (µm)
	Type of reactor for biofilm growth / experiments	Incubation time	Inoculum / Bacterial community	Substrate medium	Method for measuring biofilm thickness	
Chen and Stewart (1996)	Artificial biofilms growth in flow cell	N.S	Bacteria <i>P. aeruginosa</i> ERC1 dispersed in agarose gel slabs	Rich medium	Optical method of Bakke and Olsson	773
						428
						476
						771
						456
						526
Peyton (1996)	Annular reactor	14.6 days	Bacteria <i>P. aeruginosa</i>	Minimal-salts medium with glucose	Optical method of Bakke and Olsson	6.2
						17.61
						31.85
Heydorn et al. (2000)	Laboratory channel flow cells	1 day 2 days 4 days 7 days 10 days 1 day 2 days 4 days 7 days 10 days 1 day 2 days 4 days 7 days 10 days 1 day 2 days 4 days 7 days 10 days	Bacteria <i>P. putida</i>	Modified FAB medium supplemented with sodium citrate	CLSM images processed using the program COMSTAT	0.27
						0.78
						3.03
						4.36
						7.46
			Bacteria <i>P. aureofaciens</i>			2.33
						2.41
						3.75
						5.17
						7.06
			Bacteria <i>P. fluorescens</i>			0.66
						1.37
						3.21
						5.61
						8.47
			Bacteria <i>P. aeruginosa</i>			3.43
						2.49
						4.96
						4.52
						5.65
Xue et al. (2012)	Laboratory channel flow cells	6 days	Bacteria <i>P. aeruginosa</i>	0.02 strength LB broth	CLSM images processed using the program COMSTAT	30
						40
Xue and Seo (2013)	Laboratory channel flow cell	6 days	Bacteria <i>P. aeruginosa</i> - algT(U) - no disinfection	Nutrient growth medium: 0.02	CLSM images processed using the	159

Study	Tests description					Biofilm thickness (µm)
	Type of reactor for biofilm growth / experiments	Incubation time	Inoculum / Bacterial community	Substrate medium	Method for measuring biofilm thickness	
			Bacteria <i>P. aeruginosa</i> - PAO1 - no disinfection	strength LB broth	program COMSTAT	162
			Bacteria <i>P. aeruginosa</i> - mucA22 - no disinfection			164
			Bacteria <i>P. aeruginosa</i> - algT(U) - chlorine disinfection (0.5 mg/L)			44
			Bacteria <i>P. aeruginosa</i> - PAO1 - chlorine disinfection (0.5 mg/L)			85
			Bacteria <i>P. aeruginosa</i> - mucA22 - chlorine disinfection (0.5 mg/L)			149
Xue et al. (2014)	Laboratory channel flow cells	6 days	Bacteria <i>P. aeruginosa</i> - algT(U) - disinfected with monochloramine	0.02 strength LB broth	CLSM images processed using the program COMSTAT	38
			Bacteria <i>P. aeruginosa</i> - PAO1 - disinfected with monochloramine			47
			Bacteria <i>P. aeruginosa</i> - mucA22 - disinfected with monochloramine			46
			Bacteria <i>P. putida</i> - disinfected with monochloramine			48
Shen et al. (2016)	PVC coupons in CDC laboratory reactors	1 year	Groundwater source for drinking water		Optical coherence tomography	120
		1 month				93

N.R: not reported | CLSM: confocal laser scanning microscopy | CDC: Centres for disease control and prevention

From Table 4-2, 43 BT values were reported in seven studies and their descriptive statistics are included in Table 4-3. Figure 4-3 revealed that 50% of biofilm thickness values varied between 4 and 107 µm (quartiles 1 and 3 -Q1, Q3-). This range was used to randomly vary this parameter in

simulations with the current model. It is worth noting that all the reviewed studies (Table 4-2) used bacteria *Pseudomonas* for their experiments since they are EPS producers, then biofilm formers, and have been identified in DWDNs, in both temperate and tropical climate locations. As described in Chapter 3, *Pseudomonas* genus was common in most of the biofilm samples (8 of 9 points) collected in Colombia. Douterelo et al. (2014c) identified *Pseudomonas* genus as the dominant group in the initial process of biofilm formation in 28-days-old biofilms in a laboratory-based full scale DWDN fed with drinking water supplied to the city of Sheffield (UK).

On the other hand, the study of influence of long-term disinfection on mechanical properties of biofilms (Shen et al., 2016) found that BT is recovered after one month of continuous chlorination (4 mg/L), in relation to initial BT before tests. It is therefore reasonable to assume that the thickness of laboratory-incubated biofilms over two weeks is fairly presentative of more established biofilms.

Table 4-3. Descriptive statistics of biofilm thickness reported in Table 4-2

Descriptive statistic	Biofilm thickness (μm)
Minimum	0.27
Q1	4
Median	18
Q3	107
Maximum	773
Average	111
Std. deviation	199
CV	178%
Number of data	43

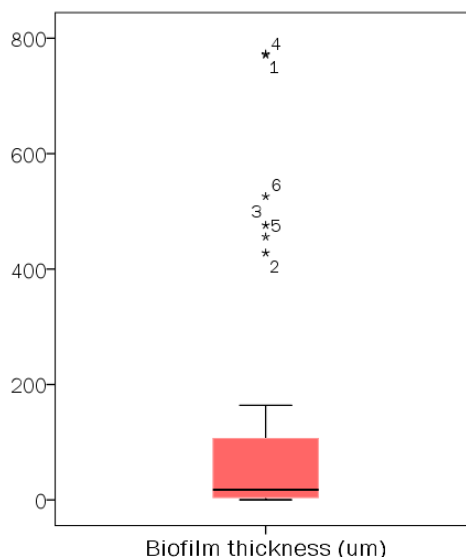


Figure 4-3. Box plot biofilm thickness data

4.2.3.2 Initial volumetric biofilm density (X_0)

The DBP potential formation experiments developed by Wang et al. (2013a) managed cells density 6.5 ± 0.6 CFU/cm², on a PVC surface, in glass vial volume (65 mL), chip area (1×10^{-4} m²), and number of chips per disinfection tests (10)¹⁰. In order to convert the cell density data into volumetric density, the relationship between cell counting units and biomass for *P. aeruginosa* developed by Kim et al. (2012) was used (Equation (4-5)). They cultured bacteria on Luria-Bertani medium, in 1 L flask, and harvested them for further colony counting and measurement of dry weight of biomass (Kim et al., 2012). The authors recommended application of this relationship in transport models in

¹⁰ J.J. Wang, 2016, personal communication, 19th January 2017

aquifers since cell concentrations in water samples are usually determined by counting methods (Kim et al., 2012). The initial volumetric biofilm density was then established equal to 40.87 mg/L.

$$Y = 1.8 \times 10^8 X - 3.6 \times 10^6 \quad (4-5)$$

Here Y is colony forming unit (CFU/mL) and X is biomass (mg/mL). In order to simulate the formation of DBPs in pipe/plumbing systems, cell density data was reviewed in studies previously published, which consisted of biofilm monitoring in real-scale DWDNs by installation of coupons or biofilm reactors. The cell density was determined by the methods 4',6-diamidino-2-phenylindole staining and epifluorescence microscope; data and further details of the reviewed studies are presented in Table 4-4.

Table 4-4. Review of cell density data in drinking water biofilm reported by other researchers

Author	Tests description					Total cell count (cells/cm ²) (a)
	Type of reactor	Biofilm age	Pipe/coupon material	Water quality	Area	
Kalmbach et al. (1997)	Two reactors were installed in a domestic DWDN at U. of Berlin (water taps)	35 days	Glass	Cl: 0 mg/L, T: 12.2 °C, TOC: 3.3 mg/L	2 cm ²	7.20E+05
			PE			4.30E+06
		56 days	Glass			7.20E+05
			PE			1.80E+06
		70 days	Glass			7.00E+05
			PE			1.50E+06
Wingender and Flemming (2004)	Two biofilm reactors located at the outlet of WTP in Germany (no disinfected drinking water) and within the DWDN	18 months	Steel, PVC, and PE	T: 11.7 °C	1650 mm ²	3.60E+06
						3.10E+07
	18 pipe sections	(2-99 years old)	Cl	Cl: <0.01 - 0.13 mg/L	Several	7.00E+06
			Cement-lined			3.00E+05
			Galvanized steel			2.00E+08
			PVC			4.80E+05
						5.00E+07
						8.00E+05
1.60E+07						
Lee and Schwab (2005)	Semi-pilot ϕ 13 mm, L=8.8 m connected to a DWDN in Seoul	84 days	Galvanized iron	Cl < 0.3 mg/L, T: 16.0 - 25.1 °C, TOC: 1.27 - 2.65 mg/L	975 mm ²	7.00E+06
Långmark et al. (2005)	Pilot plant prior to the distribution in two systems, outlet	80-90 days	PE	Cl: 0.26 mg/L, AOC: 34 mg/L, T (winter): 6.6 °C	N.R	3.00E+04

Author	Tests description					Total cell count (cells/cm ²) ^(a)	
	Type of reactor	Biofilm age	Pipe/coupon material	Water quality	Area		
	of the WTP, PE tubing, system A			T (autumn): 7.4 °C T (summer): 18.8 °C		6.00E+04	
	System A - DWDN					4.00E+04	
	System A - Pilot plant					Cl: 0.24 mg/L, AOC: 36 mg/L, T (winter): 8.5 °C	1.00E+04
						T (autumn): 11.5 °C	8.00E+04
						T (summer): 13.2 °C	1.00E+05
	Coupons were located post treatment and at the end of the DWDN. System B					Glass	Cl: 0.09 mg/L, AOC: 15 mg/L, T (winter): 8.8 °C T (autumn): 10.7 °C T (summer): 20.8 °C Cl: 0.02 mg/L, AOC: 27 mg/L, T (winter): 9.4 °C T (autumn): 14.4 °C T (summer): 15.2 °C
	System B - DWDN			9.00E+04			
				3.00E+05			
	System B - Pilot plant			3.00E+05			
				3.50E+05			
				7.00E+05			
	Manuel et al. (2007)			Three reactors: Batch, Propella, Flow cell connected to Porto's DWDN. Batch	56 days	PVC	Cl: 0.15 mg/L, T: 15.9 °C, TOC: 2.32 mg/L, DOC: 2.12 mg/L
Propella and Flow cell		2 cm ²	5.00E+07				
Manuel et al. (2009)	Flow cell reactor connected to Porto's DWDS at different flow regimes. Stagnation - turbulent flow	20 days	PVC	Cl: 0.15 mg/L, T: 20 °C, TOC: 2.3 mg/L	2 cm ²	1.10E+07	
	Stagnation - laminar flow					2.60E+07	
	Turbulent - laminar flow					7.40E+06	
	Continuous - laminar flow					7.80E+06	

^(a) The methods 4',6-diamidino-2-phenylindole staining and epifluorescence microscope were used in every studies to count total cells

Table 4-5 and Figure 4-4 include the respective descriptive statistics of the cell density data. Ten values of X_0 were randomly selected within the range defined by Q1 and Q3 ($3 \times 10^5 - 7.8 \times 10^6$ cells/cm²) for the model developed here. By using the weight of single cell bacterium *E. coli* (6.65×10^{-10} mg), biofilm area and reactor volume, cell density count values were transformed into volumetric concentration (mg/L).

Table 4-5. Descriptive statistics of cell density in drinking water biofilm reported by other researchers

Descriptive statistic	Total cell count (cells/cm ²)
Minimum	1.00E+04
Q1	3.00E+05
Median	7.20E+05
Q3	7.80E+06
Maximum	2.00E+08
Average	1.31E+07
Std. deviation	3.55E+07
CV	271.83%
Number of data	33

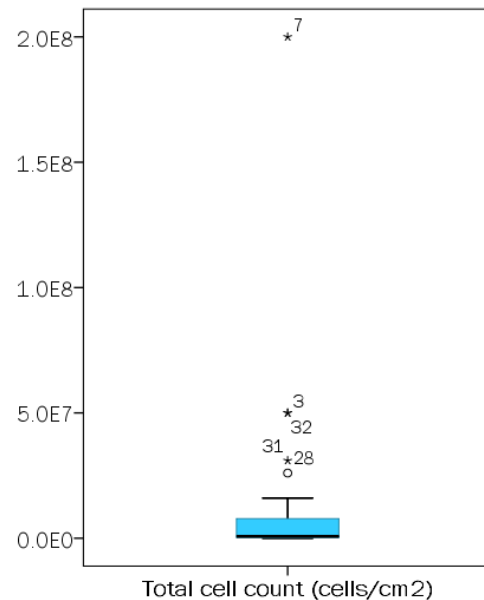


Figure 4-4. Box plot cell density data

4.2.3.3 Initial concentration of EPS (E_0)

Experimental tests of mechanical properties of drinking water biofilms indicate that EPS concentration depends on biofilm thickness. Kundukad et al. (2016) found that polysaccharides contribute to the stiffening of *P. aeruginosa* biofilms. A positive correlation was found between the biofilm surface stiffness and the micro-colony size, which was attributed to the differential expression of the biofilm's EPS according to the stages of biofilm growth. Similarly, Shen et al. (2016) concluded that long-term disinfection of one-year-old drinking water biofilms may not significantly remove net biomass; after one month of disinfection, bacteria adapt to disinfectant, produce EPS and replenish the outer layer.

Celmer et al. (2008) grew biofilms from autotrophic denitrifiers in two laboratory-scale membrane biofilm reactors, at temperatures 19.61 and 19.18 °C, and pH 7.09 and 7.02. These authors reported data of biofilm thickness, total and volatile solids, and EPS concentrations, which were used to define the linear correlation presented in Figure 4-5. This equation was included in the current model as an indirect way to involve the EPS production by cells.

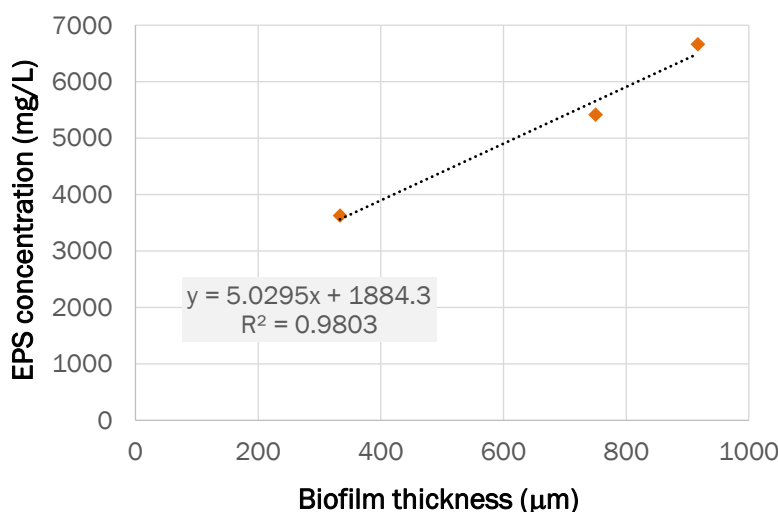


Figure 4-5. Linear correlation between biofilm thickness and EPS concentration (Celmer et al., 2008)

4.2.3.4 Effective diffusion coefficient of dissolved substances (τ_c and τ_s)

Taking into account that DBP formation from biofilm disinfection under stagnation conditions is represented by the Fick's law for the diffusive processes of chlorine and DBP that are involved, diffusion of substances reduces within the biofilm matrix in comparison to the liquid phase as a consequence of the presence of EPS (Westrin and Axelsson, 1991). Therefore, it is necessary to define a ratio of diffusion coefficients, $D_{\text{liquid}} / D_{\text{biofilm}}$ for each substance. This ratio is referred to as τ_c for chlorine and τ_s for DBPs. Chlorine diffusion coefficient in liquid and biofilm reported by Chen and Stewart (1996) were used in the present model; resulting in $\tau_c = 0.94$. The value of τ_s was defined by using several values within the range 0.016-1.0. The diffusion coefficient in liquid for chloroform and DCAN were $9.288 \times 10^{-10} \text{ m}^2/\text{s}$ and $2.67 \times 10^{-5} \text{ m}^2/\text{s}$, respectively (Buzatu et al., 2007; Poling et al., 2007).

4.2.3.5 Reaction rates (k_1 and k_2) and yield coefficients (Y_1 and Y_2)

Yield coefficients represent the mass of cells or EPS in which reactive sites have been depleted per mass or chlorine consumed (Chen and Stewart, 1996). Chlorine-cell and chlorine-EPS reaction rates and yield coefficients found by Chen and Stewart (1996) in the short-duration batch experiment (20 min) were used in the present 1D model (see Table 4-6). However these authors did not specify the temperature at which tests were carried out; for the current study, it was assumed to be 20 °C as was used by Abokifa et al. (2016a). The pH of these experiments were maintained in 7.2.

Table 4-6. Values of reaction rates (k_1 and k_2) and yield coefficients (Y_1 and Y_2)

Parameter	Value
Chlorine-cell reaction rate (k_1) (m ³ /g-sec)	1.1x10 ⁻³
Chlorine-EPS reaction rate (k_2) (m ³ /g-sec)	3.7x10 ⁻⁶
Chlorine-cell yield coefficient (Y_1) (g/g)	1.85
Chlorine-EPS yield coefficient (Y_2) (g/g)	540

4.2.3.6 Factors F_X and F_E

Factors F_X (0.7) and F_E (0.3) were used in the DBP formation equation to represent the portion of cells and EPS transformed into DBPs. Experimental data reported by Fang et al. (2010b) were processed to find the fractions of chloroform formed from disinfection of extracellular organic matter and algal cells. *M. aeruginosa* laboratory tests consisted on chlorination and chloramination of 100 mL of solutions of extracellular organic matter, intracellular organic matter, and NOM, with TOC content 5 mg/L, temperature 22 °C, pH = 7.0, during three days (Fang et al., 2010b). For DCAN, such factors were adjusted to find similar values of this DBP reported by Wang et al. (2013a) with the same values of BT resulting in similar values of chloroform reported by these authors. Such adjustment resulted in $F_X = 0.3$ and $F_E = 0.17$. These factors do not necessarily sum to one, since several DBPs may be formed simultaneously and the current model is simulating chloroform and DCAN separately.

4.2.3.7 Temperature

Temperature is widely recognized as one of the most important factors in chemical reactions by increasing reaction rates at higher temperatures. Temperature dependence of reaction rate is expressed in terms of the Arrhenius equation (Levenspiel, 1999). Having this in mind, the empirical relationship derived by Ki  n   et al. (1998) was used to indirectly include temperature within the model by adjusting the reaction rates k_1 and k_2 in the range 5-25 °C (Equations (4-6) and (4-7)).

$$k_1 = 0.0011x e^{\left(\frac{-6050}{T+273}\right)} \quad (4-6) \quad k_2 = 3.70x10^{-6}x e^{\left(\frac{-6050}{T+273}\right)} \quad (4-7)$$

Units of constants are: 0.011 m³/g-sec, -6050 K, T+273 K, and 3.70 x 10⁻⁶ m³/g-sec.

4.2.4 Boundary conditions

Table 4-7 includes the initial and boundary conditions of the model. At $t = 0$, chlorine is assumed to be completely mixed in bulk water and its concentration within the biofilm is zero; DBP concentration is also assumed to be zero in the entire domain at $t = 0$. The flux boundary condition is included in the biofilm surface (B_s) (Equations (4-8) and (4-14)); dissolved substances decay or increase according to this flux, biofilm area and reactor volume (IWA Task Group on Biofilm Modeling et al., 2006). On the substratum (pipe wall), there is no exchange of dissolved and particulate substances (i.e., no flux).

Table 4-7. Initial and boundary conditions in 1D model

Initial conditions	Boundary conditions	Description of variables	Subscripts
$t = 0$ $C_B = 0$ $C_{B_s} = C_0$	$\frac{dC}{dt} = -D_{C-B} \frac{dC}{dz} \Big _{B_s} \left(\frac{A_B}{V} \right)$ <p style="text-align: center;">(4-8)</p> $j_{substratum} = -D_{C-B} \frac{dC}{dz} = 0$ <p style="text-align: center;">(4-9)</p>	C: Disinfectant concentration D_{C-B} : Molecular diffusion coefficient of chlorine in biofilm A_b : Biofilm surface V: Reactor volume C_0 : Initial concentration of chlorine t: Time	
$t = 0$ $X_B = X_0$	$j_{B_s} = -D_{X-L} \frac{dX}{dz} \Big _{B_s} = 0$ <p style="text-align: center;">(4-10)</p> $j_{substratum} = -D_{X-B} \frac{dX}{dz} = 0$ <p style="text-align: center;">(4-11)</p>	X: Cells concentration X_0 : Initial cell concentration	C: Chlorine S: DBP X: Cells E: EPS B: Biofilm
$t = 0$ $E_B = E_0$	$j_{B_s} = -D_{E-B} \frac{dE}{dz} \Big _{B_s} = 0$ <p style="text-align: center;">(4-12)</p> $j_{substratum} = -D_{E-B} \frac{dE}{dz} = 0$ <p style="text-align: center;">(4-13)</p>	E: EPS concentration E_0 : Initial EPS concentration	L: Bulk liquid B _s : Biofilm surface
$t = 0$ $S_{B_s} = 0$ $S_B = 0$	$\frac{dS}{dt} = -D_{S-B} \frac{dS}{dz} \Big _{B_s} \left(\frac{A_B}{V} \right)$ <p style="text-align: center;">(4-14)</p>	S: DBP concentration D_{S-B} : Diffusion coefficient of chloroform/DCAN in biofilm A_b : Biofilm area V: Reactor volume	

Initial conditions	Boundary conditions	Description of variables	Subscripts
	$j_{substratum} = -D_{S-B} \frac{dS}{dz} = 0$ <p style="text-align: center;">(4-15)</p>		

4.2.5 Geometry and mesh

The current model was developed in one dimension. In this case the geometry is represented by a line with length representing the biofilm thickness. The mesh was built by dividing the line into several elements (see Figure 4-6). It was implemented within the software COMSOL Multiphysics 5.2a.

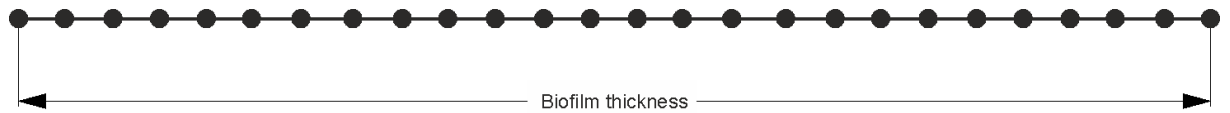


Figure 4-6. Representation of the 1D model mesh

4.2.6 Analysis of mesh dependence

Figure 4-7 shows the influence of element size on the chloroform concentration in bulk water. As it is expected, data from coarser grids are more dissimilar than those from finer grids. The percentage of difference pairs of maximal, median and average values for extremely fine and extremely coarse meshes is 17.7%, while this parameter resulted in 0.5% among extremely fine and extra fine meshes. The results presented in this chapter were obtained by employing extremely fine grids, since the computational time was very low (less than 9 s). The number of elements of every type of mesh is indicated in Table 4-8.

It is important to mention that, for simulations with the lowest BT (7 μm), the length of the elements was 0.07 μm , which may challenge the applicability of the use of continuous equations. However, implementing such low resolution was necessary in order to solve the equations representing the fast reaction between chlorine and biomass, as mentioned in section 4.2.7. Furthermore, the results of the model developed here resulted in agreement with experimental data obtained by other researchers, as discussed in the section 4.3.5.

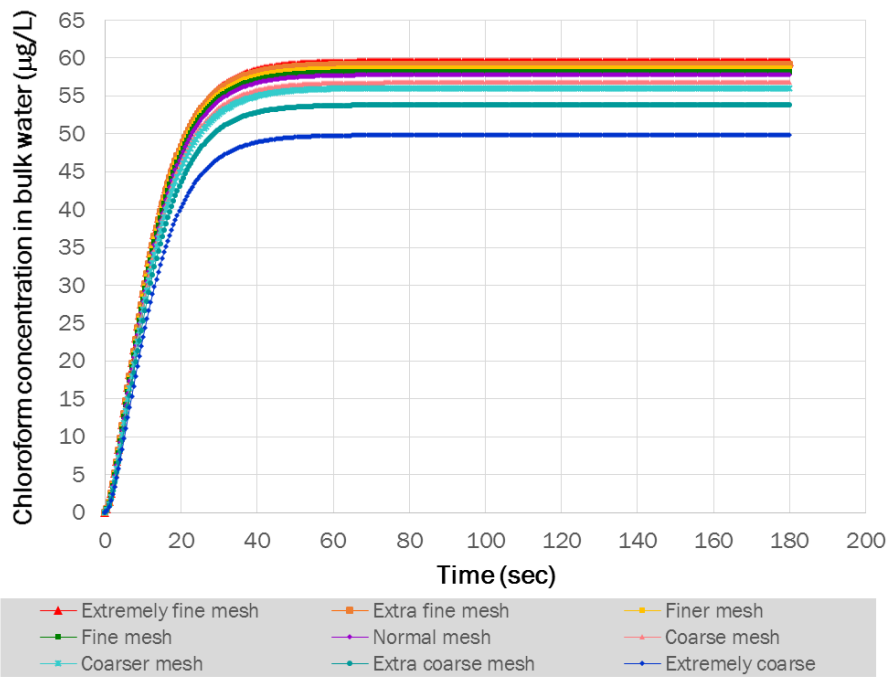


Figure 4-7. Influence of grid size on simulation results

Table 4-8. Number of elements of every type of mesh

Type of mesh	Number of domain elements	Type of mesh	Number of domain elements
Extremely fine	100	Coarse	10
Extra fine	50	Coarser	8
Finer	27	Extra coarse	5
Fine	19	Extremely coarse	3
Normal	15		

4.2.7 Processing and numerical methods

Initially, model equations were coded and solved in MATLAB R2015b by discretizing them with the explicit scheme finite difference scheme, central difference in space, and forward in time. As a consequence of the small diffusion coefficients, the model is represented by stiff equations. Therefore, small time step and grid size have to be used in order to keep the stability of the solution. This resulted in high computational time: up to 6 hours for chloroform and more than one week for DCAN simulations. For reasons of numerical efficiency, the model was implemented in COMSOL Multiphysics 5.2a, which also applies finite difference elements as numerical method and employs stabilization methods to solve the transport of species module. The computational time of COMSOL is up to 9 s using an extremely fine mesh.

The implementation of the model in MATLAB was an important step in this project because the author acquired modelling and a deeper understanding of the governing equations during this phase. Consequently, the discretization of the equations is described as it follows. Equations (4-16) and (4-17) shows the forward difference in time approximation for the dissolved substances chlorine and DBP, respectively. For the second order derivative of both chlorine and DBP, central difference in space is used (Equations (4-18) and (4-19), respectively). Then, by combining both approximations, the solution for the time and space variation of chlorine and DBP is given by Equations (4-20) and (4-21), respectively, which also include the reaction terms.

a) Biofilm sub-domain

$$\delta_t C = \frac{C^{(t+\delta t)} - C^{(t)}}{\Delta t} \quad (4-16) \quad \delta_t S = \frac{S^{(t+\delta t)} - S^{(t)}}{\Delta t} \quad (4-17)$$

$$\delta_z^2 C = \frac{(C_{i+1} - 2C_i + C_{i-1})^{(t)}}{\Delta z^2} \quad (4-18) \quad \delta_z^2 S = \frac{(S_{i+1} - 2S_i + S_{i-1})^{(t)}}{\Delta z^2} \quad (4-19)$$

$$C_i^{n+1} = C_i^n + \Delta t * \left[D_c \left(\frac{C_{i+1}^n - 2C_i^n + C_{i-1}^n}{\Delta z^2} \right) - k_1 C_i^n X_i^n - k_2 C_i^n E_i^n \right] \quad (4-20)$$

$$S_i^{n+1} = S_i^n + \Delta t * \left[D_s \left(\frac{S_{i+1}^n - 2S_i^n + S_{i-1}^n}{\Delta z^2} \right) + F_X k_1 S_i^n X_i^n + F_E k_2 S_i^n E_i^n \right] \quad (4-21)$$

To solve the boundary condition in the biofilm surface for dissolved substances, the same approximations described previously were applied (Equations (4-22) and (4-24) for chlorine and DBP, respectively). The solution of the boundary condition is given by the Equations (4-23) and (4-25); the terms with the subscript Bs+1 and Bs-1 refers to the adjacent elements to the biofilm surface in bulk water and biofilm, respectively.

b) Biofilm surface (Bs)

$$C_i^{n+1} = C_i^n - \Delta t * j_{C-Bs} \left(\frac{A_B}{V} \right) \quad (4-22) \quad j_{C-Bs} = D_{C-L} \left(\frac{C_{Bs+1} - C_{Bs-1}}{2\Delta z} \right) \frac{A_b}{V} \quad (4-23)$$

$$S_i^{n+1} = S_i^n + \Delta t * j_{S-Bs} \left(\frac{A_B}{V} \right) \quad (4-24) \quad j_{S-Bs} = D_{S-L} \left(\frac{S_{Bs+1} - S_{Bs-1}}{2\Delta z} \right) \frac{A_b}{V} \quad (4-25)$$

4.2.8 Model implementation in COMSOL Multiphysics

The current model for prediction of DBP in drinking water under stagnation conditions was implemented in the software COMSOL Multiphysics 5.2a. This software is structured by modules to represent physical and chemical processes taking place within a system. According to the specific needs of the modeller, COMSOL allows the addition of the required modules and their coupling. The modules used for running the current model and the boundary and initial conditions are described in Table 4-9.

Table 4-9. Main features for model implementation in COMSOL Multiphysics 5.2a

Module	Boundary / Domain	Condition	Initial condition (t=0)
Transport of diluted species (tds)	Wall	No flux	Co = 0 ; So = 0
	Biofilm surface (Bs)	Concentration obtained from Boundary ODE module ^(a)	
	Domain	Reactions for chlorine decay and chloroform formation	
Domain ODE	Domain	Reactions for cells and EPS decay	Xo = Xo; Eo = Eo
Boundary ODE	Biofilm surface (Bs)	Source term: Flux	Co = Co and So = 0

ODE: ordinary differential equations | ^(a) Constraint Individual dependent variables was included for coupling tds with Boundary ODE module

4.2.9 Selection of time step

Time step was determined after a sensitivity study, testing several values (i.e., 1 s, 5 s, 10 s, 30 s, 1 min, 5 min, 10 min, and 15 min). As it can be observed in Figure 4-8, no differences were identified among the eight sets of data. Percentage of difference between each consecutive pair of maximal and median values was 0.0% and less than 4.2% for average values. Thus, for short time simulations (less than 3 hours), time step was 30 s and 15 min for long time simulations (i.e., more than 8 hours).

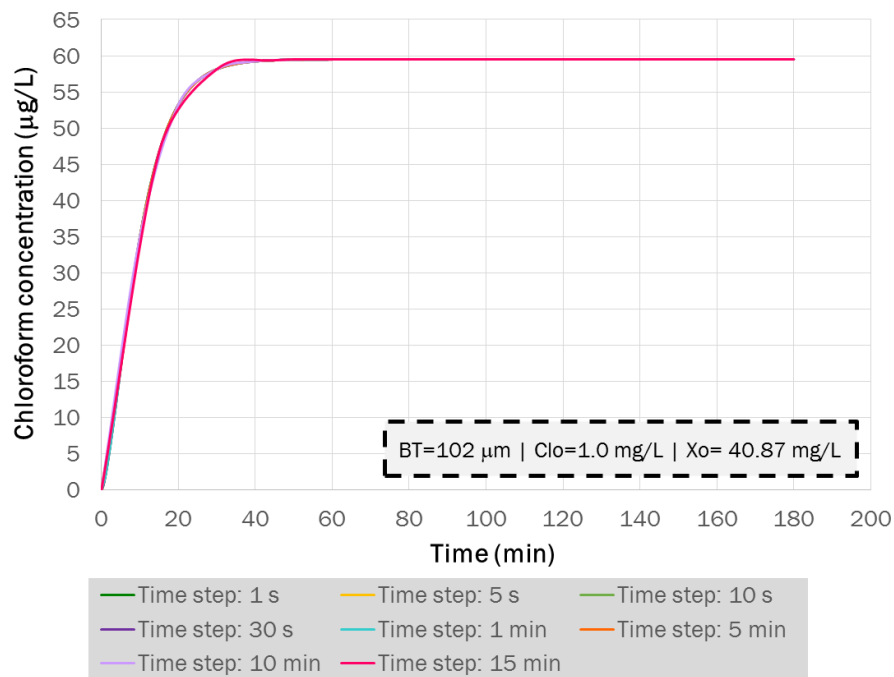


Figure 4-8. Time step comparison among chloroform concentrations in bulk water

4.2.10 Experimental study used as a reference

The work of Wang et al. (2013a) was used as a reference to compare the current model results with those obtained in their DBP formation potential tests. Their experiments considered chlorine and chloramine disinfection of *P. aeruginosa* (PAO1) biofilms, which were grown on chips with area equal to 100 mm². They used 100 mL bacterial solution and 20 mL of nutrient broth solution for both PVC and galvanized zinc chips, which were incubated at 25 °C in the dark. The cell density biofilm was monitored at 4, 8, 12, 24, 36 and 60 h; the biofilms from both types of chips reached maturation after 24 h incubation. Biofilm thickness was not reported in this study. Then, DBP formation potential was tested by disinfection of chips in 65-mL vials, at pH 8 and temperature of 20 °C, for 24 hours. The cell density was adjusted to 6.5 CFU/m².

The results for PVC chips were considered here since this material is commonly used in the DWDN of the city of Cali (53.3% of the total network length), as discussed in Chapter 3. THM and haloacetonitrile (HAN) yielded 7.7 ± 1.1 µg/mg C and 1.9 ± 0.3 µg/mg C, respectively. By considering TOC content of biofilms of ≈ 0.1 mg¹¹ and assuming that chloroform represents 71%¹² of total THMs (TTHMs) allowed determining the range of 6.6–9.6 µg/L for chloroform and 2.6-3.3

¹¹ Email: J.J. Wang, 2016, personal communication, 25th August 2016

¹² This percentage was determined by results of chlorination of *E. coli* suspension. Wang, J.-J. et al. 2013a. Disinfection byproduct formation from chlorination of pure bacterial cells and pipeline biofilms. *Water Research*. **47**(8), pp.2701-2709.

µg/L for HANs¹³. The summary of their experimental conditions and results are presented in Table 4-10.

Table 4-10. Experimental conditions and results of tests developed by Wang et al. (2013a)

Parameter	Value
pH (chlorination reactions)	8.0 ± 0.2
Temperature (chlorination reactions)	25 °C
Biofilm incubation	60 hours at 25 °C
Contact time for DBP formation potential	24 hours
TOC	0.1 mg C / 65 mL
	1.54 mg/L
Amount of chips used in DBP potential formation	10
TTHMs yields (PVC chips)	7.7 ± 1.1 mg-Cl ₂ /mg-C
HANs yields (PVC chips)	1.9 ± 0.3 mg/mg-C
Chloroform range concentration	6.62-9.46 µg/L
DCAN range concentration	2.62-3.22 µg/L

4.2.11 Data analysis

The indicator percentage of difference was widely used in order to quantify the similarities and dissimilarities among results obtained with different features of the 1D model. Percentage of difference between “value 1” and “value 2” is expressed in the Equation (4-28).

$$Difference = Value 1 - Value 2 \quad (4-26)$$

$$Average = \frac{Value 1 + Value 2}{2} \quad (4-27)$$

$$Percentage\ of\ difference = \frac{Difference}{Average} \times 100 \quad (4-28)$$

Here value 1 and value 2 are any number of the statistic descriptors mentioned previously, which are object of comparison. In some cases, maximal values were compared and, in others, the median and average of entire sets of data were used to calculate the percentage of difference. Median was also included here because it was more suitable for comparison purposes since this descriptor is less sensitive to extreme values. In general, percentage of difference of 5% was used as criteria to define whether pairs of values were different or similar.

¹³ 100% of reported concentrations of HANs was assumed as DCAN as predominant specie within this group of DBP

4.3 RESULTS AND DISCUSSION

4.3.1 Typical model behaviour

To illustrate the general behaviour of the model, a simulation was run with $BT=16\ \mu\text{m}$, $Clo=1\ \text{mg/L}$, $Xo=40.87\ \text{mg/L}$, which corresponded to biomass-limiting conditions, i.e., chlorine concentration is enough to completely oxidize biomass and still residual concentrations remain within the biofilm. Figure 4-9 presents the variation of dissolved substances within the biofilm, Figure 4-10 shows the behaviour of the same variables in bulk water, and Figure 4-11 illustrates the decay or particulate substances within the biofilm. Chlorine rapidly penetrates the biofilm (after 1 s) and chloroform concentration varies from zero (at $t=0$) until a maximum value, then it decreases to very small values due to the decay of cells and EPS and diffusion to the bulk water. In the bulk water, chlorine decays while chloroform increases, until steady state is reached due to complete depletion of cells and EPS, when chlorine has fully penetrated the biofilm.

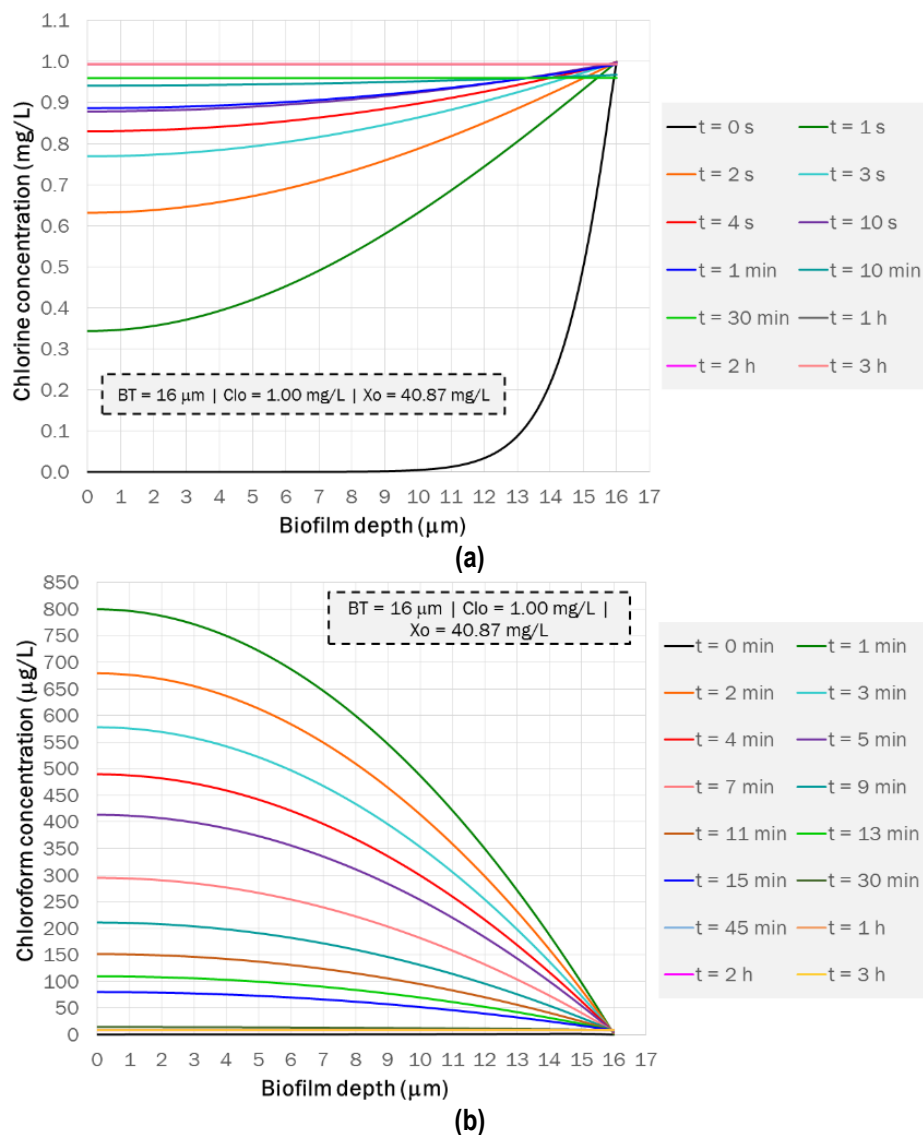


Figure 4-9. Dissolved substances within biofilm (a) Chlorine (b) Chloroform

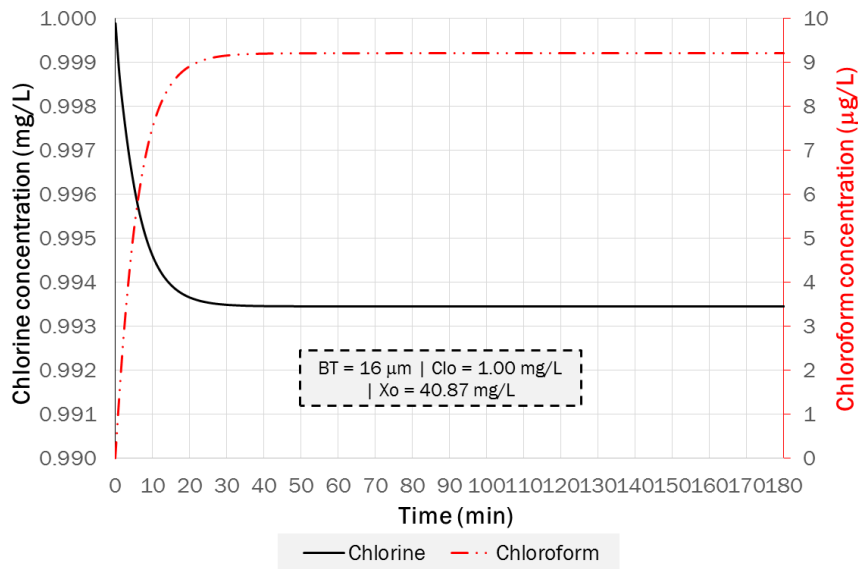


Figure 4-10. Dissolved substances in bulk water after 3 hours

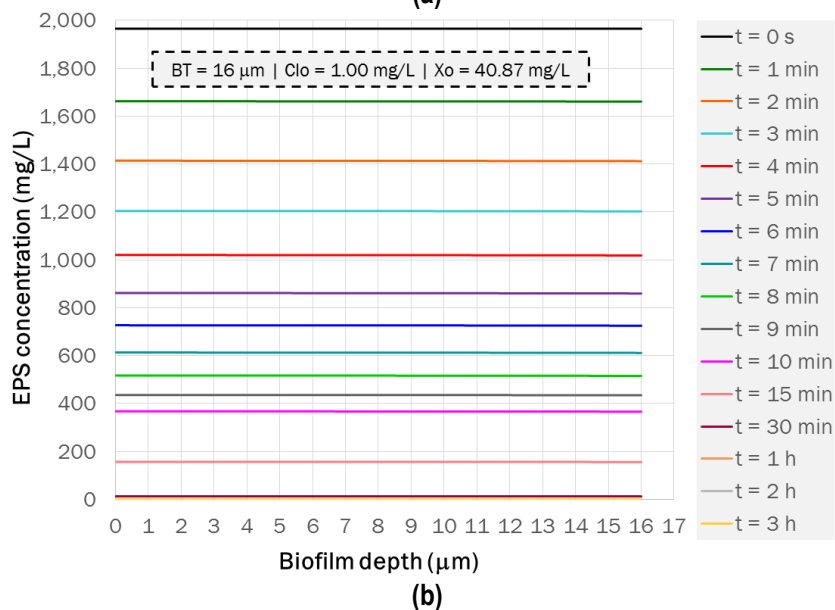
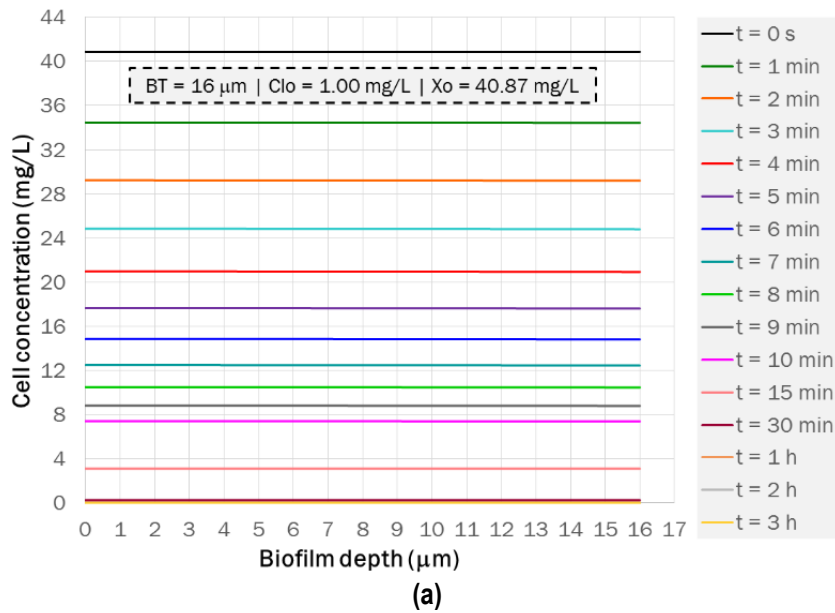
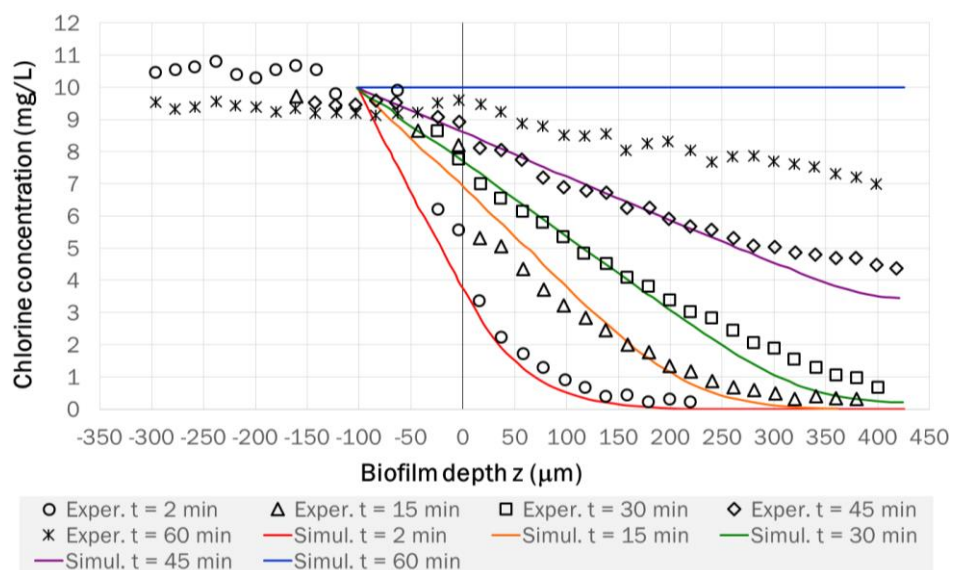


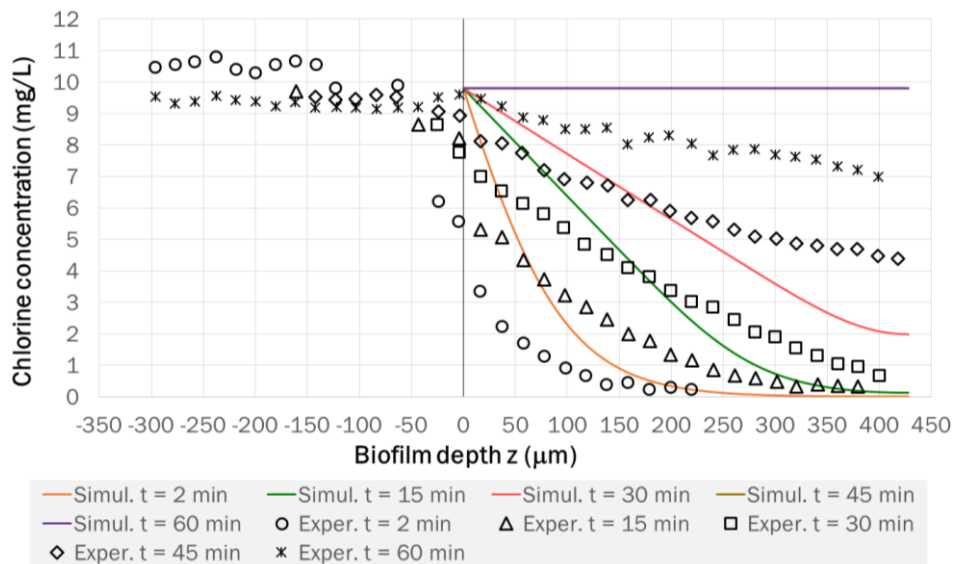
Figure 4-11. Decay of particulate substances (a) Cells (b) EPS

4.3.2 Chlorine penetration within the biofilm

Chen and Stewart (1996) grew artificial biofilms with bacteria *P. aeruginosa* and polysaccharide alginate to experimentally study the chlorine penetration within biofilms and modelled the process by a mathematical representation of diffusion and chemical reactions. The experiments were carried out in a flow cell with flow rate equal to 400 mL/min. The first step in the construction of the current model was to compare the diffusion of chlorine within the biofilm to the results reported by these researchers. Figure 4-12 indicates that, after 2 min, both models are able to reproduce the experimental results; chlorine penetrates the biofilm up to 200 μm . For $t=15$ min, both modelled chlorine profiles also match with experimental data. Chlorine profiles from simulated data with the current model, after 30 min and up to 1 hour, represents a faster diffusion of the disinfectant and complete penetration of the biofilm, which may be related to the boundary condition used in both models. The current model includes a stagnation condition and diffusion starts in the biofilm surface (Figure 4-12b). Chen and Stewart (1996) was developed under flow condition and used the film theory in the mass transfer boundary layer (IWA Task Group on Biofilm Modeling et al., 2006), then diffusion starts in a small layer adjacent to the biofilm surface (Figure 4-12a). In general terms, the mathematical representation of chlorine diffusion was acceptable to proceed with DBP simulations.



(a)



(b)

Figure 4-12. Comparison of chlorine penetration within biofilm (a) Chen and Stewart (1996): experimental vs model data (b) Experimental data from Chen and Stewart (1996) vs simulated data from current model

4.3.3 Sensitivity analysis

A single parametric sensitivity analysis (Loucks and van Beek, 2005) was done in order to define the influence of the 14 parameters that compose the proposed model. This analysis was carried out by varying each parameter one at a time while others were kept constant. Then, such influence among parameters was compared by plotting the percentage of change of every parameter vs the chloroform concentration in bulk water. The base values of each parameter used in this sensitivity analysis are indicated in Table 4-11.

Table 4-11. Base parameters used in the sensitivity analysis

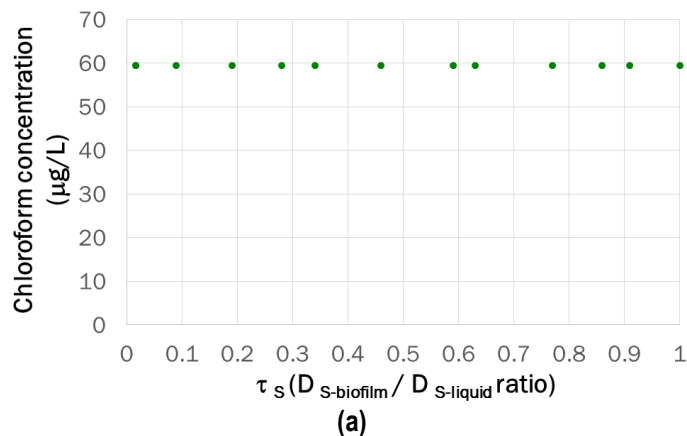
Parameter	Base value
τ_s	0.46
Biofilm thickness (BT)	49 μm
Initial EPS concentration (E_0)	4775 mg/L
Initial chlorine concentration (C_{l0})	1 mg/L
Initial cell concentration (X_0)	40.87 mg/L
Temperature (T)	15 $^{\circ}\text{C}$
Fraction of cells transformed into DBPs (F_x)	0.5
Fraction of EPS transformed into DBPs (F_E)	0.5
Cell-chlorine yield coefficient (Y_1)	1.85 (g/g)
EPS-chlorine yield coefficient (Y_2)	540 (g/g)
Biofilm area (A_b)	10 cm^2
Reactor volume (V)	65 mL

The analytical solution to Equation (4-14) is given in Equation (4-29), which allows for calculating the maximum DBP concentration extractable from the biofilm. According to this, the parameters biofilm area (A_b), reactor volume (V), biofilm thickness (BT), fraction of cells transformed into chloroform (F_x), cell-chlorine yield coefficient (Y_1), initial cells concentration (X_0), fraction of EPS transformed into chloroform (F_E), EPS-chlorine yield coefficient (Y_2), and initial EPS concentration (E_0) directly influence the DBP formation potential. Here M_s is the molar mass of the DBP substance.

$$Max S_{ext-bio} = M_s \frac{A_b}{V} (BT) \left(\frac{F_x}{Y_1} X_0 + \frac{F_E}{Y_2} E_0 \right) \quad (4-29)$$

4.3.3.1 τ_s , reaction rates k_1 and k_2 , and initial chlorine concentration

Similar influence of parameters τ_s , k_1 , k_2 , and Cl_0 on bulk water concentrations of chloroform can be observed in Figure 4-13a, Figure 4-14a, Figure 4-15a, and Figure 4-16a, respectively; it can be observed that such concentrations do not change for every tested parameter value, after 3 hours of contact time. However, the significance of such behaviour is different for every case. τ_s is related to speed at which chloroform is being transported, due to the reduction of the substance diffusion coefficient within the biofilm. Thus, values of τ_s as small as 0.016 allows obtaining the maximum concentration of chloroform in bulk water in shorter time in comparison to ratios higher than 0.09. Such difference is observable in less than 40 min (Figure 4-13b). For values of τ_s higher than 0.09, there is not obvious difference on the time when maximal concentrations of chloroform are reached.



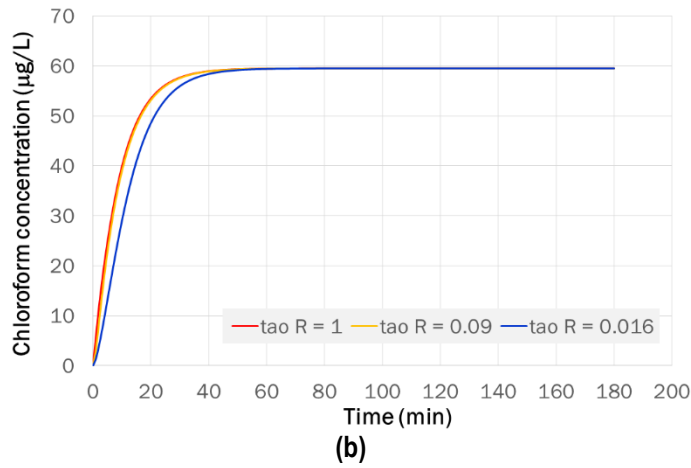
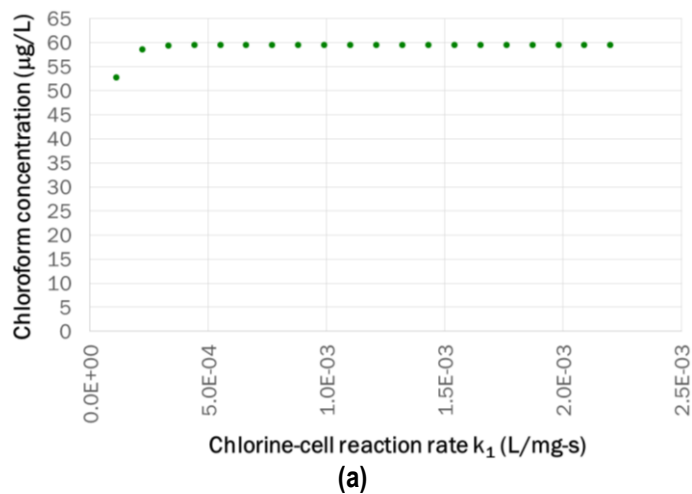
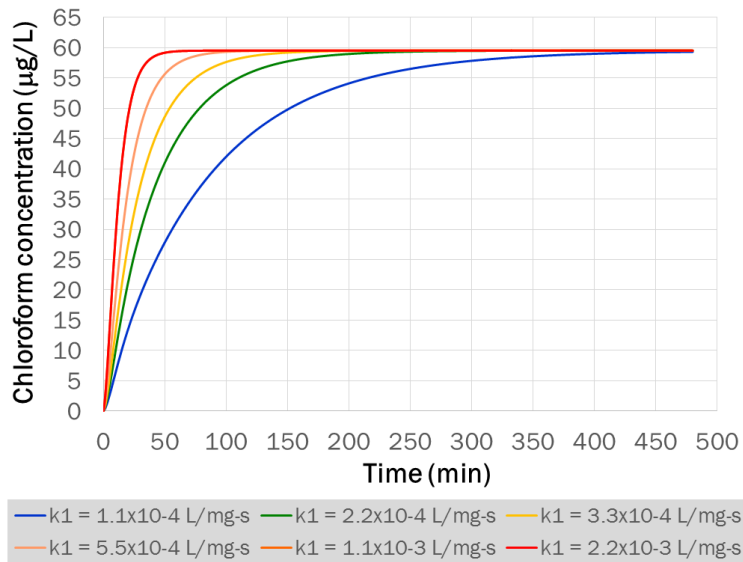


Figure 4-13. Influence of τ_s on chloroform concentration in bulk water (a) Chloroform concentrations in bulk water at different values of τ_s after $t = 3$ h (b) Temporal variation of chloroform concentrations in bulk water for three values of τ_s

With regard to reaction rates k_1 and k_2 , the influence of these parameters on chloroform concentrations is actually related to the speed of the reactions; such influence is more significant for k_1 . The time required to reach the maximum potential chloroform concentration is reduced from eight hours corresponding to the minimum value tested (1.1×10^{-4} L/mg-s) down to one hour for the maximum value considered here (2.2×10^{-3} L/mg-s) (Figure 4-14b).

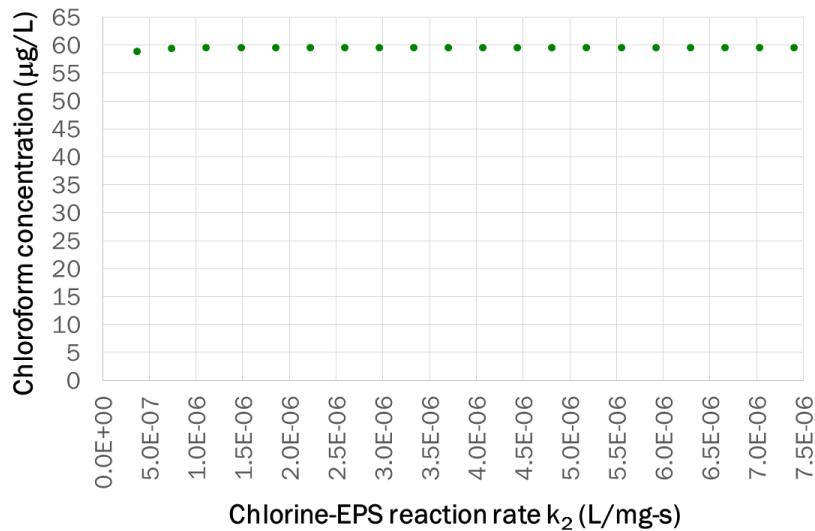




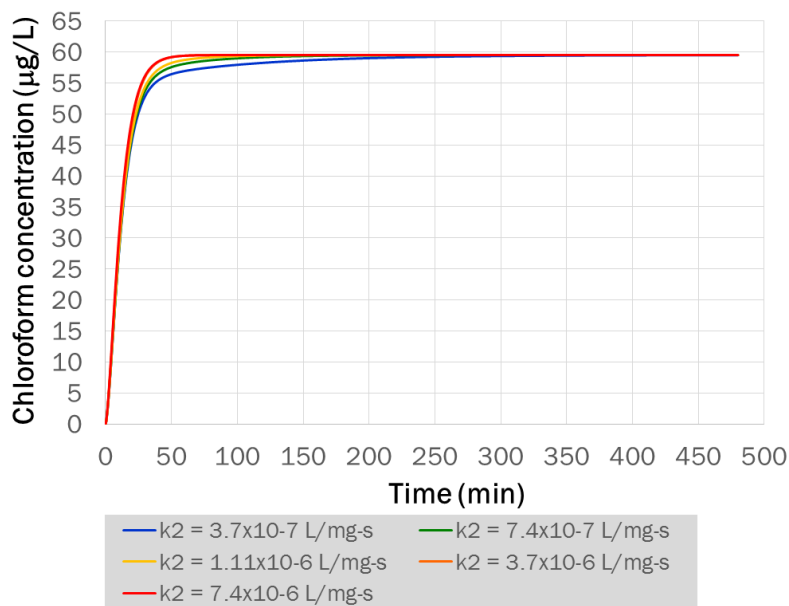
(b)

Figure 4-14. Influence of reaction rate k_1 on chloroform concentration in bulk water (a) Chloroform concentrations in bulk water at different values of k_1 after $t = 3$ h (b) Temporal variation of chloroform concentrations in bulk water for several values of k_1

The influence of reaction rate k_2 is less pronounced than k_1 , due to the contribution of EPS to DBP formation potential is smaller in comparison to cells. The value of k_2 small as 3.7×10^{-7} L/mg-s generated complete transformation of cells and EPS into chloroform in four hours. Higher values of k_2 increases the speed of the reactions and the time required to reach the maximal potential concentration of chloroform is the same (1 h) for k_2 ranging between 2.22×10^{-6} and 7.4×10^{-6} L/mg-s (Figure 4-15b).



(a)



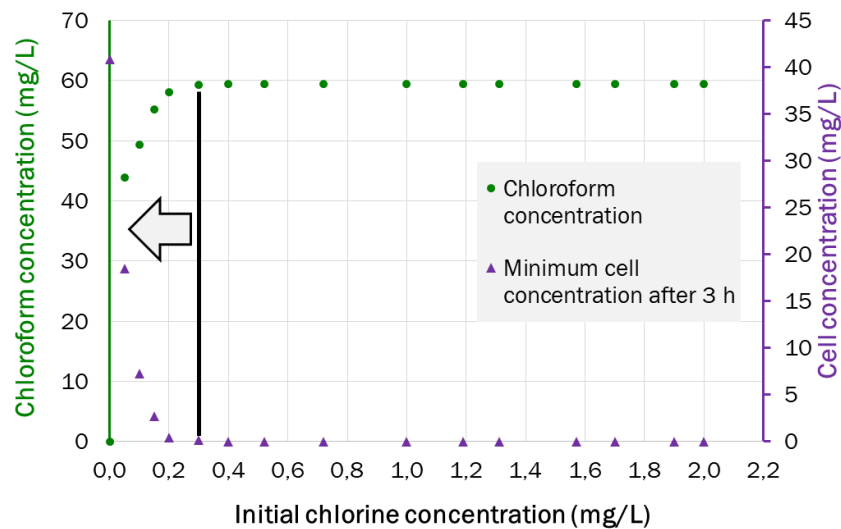
(b)

Figure 4-15. Influence of reaction rate k_2 on chloroform concentration in bulk water (a) Chloroform concentrations in bulk water at different values of k_2 after $t = 3$ h (b) Temporal variation of chloroform concentrations in bulk water for several values of k_2

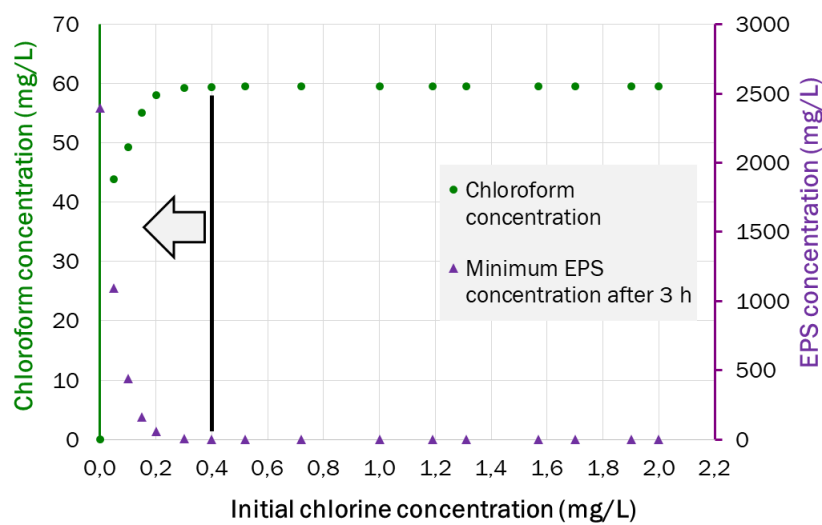
In relation to Clo, influence of this parameter on chloroform concentrations allows identifying whether the reactions are chlorine or biomass limiting. Values of Clo smaller than 0.3 mg/L are not able to completely oxidize cells and EPS, then this model turns to be chlorine limiting. For such chlorine concentrations, the model resulted in minimum remaining concentrations of cells and EPS between 0.38-40.87 mg/L (Figure 4-16a) and 58.69-2397.3 mg/L (Figure 4-16b), respectively, after 3 hours of contact time. For Clo higher than 0.3 mg/L, the model turns biomass limiting, since the DBP concentrations depend on the amount of biomass available for reaction with chlorine.

This indicates that, under certain values of Xo and Clo, the model can be either chlorine or biomass limiting. The same condition was found by Wang et al. (2012c) in batch experiment tests with culture suspensions of different strains of *P. aeruginosa*. By using initial cell density of 1.04 and 0.05 mg/L¹⁴ and chlorine dose between 0.5 and 5.0 mg/L, the disinfection experiments were biomass limiting since free chlorine concentrations were negligible in all tested samples. Abokifa et al. (2016a) also included in their multicomponent model a second order reaction limited by the biomass concentration to predict the THM formation from chlorination of biofilm, planktonic cells, and detached biofilm clusters.

¹⁴ Cell density was reported as 10^8 and 10^6 CFU/mL, which were transformed into volumetric cell density



(a)

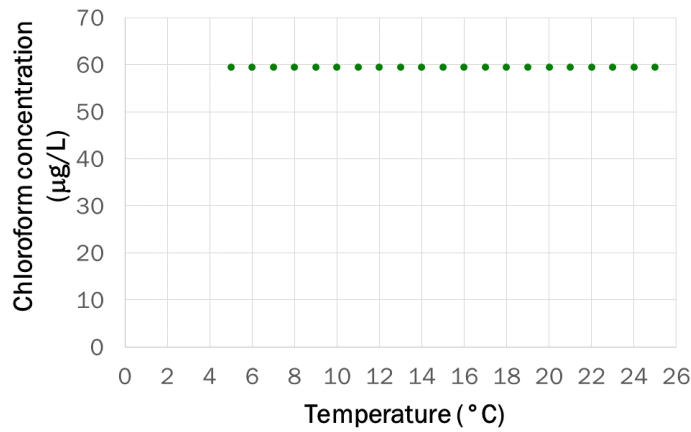


(b)

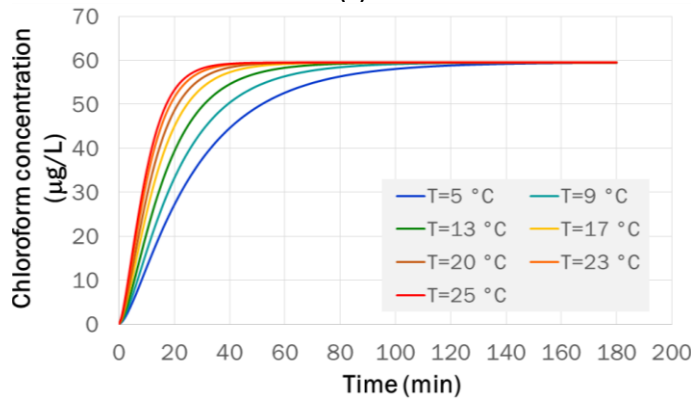
Figure 4-16. Influence of initial chlorine concentration on chloroform concentration in bulk water
(a) Comparison between Clo and minimum cell concentration (b) Comparison between Clo and minimum EPS concentration

4.3.3.2 Temperature

The effect of temperature over the chloroform formation potentials is associated with the change of reaction rates k_1 and k_2 , as explained in the previous section. Despite this, a similar analysis is presented here however based on the variation of the water temperature. According to the results in Figure 4-17, temperature does not affect the steady state concentrations of chloroform in bulk water after three hours of reaction time but does influence the speed of the reactions (Figure 4-17a). As was expected, the model is able to represent that the time required to obtain the maximal potential concentration of chloroform increases as temperature rises through the range 5-25 °C (Figure 4-17b). For instance, at 5 °C, two hours are required for entire reaction between chlorine and cells and EPS; while, at 25 °C, this happens in 45 min.



(a)



(b)

Figure 4-17. Temperature influence on chloroform concentration in bulk water (a) Chloroform concentrations in bulk water at different temperatures after t = 3 h (b) Temporal variation of chloroform concentrations in bulk water at the temperature range 5-25 °C

4.3.3.3 Yield coefficients Y_1 and Y_2 and reactor volume

Parameters such as cell and EPS yield coefficients and reactor volume result in chloroform in exponential decay of chloroform in bulk water (Figure 4-18). Therefore, up to certain values of these parameters, concentration of chloroform is minimum and does not vary significantly if these parameters increase. Particularly, small values of V resulted in high concentration of chloroform, which represents that this substance is dissolved in a low amount of solvent. Similarly, low yield coefficients represent that higher amount of mass of cells or EPS have been depleted per mass of chlorine consumed; therefore, more chloroform will be formed.

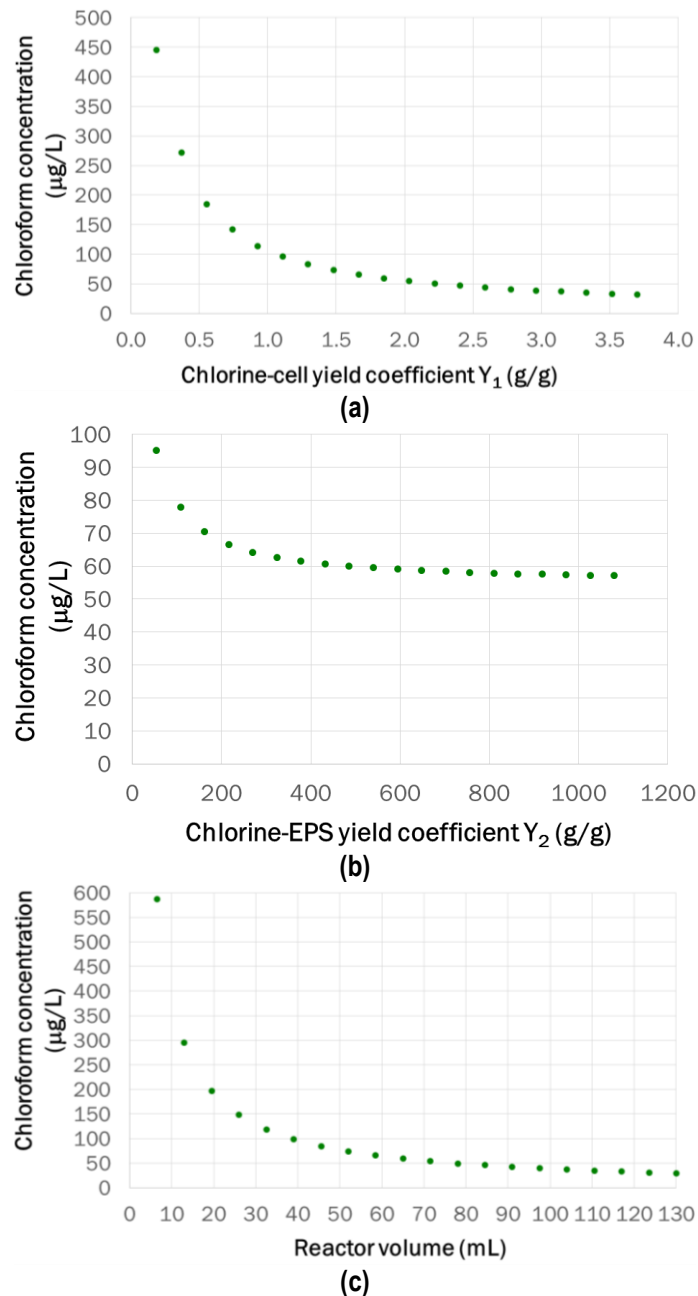


Figure 4-18. Influence of (a) Y_1 , (b) Y_2 , and (c) reactor volume on chloroform concentration in bulk water after $t = 3$ h

4.3.3.4 Biofilm thickness, initial cell and EPS concentration, fraction of cells and EPS transformed into DBP and biofilm area

Parameters such as biofilm thickness (BT), initial cell and EPS concentration (E_0), fraction of cells and EPS transformed into DBP (F_E) and biofilm area (A_b) have a linear effect on bulk water concentrations of chloroform (see Figure 4-19).

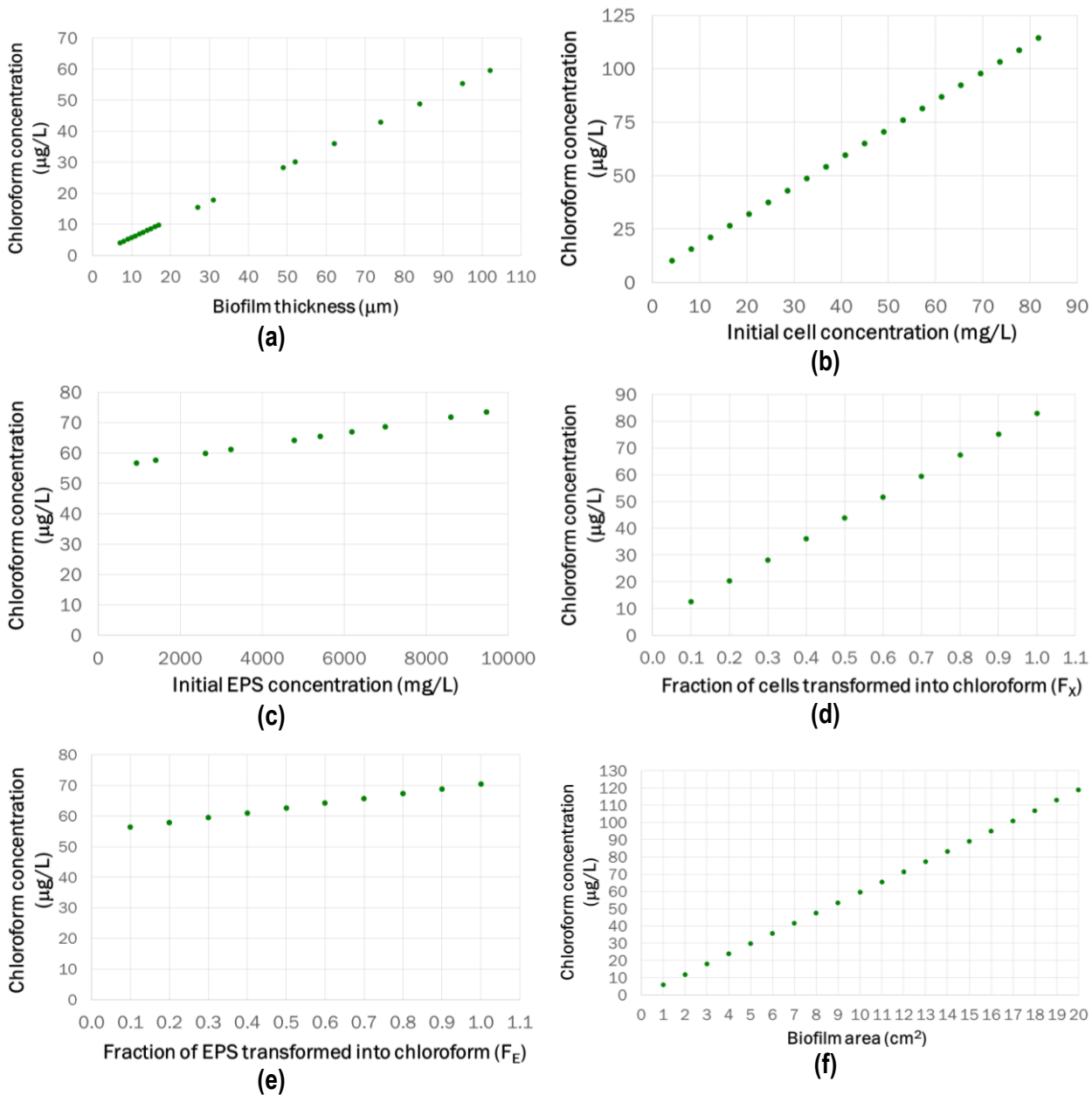


Figure 4-19. Parameters with linear influence on chloroform concentration in bulk water (a) Biofilm thickness (b) Initial cell concentration (c) Initial EPS concentration (d) F_x (e) F_E (f) Biofilm area

4.3.3.5 Comparison among parameters

This comparison was carried out in order to identify the parameters with more influence on bulk water concentrations of chloroform. The 14 parameters assessed in this sensitivity analysis are compared in Figure 4-20. The percentage of change in relation to the base value of both parameters and the respective chloroform concentrations were calculated and presented in Table 4-12. Reactor volume (V) and chlorine-cell yield coefficient (Y_1) were the parameters with influenced most the response variable (Figure 4-20a); reduction on 90% of these values represents an increase of 886% and 649% on chloroform concentrations, respectively (Table 4-12 and Table 4-13).

To clarify which parameters were also influencing in second place, another graph was plotted eliminating the two parameters mentioned previously (Figure 4-20b). Then, variation among -90% - 100% of initial cell concentrations, biofilm area, and biofilm thickness, parameters with linear influence on chloroform concentrations, produces the same degree of variation in such concentrations (Table 4-13). Chlorine-EPS yield coefficient (Y_2) is a parameter with some degree of influence on bulk concentrations of chloroform; a reduction of this of 90% causes an increase of this DBP in approximately 60% (Table 4-12). A more detailed sensitivity analysis can help to better rank the parameter influence on model outputs and identify interrelations existing between parameters. This is addressed in Chapter 5.

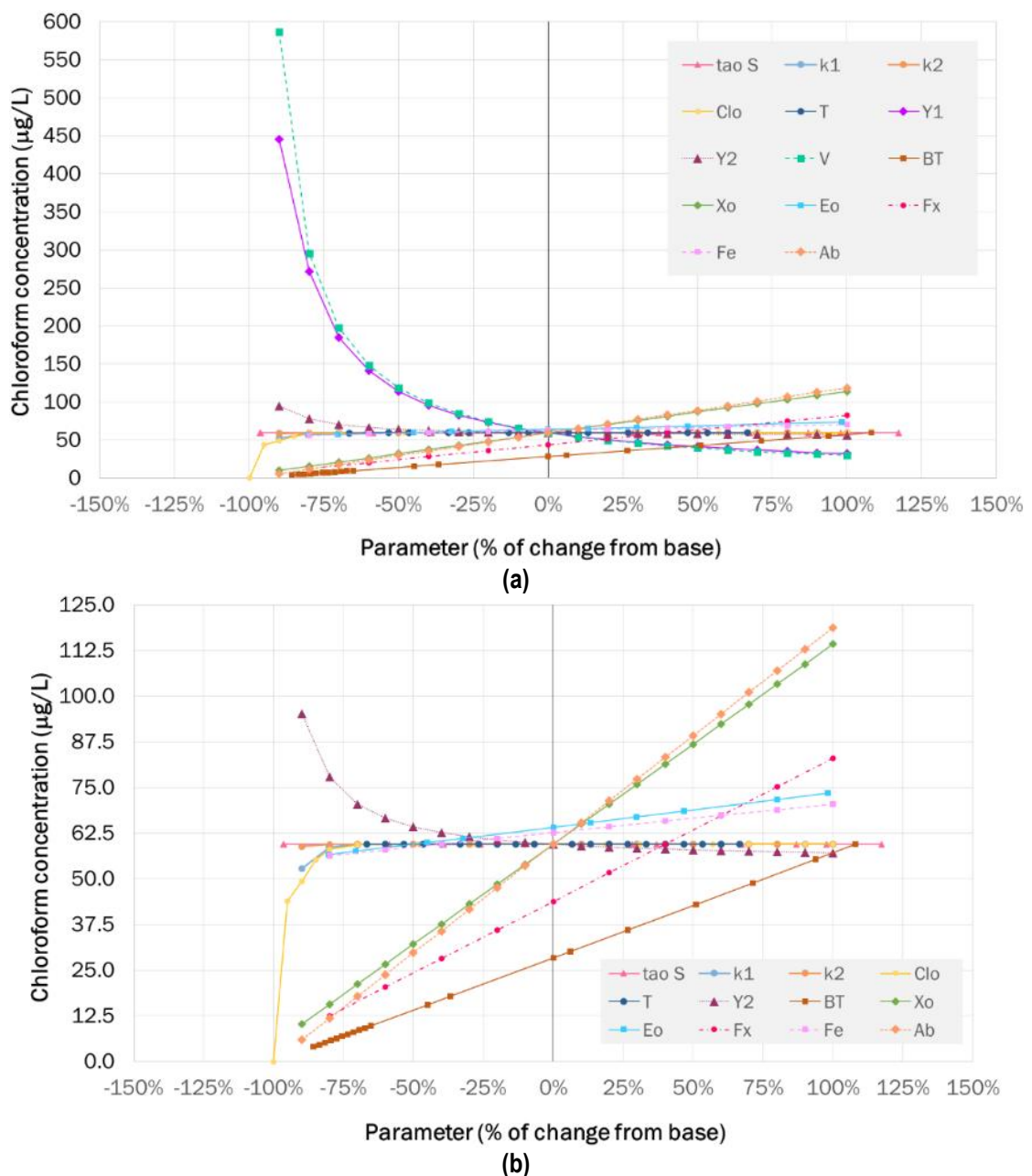


Figure 4-20. Comparison of influence on chloroform concentration in bulk water among parameters (a) 14 parameters tested (b) 12 parameters tested excluding V and Y_1

Table 4-12. Percentage of change of parameters and the respective chloroform concentrations in bulk water

Percentage of change													
τ_s	CHCl ₃	k ₁	CHCl ₃	k ₂	CHCl ₃	Cl _o	CHCl ₃	T	CHCl ₃	Y ₁	CHCl ₃	Y ₂	CHCl ₃
-96,52%	0,00%	-90,00%	-11,29%	-90,00%	-1,04%	-100,00%	-100,00%	-66,7%	-0,1%	-90,0%	649,1%	-90,0%	60,1%
-96,30%	0,00%	-80,00%	-1,45%	-80,00%	-0,14%	-95,00%	-26,29%	-60,0%	-0,1%	-80,0%	356,6%	-80,0%	31,0%
-80,43%	0,00%	-70,00%	-0,18%	-70,00%	-0,02%	-90,00%	-17,11%	-53,3%	0,0%	-70,0%	211,2%	-70,0%	18,4%
-58,70%	0,00%	-60,00%	-0,02%	-60,00%	0,00%	-85,00%	-7,30%	-46,7%	0,0%	-60,0%	138,0%	-60,0%	11,9%
-39,13%	0,00%	-50,00%	0,00%	-50,00%	0,00%	-80,00%	-2,46%	-40,0%	0,0%	-50,0%	91,1%	-50,0%	7,9%
-26,09%	0,00%	-40,00%	0,00%	-40,00%	0,00%	-70,00%	-0,29%	-33,3%	0,0%	-40,0%	61,4%	-40,0%	5,3%
0,00%	0,00%	-30,00%	0,00%	-30,00%	0,00%	-60,00%	-0,04%	-26,7%	0,0%	-30,0%	39,0%	-30,0%	3,4%
28,26%	0,00%	-20,00%	0,00%	-20,00%	0,00%	-48,00%	0,00%	-20,0%	0,0%	-20,0%	23,0%	-20,0%	2,0%
36,96%	0,00%	-10,00%	0,00%	-10,00%	0,00%	-28,00%	0,00%	-13,3%	0,0%	-10,0%	9,9%	-10,0%	0,9%
67,39%	0,00%	0,00%	0,00%	0,00%	0,00%	0,00%	0,00%	-6,7%	0,0%	0,0%	0,0%	0,0%	0,0%
86,96%	0,00%	10,00%	0,00%	10,00%	0,00%	19,00%	0,00%	0,0%	0,0%	10,0%	-8,6%	10,0%	-0,7%
97,83%	0,00%	20,00%	0,00%	20,00%	0,00%	31,00%	0,00%	6,7%	0,0%	20,0%	-15,3%	20,0%	-1,3%
117,39%	0,00%	30,00%	0,00%	30,00%	0,00%	57,00%	0,00%	13,3%	0,0%	30,0%	-21,4%	30,0%	-1,8%
		40,00%	0,00%	40,00%	0,00%	70,00%	0,00%	20,0%	0,0%	40,0%	-26,3%	40,0%	-2,3%
		50,00%	0,00%	50,00%	0,00%	90,00%	0,00%	26,7%	0,0%	50,0%	-30,8%	50,0%	-2,6%
		60,00%	0,00%	60,00%	0,00%	100,00%	0,00%	33,3%	0,0%	60,0%	-34,5%	60,0%	-3,0%
		70,00%	0,00%	70,00%	0,00%			40,0%	0,0%	70,0%	-38,0%	70,0%	-3,3%
		80,00%	0,00%	80,00%	0,00%			46,7%	0,0%	80,0%	-40,9%	80,0%	-3,5%
		90,00%	0,00%	90,00%	0,00%			53,3%	0,0%	90,0%	-43,7%	90,0%	-3,8%
		100,00%	0,00%	100,00%	0,00%			60,0%	0,0%	100,0%	-46,0%	100,0%	-4,0%
								66,7%	0,0%				

Table 4-13. Percentage of change of parameters and the respective chloroform concentrations in bulk water

Percentage of change													
V	CHCl ₃	BT	CHCl ₃	Xo	CHCl ₃	Eo	CHCl ₃	Fx	CHCl ₃	F _E	CHCl ₃	Ab	CHCl ₃
-90%	886,2%	-85,71%	-85,81%	-90%	-82,86%	-80,42%	-11,77%	-80,0%	-71,4%	-80,0%	-10,0%	-90%	-90,0%
-80%	396,9%	-83,67%	-83,78%	-80%	-73,67%	-70,53%	-10,33%	-60,0%	-53,5%	-60,0%	-7,5%	-80%	-80,0%
-70%	232,1%	-81,63%	-81,74%	-70%	-64,45%	-45,13%	-6,61%	-40,0%	-35,7%	-40,0%	-5,0%	-70%	-70,0%
-60%	149,4%	-79,59%	-79,71%	-60%	-55,24%	-32,17%	-4,71%	-20,0%	-17,8%	-20,0%	-2,5%	-60%	-60,0%
-50%	99,7%	-77,55%	-77,68%	-50%	-46,02%	0,00%	0,00%	0,0%	0,0%	0,0%	0,0%	-50%	-50,0%
-40%	66,5%	-75,51%	-75,65%	-40%	-36,83%	13,34%	1,95%	20,0%	17,8%	20,0%	2,5%	-40%	-40,0%
-30%	42,8%	-73,47%	-73,61%	-30%	-27,62%	29,65%	4,34%	40,0%	35,7%	40,0%	5,0%	-30%	-30,0%
-20%	25,0%	-71,43%	-71,58%	-20%	-18,41%	46,70%	6,84%	60,0%	53,5%	60,0%	7,5%	-20%	-20,0%
-10%	11,1%	-69,39%	-69,55%	-10%	-9,21%	80,19%	11,74%	80,0%	71,4%	80,0%	10,0%	-10%	-10,0%
0%	0,0%	-67,35%	-67,51%	0%	0,00%	98,22%	14,38%	100,0%	89,2%	100,0%	12,6%	0%	0,0%
10%	-9,1%	-65,31%	-65,48%	10%	9,21%							10%	10,0%
20%	-16,6%	-44,90%	-45,08%	20%	18,40%							20%	20,0%
30%	-23,1%	-36,73%	-36,91%	30%	27,62%							30%	29,9%
40%	-28,5%	0,00%	0,00%	40%	36,83%							40%	39,9%
50%	-33,3%	6,12%	6,17%	50%	46,04%							50%	49,9%
60%	-37,5%	26,53%	26,78%	60%	55,24%							60%	59,8%
70%	-41,1%	51,02%	51,60%	70%	64,45%							70%	69,8%
80%	-44,4%	71,43%	72,34%	80%	73,66%							80%	79,8%
90%	-47,3%	93,88%	95,24%	90%	82,86%							90%	89,7%
100%	-50,0%	108,16%	109,85%	100%	92,07%							100%	99,7%

In relation to reactor volume and biofilm area, these parameters can be easily determined in a DWDN from geometrical characteristics of the water pipes, or surfaces and reactors used in-situ or laboratories. Then, low uncertainty is expected from these parameters. Yield coefficients were determined by Chen and Stewart (1996) from several experimental data sets by the method of nonlinear least-squares; such experiments consisted of measuring chlorine profiles within artificial biofilms of *P. aeruginosa*. Therefore, further adjustments of this parameter can be done by laboratory tests with heterogeneous biofilms growth under real-scale DWDN conditions.

In relation to initial cell concentration, it is important to remark that the specific chemical, physical and hydraulic conditions of the DWDNs shape the bacterial communities of biofilms as discussed in Chapter 3. Consequently, it is necessary to collect cell density data from the biofilms growing in the DWDN of interest. Despite initial EPS concentration having a lower impact on variation of chloroform bulk concentrations, it is also important to measure the EPS content in biofilms of real-scale DWDN to improve the reliability of the model predictions. Biofilm thickness is also an important parameter influencing the model results and is clearly interacting with parameter E_0 , since the latter is calculated using BT values (Section 4.2.3.3). Additionally, further biofilm research could lead to the formulation of a relationship between EPS concentration and biofilm thickness in biofilms naturally found in real-scale DWDNs.

Biofilm thickness can be determined by microscopy and imaging techniques (Shen et al., 2016). As presented in Table 4-2, biofilm thickness for drinking water biofilms have been measured in those grown in laboratory reactors. In a personal communication with Dr Isabel Douterelo, she mentioned the difficulty faced by measuring this parameter in biofilms grown on coupons installed in real-scale DWDNs, since the biomass content was very high and dyes were not able to fully penetrate the biofilms, then they were not completely observable through the microscope¹⁵.

Other factors such as chlorine concentration and temperature can be defined by historical records supplied by the water utilities or direct measurement in the field (Nescerecka et al., 2014; Dippong et al., 2016). Parameters such as fraction of cells and EPS transformed into DBPs can be adapted from experimental studies reporting results of the DBP of interest (Fang et al., 2010b; Wang et al., 2013a) or adjusted to fit the model, if there were experimental data to compare to or validate. The diffusion coefficient of DBP within the biofilm may also be adjusted if the model is coupled to cells growth and EPS production simultaneously. This factor can also be calculated by measuring DBP

¹⁵ Technical meeting at the University of Sheffield, 24th March 2017. E-mail: i.douterelo@sheffield.ac.uk

concentration profiles within biofilms; however, it is not clear if the micro-sensors for such substances are already available for laboratory applications.

4.3.4 Factors affecting the DBP formation

As explained in Chapter 2, the factors which affect the DBP formation are the concentration and type of NOM, type and concentration of disinfectant, pH, temperature, contact time and bromide concentration. The current model was developed for water systems using chlorine as disinfectant. The type of organic matter is included through the parameters corresponding to DBP precursors such as bacteria and EPS (k_1 , k_2 , Y_1 , Y_2 , F_X , F_E). These substances are mainly composed by biomolecules such as genetic material, proteins, lipids, and polymers (Wang et al., 2012b; Fish et al., 2015). Particularly, it has been identified that EPS contain aromatic molecules, are hydrophilic and contain fulvic like substances (Wang et al., 2012c; Lemus Pérez and Rodríguez Susa, 2017).

As also mentioned before, temperature is indirectly included through the reaction rates k_1 and k_2 . Equations (4-6) and (4-7) can be used to adjust these rates to the local temperature of the DWDN of interest. Parameters such as τ_S , k_1 , and k_2 affect the time when maximal potential concentration of DBP is reached. Higher rates and diffusion coefficient of DBP substance accelerate the reactions; therefore, less time is required to oxidize the entire biomass of the biofilm. This model did not include pH variable directly; however experimental results and field data matched with simulated results, as discussed in Sections 4.3.5 and 4.3.6.1. The influence of bromide concentration is not included in the current model; it is accepted that bromide presence in disinfected water favours the formation of brominated DBPs (Chowdhury et al., 2009). More information is required to determine the presence and amount of bromide within biofilms.

4.3.5 Comparison between model results and experimental data

According to Wang et al. (2013a), tests of DBP formation potentials resulted in ranges of 6.6–9.4 $\mu\text{g/L}$ and 2.6–3.2 $\mu\text{g/L}$ for chloroform and DCAN, respectively. The current model reproduced such results for BT in ranges of 12–16 μm and 12–14 μm , for these substances, respectively (Figure 4-21). These outcomes are consistent with the conditions of biofilm growth reported by Wang et al. (2013a); who incubated biofilm, in an enriched medium, for 60 hours, and the steady state was reached after 24 hours. Hence, thin biofilms may be expected under such condition.

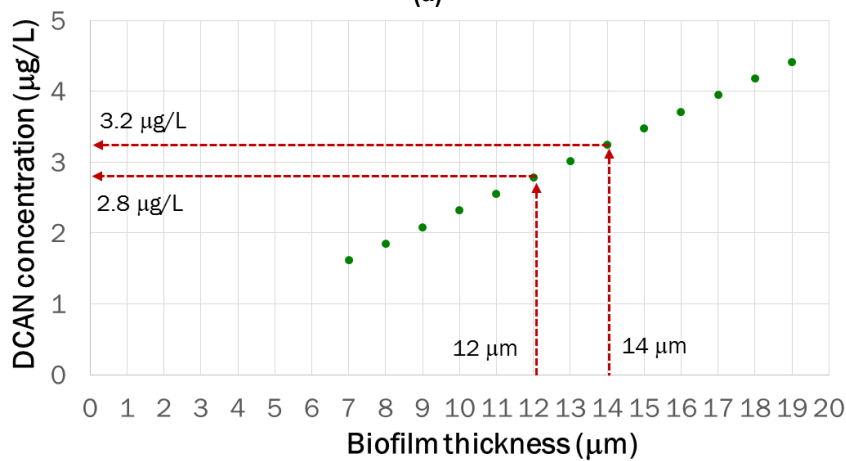
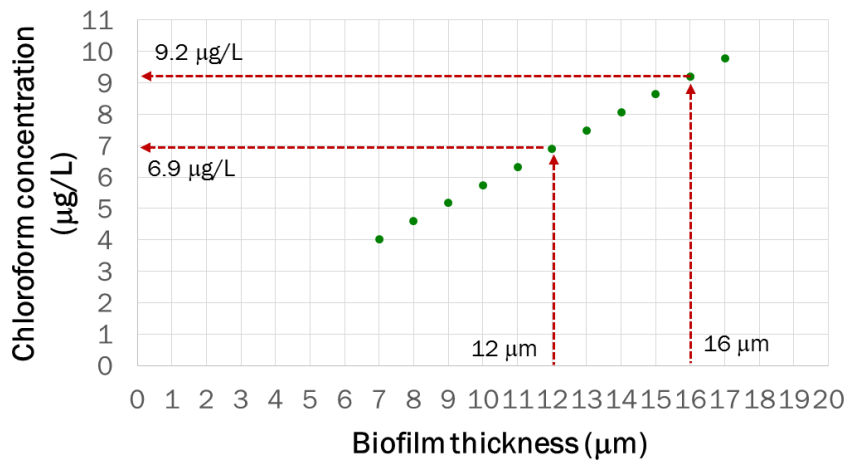


Figure 4-21. (a) Chloroform and (b) DCAN concentrations according to results of Wang et al. (2013a)

4.3.6 Simulation of scenarios: building plumbing system supplied with warm water

DBPs are monitored in the distribution network by water utilities and regulation agencies, but people are exposed to them inside of the facilities. Exposure occurs by inhalation, dermal contact, and ingestion; through domestic activities such as bathing, showering, cooking, and drinking (Chowdhury, 2016). The same chemical, biological and hydraulic processes occurring in the distribution network also take place in plumbing systems. In addition, such systems are characterised by high stagnation times and temperatures, therefore water age increases inside of the buildings, disinfectant decays faster, and more favourable conditions exist for bulk bacteria regrowth, biofilm growth and DBP formation (Ji et al., 2015; Chowdhury, 2016). Overnight sleeping time, working hours, and weekends in commercial buildings are examples of stagnation conditions in plumbing systems. Stagnation on dead-end sections of DWDNs can also take place during overnight sleeping time. Higher water temperatures in plumbing systems can occur due to the heating system used to raise the temperature of the building or only for domestic activities

(showering, bathing, and washing). This causes the temperature of water flowing in the plumbing pipes to increase.

To analyse the scenario of chloroform and DCAN formation in Colombian plumbing systems, the parameters included in Table 4-14 were used when running the current model, which yielded 12 scenarios in total (Table 4-16). The scenario 1 is the least critical one, since it includes the lowest values of Clo, Xo, and BT, according to the ranges defined in Section 4.2.3. On the other hand, scenario 12 corresponds to the most critical one.

Table 4-14. Parameters used to simulate DBP formation in plumbing systems

Parameters	Value	Source
Stagnation times	11 h (morning – afternoon)	Assuming typical domestic activities: overnight sleeping time and working hours
Pipe diameter (ϕ)	0.5 inches	Typical diameter found in houses in Colombia
Length of the pipe (L)	50 m	Assuming house depth of 25 m with two floors
Temperature	25 °C	Water temperature in Cali – Colombia (Table 3-4) and in Dhahran, Saudi Arabia (Chowdhury, 2016)
Initial chlorine concentration	0.12 and 1.66 mg/L	Minimum and maximum values found in Cali – Colombia (Table 3-4)
Biofilm thickness	7 and 102 μm	Extreme values within the range Q1-Q3 (Table 4-3)
Initial EPS concentration	2.397,3 and 1.919,5 mg/L	Calculated from BT with equation included in Figure 4-5
Initial cell concentration	0.89; 4.03; and 13.98 mg/L	Values within the range Q1-Q3 (Table 4-5)

4.3.6.1 Chloroform formation compared with field assessment (Chowdhury, 2016)

Chowdhury (2016) investigated the effects of plumbing systems on human exposure to DBPs in drinking water by measuring several species of THMs and HAAs, during one year, in two houses located in the city of Dhahran, Saudi Arabia. The sampling campaign included three points (the water network at the entry of the houses, the house tap, and the hot water tank). The results of this study are consolidated in Table 4-15; water pH ranged between 6.89-8.33. According to the author, there were not any differences between sampling points, thus DBP species data for three sampling points were presented as averages, resulting in chloroform concentrations in the water network equal to 5.51 $\mu\text{g/L}$; plumbing systems equal to 9.37 and 12.42 $\mu\text{g/L}$ for cold and hot water, respectively. This represents that 3.86 and 6.91 $\mu\text{g/L}$ of chloroform was formed in cold and hot water, respectively, under stagnation conditions (Chowdhury, 2016).

Table 4-15. TTHMs and free chlorine concentrations measured in plumbing systems (Chowdhury, 2016)

Sampling point		TTHMs ($\mu\text{g/L}$)		Free chlorine (mg/L)	
		Stagnation condition			
		PM-AM	AM-Aftern.	PM-AM	AM-Aftern.
Water network		6.94	6.50	0.33	0.26
House tap		11.1	10.40	0.14	0.14
Hot water tank		14.60	13.20	0.11	
TTHMs formed under stagnation conditions ($\mu\text{g/L}$)	Cold water	4.16	3.90	0.11 – 0.33 mg/L	
	Hot water	7.66	6.70		
Chlorine demand under stagnation conditions (mg/L)	Cold water	-		0.19	0.12
	Hot water			0.22	0.14

Figure 4-22 shows the chloroform concentrations under initial concentrations of chlorine measured in plumbing systems by Chowdhury (2016) (0.33 mg/L ; Table 4-15). Due to the average concentration of chloroform found in plumbing premises was low (3.86 $\mu\text{g/L}$), lowest biofilm thickness and cell density were tested in the model. Model outputs resulted in similar concentrations to Chowdhury (2016) for pipe diameter between $\frac{3}{4}$ - 1 inches. The diameters of the plumbing networks were not reported by the author. However, these results confirm that the model is able to reproduce DBP concentrations associated with field conditions.

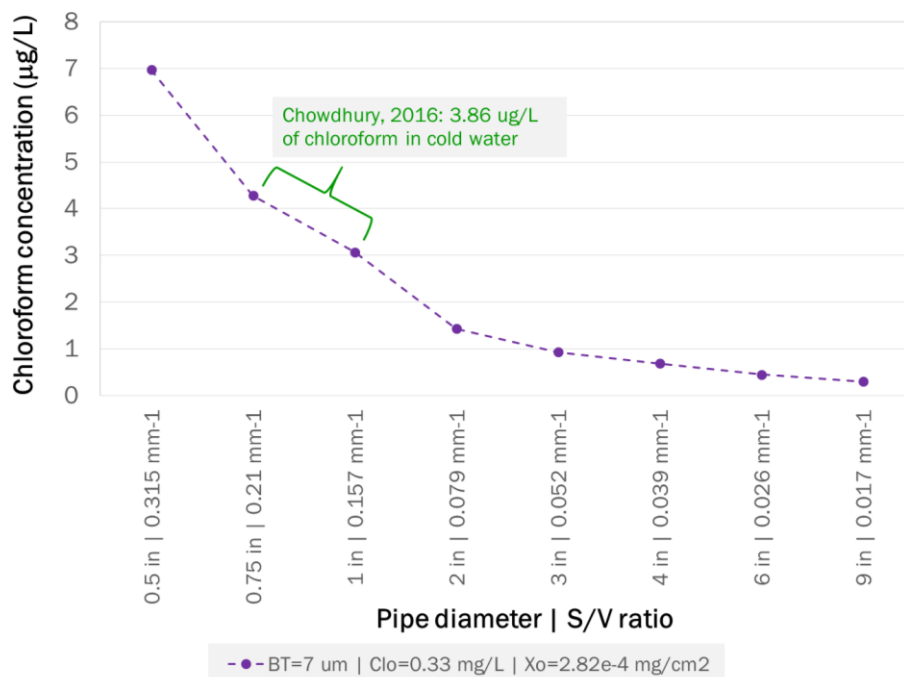


Figure 4-22. Chloroform concentrations in bulk water for different pipe diameter

4.3.6.2 Chloroform formation

Figure 4-23 presents the chloroform concentrations in bulk water for BT of 7 μm and 102 μm . Simulated chloroform concentrations ranged between 6.98-31.62 $\mu\text{g/L}$ and 89.29-466.20 $\mu\text{g/L}$ for 7 μm and 102 μm of BT, respectively. For BT=7 μm , 5.25 hours were required to achieve the maximum DBP concentration in bulk water with the lowest chlorine concentration of 0.12 mg/L and X_0 of 0.89 and 4.03 mg/L. In the case of the highest X_0 (13.98 mg/L), six hours were needed to reach the maximal potential chloroform concentration. For chlorine concentration of 1.66 mg/L, complete transformation of cells and EPS into chloroform occurred in less than 30 minutes (Figure 4-23a).

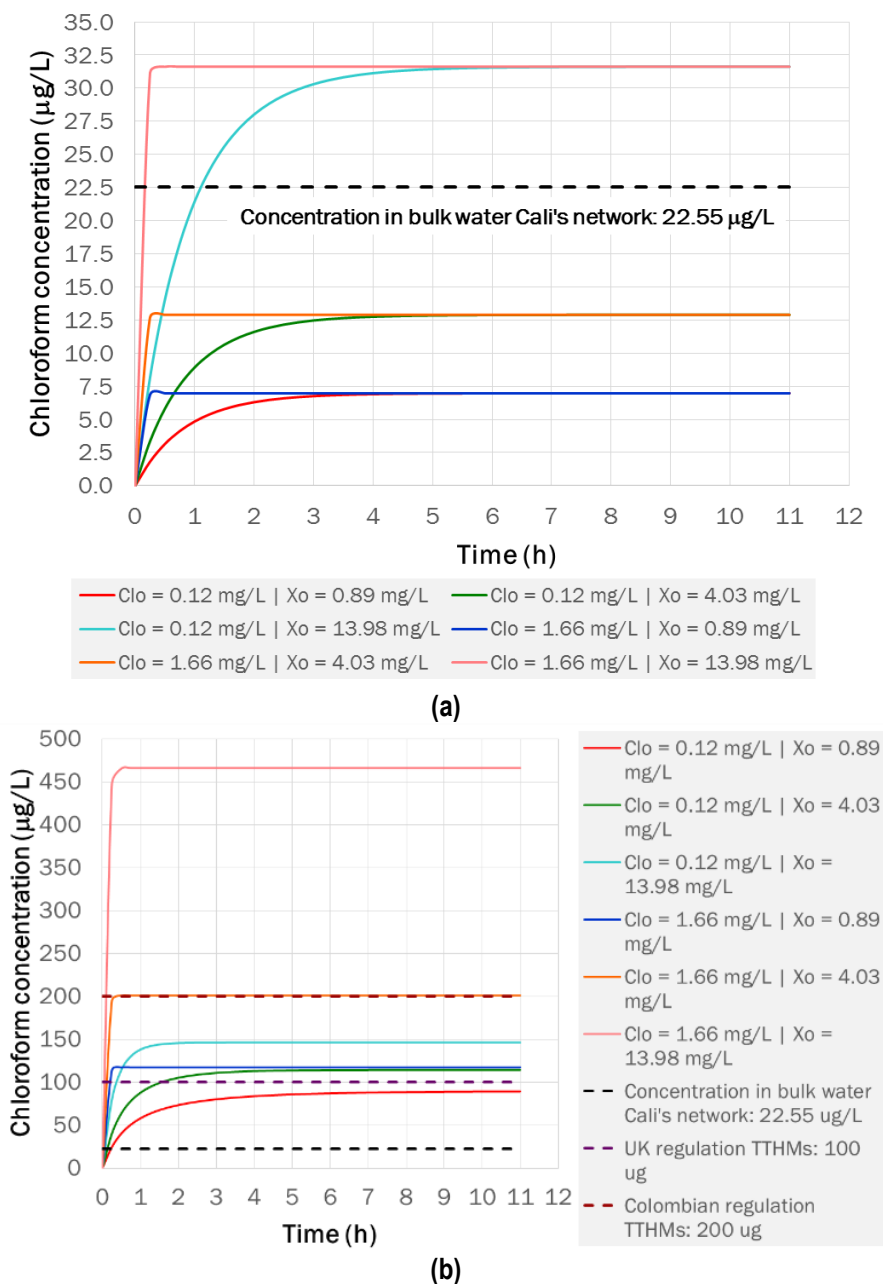


Figure 4-23. Chloroform concentrations in bulk water for several scenarios of initial chlorine and cell concentration (a) BT = 7 μm (b) BT = 102 μm

For $BT=102 \mu\text{m}$ and Clo of 0.12 mg/L , simulations indicated that the time required for complete reaction chlorine-biomass reduces as X_o increases (7.0, 5.5, and 4.25 hours for X_o of 0.89, 4.03, and 13.98 mg/L , respectively). This is related to faster production of DBP when more biomass is available, which is given by the expression $F_X \times k_1 \times C \times X$ of Equation (4-4). This expression indicates that more DBP is formed per unit of time for high cell concentration, then the maximal potential concentration of DBP is reached in shorter time in comparison to low concentrations of cells.

The different pattern between two BT values in relation to reaction time is explained by whether the reactions are chlorine or biomass limiting. For $7 \mu\text{m}$, reactions can be biomass limiting, residual concentration is 0.11 mg/L (Figure 4-25), and reaction time is directly proportional to cell concentration. On the contrary, reactions can be chlorine limiting for $102 \mu\text{m}$, residual concentrations are almost negligible, and reaction time is inversely proportional to cell concentration. For Clo of 1.66 mg/L , complete transformation of cells and EPS into chloroform also occurred in less than 30 minutes (Figure 4-23b).

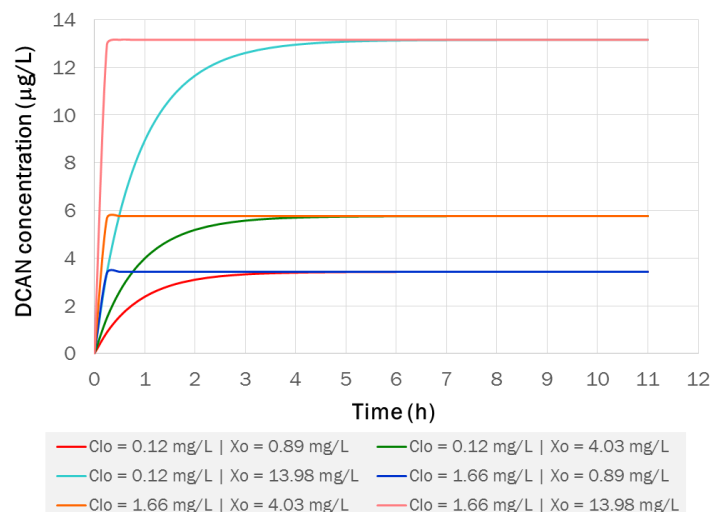
In comparison to reference values, for $BT=7 \mu\text{m}$, the highest X_o led to a maximal potential concentration of chloroform higher than the concentration found in the field work developed in the city of Cali (average $31.62 \mu\text{g/L}$ vs $22.55 \mu\text{g/L}$ ¹⁶ - Section 3.3.5). For $BT=102 \mu\text{m}$, it is worth noting that most of the scenarios considered here resulted in potential concentrations of chloroform higher than the limit defined in the UK regulations ($100 \mu\text{g/L}$) (UK Parliament, 2000). In relation to Colombian standards ($200 \mu\text{g/L}$) (Ministerio de la Protección Social and Ministerio de Ambiente Vivienda y Desarrollo Territorial, 2007), only the scenario of $Clo=1.66 \text{ mg/L}$ and $X_o = 13.98 \text{ mg/L}$ resulted in notably greater concentration ($466.2 \mu\text{g/L}$). Such value can be perceived as unrealistic or improbable, but it is difficult to confirm due to the lack of field data to use as inputs of the model. Therefore, it is important to highlight the importance of studying biofilm properties in DWDNs of developing countries for collecting reliable field data and define real scenarios of these networks. In general, biofilms can be understood as potential chronic risk sources in DWDNs, which may even lead to non-compliance of local regulations for chloroform and TTHMs, according to model results.

¹⁶ 71% of TTHMs represent chloroform – section 4.2.10

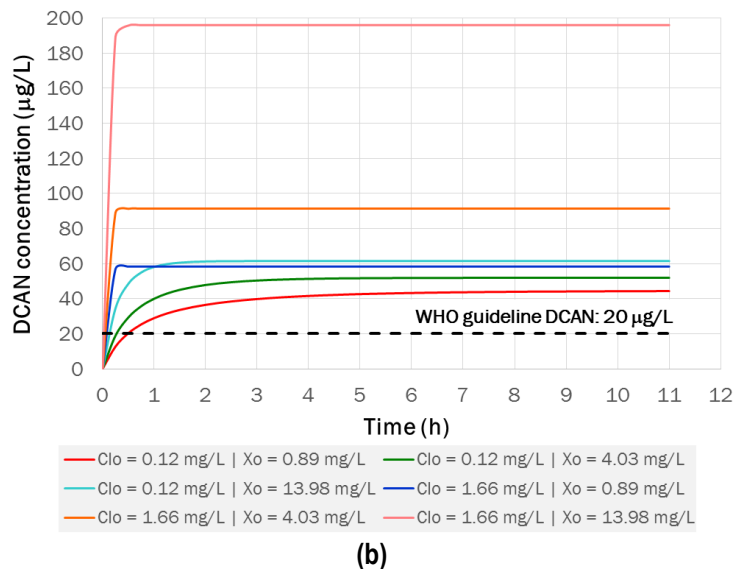
4.3.6.3 Dichloroacetonitrile formation

As expected, the model suggests that thicker biofilms promote the formation of higher potential DCAN concentrations. For BT=7 μm and 102 μm , the simulated DCAN concentrations ranged between 3.43-13.16 $\mu\text{g/L}$ and 44.3-195.94 $\mu\text{g/L}$, respectively (Figure 4-24a and b). In relation to reaction time needed to get to the maximal potential DCAN concentration, the same pattern of chloroform was found for this substance and the two values of BT tested and Clo=0.12 mg/L. For BT=7 μm , reaction time increases as X_o increases, while this time is shorter as X_o increases for BT=102 μm . As mentioned previously, this is related to faster chlorine depletion when more biomass is available, since more DBPs are being formed. For chlorine concentration of 1.66 mg/L, complete transformation of cells and EPS into DCAN occurs in less than 30 minutes (see Figure 4-24a and b). For BT=102 μm , following DCAN guidelines (WHO, 2017) becomes more challenging, since all the tested scenarios produced concentrations higher than 20 $\mu\text{g/L}$ (Figure 4-24b) and a maximum of 195.94 $\mu\text{g/L}$ is obtained for the most critical conditions (Clo=1.66 mg/L, X_o =13.98 mg/L).

It is important to highlight that DCAN is an unstable DBP species, which degrades under certain conditions of free chlorine and pH. DCAN degrades in the absence of chlorine above pH 7 and below pH 6.5. In the presence of free chlorine, DCAN degradation can be much faster in the condition of a pH of about 6–8.5 under low to moderate chlorine residuals (Reckhow et al., 2001). Therefore, despite of the formation of this DBP under stagnation conditions, DCAN concentrations may reduce if conditions of pH and free chlorine are the appropriate for its degradation. Finally, it is important to remark that HANs can be more toxic than THMs and its control must follow the WHO recommendation of 20 $\mu\text{g/L}$ (WHO, 2017), while further research leads to a precautionary threshold based on health effects.



(a)



(b)
Figure 4-24. DCAN concentrations in bulk water for several scenarios of initial chlorine and cell concentration (a) BT = 7 µm (b) BT = 102 µm

4.3.6.4 Chlorine demand

Figure 4-25 shows chlorine decay in bulk water during the formation of DBPs and Table 4-16 includes the chlorine demand exerted by biomass for each scenario. While Chowdhury (2016) found chlorine demands of 0.19 and 0.12 mg/L in morning and afternoon measurements, respectively (Table 4-15), the chlorine demands exerted by cells and EPS in the current model resulted in much lower values (0.009-0.42 mg/L) (Table 4-16). Since chlorine decay was calculated based on the reaction rates and yield coefficients found by Chen and Stewart (1996), chlorine demand does not change with the amount of chloroform and DCAN produced. In addition, the recent experimental study by Lemus Pérez and Rodríguez Susa (2017) determined that all the chlorine consumed by the biofilm matrix was not transformed into DBPs. The current model approach considers the consumption of chlorine only by cells and EPS and separately simulates the formation potentials of two DBP species. In real systems, chlorine reacts with organic and inorganic substances contained in the biofilm matrix such as iron, adsorbed organic matter, and soluble microbial products; and several DBP species are simultaneously formed according to the physico-chemical conditions, chlorine dose, and amount and type of precursors (Wang et al., 2012b; Xue et al., 2013; Lemus Pérez and Rodríguez Susa, 2017).

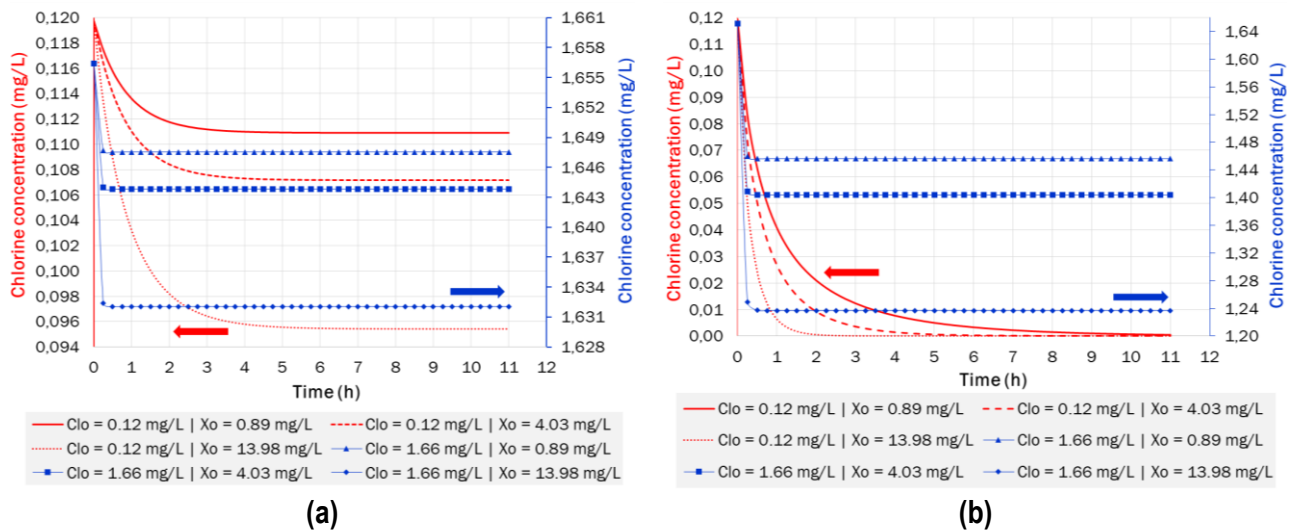


Figure 4-25. Chlorine concentrations in bulk water, under several scenarios of initial chlorine and cell concentration (a) BT = 7 μm (b) BT = 102 μm

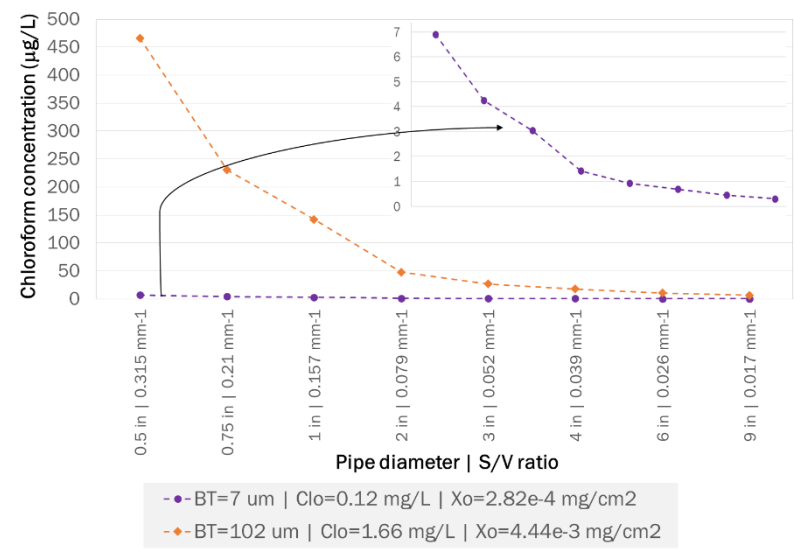
Table 4-16. Chlorine demand on plumbing system scenarios

Scenario		Chlorine demand (mg/L)
1	BT = 7 μm Clo = 0.12 mg/L Xo = 0.89 mg/L	0.009
2	BT = 7 μm Clo = 0.12 mg/L Xo = 4.03 mg/L	0.013
3	BT = 7 μm Clo = 0.12 mg/L Xo = 13.98 mg/L	0.025
4	BT = 7 μm Clo = 1.66 mg/L Xo = 0.89 mg/L	0.012
5	BT = 7 μm Clo = 1.66 mg/L Xo = 4.03 mg/L	0.016
6	BT = 7 μm Clo = 1.66 mg/L Xo = 13.98 mg/L	0.028
7	BT = 102 μm Clo = 0.12 mg/L Xo = 0.89 mg/L	0.120
8	BT = 102 μm Clo = 0.12 mg/L Xo = 4.03 mg/L	0.120
9	BT = 102 μm Clo = 0.12 mg/L Xo = 13.98 mg/L	0.120
10	BT = 102 μm Clo = 1.66 mg/L Xo = 0.89 mg/L	0.204
11	BT = 102 μm Clo = 1.66 mg/L Xo = 4.03 mg/L	0.256
12	BT = 102 μm Clo = 1.66 mg/L Xo = 13.98 mg/L	0.423

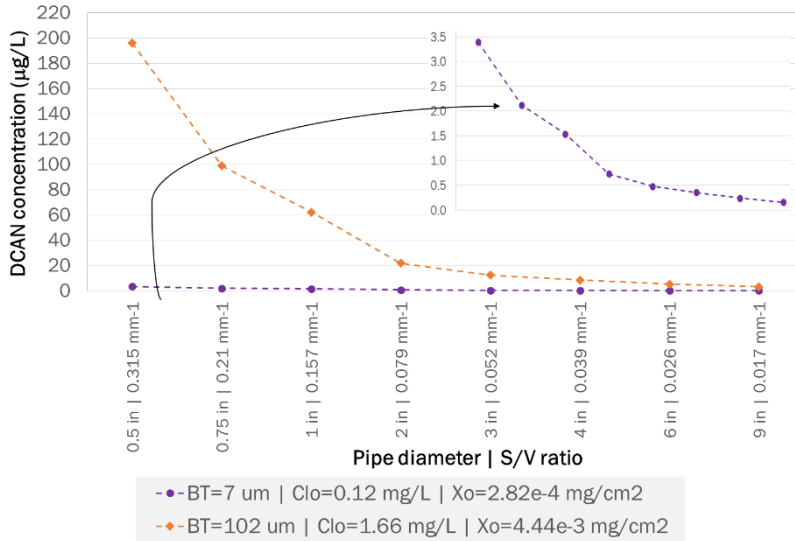
4.3.6.5 Influence of S/V ratio on DBP formation

One of the main characteristics of plumbing systems is the high S/V ratio, as explained in Section 2.2.4. The S/V ratio is included in the current biofilm chlorination model in the boundary condition at the biofilm surface, which represents the variation of dissolved substances in the bulk water (Equations (4-8) and (4-14)). Results for 12 scenarios corresponding to pipe diameter of 1/2 inches, which is commonly used in small building facilities in Colombia, were presented previously. In order to illustrate the influence of this parameter of DBP concentrations, simulations for the least and most critical scenarios were run (1 and 12, respectively) (Table 4-16).

Considering that S/V ratio is inversely proportional to pipe diameter ($4/\phi$), increasing the pipe diameter resulted in reduction of DBP concentrations in bulk water. Simulated chloroform ranged between 0.30-6.91 $\mu\text{g/L}$ (scenario 1) and between 6.55-466.2 $\mu\text{g/L}$ (scenario 12), for ϕ between 1/2 - 9 inches (Figure 4-26a). Similarly, modelled DCAN ranged between 0.16-3.39 $\mu\text{g/L}$ (scenario 1) and between 3.27-195.94 $\mu\text{g/L}$ (scenario 12), for the same ϕ range (Figure 4-26b). The analysis of chlorine wall decay has determined that, as pipe diameter increases, the wall reactions becomes less important and chlorine decay mainly relies on bulk water reactions (Lu et al., 1999; Hallam et al., 2002; Buamah et al., 2014; Lee et al., 2014). For DBP analysis carried out here, pipe diameter as big as 9 inches may lead to potential concentrations of 0.30-6.55 $\mu\text{g/L}$ and 0.16-3.27 $\mu\text{g/L}$ of chloroform and DCAN, respectively, which represent small fractions of the UK and Colombian regulation and WHO guidelines.



(a)



(b)

Figure 4-26. Influence of S/V ratio on DBP concentrations in bulk water (a) Chloroform (b) DCAN

In order to improve the comparison of DBP concentrations to regulation compliance and guidelines, several simulations for both chloroform and DCAN were run for several values of BT and S/V ratio. This was done in order to find the values of this parameter which resulted in lower concentrations than the suggested or regulated ones. Figure 4-27 shows the results of DBP concentrations for $Clo=1.66 \text{ mg/L}$ and X_o of $1.28 \times 10^{-4} \text{ mg/cm}^2$ and $4.44 \times 10^{-3} \text{ mg/cm}^2$ for DCAN and chloroform, respectively. Due to X_o is expressed in terms of surface density, the volumetric concentrations are specified in Figure 4-28, according to the pipe diameter.

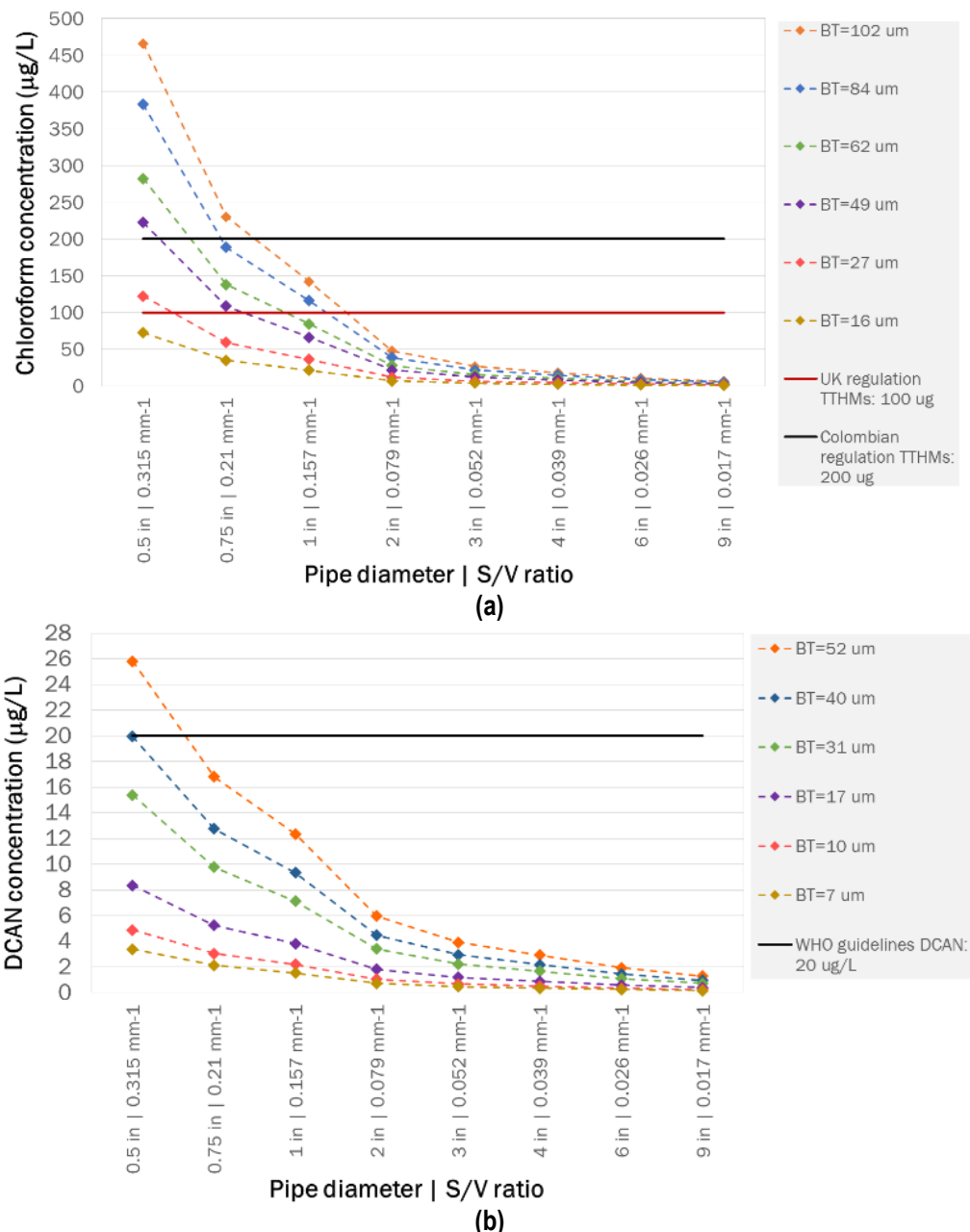


Figure 4-27. DBP concentrations in bulk water and regulation limits / guidelines (a) Chloroform, $Clo = 1.66 \text{ mg/L}$, $X_o = 4.44 \times 10^{-3} \text{ mg/cm}^2$ (b) DCAN, $Clo = 1.66 \text{ mg/L}$, $X_o = 1.28 \times 10^{-4} \text{ mg/cm}^2$

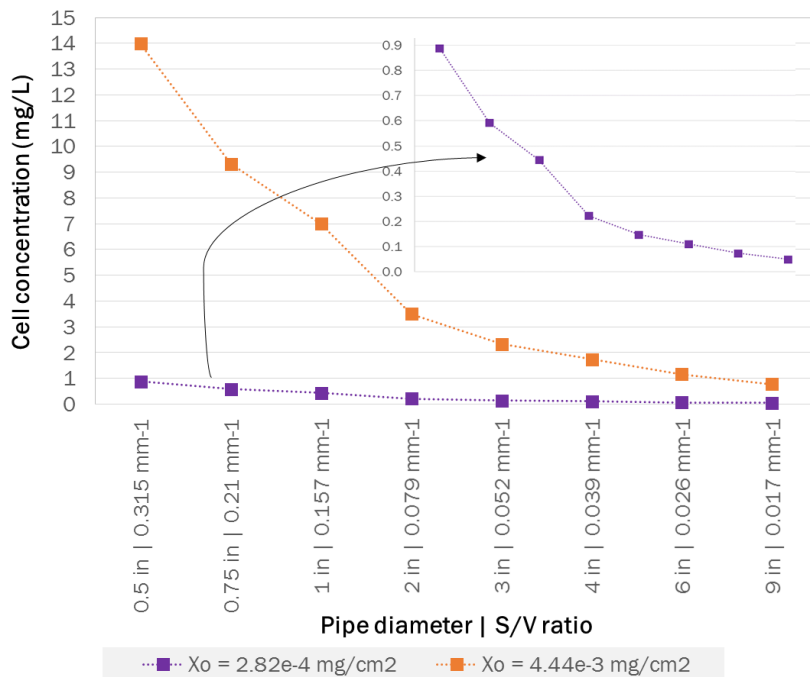


Figure 4-28. Cell concentration according to pipe diameter

Particularly, for the given C_{lo} and X_o , chloroform concentrations fall below the Colombian and UK regulated values (200 and 100 $\mu\text{g/L}$, respectively), for BT values smaller than 49 μm and 16 μm , respectively, and pipe diameter of $\frac{1}{2}$ inches. However, by increasing the pipe diameter to only $\frac{3}{4}$ inches, chloroform concentrations reduce around 51%. Therefore, thicker biofilms result in chloroform concentrations lower than the regulated thresholds. For instance, 84 μm potentially yields 188.5 $\mu\text{g/L}$ and 27 μm potentially yields 59.3 $\mu\text{g/L}$ in ϕ of $\frac{3}{4}$ inches. The same occurs with DCAN concentrations; BT smaller than 40 μm yields potential concentrations lower than the value suggested by the WHO (20 $\mu\text{g/L}$) (WHO, 2017) for every ϕ considered here. Increasing diameter from $\frac{1}{2}$ inches to $\frac{3}{4}$ inches, DCAN concentrations reduce around 36%. Such values of pipe diameter may offer a guideline for future recommendations for design and installation of plumbing pipes in small buildings, where low water consumption is expected. In order to properly propose a minimum pipe diameter for plumbing facilities, further hydraulic analysis must be done to determine the influence of such change on pressure, velocities, and residence time.

4.3.6.6 Discussion of DBP formation potentials simulated under stagnation conditions

The discussion presented in Sections 4.3.6.2 and 4.3.6.3 was based on regulation limits or guideline values; however, such thresholds are more related to precautionary limits rather than health-based recommendations. The toxicity of some DBPs, from around 600 DBPs species discovered to date, has been tested on bioassays with mice and cells using concentrations higher than those found in drinking water (Hrudey, 2009). Overall, the epidemiological evidence is

insufficient to declare chlorinated DBPs as carcinogenic in humans or a cause of birth defects (Hrudey, 2009; Hrudey et al., 2015a). On the other hand, the presence of pathogenic microorganisms in tap water will certainly cause negative public health impacts (Hrudey, 2009). In this line, the risk management alternative is to reduce the precursors of DBPs in the water source, maintaining efficient treatment processes and proper O&M of distribution networks. For plumbing systems, consumers should be advised on flushing the tap water, for the first use of water after a period of stagnation.

In relation to reduce DBPs precursors, it is in this point that biofilm formation and disinfection becomes relevant. Biofilms in drinking water have only been approached in research as potential reservoirs of pathogens, which can be released to bulk water and reach the consumers (Wingender and Flemming, 2011). Biofilm monitoring is not included neither in routine O&M of distribution networks by water utilities nor by regulatory agencies. The current model, based on experimental data reported by other researchers, does acknowledge the role of biofilms as DBP precursors and present the potential concentrations of chloroform and DCAN under certain scenarios. The model presented here allows identifying the most significant parameters and better understanding of the interaction of those involved in the formation of two DBP species formed from the chlorination of drinking water biofilms. In addition, the model gives a better understanding of the rates at which chloroform and DCAN are formed; which is not always evident with solely laboratory data.

4.4 MODEL APPLICATIONS AND LIMITATIONS

The current model can only predict the chlorine decay according to the demand exerted by EPS and cells. The reactions of this disinfectant with other substances contained in the biofilm matrix and attached to the pipe walls such as sediments and loose deposits and bulk water reactions are not included; therefore, chlorine is exclusively available for biofilm reactions. This means that reactions occur faster compared to inclusion of total demand of chlorine in water pipes.

The proposed model does not include neither cell growth nor EPS production. For long term assessment, i.e., days and weeks, biofilm growth should be incorporated in order to completely analyse the dynamics between disinfectant and biofilm matrix; and influence of hydraulics in mass transfer and biofilm detachment. For instance, Abokifa et al. (2016a) found that maximal bacteria growth (biofilm and planktonic cells together) occur after six hours, while cell death and inactivation was reduced. Then, mortality rate increased for the next 12 hours. As a consequence, THM formation reached a plateau for the next 30 hours and constant THM concentration was produced

during this period of time (Abokifa et al., 2016a). Further re-chlorination led to extra reaction with remaining biomass and increasing THM formation; then another plateau was observed until 60 hours of simulation. This indicates that THM formation reached a peak and remained constant until re-chlorination was applied, then another peak was found and remained constant until 60 hours (Abokifa et al., 2016a).

It is known that biofilm growth is a slow process (e.g., hours or days; see modelling and experimental data in Sections 2.4.3 and 4.2.3.1) compared to oxidative reactions with chlorine. Despite this the current model did not include biofilm growth and chlorine demand exerted by other substances present in water pipes, the proposed model developed here is applicable to determine the DBP formation potentials under different of scenarios of biofilm properties and drinking water quality. Model applications also include improving the understanding of field and experimental tests, which are carried out under controlled conditions, as demonstrated by the comparison of results to other studies. Additionally, this model can be applied to plumbing systems and dead-end sections of DWDNs under stagnation conditions in order to predict the potential DBP formation under specific conditions of the assessed system.

On the other hand, this model does differentiate between cells and EPS contribution to DBP formation, which allows the incorporation of kinetic variables resulting from experimental studies carried out for both particulate substances. It is important to highlight that the interest on studying the role of EPS as a protective barrier for bacteria within the biofilm and as DBP precursor is increasing (Fang et al., 2010b; Huang et al., 2012; Wang et al., 2012c; Xue et al., 2012; Wang et al., 2013b; Lemus Pérez and Rodríguez Susa, 2017). Other advantages of the proposed model is the low computational cost due to it is simulating in one dimension; and is able to predict individual DBP species by incorporating their respective diffusion coefficients. Further development of this model may support the improvement of exposure assessment in humans and comparison to maximum concentrations established by toxicological studies. Particularly, this model simulates the formation of DCAN, which can be more toxic substance than other DBPs, and there has not been regulated yet for any national regulatory agency. Long term prediction of DCAN should include a sink term since it degrades over a period of hours or days, depending on pH and chlorine concentration (Reckhow et al., 2001).

The current model relies on microbiological variables such as parameters of biofilm thickness, and initial cell and EPS concentration. As discussed above, biofilms are not frequently monitored in DWDNs by neither water utilities nor regulatory agencies. Therefore, data of these parameters are not often available in real-scale water networks; and to interpret idealized laboratory data can be

challenging in the context of real DWDNs. As a first step, initial EPS concentration was calculated in this study with a linear equation originated from an experimental study with municipal wastewater. Field-work information collected in Cali's DWDN related to water quality was used as inputs for the several scenarios simulated with the current model. However, to the author's knowledge, biofilm thickness, and initial cell and EPS concentration data for this network have not yet been published. This indicates that more effort is required in promoting drinking-water-biofilm research in developing countries by improving international collaborations, laboratory facilities, molecular analysis techniques, protocols for sampling in real-scale DWDNs, among others.

Finally, as human exposure to water substances occur within the facilities, drinking water quality in plumbing systems becomes relevant in public health topics. The epidemiological study by Wright et al. (2017) found that DBP exposure classification may be improved if models were available for the studied network. On the other hand, DBP monitoring take place in the distribution network, which is characterized for flow rates leading to slow velocities in dead-end zones or normal velocities in the main pipes. The current model is applicable under stagnation conditions, which are present in dead-end sections of a network or in plumbing facilities, where water consumption actually occurs. To analyse the mass transfer rate of dissolved substance in the biofilm surface, hydrodynamics are included in a 2D model for water pipes. The definition, development, results and discussion of this model can be found in the following chapter.

4.5 CONCLUSIONS

Biofilms attached to the pipe walls have been acknowledged as a cause for chlorine decay in water pipes but they have not yet been included in DBP models for DWDNs. To the author's knowledge, this is the first model including biofilm EPS oxidation as precursor of DBPs together with cell disinfection. The current study led to the following conclusions:

- Under stagnation conditions and small pipes, biofilm-chlorine reactions at the pipe walls are important for DBP contribution to the bulk water.
- Increasing the complexity of a model is not necessarily directly related to a better approximation of the process. The current 1D model of chlorine disinfection of flat biofilms is able to predict the chloroform and DCAN formation potentials in bulk drinking water, under stagnation conditions.
- Chloroform and DCAN formation from biofilm chlorination can be expressed in terms of cell and EPS concentrations, chlorine yields, reaction rates, and fraction of cells and EPS transformed into DBP.

- Due to the slow process of biofilm growth and EPS production, fixed initial cell and EPS concentration are an appropriate approach to simulate DBP formation potentials occurring in few hours.
- Whether the reactions are chlorine or biomass limiting depends on the parameters biofilm thickness and initial chlorine and cell concentrations together.
- In the current model, DBP diffusion coefficient within the biofilm is relevant only for analysis on short time as 40 minutes.
- Temperature effects are indirectly included in the model by adjusting the reaction rates of chlorine with cells and EPS. Higher temperature leads to acceleration of reactions.
- Parameters biofilm thickness, initial cell and EPS concentration, fraction of cells and EPS transformed into DBP and biofilm area have a linear effect on bulk water concentrations of DBPs. Reactor volume and chlorine yield coefficients have a decreasing exponential effect of DBP concentrations in bulk water.
- Reactor volume and chlorine-cell yield coefficient are the most influencing parameters on bulk water concentrations of DBPs, followed by biofilm area and initial cell concentration. Biofilm thickness also has an important effect on the model results by the direct relationship with cell and EPS concentrations and the definition of the domain dimension.
- To promote biofilm research in real-scale drinking water systems will increase the availability of data useful for DBP models, considering biofilms as precursors.
- Plumbing systems can favour the DBP formation from disinfection of biofilms due to the high stagnation time and high S/V ratios.
- Pipe diameters as small as ½ inches in plumbing facilities may lead to DBP concentrations higher than the regulated or guidance values. Increasing the diameter to ¾ inches can significantly reduce the concentrations even to values under such thresholds.

5 MODELLING DBP FORMATION FROM BIOFILM CHLORINATION UNDER HYDRODYNAMIC CONDITIONS

5.1 INTRODUCTION

This chapter aims to explain the process of developing a 2D model, coupled to a pipe flow, in order to assess the influence of hydraulics over mass transport and formation potentials of chloroform and DCAN from the chlorination of biofilms in drinking water. This study aimed to improve the DBP prediction in water pipes under hydrodynamics conditions. While the simple model developed in Chapter 4 can be applied in water systems under stagnation conditions, the coupled-flow model can be used, in general, in DWDNs with bulk flow. By the current model, chlorine and DBP mass transfer were assessed under different scenarios according to the flow regime, Reynolds number, pipe diameter; and initial chlorine, cell, and EPS concentrations. A sensitivity analysis based on Morris method was also carried out to screen the parameters influence on model outputs.

5.2 MODEL DEVELOPMENT

5.2.1 Model definition

The model described here simulates the formation potentials of chloroform and DCAN from chlorination of flat biofilms in drinking water pipes, in two dimensions, under bulk flow. This model is based on the 1D model previously developed; initial constant concentration of cells and EPS and their decay due to the reaction with chlorine within the biofilm were considered. The schematic representation of the model is presented in Figure 5-1. The starting point for developing the current model was the simple model presented in Chapter 4 and the physico-chemical data collected in the field work discussed in Chapter 3 (see Figure 5-2).

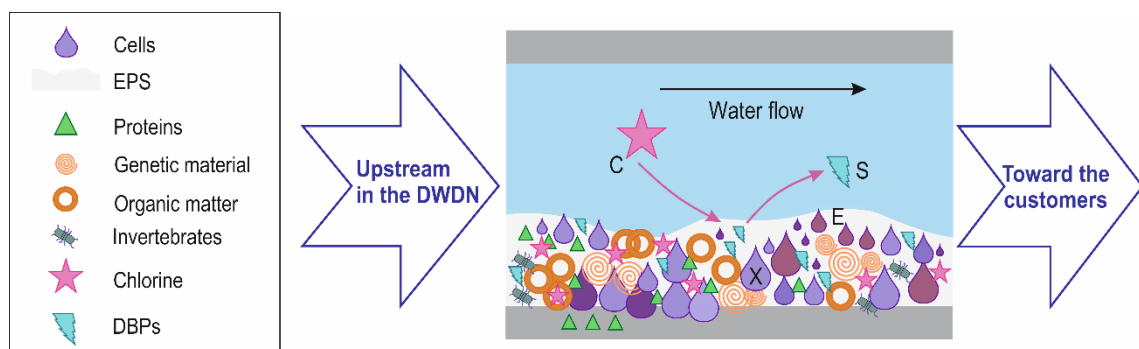


Figure 5-1. Schematic representation of the 2D model

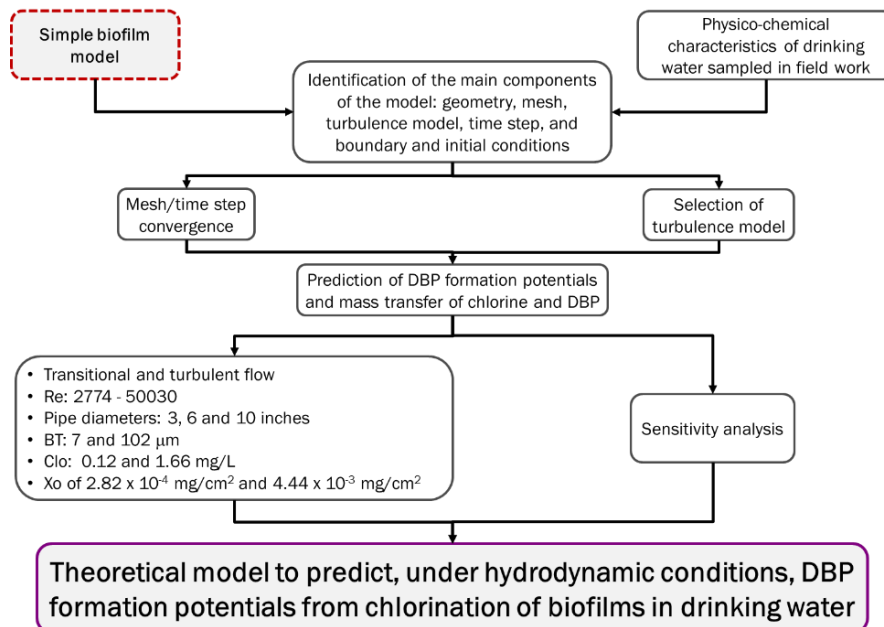


Figure 5-2. Process for building a flow-coupled model to predict DBP formation potentials from chlorination of biofilms

The main assumptions made to develop the current model are:

- Flow field solution: DWDNs are built to transport water from the WTPs to the consumers. Therefore, pipelines are characterized by bulk flow and the flow rates depend on the water demand. Transitional and turbulent flow were considered here because the first one can be present in dead-end sections of DWNs (Abokifa et al., 2016b) and the latter one is predominant in water pipes under normal operation (Cogan, 2010). Laminar flow was also included for comparison purposes, since the biofilm modelling was developed under this flow regime to reduce computational cost.
- Flat biofilm: As explained in Chapter 4, a biofilm can be compact or present voids and channels within in, according to the nutrients availability. This means that biofilm growth under limited transport of nutrients (slow flow) leads to thicker biofilms due to the presence of voids channels rather than higher cell density (Picioreanu et al., 1998b; Picioreanu et al., 2000b). Considering that the current model is mainly focused on transitional and turbulent flow (Re: 2,300-10,000), flat biofilm surface is considered here as a reasonable approximation to the biofilm morphology in drinking water pipes.
- Sherwood number and mass transfer rate of dissolved substances (chlorine and DBPs) are used to characterize the mass transport at the biofilm surface: similar approach has been applied for biofilm modelling, which includes biofilm growth and transport of substrates from bulk

water to the biofilm matrix, through the biofilm surface (IWA Task Group on Biofilm Modeling et al., 2006).

Other assumptions were also made for the 2D model, which were also presented in Chapter 4:

- Biofilm is continuous medium
- Constant biofilm thickness
- Cells and EPS are homogeneously mixed in biofilm matrix
- Fixed initial concentration of cells (X_0) and EPS (E_0)
- Chloroform (S) and DCAN (S) are modelled separately according to fraction of cells and EPS converted into the respective DBP

5.2.2 Model equations and initial and boundary conditions – Reactions

Figure 5-3 sketches the 2D-bulk flow model and the corresponding equations are included in Table 5-1. Under isothermal and isotropic conditions (i.e., constant temperature and constant diffusion coefficient), chlorine diffuses through the biofilm matrix, reacting with cells and EPS (Equation (5-1)). Since this model includes fixed initial concentrations of cells and EPS, the variation of both particulate substances is given by their decay according to reactions with chlorine (Equations (5-2) and (5-3)). Such reaction leads to the formation of DBPs (Equation (5-4)). Parameters F_x and F_E in Equation (5-4) allows simulating the formation of individual species of DBPs, according to experimental data reported by other researchers, as was explained in Section 4.2.3.6. In bulk water, transport of dissolved substances is including both convection and diffusion (Equations (5-5) and (5-6)). The source term in both equations is defined by the consumption of chlorine by biofilm reactions and the formation of DBPs (expression in the right side of the equations).

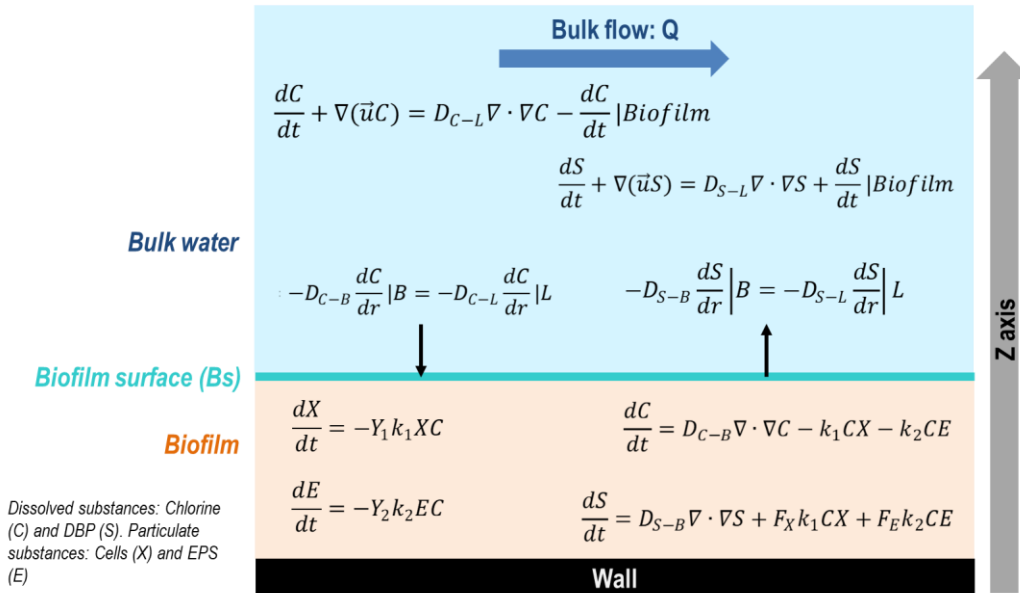


Figure 5-3. 2D mass balance equations for soluble and particulate components in biofilm, biofilm surface, and bulk water

Regarding the initial conditions, at $t=0$, chlorine is completely mixed in bulk water with concentration C_0 , which was also specified at the inlet. Within the biofilm, chlorine concentration is zero. DBP concentration is zero everywhere at $t=0$. Initial concentration of cells and EPS (particulate substances) are X_0 and E_0 at $t=0$. When reactions start, these substances decay until complete depletion, according to contact time with chlorine.

Table 5-1. Mass balance equations and initial conditions in 2D model – Cylindrical pipes

Phase	Equation	Initial conditions	Description of variables	Subscripts
Biofilm	$\frac{dC}{dt} = D_{C-B} \nabla \cdot \nabla C - k_1 CX - k_2 CE$ <p style="text-align: center;">(5-1)</p> <p>Divergence of a vector: $[\nabla]_r = \frac{1}{r} \frac{\partial}{\partial r} (r) [\nabla]_z = \frac{\partial}{\partial z}$</p> <p>Gradient of a scalar: $[\nabla]_r = \frac{\partial}{\partial r} [\nabla]_z = \frac{\partial}{\partial z}$</p>	$t = 0$ $C_{B0} = 0$	C: Disinfectant concentration X: Cell concentration E: EPS concentration k ₁ : Disinfectant decay rate – cells disinfection k ₂ : Disinfectant decay rate – EPS oxidation D _{C-B} : Molecular diffusion coefficient of chlorine in biofilm C _o : Initial concentration of chlorine t: Time	C: Chlorine S: DBP X: Cells E: EPS B: Biofilm L: Bulk liquid Bs: Biofilm surface r: Pipe radius, r-coordinate z: z-coordinate along the pipe length
	$\frac{dX}{dt} = -Y_1 k_1 XC$ <p style="text-align: center;">(5-2)</p>	$t = 0$ $X_{B0} = X_o$	X: Cell concentration C: Disinfectant concentration k ₁ : Disinfectant decay rate – cells disinfection Y ₁ : Cell-chlorine yield coefficient X _o : Initial concentration of cells t: Time	

Phase	Equation	Initial conditions	Description of variables	Subscripts
	$\frac{dE}{dt} = -Y_2 k_2 EC$ <p style="text-align: center;">(5-3)</p>	$t = 0$ $E_{B0} = E_0$	E: EPS concentration C: Disinfectant concentration k_2 : Disinfectant decay rate – EPS oxidation Y_2 : EPS-chlorine yield coefficient E_0 : Initial concentration of EPS t: Time	
	$\frac{dS}{dt} = D_{S-B} \nabla \cdot \nabla S + F_X k_1 CX + F_E k_2 CE$ <p style="text-align: center;">(5-4)</p>	$t = 0$ $S_{Bs} = 0$ $S_{B0} = 0$	S: DBP concentration X: Cell concentration E: EPS concentration k_1 : Disinfectant decay rate – cells disinfection k_2 : Disinfectant decay rate – EPS oxidation D_{S-B} : Diffusion coefficient of DBP in biofilm F_X : Fraction of cells transformed into DBP F_E : Fraction of EPS transformed into DBP S_0 : Initial concentration of DBP t: Time	

Phase	Equation	Initial conditions	Description of variables	Subscripts
Bulk water	$\frac{dC}{dt} + \nabla(\vec{u}C) = D_{C-L}\nabla \cdot \nabla C - \frac{dC}{dt} _{Biofilm}$ <p style="text-align: center;">(5-5)</p>	$t = 0$ $C_{Lo} = C_o$	C: Chlorine concentration \vec{u} : Velocity vector D_{C-L} : Molecular diffusion coefficient of chlorine in liquid C_o : Initial concentration of chlorine t: Time	
	$\frac{dS}{dt} + \nabla(\vec{u}S) = D_{S-L}\nabla \cdot \nabla S + \frac{dS}{dt} _{Biofilm}$ <p style="text-align: center;">(5-6)</p>	$t = 0$ $S_{Lo} = 0$	S: DBP concentration X: Cells concentration E: EPS concentration D_{S-L} : Diffusion coefficient of DBP in liquid t: Time	

Table 5-2 presents the boundary conditions for the transport of dissolved substances. Continuity flux boundary condition is included at the biofilm surface (Bs) for chlorine (Equation (5-7)) and DBP (Equation (5-8)). This boundary condition means that substance concentrations and flux are the same on both sides of the interface between bulk water and biofilm (IWA Task Group on Biofilm Modeling et al., 2006). On the other hand, there is no exchange of particulate substances, cells and EPS, between biofilm and bulk flow (no flux condition – Equation (5-9)). At the pipe inlet, the boundary condition is the concentration of chlorine and DBP (Equations (5-10) and (5-11), respectively). At the pipe outlet, the boundary condition is represented by the outflow, which assumes that there is zero gradient in the normal direction, of neither chlorine (Equation (5-12)) nor DBP (Equation (5-13)) at this boundary. At the substratum (pipe wall), there is no exchange of neither particulate nor dissolved substances (no flux condition – Equations (5-14) and (5-15), respectively).

Table 5-2. Boundary conditions for transport of dissolved substances in 2D model – Cylindrical pipes

Boundary	Boundary conditions	Description of variables	Subscripts
Biofilm surface (Bs)	$j_{C-Bs} = -D_{C-B} \frac{dC}{dr} \Big _B = -D_{C-L} \frac{dC}{dr} \Big _L$ <p style="text-align: center;">(5-7)</p> $j_{S-Bs} = -D_{S-B} \frac{dS}{dr} \Big _B = -D_{S-L} \frac{dS}{dr} \Big _L$ <p style="text-align: center;">(5-8)</p> $j_{X-Bs} = j_{E-Bs} = 0$ <p style="text-align: center;">(5-9)</p>	j: Flux C: Chlorine concentration S: DBP concentration D _{C-B} : Molecular diffusion coefficient of chlorine in biofilm D _{C-L} : Molecular diffusion coefficient of chlorine in liquid	C: Chlorine S: DBP X: Cells E: EPS B: Biofilm L: Bulk liquid Bs: Biofilm surface
Inlet	$C_{inlet} = C_0$ <p style="text-align: center;">(5-10)</p> $S_{inlet} = 0$ <p style="text-align: center;">(5-11)</p>	C _{inlet} : Chlorine concentration at the pipe inlet C ₀ : Initial concentration of chlorine S _{inlet} : DBP concentration at the pipe inlet	r: Pipe radius, r-coordinate z: z-coordinate

Boundary	Boundary conditions	Description of variables	Subscripts
Outlet	$n \cdot -D_{C-L} \nabla C = 0$ <p style="text-align: center;">(5-12)</p> $n \cdot -D_{S-L} \nabla S = 0$ <p style="text-align: center;">(5-13)</p>	n: Normal vector D _{C-L} : Molecular diffusion coefficient of chlorine in liquid D _{S-L} : Diffusion coefficient of DBP in liquid ∇C: Gradient of chlorine concentration ∇S: Gradient of DBP concentration	
Walls	$j_{X-wall} = j_{E-wall} = 0$ <p style="text-align: center;">(5-14)</p> $j_{C-wall} = j_{S-wall} = 0$ <p style="text-align: center;">(5-15)</p>	j: Flux	

5.2.3 Model equations and initial and boundary conditions – Bulk flow

Table 5-3 shows the Navier-Stokes equations for solving the flow field for incompressible flow (mass-continuity and momentum). Here, drinking water is treated in its liquid phase and energy conservation equation was not solved because the model was developed for isothermal conditions. Navier (1827; cited by Canuto et al. (2007)) must be credited with the first attempt at deriving the equations for homogeneous incompressible viscous fluids on the basis of considerations involving the action of intermolecular forces. Stokes (1845; cited by Canuto et al. (2007)) who, under the sole assumption that the stresses are linear functions of the strain rates, derived the equations in the form that is currently in use. Equation (5-16) is the equation of mass conservation, also known as the continuity equation. The equation for momentum conservation is given by Equation (5-17). The expression on the right-hand side of this equation ($\nabla(\mu \nabla \vec{u})$) corresponds to the viscous stress tensor.

Table 5-3. Navier-Stokes equations for incompressible flow

Component	Equation	Description of variables
Mass	$\frac{\partial \rho}{\partial t} + \nabla(\rho \vec{u}) = 0$ <p style="text-align: center;">(5-16)</p>	ρ: Fluid density \vec{u} : Velocity vector t: Time

Component	Equation	Description of variables
Momentum	$\frac{\partial(\rho\vec{u})}{\partial t} + \nabla(\rho\vec{u}\vec{u}) = -\nabla p + \nabla(\mu\nabla\vec{u})$ <p style="text-align: center;">(5-17)</p>	<p>p: Pressure</p> <p>μ: Molecular viscosity</p>

Table 5-4 presents the boundary conditions for the flow field. Normal velocity condition is specified at the inlet (Equation (5-18)), pressure at the outlet (Equation (5-19)), and no slip at the walls (Equation (5-20)).

Table 5-4. Boundary conditions for flow field in 2D model – Cylindrical pipes

Boundary	Boundary conditions	Initial conditions	Description of variables
Inlet	$u = -nUo$ <p style="text-align: center;">(5-18)</p>	<p>Uo: parabolic profile of Vo</p> <p><i>Turbulence conditions:</i></p> <p>Turbulent intensity = 0.1</p> <p>Turbulent length scale = φ</p>	<p>u: Normal inflow velocity magnitude</p> <p>Uo: Velocity magnitude</p> <p>Vo: Average velocity</p>
Outlet	$p = 0$ <p style="text-align: center;">(5-19)</p>	-	p: Pressure
Walls and Biofilm surface (Bs)	$\vec{u} = 0$ <p style="text-align: center;">(5-20)</p>	-	\vec{u} : Velocity vector

The model SST (Shear Stress Transport) was chosen for solving the transitional and turbulent flow. Details about the process to select the appropriate turbulence model are presented in the Section 5.2.4.3. Turbulence is a property of the flow and it is measured by the Reynolds number (Re). In this study, the range Re = 2300 – 10,000 was used as the range for the transition regime between laminar and turbulent flow (Abraham et al., 2009). Turbulence is characterized by a wide range of flow scales: the largest occurring scales, which depend on the geometry, the smallest, quickly fluctuating scales, and all the scales in between (COMSOL, 2013). The Navier-Stokes equations can be used for turbulent flow simulations, although this would require a large number of elements in order to capture the turbulent flow fluctuations in time and space. A strategy to tackle this issue is to divide the flow into large, resolved scales and small, unresolved scales. The small scales are then modelled using a turbulence model to reduce the numerical cost of resolving all present scales (COMSOL, 2013).

In this line, the Navier-Stokes equations for incompressible flow are adapted to include the flow quantities into an averaged value and a fluctuating part. Then, \vec{u} is replaced by the averaged velocity field \mathbf{U} (COMSOL, 2013) (Table 5-5 and Table 5-6). The term $\nabla \cdot (\rho \mathbf{u}' \otimes \mathbf{u}')$ specified in the Equation (5-22) is called the Reynolds stress tensor (COMSOL, 2013).

Table 5-5. Navier-Stokes equations for turbulent incompressible flow

Component	Equation	Description of variables
Mass	$\frac{\partial \rho}{\partial t} + \nabla(\rho \mathbf{U}) = \mathbf{0}$ <p style="text-align: center;">(5-21)</p>	<p>ρ: Fluid density</p> <p>\mathbf{U}: Averaged velocity field</p> <p>t: Time</p>
Momentum	$\frac{\partial(\rho \mathbf{U})}{\partial t} + \nabla(\rho \mathbf{U}) + \nabla \cdot (\rho \mathbf{u}' \otimes \mathbf{u}') = -\nabla p + \nabla(\mu \nabla \mathbf{U})$ <p style="text-align: center;">(5-22)</p>	<p>p: Pressure</p> <p>μ: Molecular viscosity</p>

The equations of the turbulence model SST are included in Table 5-6. The SST turbulence model combines the κ - ϵ and κ - ω turbulence models. The model equations are formulated in terms of turbulent kinetic energy (κ) (Equation (5-23)) and the dissipation per unit turbulent kinetic energy (ω) (Equation (5-24)). The turbulent viscosity is expressed by the Equation (5-25). E is the characteristic magnitude of the average velocity gradients (Equation (5-26)). P is a function of P_k (Equation (5-27)), which is the rate of production of the turbulent kinetic energy κ (Equation (5-28)), and the terms σ_κ , σ_ω , $\sigma_{\omega 2}$ are Prandtl number-like parameters for the transport κ and ω (Abraham et al., 2009). The model constants are defined through interpolation of appropriate inner and outer values (Equation (5-29)). F_1 is a blending function (Equation (5-30)) that facilitates the combination of the standard κ - ϵ and κ - ω models. The β terms are model constants.

The factor γ , which multiplies the production term P in Equation (5-24), has the role of diminishing the rate of turbulence production in flows that are not fully turbulent (Abraham et al., 2009). The values of γ range between 0 and 1. COMSOL interpolates γ by Equation (5-29) with default values $\gamma_1 = 5/9$ and $\gamma_2 = 0.44$ (Table 5-6). On the other hand, Abraham et al. (2009) presented a transition model to adapt the SST turbulence model to non-fully turbulent flows for the simulation of heat transfer in round pipes. The adaptation was made via the damping factor γ , which depends also on the local stability status of the flow in the near-wall region. Complete development of the transition model can be found in Abraham et al. (2009). Despite of some Re of the simulations presented in

this study fall into the transitional flow regime, the SST model included in COMSOL Multiphysics 5.2a was used (see Section 5.2.4.3).

SST model uses the wall distance parameter (l_w ; Equations (5-31) and (5-34)), which is provided by a mathematical *Wall Distance* interface. *Wall distance* is included when using the SST model implemented with COMSOL Multiphysics 5.2a. The solution to the wall distance equation is controlled using the parameter l_{ref} . The distance to objects larger than l_{ref} is represented accurately, while objects smaller than l_{ref} are effectively diminished by appearing to be farther away than they actually are. This is a desirable feature in turbulence modelling since small objects would get too large impact on the solution if the wall distance were measured exactly (COMSOL, 2013). Finally, the model SST in COMSOL Multiphysics 5.2a includes the default constants specified in Table 5-6, which remained unchanged in the application to the current biofilm chlorination model.

Table 5-6. Equations of the turbulent model SST

Equations	Description of variables
$\frac{\partial(\rho k)}{\partial t} + \nabla(\rho k \vec{u}) = P - \rho \beta_o^* k \omega \nabla \cdot [(\mu + \sigma_k \mu_T) \nabla k]$	(5-23) t: Time
$\frac{\partial(\rho \omega)}{\partial t} + \nabla(\rho \omega \vec{u}) = \frac{\rho \gamma}{\mu_T} P - \rho \beta \omega^2 + \nabla \cdot [(\mu + \sigma_k \mu_T) \nabla k] + 2(1 - F_1) \frac{\rho \sigma_{\omega 2}}{\omega} \nabla \omega \cdot \nabla k$	(5-24) k: Turbulent kinetic energy ω: Dissipation per unit turbulent
$\mu_T = \frac{\rho a_1 k}{\max(a_1 \omega, E F_2)}$	(5-25) kinetic energy
$E = \sqrt{2 E_{ij} E_{ij}}$	(5-26) turbulent kinetic energy
$P = \min(P_k, 10 \beta_o^* k \omega)$	(5-27) ρ: Fluid density
$P_k = \mu_T (\nabla \vec{u} : (\nabla \vec{u} + (\nabla \vec{u})^T) - \frac{2}{3} (\nabla \cdot \vec{u})^2) - \frac{2}{3} \rho k \nabla \cdot \vec{u}$	(5-28) μ: Molecular viscosity μ _T : Turbulent viscosity
<p>Constants of the model: $\lambda = F_1 \lambda_1 + (1 - F_1) \lambda_2$ for $\lambda = \beta, \gamma, \sigma_k, \sigma_\omega$</p>	(5-29) F ₁ , F ₂ : Interpolation functions
$F_1 = \tanh(\theta_1^4)$	(5-30) E: Characteristic magnitude of the
$\theta_1 = \min \left[\max \left(\frac{\sqrt{k}}{\beta_o^* \omega l_w}, \frac{500 \mu}{\rho \omega l_w^2} \right), \frac{4 \rho \sigma_{\omega 2} k}{CD_{k\omega} l_w^2} \right]$	(5-31) average velocity gradients
$CD_{k\omega} = \max \left(\frac{2 \rho \sigma_{\omega 2}}{\omega} \nabla \omega \cdot \nabla k, 10^{-10} \right)$	(5-32) T: Temperature
$F_2 = \tanh(\theta_2^2)$	(5-33) P _k : Production term
$\theta_2 = \max \left(\frac{2 \sqrt{k}}{\beta_o^* \omega l_w}, \frac{500 \mu}{\rho \omega l_w^2} \right)$	(5-34) l _w : Distance to the closest wall β ₁ , β ₁ , β* ₀ , γ ₁ , γ ₂ , σ _{k1} , σ _{k2} , σ _{ω1} , σ _{ω2} , a ₁ : constants of the model
<p>Turbulence model parameters: The default model constants are given by: β₁=0.075 β₂=0.0828 β*₀=0.09 γ₁=5/9 γ₂=0.44 σ_{k1}=0.85 σ_{k2}=1.0 σ_{ω1}=0.5 σ_{ω2}=0.856 a₁=0.31</p>	

Source: adapted from COMSOL (2013)

5.2.4 Pre-processing

5.2.4.1 Geometry and mesh

The current model presents some mathematical challenges at the biofilm surface; fluxes vary from zero to a finite value in few seconds. Several mesh and geometry configurations were tested and it was observed that, when the mesh size in this region was higher than the length scale of the mathematical solution, negative concentrations of the dissolved substances arose at the pipe wall and/or outlet. In order to avoid this, the optimal geometry and mesh were selected in function of obtaining positive concentrations of chlorine and chloroform and positive fluxes, under laminar and transition flow regimes. Therefore, five configurations were tested by a combination of several geometry and model characteristics, which are specified in Table 5-7.

Table 5-7. Geometry configurations tested in the current model

Configuration Nr.	Main bulk water domain	Surface reactions	Full biofilm thickness	Stabilization domain with no reaction	
				Before main bulk water domain	After main bulk water domain
1	X	X			
2	X		X		
3	X	X		X	
4	X	X		X	X
5	X		X	X	

The main bulk water domain represents the portion of the pipe where wall reactions were occurring along its length, from the beginning to the end. Surface reactions indicated the solution of wall reactions in COMSOL by assuming that the biofilm is completely mixed, then simulations of the reactions along the total biofilm thickness is not necessary. This represented a simplification of the model because specifying reactions at the wall as boundary was sufficient. Full biofilm thickness means that wall reactions were specified along the total biofilm thickness, then constructing a subdomain for this was necessary. A stabilization domain with no reactions refers to the construction of a subdomain for bulk water, where no reactions were taking place. This was made in order to allow the development of the flow and the transport of dissolved substances without steep changes of their concentrations due to reactions with biomass.

The meshes were created with COMSOL Multiphysics 5.2a. The first attempt was made with a triangular mesh refined at the wall and at the boundary between the stabilization and bulk water domains; biofilm reactions were included as surface reactions. However, fluxes at the wall presented notably oscillations. This mesh was discarded and effort was focused on rectangular element meshes. Finally, the configuration number 5 was selected together with a mapped mesh,

including boundary layers at the biofilm surface and in between stabilization and bulk water domains in order to smooth the transition between elements of different size. Figure 5-4 presents the geometry configuration and Figure 5-5 shows the mesh details.

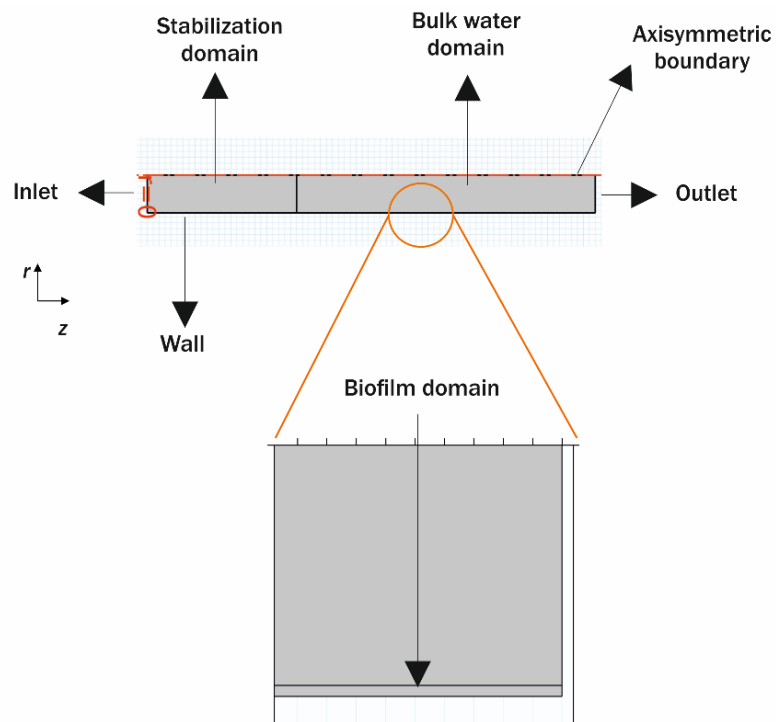


Figure 5-4. Geometry of the water pipe

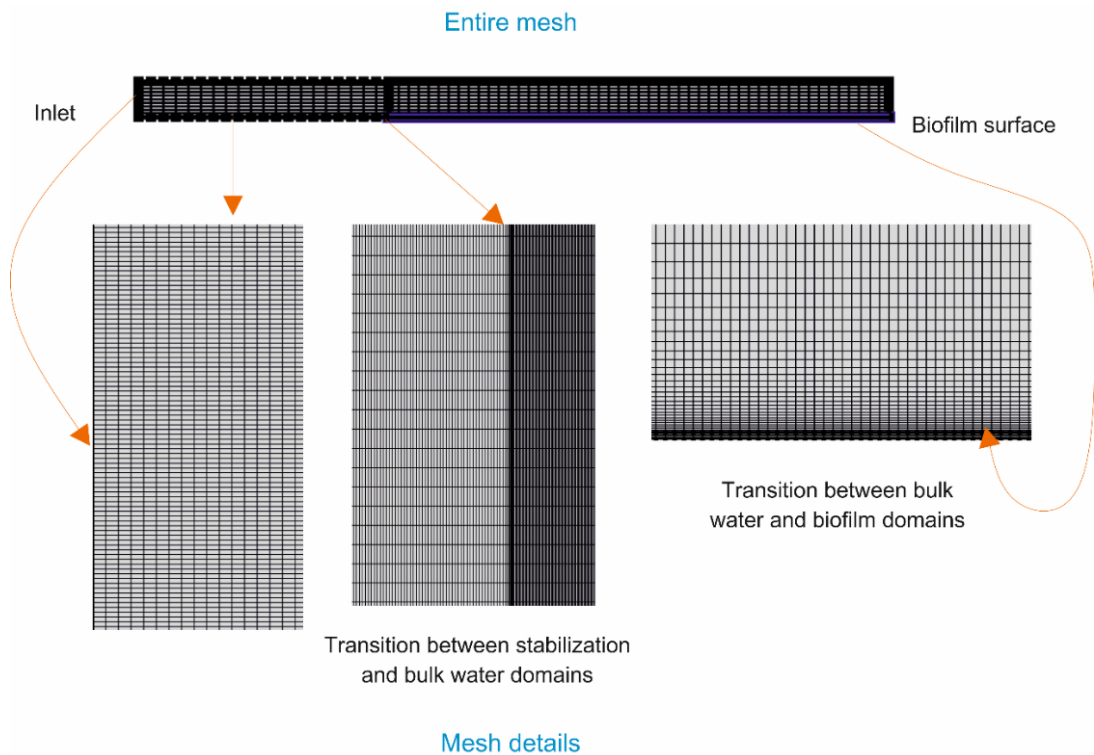


Figure 5-5. Mesh details of the water pipe

The software COMSOL offers the parameter “mesh quality” to assess the degeneration of the elements, according to their shapes. Quality varies between 0 and 1; 0 represents the presence of degenerated elements and 1 perfectly regular elements. Low mesh quality leads to inverted elements and convergence issues (COMSOL, 2012); therefore, it is preferable to obtain mesh quality near to 1 at the time of constructing the mesh. For the stabilization domain, high mesh quality was not necessary because this domain was only used for development of the flow and transport of chlorine with no reactions. The mesh quality of the biofilm subdomain is very low due to the aspect ratio of the elements; thickness varied between 7-102 μm while length was 1 m. In order to minimise this difference, a boundary layer was included at the biofilm surface to improve the transition of the element size between biofilm and bulk water domains.

The highest mesh quality was established for bulk water in order to better predict the transport of dissolved substances along the pipe. Another boundary layer was included between the stabilization and bulk water domain. Overall, the selected geometry and constructed mesh were appropriate for the scope of the current model, obtaining reasonable chlorine and chloroform concentrations and fluxes at the pipe wall and outlet, within an acceptable computational time (see Sections 5.2.4.2 and 5.3.1). Table 5-8, Table 5-9 and Table 5-10 describe the main mesh characteristics for ϕ of 10, 6, and 3 (inches), respectively. The number of elements was changed according to the pipe diameter in order to keep the same mesh quality. The length of the pipe was kept equal to 1 m to ease the interpretation of the results.

Table 5-8. Characteristics of the mapped mesh for pipe diameter of 10 inches

Domain / Region	Size elements	Element distribution on edges	Number of elements	Average quality
Stabilization	<ul style="list-style-type: none"> ▪ Length: 0.5 m ▪ Predefined size: normal 	<ul style="list-style-type: none"> ▪ Wall: 150 ▪ Inlet: 150 	34,200	0.350
Bulk water	<ul style="list-style-type: none"> ▪ Length: 1.0 m ▪ Predefined size: fine 	<ul style="list-style-type: none"> ▪ Biofilm surface: 800 ▪ Wall: 150 	152,000	0.740
Biofilm	<ul style="list-style-type: none"> ▪ Length: 1.0 m ▪ Thickness: 7-102 μm ▪ Predefined size: fine 	<ul style="list-style-type: none"> ▪ Biofilm surface: 800 ▪ Wall: 5 	4,000	0.002
Whole mesh statistics: Total number of elements / Average quality			190,200	0.651
Boundary layer in biofilm surface	<ul style="list-style-type: none"> ▪ Number of boundary layers: 40 ▪ Stretching factor: 1.1 ▪ Thickness of first layer: BT/5 			
Boundary layer in between stabilization and bulk water domain	<ul style="list-style-type: none"> ▪ Number of boundary layers: 30 ▪ Stretching factor: 1.5 ▪ Thickness of first layer: L/800 			

Table 5-9. Characteristics of the mapped mesh for pipe diameter of 6 inches

Domain / Region	Size elements	Element distribution on edges	Number of elements	Average quality
Stabilization	<ul style="list-style-type: none"> ▪ Length: 0.5 m ▪ Predefined size: normal 	<ul style="list-style-type: none"> ▪ Wall: 150 ▪ Inlet: 100 	21,600	0.340
Bulk water	<ul style="list-style-type: none"> ▪ Length: 1.0 m ▪ Predefined size: fine 	<ul style="list-style-type: none"> ▪ Biofilm surface: 800 ▪ Wall: 100 	96,000	0.740
Biofilm	<ul style="list-style-type: none"> ▪ Length: 1.0 m ▪ Thickness: 7-102 μm ▪ Predefined size: fine 	<ul style="list-style-type: none"> ▪ Biofilm surface: 800 ▪ Wall: 5 	4,000	0.002
Whole mesh statistics: Total number of elements / Average quality			121,600	0.646
Boundary layer in biofilm surface	<ul style="list-style-type: none"> ▪ Number of boundary layers: 20 ▪ Stretching factor: 1.2 ▪ Thickness of first layer: BT/5 			
Boundary layer in between stabilization and bulk water domain	<ul style="list-style-type: none"> ▪ Number of boundary layers: 30 ▪ Stretching factor: 1.5 ▪ Thickness of first layer: L/800 			

Table 5-10. Characteristics of the mapped mesh for pipe diameter of 3 inches

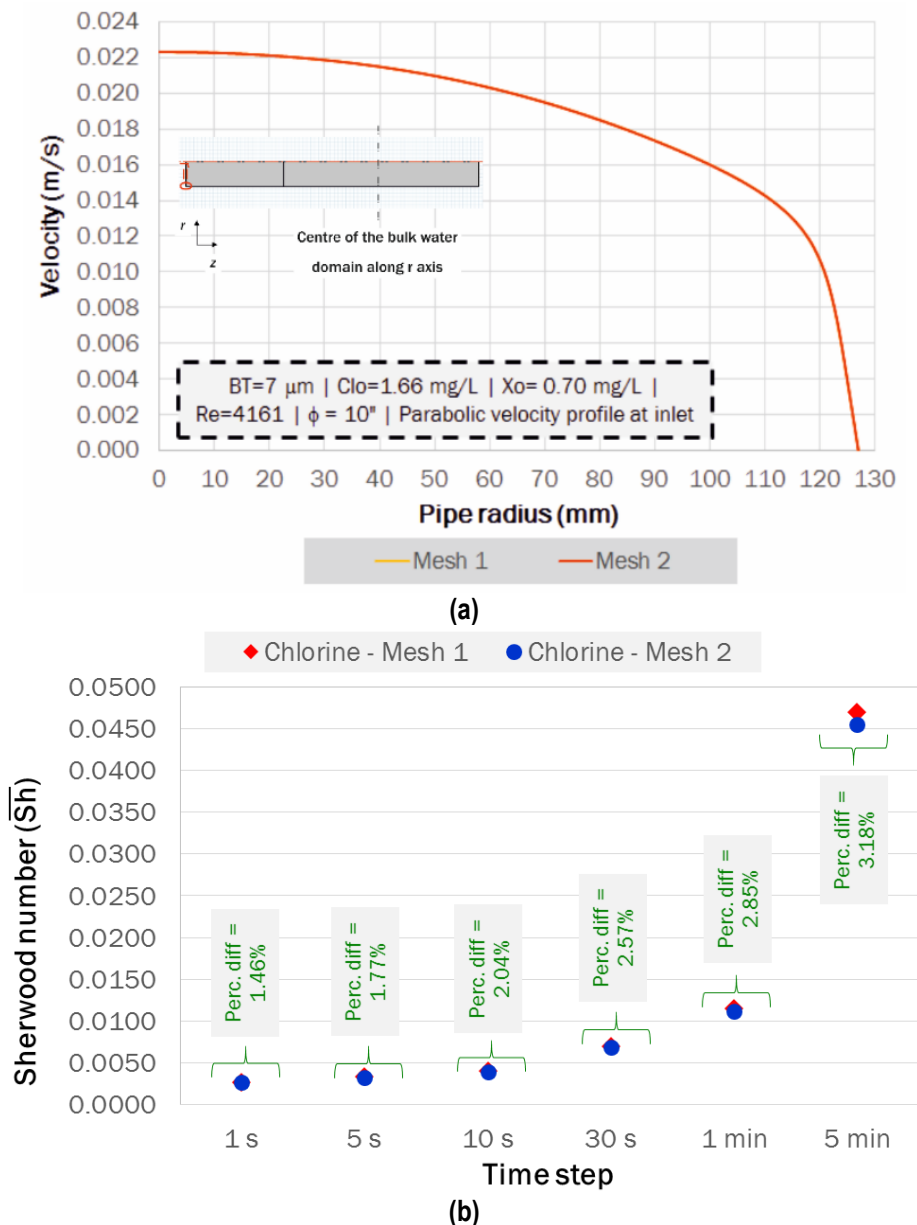
Domain / Region	Size elements	Element distribution on edges	Number of elements	Average quality
Stabilization	<ul style="list-style-type: none"> ▪ Length: 0.5 m ▪ Predefined size: normal 	<ul style="list-style-type: none"> ▪ Wall: 150 ▪ Inlet: 50 	10,800	0.340
Bulk water	<ul style="list-style-type: none"> ▪ Length: 1.0 m ▪ Predefined size: finer 	<ul style="list-style-type: none"> ▪ Biofilm surface: 800 ▪ Wall: 50 	48,000	0.741
Biofilm	<ul style="list-style-type: none"> ▪ Length: 1.0 m ▪ Thickness: 7-102 μm ▪ Predefined size: fine 	<ul style="list-style-type: none"> ▪ Biofilm surface: 800 ▪ Wall: 5 	4,000	0.002
Whole mesh statistics: Total number of elements / Average quality			62,800	0.625
Boundary layer in biofilm surface	<ul style="list-style-type: none"> ▪ Number of boundary layers: 40 ▪ Stretching factor: 1.1 ▪ Thickness of first layer: BT/5 			
Boundary layer in between stabilization and bulk water domain	<ul style="list-style-type: none"> ▪ Number of boundary layers: 30 ▪ Stretching factor: 1.4 ▪ Thickness of first layer: L/800 			

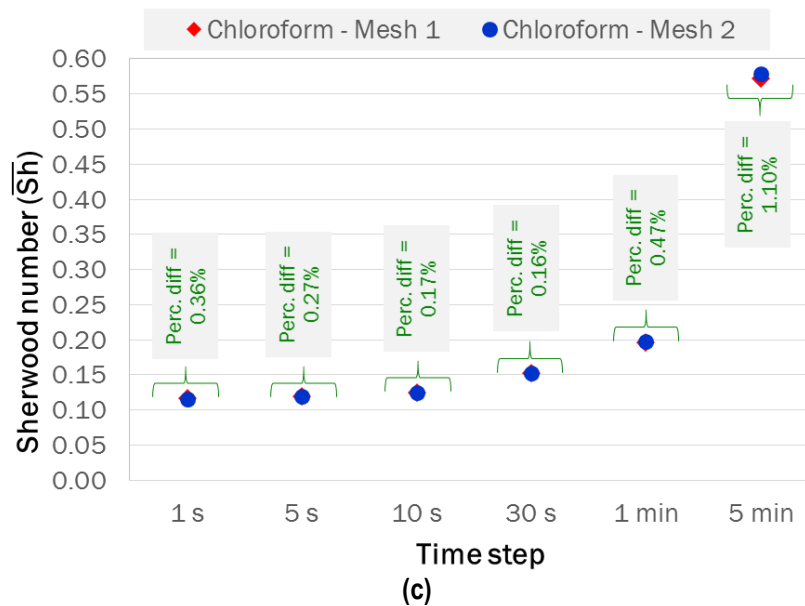
5.2.4.2 Mesh convergence and selection of time step

Once the base mesh was defined for 10-inch pipes (mesh 1, 190.200 elements, Table 5-8), the next step was to determine the mesh convergence. This was done by refining that mesh in both directions (r, z), including the boundary layers; such refinement consisted on doubling the number of elements. The mesh 2 resulted in 752.800 elements. Taking into account that the current model was applied for prediction of bulk concentrations of DBPs and characterisation of mass transport of dissolved substances at the biofilm surface, velocity at the centre of the bulk water domain along r axis and the parameter \bar{Sh} (Equation (2-11)) for both chlorine and chloroform were used to compare both meshes. These parameters are representing the flow regime and mass transport

simulations of the model. Several time steps (i.e., 1s, 5 s, 10 s, 30 s, 1 min, 5 min) were also compared for \bar{Sh} in order to identify the appropriate time step simultaneously to mesh convergence test.

Results of velocity at the centre of the bulk water domain and the parameter \bar{Sh} are presented in Figure 5-6. The conditions of the simulations are also specified in Figure 5-6a. Result comparisons allowed determining that results of velocity and \bar{Sh} obtained with both meshes are similar. Percentage of difference for maximal, median, and average velocity were 0%, 0%, and 0.11%, respectively. In the case of \bar{Sh} for chlorine, percentage of difference ranged between 1.46-3.18% for the assessed time steps. Finally, \bar{Sh} for chloroform, percentage of difference ranged between 0.16-1.10% for the assessed time steps. Due to small differences between two meshes, the mesh 1 was selected for running the subsequent simulations.





(c)
Figure 5-6. Comparison of velocity and \bar{Sh} between mesh 1 and 2 (a) Velocity monitored in the centre of bulk water domain along r axis (b) \bar{Sh} for chlorine (c) \bar{Sh} for chloroform

In relation to the time step, the selected ones resulted in dissimilar results between consecutive pairs for every mesh. The percentage of difference ranged between 19.38-121.47% and 2.54-97.87% for chlorine and chloroform, respectively with mesh 1; and between 19.07-121.26% and 2.63-98.35% for chlorine and chloroform, respectively with mesh 2. For this reason, a time step of 0.1 s was also tested with mesh 1. Figure 5-7a presents the comparison of \bar{Sh} for both chlorine and chloroform and Figure 5-7b shows the comparison of average chloroform concentrations at the pipe outlet for several time steps. In relation to the latter, percentage of difference varied between 0.0-3.98%, 0.15-86.47% and 0.02-6.33% for maximal, median and average concentrations, respectively, for consecutive pairs of time steps. In particular, percentage of difference between values corresponding to 0.1 s and 1 s resulted in 0%, 0.15% and 0.02% for maximal, median and average concentration of chloroform, respectively. In the case of \bar{Sh} , percentage of difference was reduced to 4.78% and 0.08% for chlorine and chloroform, respectively between time steps 0.1 s and 1 s. Due to small differences between time steps 0.1 s and 1 s, the latter one was selected for the subsequent simulations.

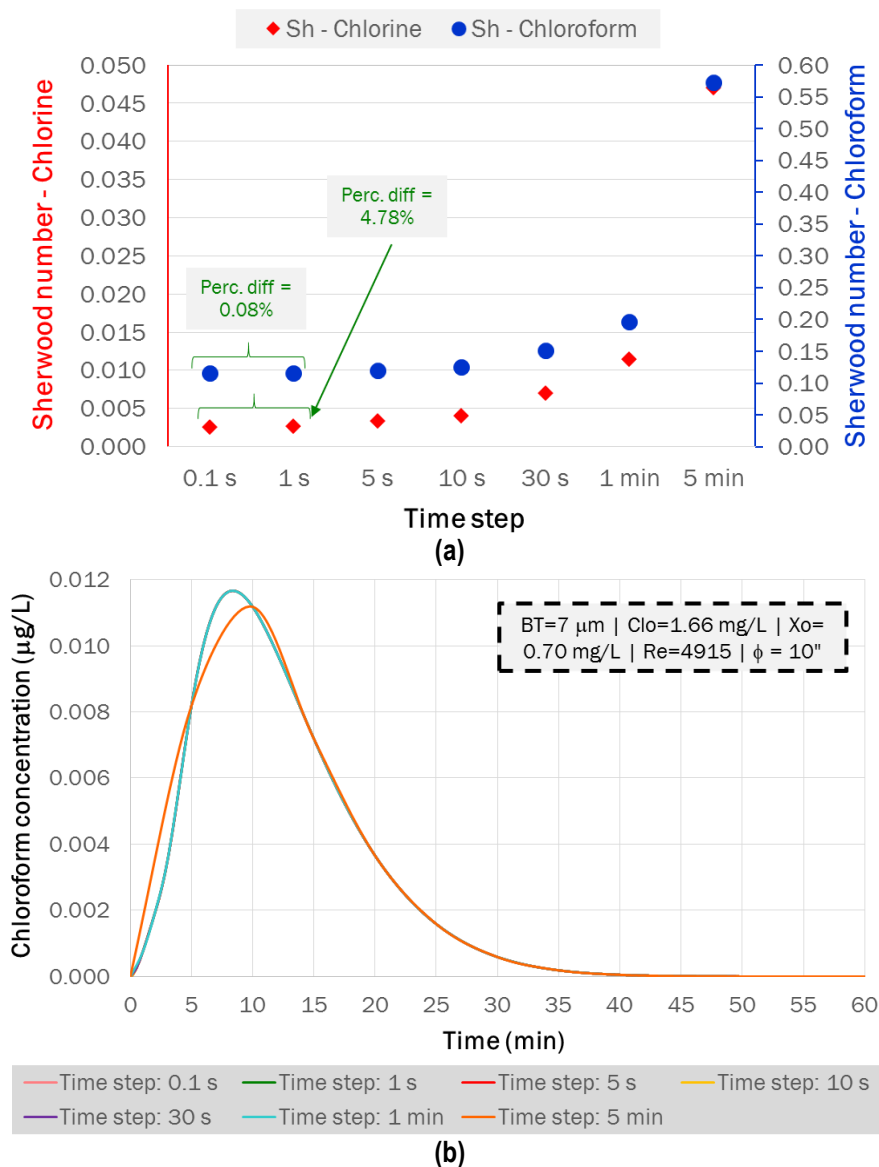


Figure 5-7. Comparison of \bar{Sh} (a) and average chloroform concentration at the pipe outlet (b) in mesh 1

5.2.4.3 Selection of turbulence model

Considering that drinking water pipes are characterized by turbulent flow regime (Cogan, 2010), it is important to analyse the mass transport of chlorine and DBPs in the current 2D model under high Re . In addition, the current model involves reactions at the pipe wall; therefore, the flow near to it becomes important to simulate correctly. In this line, a brief background on turbulence models is presented here in order to better explain the selection of the turbulence model for the subsequent simulations. According to Frei (2013), the turbulent flow near a flat wall can be divided up into four regimes (Figure 5-8). At the wall, the fluid velocity is zero, and for a thin layer above this, called the viscous sublayer or laminar sublayer, the flow velocity is linear with distance from the wall. Further away from the wall, the region buffer layer is located. In the buffer region, the flow begins to

transition to turbulent and it eventually transitions to a region where the flow is fully turbulent and the average flow velocity is related to the log of the distance to the wall. This is known as the log-law region. Even further away from the wall, the flow transitions to the free-stream region. The viscous and buffer layers are very thin and, if the distance to the end of the buffer layer is δ , then the log-law region will extend about away from the wall.

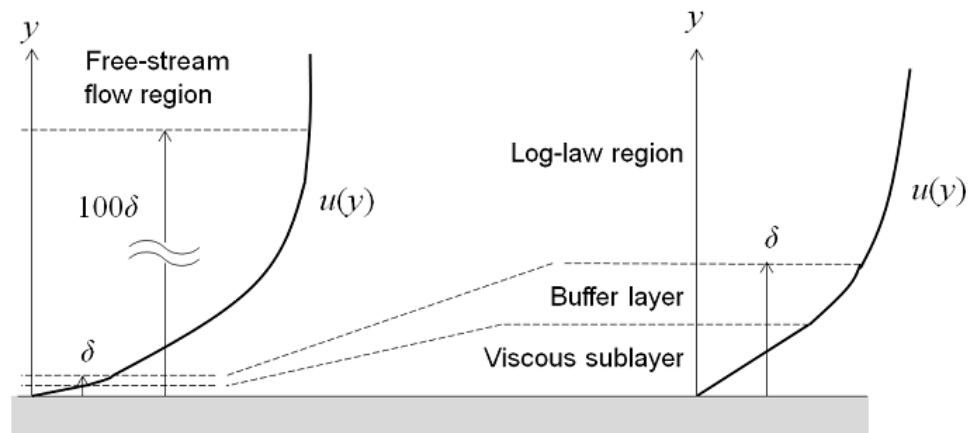


Figure 5-8. Regimes of the turbulent flow near to a flat wall

Source: Frei (2013)

Three Reynolds-averaged Navier-Stokes turbulence models from seven models available in COMSOL Multiphysics 5.2a were tested in order to select the most appropriate one to simulate the mass transfer at the biofilm surface. Table 5-11 presents a brief description of the models SST, yPlus, and Low Reynolds number κ - ϵ . These models were selected as they solve the flow everywhere, therefore a detailed comparison on velocity magnitude and concentrations of DBPs at the pipe outlet could be carried out. In the case of simulations of heat transfer in round pipes, versions of low Reynolds number κ - ϵ and low Reynolds number Reynolds stress turbulence models (Thakre and Joshi, 2000), κ - ϵ with standard wall functions (Jayakumar et al., 2008), and SST (Abraham et al., 2009; Di Piazza and Ciofalo, 2010) have been used in comparison with experimental data, for transitional and fully developed turbulent flows.

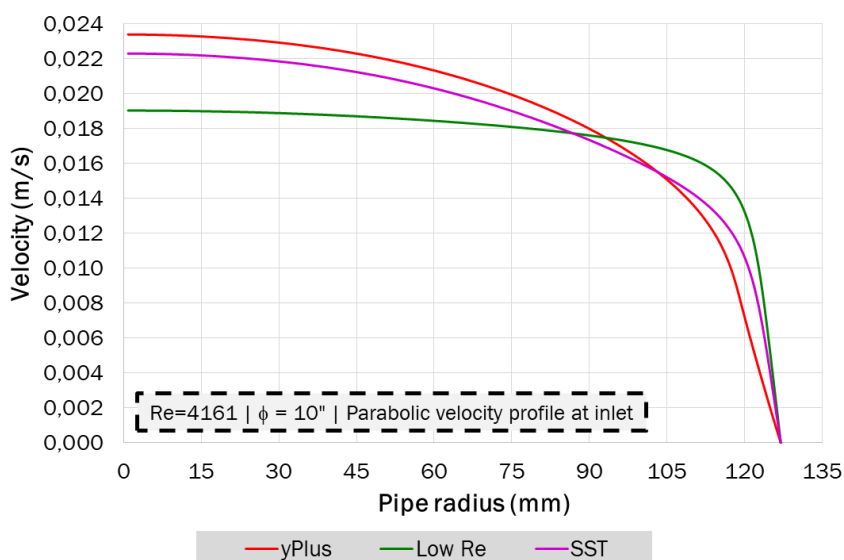
Table 5-11. Description of five turbulence models included in COMSOL Multiphysics 5.2a

Turbulence model	Variables computed	Regions where the flow is solved / not solved	Applications	Limitations
SST	It is a combination of the κ - ϵ in the free stream and the κ - ω	Everywhere It does not use wall functions	It tends to be most accurate when solving the flow near the wall Flow over an aerofoil	--

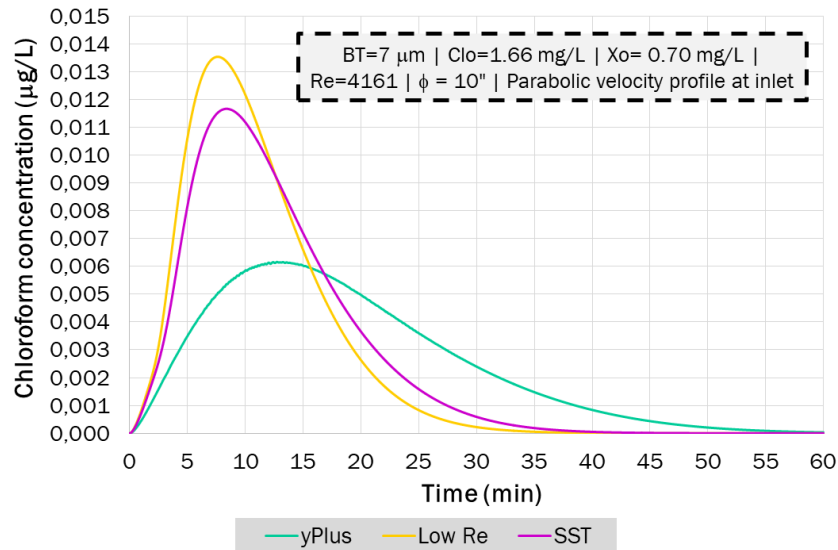
Turbulence model	Variables computed	Regions where the flow is solved / not solved	Applications	Limitations
	models near the walls			
yPlus	Turbulence viscosity	Everywhere It does not use wall functions	It provides good approximations for internal flow, especially in electronic cooling applications	The least accurate model
Low Reynolds number κ - ϵ	κ : turbulent kinetic energy ϵ : rate of dissipation of kinetic energy	Everywhere It does not use wall functions	Lift and drag forces and heat flux can be modelled with higher accuracy	It uses more memory than standard κ - ϵ

Adapted from Frei (2013)

To select the appropriate turbulence model for the subsequent simulations, simulations with the five turbulence models described in Table 5-11 were run. Velocity magnitude at the centre of bulk water domain along r axis (see Figure 5-6a) and chloroform concentrations at the pipe outlet were used to compare the performance of these models (Figure 5-9). The three models solved the flow in this region and the velocity magnitude is zero at the pipe wall. In order to quantify the similarity between turbulence models, percentage of difference was calculated for pairs or maximal (Table 5-12), median (Table 5-13), and average (Table 5-14) velocity. Pair of models yPlus/SST was the only one which resulted in percentage of difference lower than 5% for every velocity value compared.



(a)



(b)

Figure 5-9. Comparison of five turbulence models included in COMSOL Multiphysics 5.2a (a) Velocity monitored at the middle of bulk water domain (b) Average chloroform concentrations at the pipe outlet

Table 5-12. Percentage of difference between pairs of turbulence model – Maximal velocity

Turbulence model	yPlus	Low Re κ-ε	SST
yPlus	-		
Low Re κ-ε	20.53%	-	
SST	4.77%	15.80%	-

Table 5-13. Percentage of difference between pairs of turbulence model – Median velocity

Turbulence model	yPlus	Low Re κ-ε	SST
yPlus	-		
Low Re κ-ε	7.14%	-	
SST	4.54%	2.60%	-

Table 5-14. Percentage of difference between pairs of turbulence model – Average velocity

Turbulence model	yPlus	Low Re κ-ε	SST
yPlus	-		
Low Re κ-ε	8.05%	-	
SST	2.24%	5.81%	-

The effect of turbulence on concentrations of chloroform is observed in Figure 5-9b. Concentration curves are very dissimilar. Percentage of difference of pairs of turbulence models were higher than 5% for all the values assessed here, except for average values of the pair Low Reynolds/SST.

Up to this point, it is clear that solution of the flow near to the wall is crucial as the current model involves reactions at the pipe wall and mass transport at the biofilm surface. For instance, Di Piazza and Ciofalo (2010) found that models SST and Reynolds stress model – ω were in excellent agreement with direct numerical simulation results in relation to pressure drop in helically coiled heat exchanger and Re of 14,000 and 80,000. With regards to heat transfer, the predicted temperature with both models were in satisfactory agreement (Di Piazza and Ciofalo, 2010).

Taking into account that there are no experimental data to compare with in order to select the most appropriate turbulence model, comparisons between results obtained with the software Ansys Fluent 16.0 were made. Simulations using Ansys Fluent 16.0 used an axisymmetric mesh, with 64,135 rectangular elements, $\phi = 10$ inches and $L = 1$ m. The selected models were laminar and SST; laminar was included because low Re (1248) was used in this analysis. Laminar flow regime was included in order to analyse a wider range of Re. Figure 5-10a shows the comparison of velocity magnitude monitored in the middle of bulk water domain for models laminar and SST run in both software COMSOL and Ansys Fluent. Similarly, maximal (Table 5-15), median (Table 5-16), average (Table 5-17) velocities were compared for each turbulence model between both software.

Velocity profile of laminar and SST model resulting from both software are similar for maximal and median velocity (percentage of difference lower than 5%), but percentage of difference for average velocity was higher than 23%. This similarity between both software for laminar and SST turbulence models represents that the solution is solver independent and that the model can be replicated in both software. In conclusion, the turbulence model selected for the subsequent simulations in this study was SST; the curves of this model obtained from COMSOL and Ansys Fluent are included in Figure 5-10b for better illustration. It is important to highlight that SST tends to be more accurate solving the flow near the wall because it combines κ - ϵ and κ - ω models (Frei, 2013).

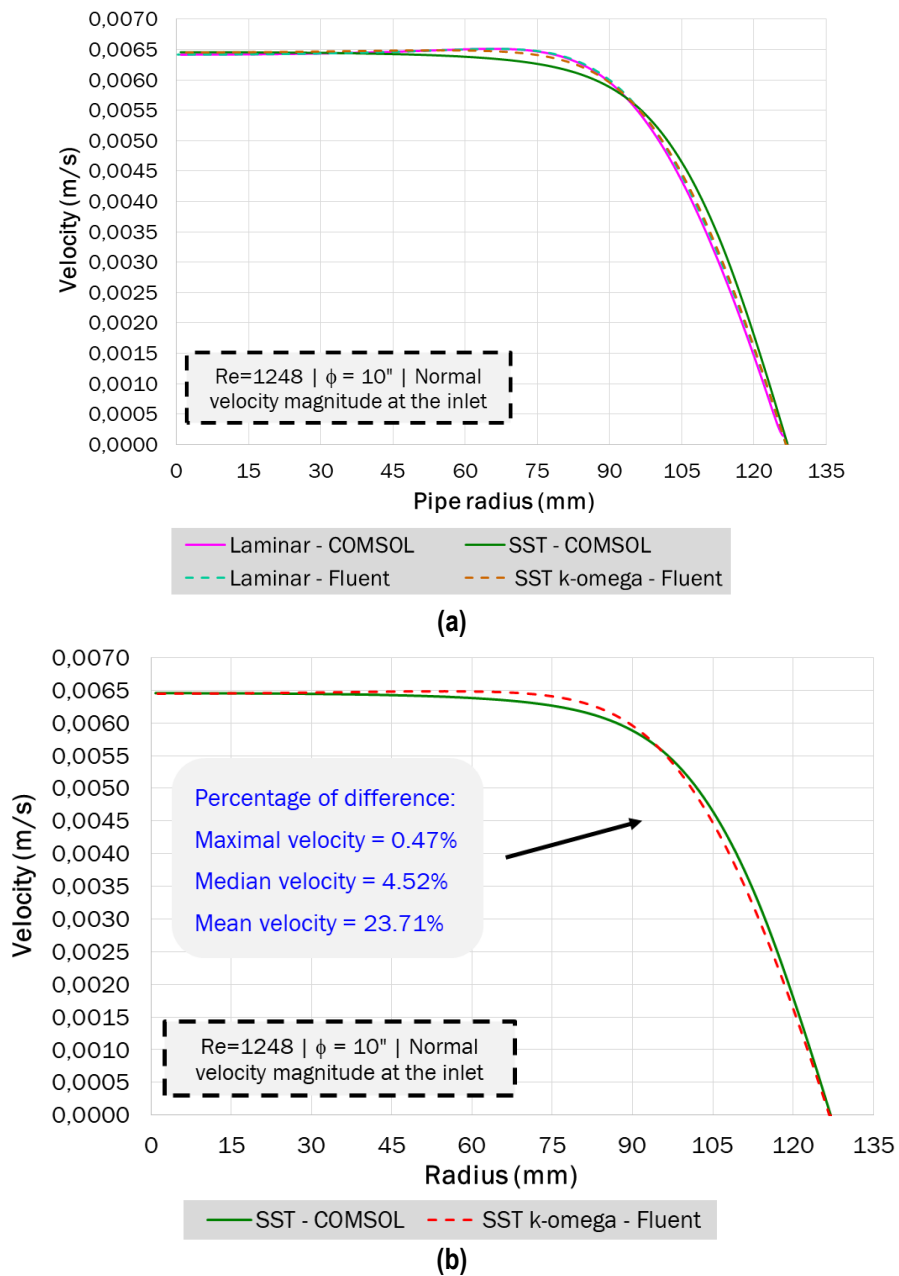


Figure 5-10. Comparison of velocity monitored at the middle of bulk water domain between software COMSOL and Fluent (a) Laminar and SST (b) SST

Table 5-15. Percentage of difference between COMSOL and Fluent for the same turbulence model – Maximum velocity

Software	Fluent		
	Turbulence model	Laminar	SST
COMSOL	Laminar	0.02%	-
	SST	-	0.47%

Table 5-16. Percentage of difference between COMSOL and Fluent for the same turbulence model – Median velocity

Software	Fluent		
	Turbulence model	Laminar	SST
COMSOL	Laminar	0.88%	
	SST	-	4.52%

Table 5-17. Percentage of difference between COMSOL and Fluent for the same turbulence model – Average velocity

Software	Fluent		
	Turbulence model	Laminar	SST
COMSOL	Laminar	24.12%	
	SST	-	23.71%

Due to the importance of coupling flow and mass transport, further analysis of the influence of turbulence on mass transport was carried out by comparing \bar{Sh} of chlorine and chloroform resulting from conditions described in Figure 5-9 and Figure 5-10. Results are shown in Table 5-18; the typical behaviour of the model described in Section 5.3.1 presents the normal variation in time of Sh . The \bar{Sh} calculated for the turbulence models presented in Table 5-18 are dissimilar; percentage of difference for every pair of \bar{Sh} were as high as 173%. \bar{Sh} for chloroform with laminar flow and SST turbulence model corresponding to simulation with inlet velocity equal to the normal velocity magnitude were the only pair of similar values (0.0011925 vs. 0.0012109; percentage of difference = 1.53%).

Table 5-18. \bar{Sh} for different turbulent models

Turbulence model	Inlet velocity: Parabolic profile		Inlet velocity: Normal velocity magnitude	
	Chlorine	Chloroform	Chlorine	Chloroform
Laminar	N.A	N.A	0.0011925	0.0056078
yPlus	0.0014186	0.082039	N.A	N.A
Low Re	0.0041935	0.170580	N.A	N.A
SST	0.0027529	0.116310	0.0012109	0.076996

N.D: Not Defined | N.A: Not Apply

The previous analysis was undertaken to select the most appropriate turbulence model for coupling flow and mass transport during the formation of chloroform from chlorine disinfection. This enabled the conclusion to be drawn that DBP concentrations are highly sensitive to the turbulence model used in the simulations. Therefore, further field or laboratory research regarding DBP formation

from biofilms under hydrodynamic conditions should consider turbulence as an important factor influencing the results.

5.2.5 Implementing the model in COMSOL

As explained previously, rectangular meshes (Table 5-8, Table 5-9, and Table 5-10), time step of 1 s, and SST turbulence model were chosen to predict the DBP formation potentials, in drinking water pipes, by chlorination of biofilms, under hydrodynamic conditions. First, the flow field was solved under steady state, then transient simulations for substance transport from this converged steady flow field were performed; it was assumed dissolved substances (chlorine and DBPs) do not affect the flow field. The discretization approach was P1+P1 (linear elements for both the velocity components and the pressure field) for solution of flow, linear for solution of transport of dissolved substances, and quadratic discretization for solution of decay of cells and EPS.

The solver was “Direct” for both transitional flow and transport of dissolved substances simulations. Direct methods find an approximation of the solution $A^{-1}f = u$ by matrix factorization in a number of operations that depend on the number of unknowns. Factorization is expensive, but once it has been computed, it is relatively inexpensive to solve for new right-hand sides. Since direct methods are expensive in terms of memory and time intensive for CPUs, they are preferable for small- to medium-sized 2D and 3D applications (Marra, 2013). This is the case of the current model; therefore, direct solver was selected.

The numerical simulations were run in a computer with a processor Intel® Core™ i5-4430 CPU 3.00 GHz, and RAM memory of 16.0 GB. The model was implemented in the software COMSOL Multiphysics 5.2a, by a 2D axisymmetric geometry of a cylindrical pipe. Computational time ranged between 1-10 hours, according to domain size, flow regime, and simulation time. For instance, each simulation for $\phi = 3$ inches, transitional flow and simulation time of one hour lasted around 1-2 hours. Each simulations of the sensitivity analysis lasted around 3 hours. Table 5-19 presents the modules, boundary and initial conditions used in each simulated domain.

Table 5-19. Main features for model implementation in COMSOL Multiphysics 5.2a

Module	Domain	Boundary	Boundary condition	Initial values
Laminar flow	Bulk water	Inlet	Normal velocity – Parabolic profile	0
		Outlet	Pressure. $P_o = 0$	
		Bs	No slip	

Module	Domain	Boundary	Boundary condition	Initial values
		Centre of the pipe	Axial symmetry	
Transitional and turbulent flow SST model	Bulk water	Inlet	Normal velocity – Parabolic profile Turbulent intensity = 0.1 Turbulent length scale = ϕ	0
		Outlet	Pressure. $P_o = 0$	
		Wall	No slip	
		Centre of the pipe	Axial symmetry	
Transport diluted substances (tds)	Bulk water	Inlet	Inflow. $C_o = C_o; R_o = 0$	$C_o = C_o; R_o = 0$
		Outlet	Outflow	
		Bs	Continuity	
		Centre of the pipe	Axial symmetry	
	Biofilm	Wall	No flux	$C_o = 0; R_o = 0$
--	Reactions			
Domain ODEs	Biofilm	Reactions for cells and EPS decay	--	$X_o = X_o; E_o = E_o$

5.2.6 Scenarios simulated

The scenarios simulated with the model proposed here are based on the variables flow regime, Reynolds number, pipe diameter, and drinking water quality, in order to identify their influence on response variables such as average DBP concentration at the pipe outlet, \bar{S}_h and mass transfer rate of DBPs. The conditions of the simulated scenarios were as it follows:

- Laminar, transitional, and turbulent flow
- Re: 1,202 – 50,030
- Pipe diameters of 3, 6 and 10 inches
- BT of 7 μm and 102 μm , Clo of 0.12 mg/L and 1.66 mg/L, and X_o of 2.82×10^{-4} mg/cm² and 4.44×10^{-3} mg/cm²

5.2.7 Parameters selection

The selection of parameters was explained in Chapter 3. Table 5-20 presents the consolidation of the microbiological and kinetic parameters; and hydraulic-related parameters such as flow rate, velocity and pipe diameter considered for simulations of the scenarios described in the previous section.

Table 5-20. Parameters used in the 2D model simulations

Parameter	Value	Reference
Biofilm thickness (BT)	7 and 102 μm	Table 4-3
Initial biofilm density (X_0)	2.82×10^{-4} and 4.44×10^{-3} mg/cm^2	Table 4-5
Initial EPS concentration (E_0)	$E_0 = 5.0295BT + 1884.3$	Celmer et al. (2008)
Temperature (T)	25 $^{\circ}\text{C}$	Section 3.3.5
Diffusion coefficient of chlorine in liquid	2.66×10^{-9} m^2/s	Chen and Stewart (1996)
Diffusion coefficient of chloroform in liquid	9.29×10^{-10} m^2/s	Buzatu et al. (2007)
Diffusion coefficient of DCAN in liquid	1.66×10^{-9} m^2/s	Poling et al. (2007)
Chlorine-cell reaction rate (k_1)	1.1×10^{-3} $\text{m}^3/\text{g}\cdot\text{sec}$	Chen and Stewart (1996)
Chlorine-EPS reaction rate (k_2)	3.7×10^{-6} $\text{m}^3/\text{g}\cdot\text{sec}$	Chen and Stewart (1996)
Chlorine-cell yield coefficient (Y_1)	1.85 g/g	Chen and Stewart (1996)
Chlorine-EPS yield coefficient (Y_2)	540 g/g	Chen and Stewart (1996)
Portion of chlorine reacting with cells - chloroform (F_x)	0.70	Section 4.2.3.6
Portion of chlorine reacting with cells - DCAN (F_x)	0.30	Section 4.2.3.6
Portion of chlorine reacting with EPS - Chloroform (F_E)	0.30	Section 4.2.3.6
Portion of chlorine reacting with EPS - DCAN (F_E)	0.17	Section 4.2.3.6
τ_s	0.50	Section 5.2.8
Flow rate (Q)	260 – 1080 L/h	Abokifa et al. (2016a)
	2170 – 2820 L/h	-
Re	1,202 – 50,030	-
Pipe diameter (ϕ)	3, 6, 10 inches	-

5.2.8 Effective diffusion coefficient of DBPs

In Chapter 4, the influence of τ_s on chloroform concentrations was observed for time less than 60 min and values as small as $\tau_s = 0.016$, under stagnation conditions. Differences were noted on the speed of the reactions but not in the potential concentrations of chloroform. Taking into account that there are not experimental measurements of diffusion of chloroform and DCAN within biofilms, the influence of τ_s on concentrations of both substances were examined again under transitional flow. Figure 5-11 shows the chloroform concentrations in bulk water and \bar{S}_h for the same substance. Results indicate there is no significant difference among concentrations at the pipe outlet (percentage of difference 0.00-0.21%, 0.01-0.59%, and 0.00-0.04% for maximal, median and average values). However, \bar{S}_h for chloroform is very dissimilar among the three values of τ_s tested. Percentage of difference ranged between 38.14-135.31% for consecutive pair of \bar{S}_h values and it was 187% for τ_s values of 0.016 and 1.000. Such difference is due to calculation of \bar{S}_h (Equation (2-11)), which relies on concentration gradients of dissolved substances at the biofilm surface; then,

changes of diffusion coefficient of these substances within the biofilm in relation to bulk water coefficients leads to different gradients for each τ_s tested.

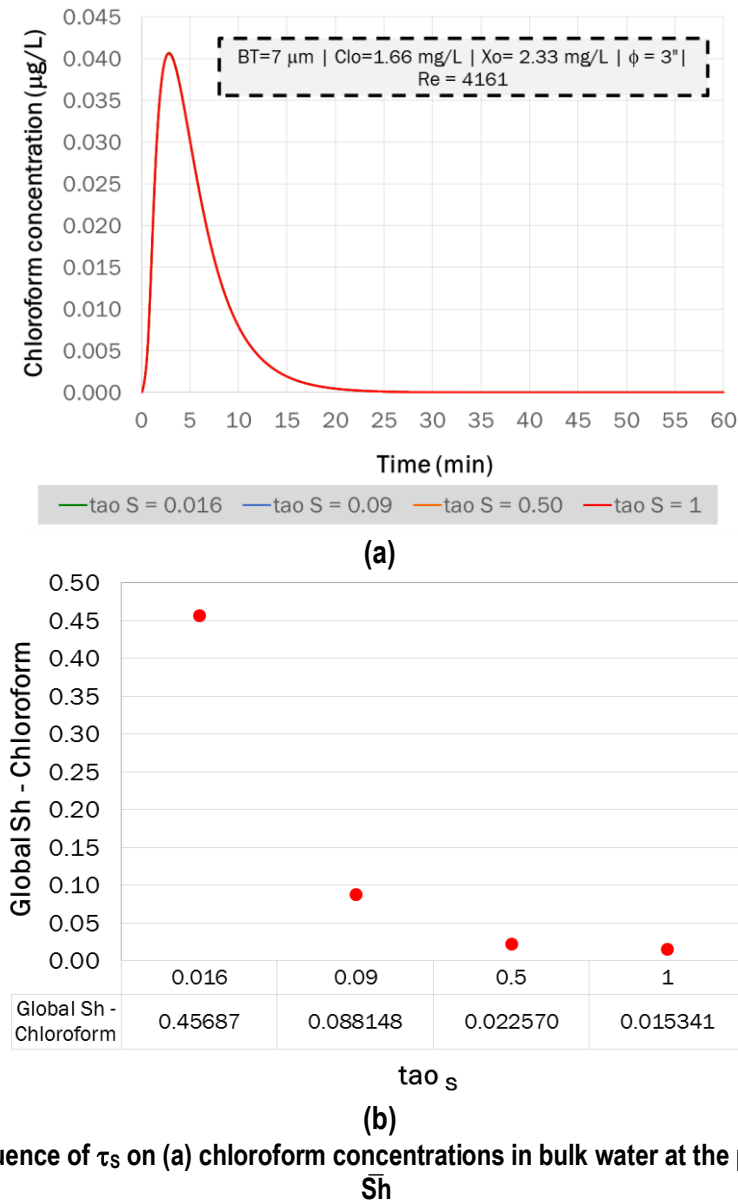


Figure 5-11. Influence of τ_s on (a) chloroform concentrations in bulk water at the pipe outlet and (b) \bar{Sh}

Figure 5-12 shows the DCAN concentrations in bulk water and the \bar{Sh} for the same substance. Similarly to chloroform, results for DCAN evidence there is no difference among concentrations at the pipe outlet (percentage of difference 0.00-0.32%, 0.24-0.56%, and 0.00-0.04% for maximal, median and average values). However, \bar{Sh} for DCAN is very dissimilar among the three values of τ_s tested. Percentage of difference ranged between 38.17-135.29% for consecutive pair of \bar{Sh} values and it was 187% for τ_s values of 0.016 and 1.000. As previously mentioned, there is not information regarding experimental studies to calculate the effective diffusion coefficients of chloroform and DCAN within biofilms. Therefore, $\tau_s=0.5$ was arbitrarily chosen as an intermediate

value within the possible range. This parameter was included in the sensitivity analysis and it was possible to determine its degree of influence on the response variables (see Section 5.3.7).

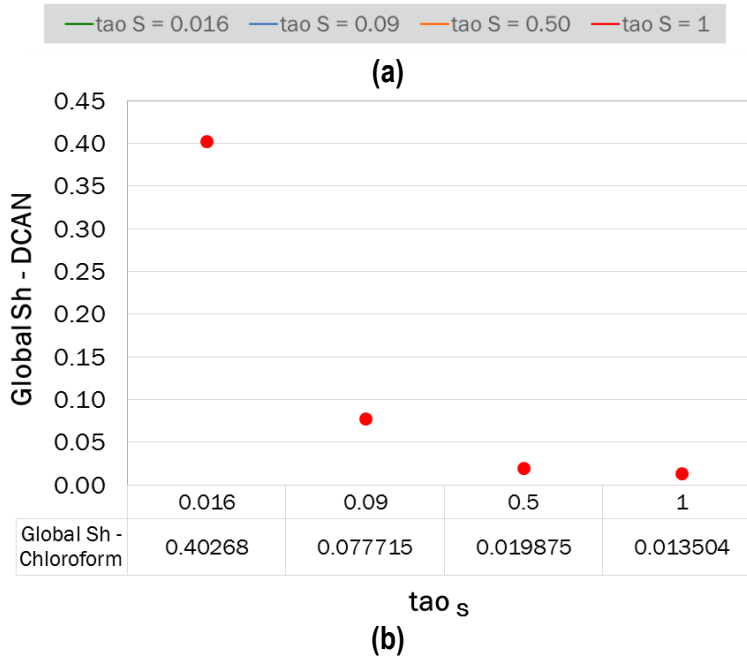
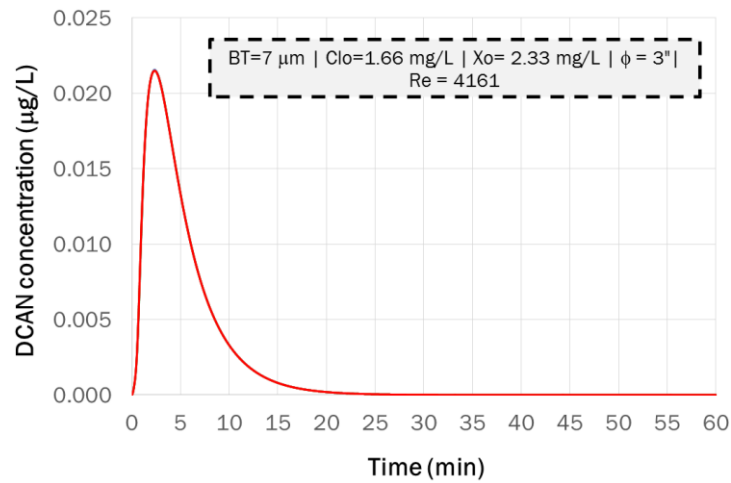


Figure 5-12. Influence of τ_s on (a) DCAN concentrations in bulk water at the pipe outlet and (b) \bar{Sh}

5.2.9 Mass transport

Mass transport of dissolved substances chlorine and DBPs was characterized by the local Sh (Equation (2-9)), average \bar{Sh} (Equation (2-11)), and \bar{k}_f (Equation (2-11)).

5.2.10 Sensitivity analysis

The aim of a sensitivity analysis in a model is to establish what factors need better determination, and to identify the weak links of the assessment chain (i.e those that propagate most variance in

the output) (Saltelli et al., 2004). For the particular model presented here, carrying out a sensitivity analysis is important because the model is based on microbiological data, which are not frequently available for full scale DWDNs. Therefore, to determine which parameters influence most the outputs is crucial for offering recommendations on further research and on where the efforts on field work and laboratory assessment must be put in. According to Menberg et al. (2016), there are three distinctive sensitivity analysis methods: i) Morris method for parameter screening (low computational cost), ii) linear regression analysis (medium computational cost), and iii) Sobol method (high computational cost).

The results of these three methods applied to an energy building model were compared and researchers concluded that, by using the median value for measuring the parameter influence, Morris method yielded robust results for evaluations with small sample size and comparable to the other two method results (Menberg et al., 2016). For instance, researchers used 10 independent evaluations and 10 trajectories and found the same information regarding the differentiation of influential and negligible parameters (Menberg et al., 2016). To investigate higher-order effects and parameter interactions, Menberg et al. (2016) used 50-150 trajectories and found that correlation of elementary effects (EEs) and parameter values in Morris method can also provide basic information about parameter interactions.

Taking into account that the proposed model here has a high computational cost (1.5-3.0 hours per each run), Morris method was chosen to perform a sensitivity analysis in order to assess the level of influence of each model parameter and define basic interactions between parameters. This was done based on the same approach of Menberg et al. (2016); median value of elementary effect measurement was used. The application of the method is presented in the following section.

5.2.10.1 Parameter screening with Morris method

Morris (1991) introduced a method for parameter screening in combination with a factorial sampling strategy in order to identify parameters that can be fixed at any value within their range without affecting the variance of the model outcome. Morris's method is based on the model output represented by a mathematical function $Y(\mathbf{Z})$ with Y as a vector of one model output. The outputs for the current analysis were the average of the average DCAN concentration at the pipe outlet and \bar{Sh} for chlorine and DCAN. \mathbf{Z} is a $N \times m$ matrix of model inputs (Z) with N samples of m parameters defined within the lower and upper bounds for each parameter Z_{\min} and Z_{\max} , respectively (Menberg et al., 2016).

For sampling, the parameter space ($Z_{\min} - Z_{\max}$) is discretized by transforming the input parameters into dimensionless variables in the interval (0;1) and dividing each parameter interval into a number of p levels, which form a regular grid in the unit-length hypercube H^m (Menberg et al., 2016). The first sample is randomly chosen and each sample differs only in one coordinate from the preceding one (Morris, 1991). A sequence of $m+1$ points is called a trajectory; in each trajectory, parameter changes only once by a pre-defined value Δ_i . One point in a trajectory represents one evaluation run of the model. The magnitude of variation in the model output due to the pre-defined variation of one parameter Z is called elementary effect (EE) (Equation (5-35)) (Morris, 1991).

$$EE_i = \frac{Y(Z + e_i \Delta_i) - Y(Z)}{\Delta_i} \quad (5-35)$$

Here e_i is a vector of zeros, except for the i -th component that equals ± 1 and represents an incremental change in parameter i (Garcia Sanchez et al., 2014). While one trajectory allows the evaluation of one elementary effect for each parameter i , a set of t trajectories enables statistical evaluation of the finite distribution of the EEs. Absolute average (μ^*) (Equation (5-36)) and standard deviation (SD) (Equation (5-37)) are the statistical measures commonly used to assess the EEs.

$$\mu_i^* = 0.5 \sum_{t=1}^r |EE_{it}| \quad (5-36)$$

$$SD = \sqrt{\frac{1}{(r-1)} \sum_{t=1}^r (EE_{it} - \mu_i)^2} \quad (5-37)$$

Here r is the number of random trajectories (with index t), and t is a set of multiple trajectories. The absolute average (μ^*) indicates the magnitude of influence of a parameter on the model outcome and is often used to rank the parameters according to their importance. Menberg et al. (2016), by 10 independent evaluations of the Morris method each with 10 trajectories, found that using μ^* can result in inconsistent ranking of parameters influence, due to some bias by the occurrence or absence of outliers and the resulting skewness in the EE distributions. In order to overcome this issue, the researchers proposed the application of the absolute median χ^* , because this measure is less influenced by the type of distribution of the EE and by outliers, then negligible parameters can be identified (Menberg et al., 2016).

The SD is a measure for the spread in the model outcome due to changes in a specific parameter. It indicates that the magnitude of influence of a parameter is dependent on the values of the

remaining parameters, and can be interpreted as a measure for non-linearity and parameter interactions (Morris, 1991). The computational cost of the Morris method depends on number of parameters m and number of t trajectories and is given by $t^*(m+1)$.

5.2.10.2 Higher-order parameter interaction effects

Menberg et al. (2016), by applying an alternative strategy, investigated the interaction effect between two parameters by utilising the results generated from the Morris method. The strategy consisted on evaluating the correlation coefficient of the first parameter (its value) with the EE of the other parameter as an indication of second-order effects identified (Menberg et al., 2016). Despite of this technique is relatively easy, large number of trajectories are required in order to interpret the correlations meaningfully. The study of Menberg et al. (2016) used the input parameter matrices and their corresponding EEs obtained from sensitivity analysis runs ranging from 50 to 150 trajectories to compute the corresponding Pearson's correlation coefficients. For each set of trajectories, correlation coefficients were calculated between the EEs for each parameter i and the corresponding parameter values resulting in a matrix of correlation coefficient for each sensitivity run (Menberg et al., 2016). Then, coefficients with p -value lower than 0.005 were selected to calculate the sum of absolute correlation coefficients for each parameter. Ranking the parameters according to such sum resulted in identical to the ranking based on Sobol indices (Menberg et al., 2016).

5.2.10.3 Implementation of Morris method

The Morris method was applied by following the same procedure adopted by Menberg et al. (2016), i.e., χ^* instead of μ^* for screening parameters; 10 trajectories and 12 parameters, which resulted in 130 simulations, corresponding to 33 days of computational time. All simulations were run for $t=3$ hours. Higher order interactions between parameters were not evaluated due to the computational cost. For instance, Menberg et al. (2016) used 50-150 trajectories, which represents for the current model a computational time of 108 days and 325 days. The method was implemented in MATLAB 2015b, using the adapted version of toolbox SAFE developed by Pianosi et al. (2015). Simulations of sensitivity analysis were run by using the tool "Batch sweep" in COMSOL Multiphysics 5.2a. Influence of parameter variation was assessed for the response variables \bar{S}_h for chlorine, \bar{S}_h for DCAN, and average and median value of average DCAN concentration at the pipe outlet. Average and median concentrations of DCAN were chosen because the typical behaviour of those curves are characterized by increasing values, reaching a maximal value and then decreasing to almost negligible concentrations. Then, average concentration at the pipe outlet may be affected by the maximal value in each run; then, it is

important to consider the peak concentrations effects. The ranges of parameters included in the sensitivity analysis are shown in Table 5-21, which are the same ranges used in the parametric sensitivity analysis applied in Chapter 4, Section 4.3.3.

Table 5-21. Ranges of parameters considered for sensitivity analysis

Range	τ_s	X_o	E_o	C_{lo}	F_x	F_E
Units	–	mg/cm ²	mg/L	mg/L	–	–
Min	0.016	6.65x10 ⁻⁶	935	0.12	0.00	0.00
Max	1.00	1.33x10 ⁻¹	9465	2.00	1.00	1.00
Range	Y_1	Y_2	k_1	k_2	Q	BT
Units	g/g	g/g	L/mg-s	L/mg-s	L/h	μ m
Min	0.19	54	1.1x10 ⁻⁴	3.7x10 ⁻⁷	600	7
Max	3.70	1080	2.2x10 ⁻³	7.4x10 ⁻⁶	1100	102

5.2.11 Post-processing

The results processing included the description of the typical behaviour of the model by explaining the flow field (contour plots of velocity and pressure magnitude in the pipe and velocity profiles); the contour plots of concentrations of substances in bulk water and biofilm; fluxes at the biofilm surface; and curves of concentrations of dissolved substances at the pipe outlet. The transport of dissolved substances was characterized by the average global \bar{Sh} for chlorine and DBPs and calculation of mass transfer rates.

5.3 RESULTS AND DISCUSSION

5.3.1 Typical model behaviour

5.3.1.1 *Flow field*

The flow field of the simulations of the 2D model is generally explained by the comparison of laminar, transitional and turbulent flow in Figure 5-13. The pressure is higher near to the pipe inlet and decreased until zero at the outlet, according to the boundary conditions. For transitional flow, pressure near to the inlet is around 0.6 Pa and it reaches the maximal value when the transitional flow is fully developed. As expected for higher flow rates, maximum pressure magnitude is higher in turbulent flow (20.5 Pa), followed by transitional flow (1.3 Pa) and laminar flow (0.14 Pa).

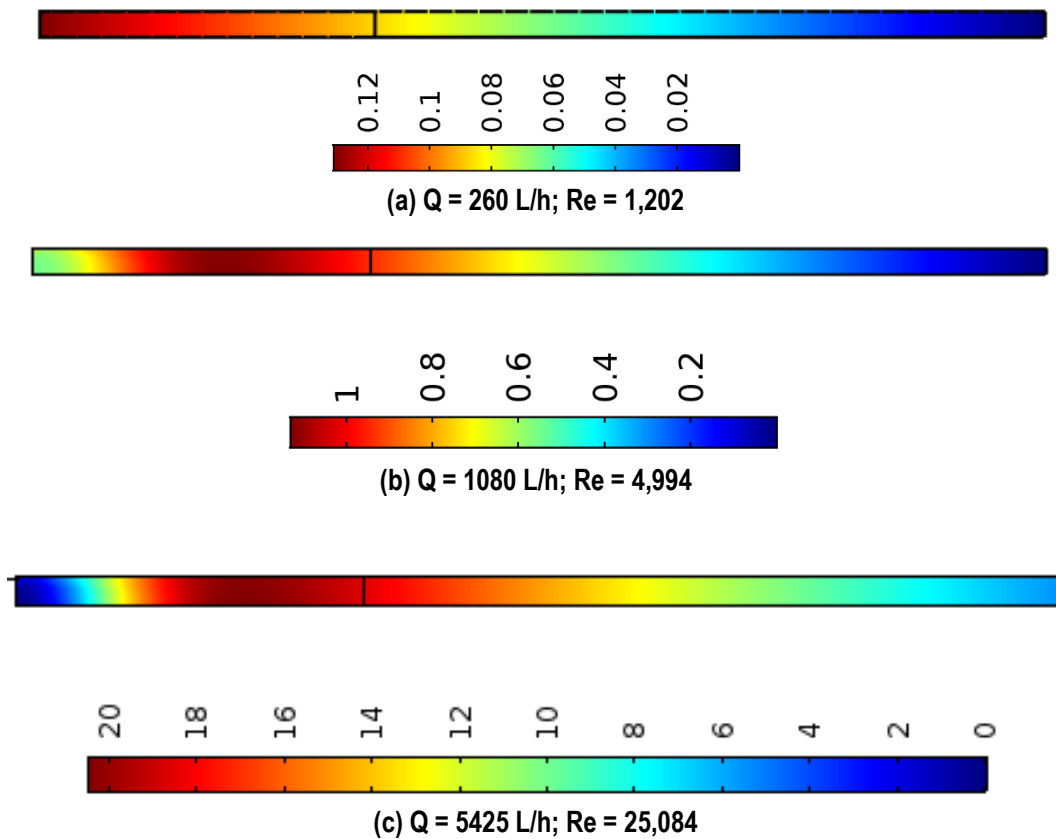


Figure 5-13. Pressure (Pa) surface plot – Inlet: left; Outlet: right (a) Laminar flow (b) Transitional flow (c) Turbulent flow

Velocity profiles of three flow regimes simulated here are observed in Figure 5-14. With regards to laminar flow, velocity profiles are uniform along the pipe (Figure 5-14a), which is characteristic of this flow regime. For transitional (Figure 5-14b) and turbulent flow (Figure 5-14c), the velocity magnitude reached a maximum near to the inlet, which has a boundary condition defined by a parabolic profile. Once the flow is developed along the pipe, maximal velocities in the centre of the pipe are reduced, then the velocity profiles are more similar.

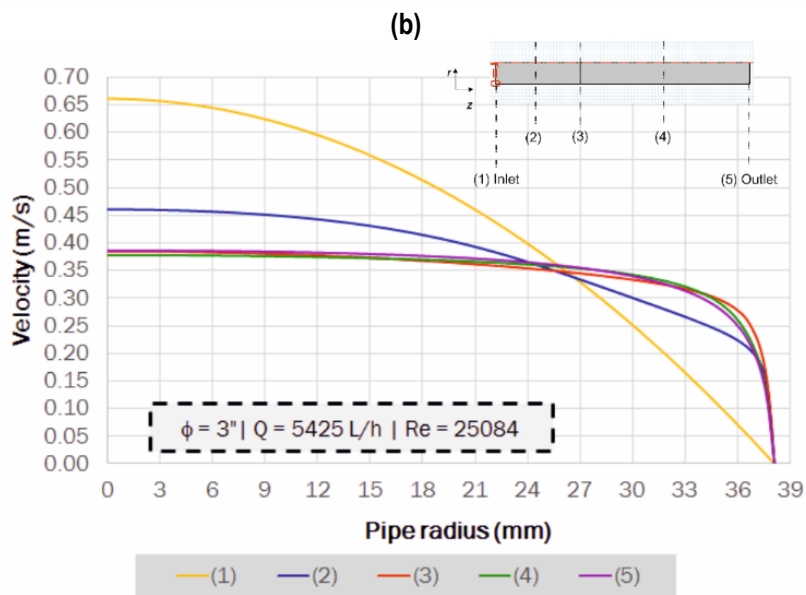
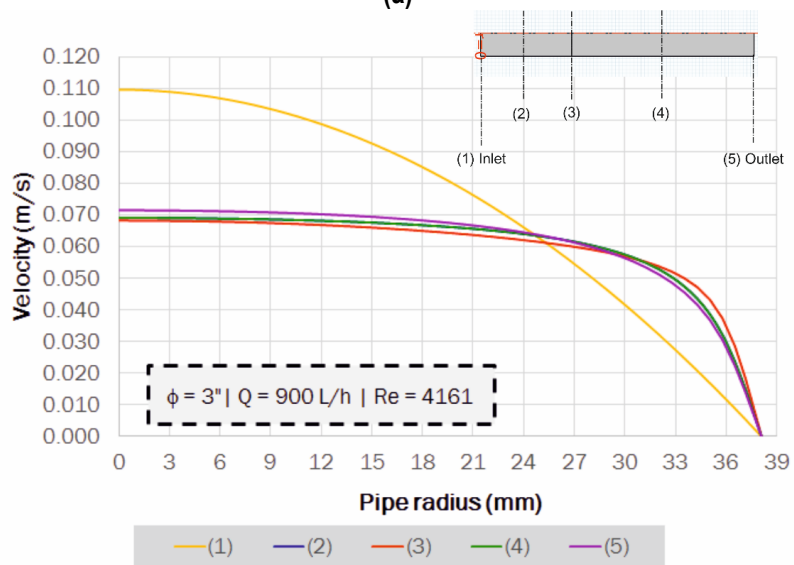
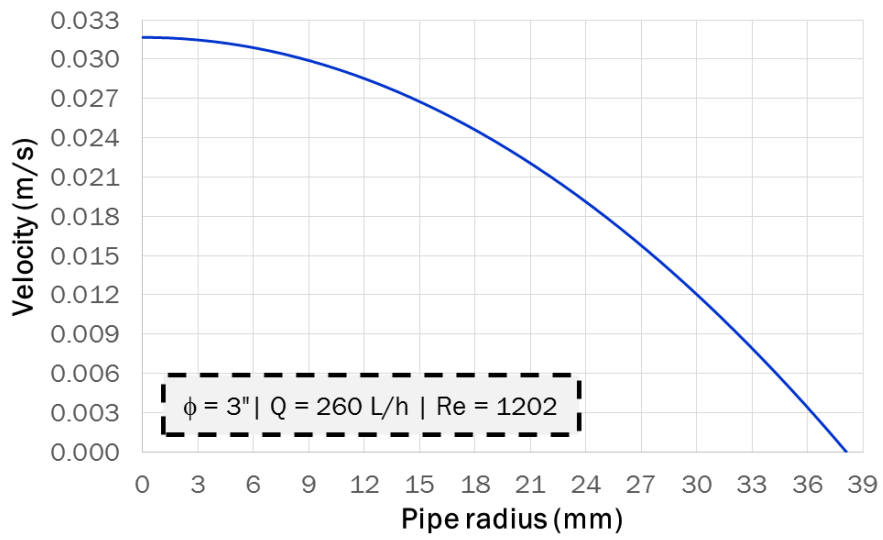


Figure 5-14. Velocity profiles (a) Laminar flow (b) Transitional flow (c) Turbulent flow

5.3.1.2 Concentrations of substances in biofilm and bulk water

Considering the current model corresponds to the simulation of the formation potentials of DBPs from chlorination of biofilms, all the simulations were run until concentrations of DBPs at the pipe outlet were almost zero. Due to the disproportion between pipe radius and biofilm thickness, results are presented in non-scaled plots for better explanation. To ease the results interpretation, Figure 5-15 shows a sketch on the non-scaled geometry and its configuration.

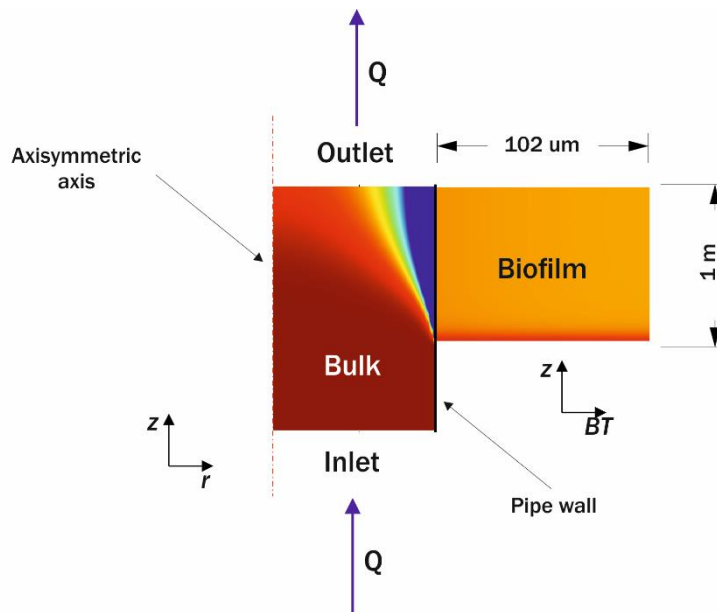


Figure 5-15. Sketch of the non-scaled geometry

The typical behaviour of dissolved and particulate substances in the biofilm corresponds to transitional flow regime ($Re = 2774$) and is presented in Figure 5-16. Chlorine penetration occurred in the first seconds; at short time as 0.1 min (6 sec), chlorine within biofilm had already reached half of the inlet concentration and DCAN was already formed. Higher concentrations of DCAN were at the bottom of the biofilm most likely due to diffusion occurring in all directions while transport to the bulk occurs at the biofilm surface, then DCAN formed near to this boundary was being evacuated first. At $t=0.1$ min, no significant decrease of cells and EPS was observed in Figure 5-16.

At $t=1$ min, chlorine in biofilm was already reaching the inlet concentration in the section near to the inlet. It is important to mention that chlorine first penetrated the biofilm thickness, then continues filling this region in the flow direction (z). Cells and EPS already showed a slight decrease and DCAN concentration reached the maximum value. At $t=5$ min, a notable reduction of cells and EPS was observed, chlorine concentration was higher within the biofilm and DCAN concentration still exhibited the highest value. At $t=15$ min, chlorine concentration within biofilm was equal to the

concentration at the pipe inlet, there were negligible concentrations of cells and EPS, and DCAN was already disappearing from the biofilm. From $t=30$ min and until the end of the simulations (1 hour), chlorine reached the maximum concentration possible and there were negligible concentrations of cells, EPS, and DCAN.

As described in Section 4.3.2, experimental data reported by Chen and Stewart (1996) indicated that complete penetration of a biofilm as thick as $428\ \mu\text{m}$ occurred after $t=60$ min, with flow rate of $450\ \text{L/min}$. Then, it is reasonable that complete penetration of biofilm by chlorine with thickness of $102\ \mu\text{m}$ and higher flow rate than $450\ \text{L/min}$ takes place in a shorter time (e.g., 15 min). These results indicate that the current model is able to represent the general pattern of the reactions between chlorine and biofilm for the subsequent formation of DBPs. Reactions occur fast, in the first 5 min, when chlorine penetrates the thickness of the biofilm, reacting with cells and EPS, which are transformed into DCAN.

With regards to dissolved substances in bulk water, Figure 5-17 shows the typical behaviour of chlorine and DCAN in this region. At $t=0.1$ min, chlorine was completely mixed in the bulk and concentration was equal to the inlet concentration, as specified in the initial conditions. DCAN was absent in the bulk at this time. After 1 min, consumption of chlorine near to the biofilm surface was observed and DCAN transport was also occurring. Chlorine concentration reached the lowest concentration at the pipe outlet at $t=1.67$ min (Figure 5-20a) and DCAN reached the highest concentration at the pipe outlet at $t=4.3$ min (Figure 5-20b). However, the surface plot of the bulk at this time did not show any evident differences in relation to these substances.

For $t=5$ min, while chlorine decreased in bulk water near to the biofilm surface, DCAN increased in bulk water. Then, at $t=15$ min, chlorine was again filling the bulk domain and DCAN concentration was decreasing because it was leaving the pipe. It is important to mention that cells and EPS were completely depleted within the biofilm (Figure 5-16) at $t=15$ min, but there was still DCAN within this region. Then, it is reasonable to still find DCAN in the bulk water, near to the biofilm surface at $t=15$ min and 30 min. For times of 45 min and 60 min, DCAN was completely evacuated from the pipe and chlorine concentration is equal to that specified at the inlet.

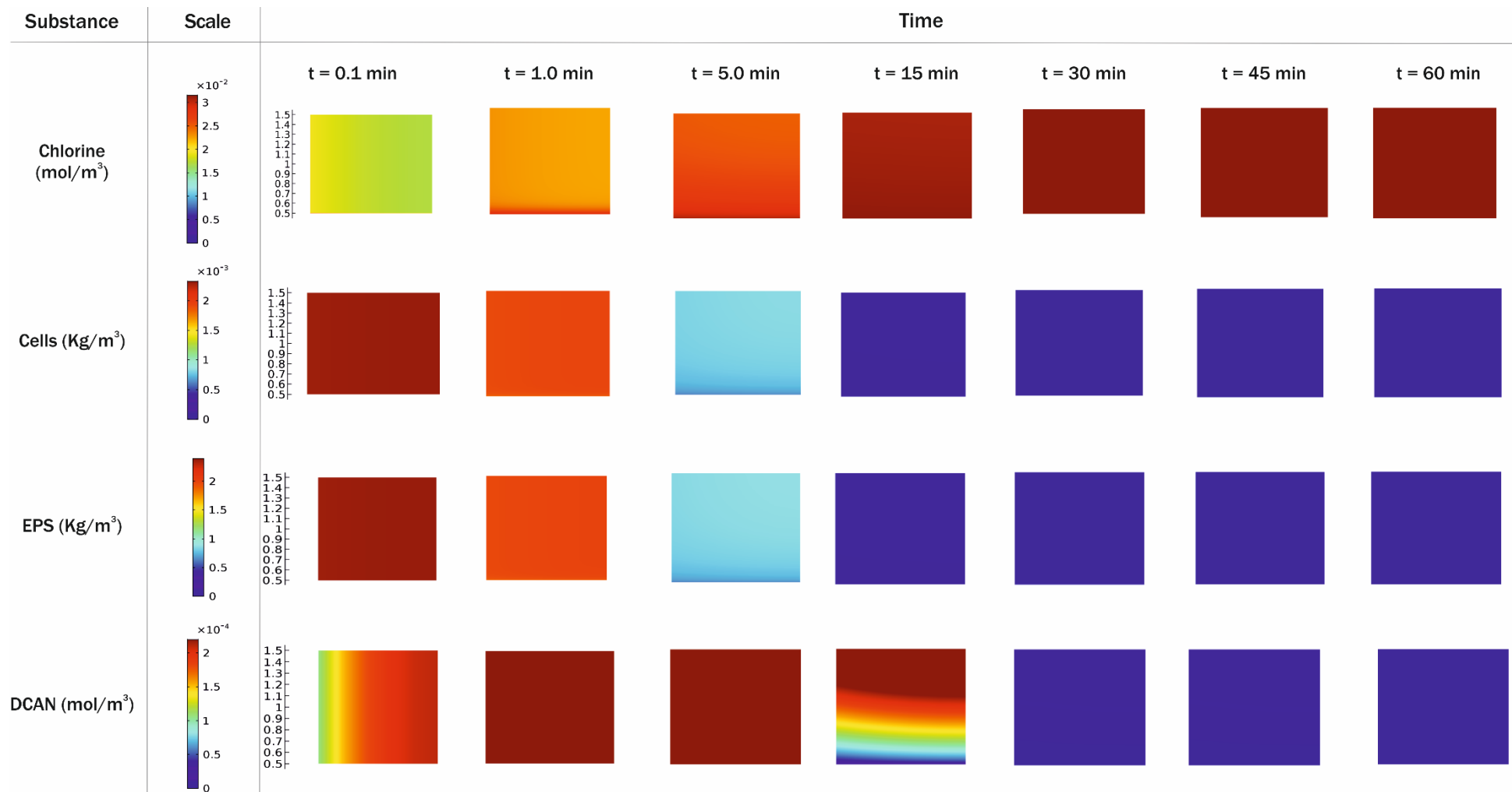


Figure 5-16. Contour plots of substance concentrations in biofilm – BT = 102 μ m, Clo = 1.66 mg/L, Xo = 2.33 mg/L, Re = 2774, ϕ = 3"

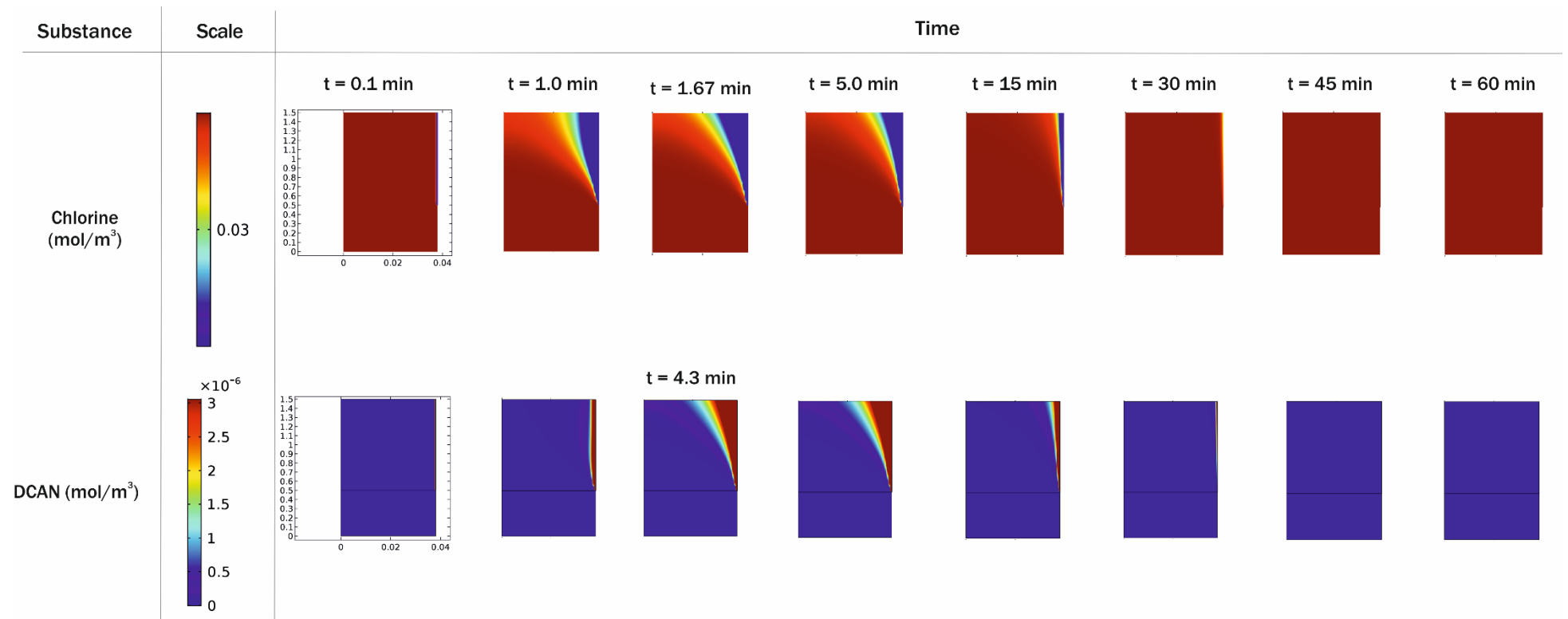


Figure 5-17. Contour plots of concentrations of dissolved substances in bulk water - BT = 102 μm, Clo = 1.66 mg/L, Xo = 2.33 mg/L, Re = 2774, φ = 3"

5.3.1.3 Fluxes of dissolved substances at biofilm surface

Figure 5-18 presents the variation of the DCAN (a) and chlorine flux (b) at the biofilm surface. Since chlorine was being transported from bulk water to the biofilm, fluxes were positive; the opposite occurred for DCAN because this substance was being transported from biofilm to bulk water. Taking into account that chlorine decay occurred faster, highest variation of its flux took place in terms of seconds. In contrast, DCAN flux variation occurred place in terms of minutes. It is also important to note that absolute values of fluxes resulted in higher values for DCAN in comparison to chlorine. This is also reflected in the \bar{Sh} for both substances; \bar{Sh} of chlorine was lower than \bar{Sh} of DCAN (0.13962 vs 0.23260). Finally, it is also worth noting that the flux curves exhibited a curvilinear shape at the beginning of the biofilm (in the flow direction), when reactions chlorine-biomass were occurring at the beginning of the reactive length of the pipe.

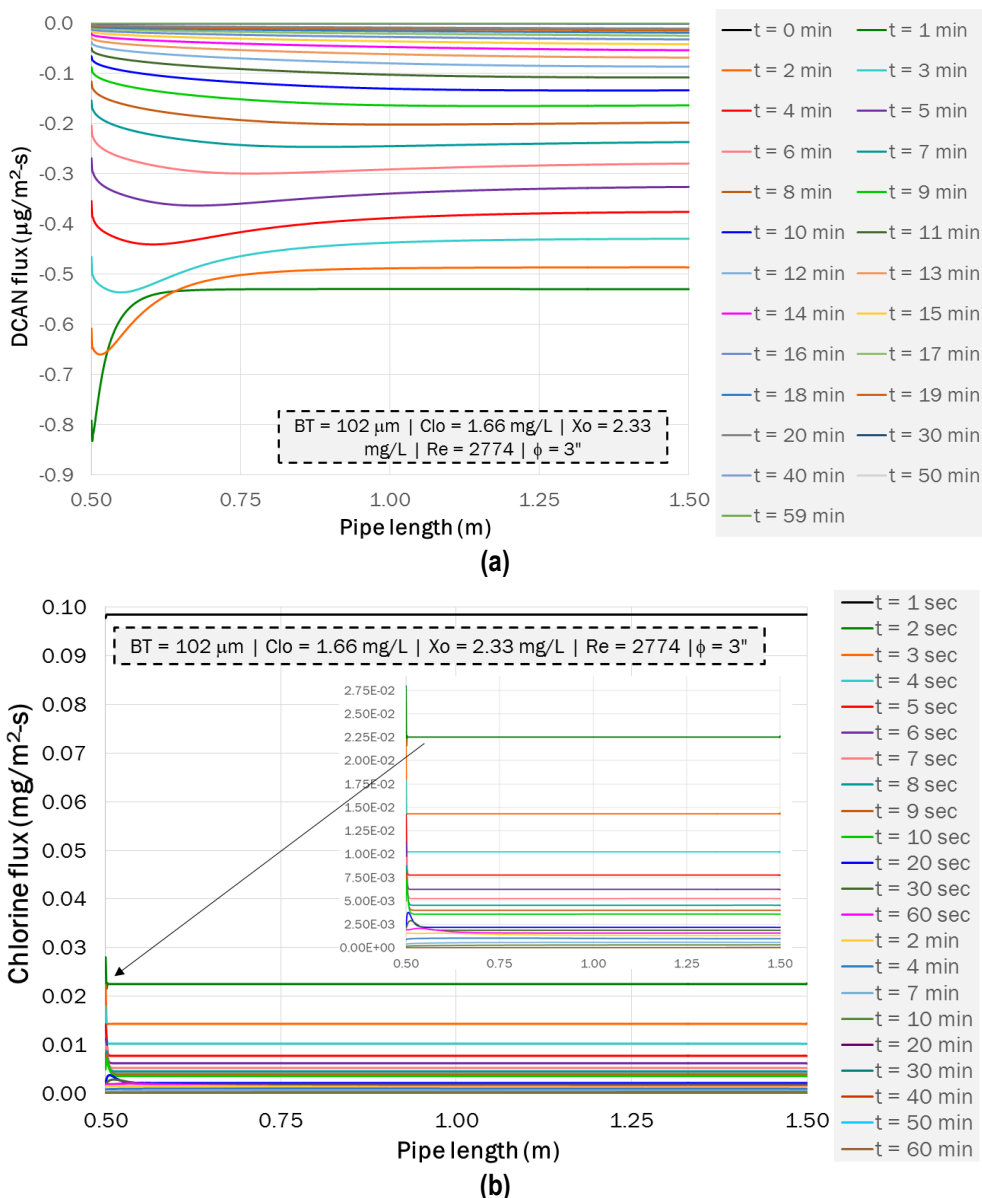


Figure 5-18. Flux of dissolved substances at the biofilm surface (a) DCAN (b) Chlorine

5.3.1.4 Variation of \bar{Sh} at the biofilm surface

Variation of \bar{Sh} of chlorine and DCAN is included in Figure 5-19. \bar{Sh} was high at the beginning of the reactions between chlorine and biomass. Then, \bar{Sh} rapidly decreased and became steady after few seconds (around 86 seconds) for chlorine and few minutes (around 5 minutes) for DCAN.

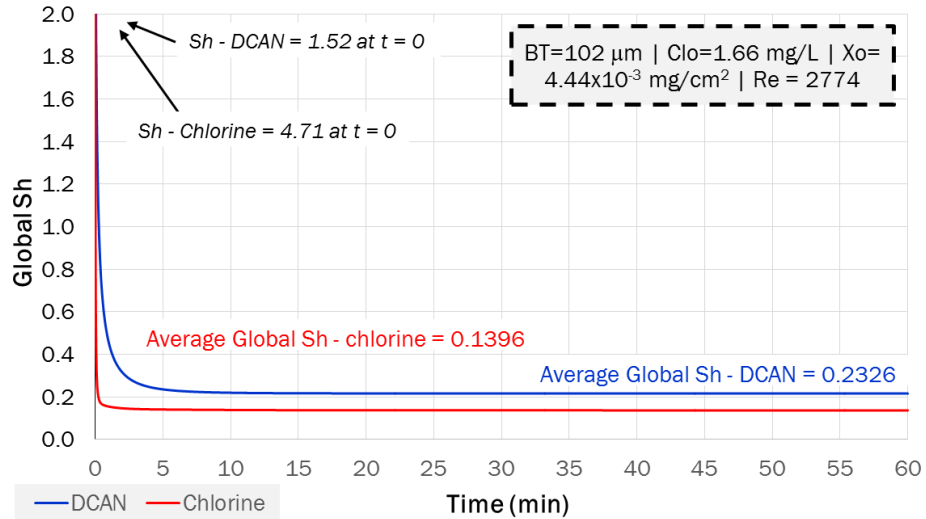


Figure 5-19. Variation of \bar{Sh} at the pipe outlet

5.3.1.5 Concentrations of dissolved substances at the pipe outlet

Variation of concentrations of DCAN and chlorine at the pipe outlet is included in Figure 5-20. As chlorine concentrations were decreasing, DCAN was increasing. Minimal and maximal values of chlorine and DCAN, respectively were reached at different times. Chlorine decayed faster in relation to the formation of DCAN. However, such decay was almost negligible for this case. The chlorine demand was 1.3×10^{-3} mg/L and maximum DCAN concentration was $0.34 \mu\text{g/L}$, for reactions occurring in a pipe with length of 1 m.

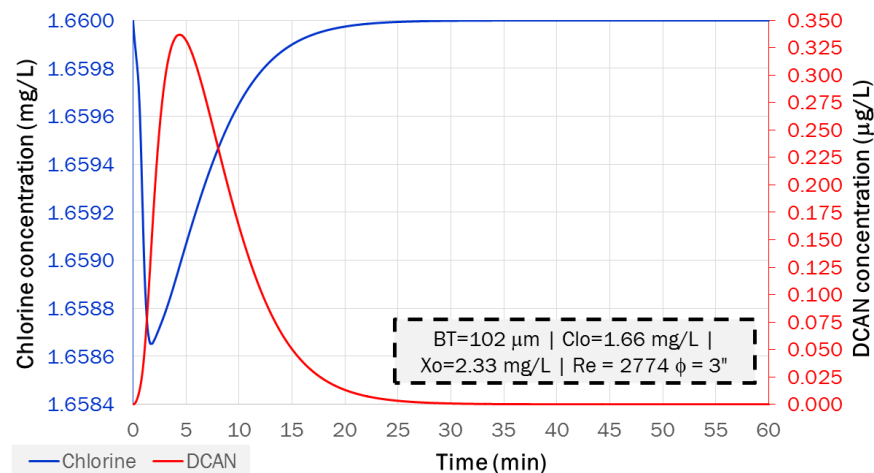


Figure 5-20. Average concentration of chlorine and DCAN at the pipe outlet

5.3.2 Influence of flow regime on DBP formation and transport

To understand how flow regime influences DBP formation and transport at the biofilm surface, results from laminar, transitional and turbulent flow simulations were assessed under the same initial conditions of chlorine concentration, cell density, and biofilm thickness. This analysis was based on the average concentration of chloroform and DCAN at the pipe outlet and \bar{Sh} of these three substances. Average concentrations of DBPs at the pipe outlet are presented in Figure 5-21 and average \bar{Sh} of chlorine and DBPs are included in Figure 5-22.

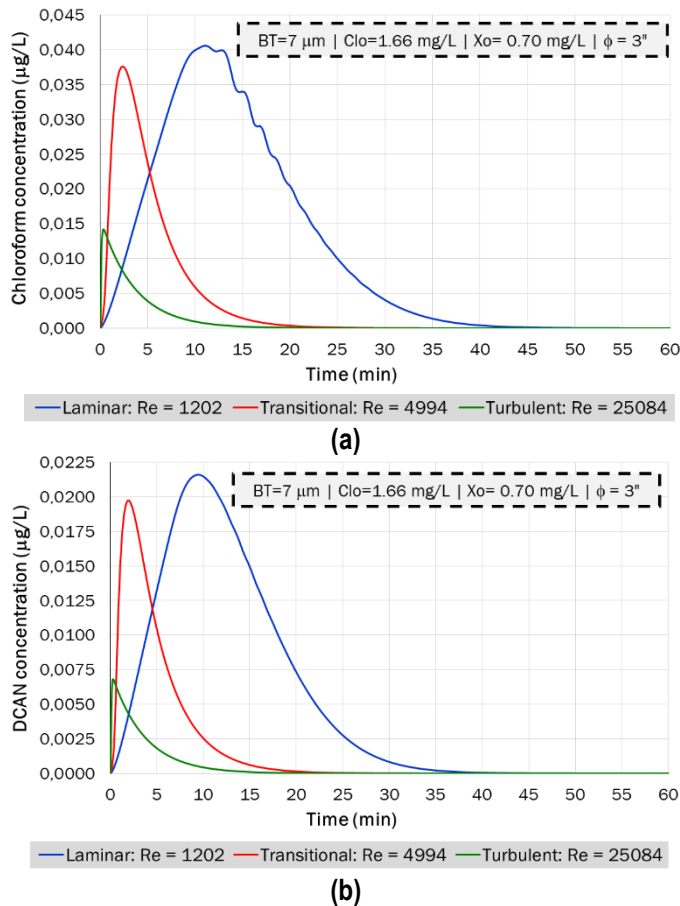


Figure 5-21. Average concentration of chloroform at the pipe outlet according to flow regime (a) Chloroform (b) DCAN

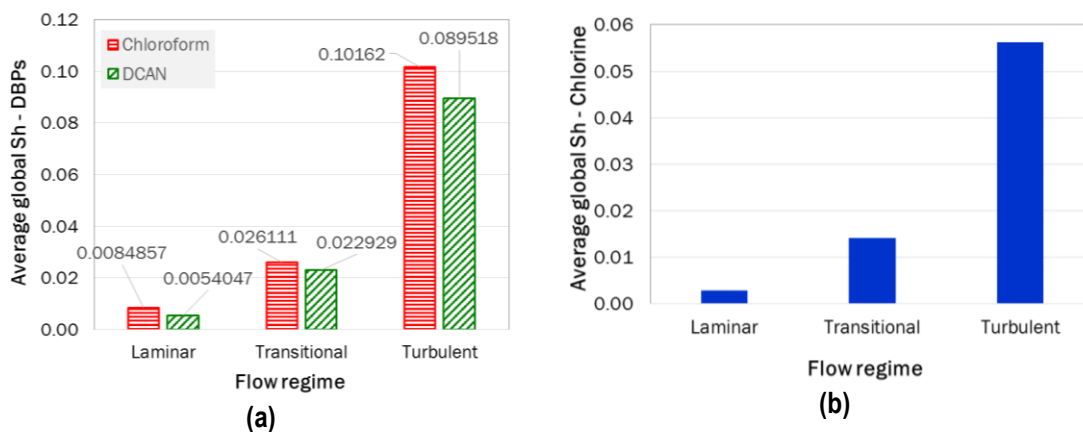


Figure 5-22. Variation of local \bar{Sh} according to flow regime (a) DBPs (b) Chlorine

Under the three flow regimes, concentrations of chloroform and DCAN were decreasing as Re increased, due to dilution effect caused by the increased of the flow rate. Similarly, DBP transport occurred faster under turbulent flow conditions, followed by transitional flow and laminar flow. This is observed by the narrowing of the concentration curves as Re increased (Figure 5-21). This is also reflected in the values of Sherwood number, which were higher for the three dissolved substances simulated for higher Re (Figure 5-22).

Although flow in drinking water pipes is frequently turbulent (Cogan, 2010), it is important to show the differences among results from three flow regimes, as laminar flow is commonly assumed in biofilm modelling, as explained in Section 2.4.3 (Table 2-3, Chapter 2), and transitional flow can be found in dead-end sections of DWDNs (Abokifa et al., 2016b). Depending on the biofilm characteristics that a modeller wants to represent, biofilm modelling is computationally expensive and improved hardware is required to efficiently carry out this task. Therefore, researchers have decided to assume laminar flow under low Re (0.32×10^{-5} - 150) to simplify the calculation of the flow next to the biofilm surface (Eberl et al., 2000; Piciooreanu et al., 2000a; Eberl and Sudarsan, 2008; Zhang et al., 2008; Duddu et al., 2009; Cogan, 2010; Lindley et al., 2012; Taherzadeh et al., 2012; Zhang, 2012; Cumsille et al., 2014; Tierra et al., 2015).

Most of the previous cited studies focused on substrate transport towards the biofilm to model its growth and influence on its morphology. Particularly, Cogan (2010); Cogan (2011) and Zhang (2012) simulated the disinfection of biofilms under laminar flow to analyse the behaviour of susceptible and persistent bacteria and the disinfection effectiveness by simulating active and dead cells. Eberl and Sudarsan (2008) presented a case similar to the one presented here; they modelled the disinfection effects on multiple colonies growing in a narrow channel, under slow flow. These authors found that hydrodynamics played an important role for the transport of substrate (dissolved oxygen); increasing the flow velocity led to faster a more stable growth. In the case of the disinfectant, the colonies located near to the inlet of the channel took the hardest hit, biomass was quickly inactivated and limited in the downstream region (Eberl and Sudarsan, 2008). The model developed here showed that, under continuous chlorine supply and transitional and turbulent flow, pipe was refilled with chlorine after few minutes (≈ 15 min, Section 5.3.1.2).

For the case of the formation potentials of DBPs from chlorination of biofilms, it is important to consider the real flow conditions found in drinking water pipes due to hydraulic variables such as water demand, velocity, and pressure are not constant along the day. Therefore, transport parameters such as Sherwood number and mass transfer rate can be affected by such variation.

5.3.3 Influence of Re on DBP transport

Once it was defined that the flow regime actually affects the transport of DBP potentially formed in drinking water pipes, several Re corresponding to transitional and turbulent flow were simulated to analyse in more detail the likely influence of flow rate on DBP formation and transport. Chlorine, chloroform and DCAN were assessed for biofilm thicknesses of 7 μm and 102 μm .

5.3.3.1 Chloroform and dichloroacetonitrile formation

Average concentrations of chloroform, DCAN and chlorine at the pipe outlet are shown in Figure 5-23, Figure 5-24, and Figure 5-25, respectively, for ten values of Re, corresponding to transitional flow. Similarly for turbulent flow, average concentrations of chloroform, DCAN and chlorine at the pipe outlet are shown in Figure 5-26, Figure 5-27, and Figure 5-28, respectively, for ten values of Re. Increasing Re was simulated by increasing velocity and keeping the same pipe diameter (3 inches).

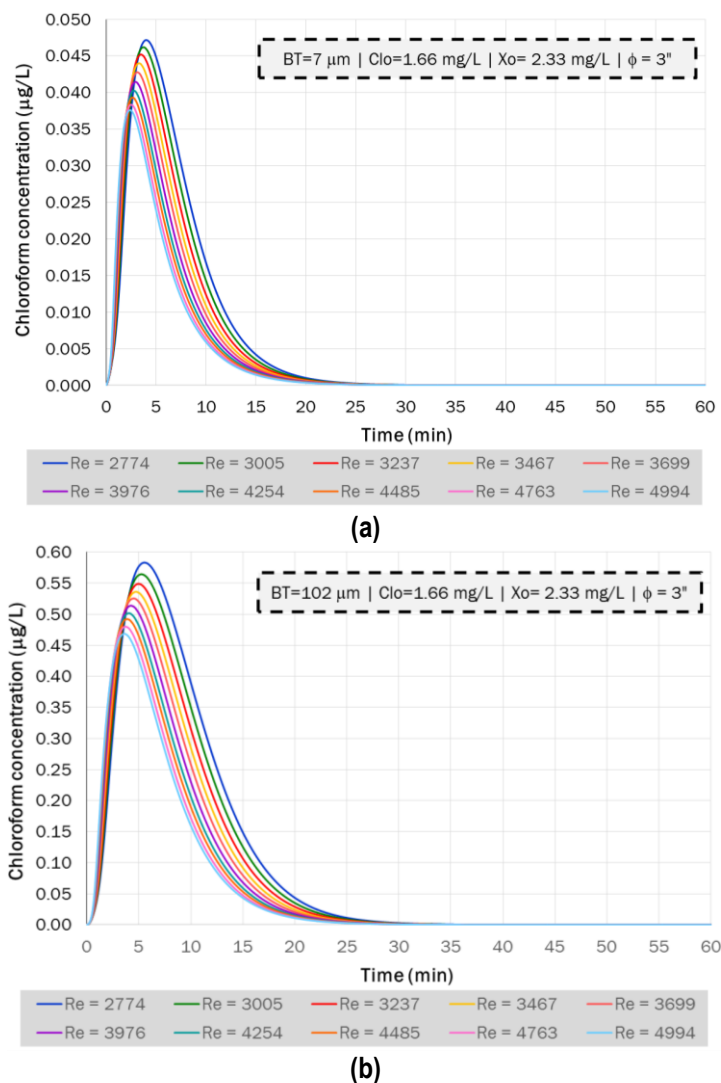
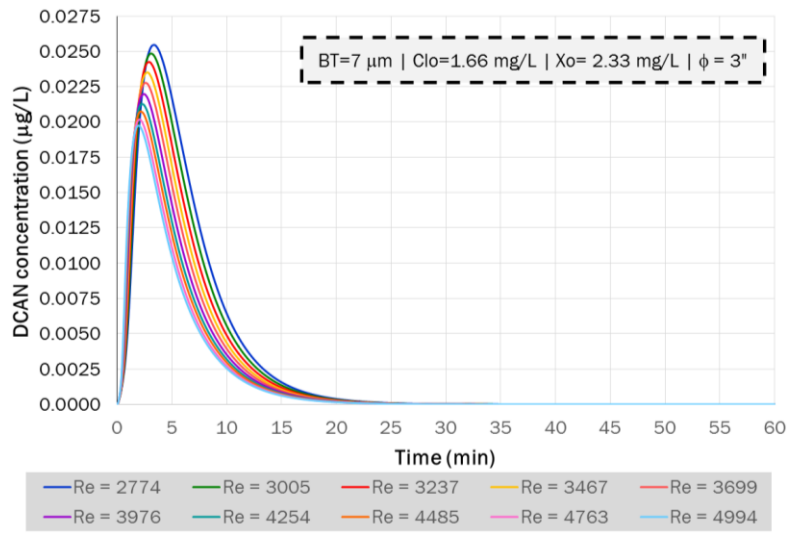
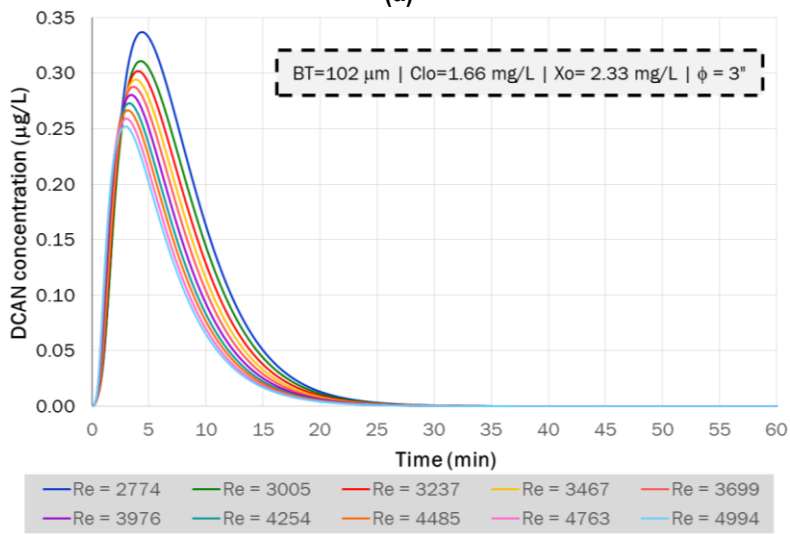


Figure 5-23. Average chloroform concentration at the pipe outlet for several Re – Transitional flow
(a) BT = 7 μm (b) BT = 102 μm

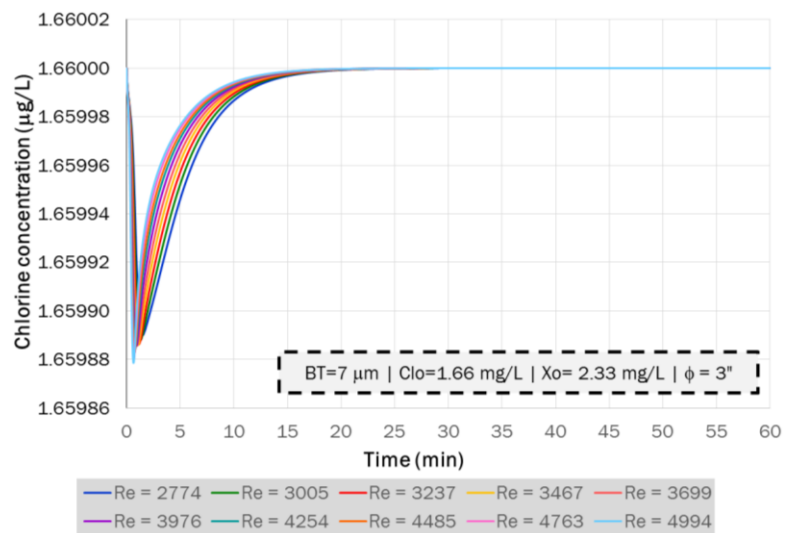


(a)

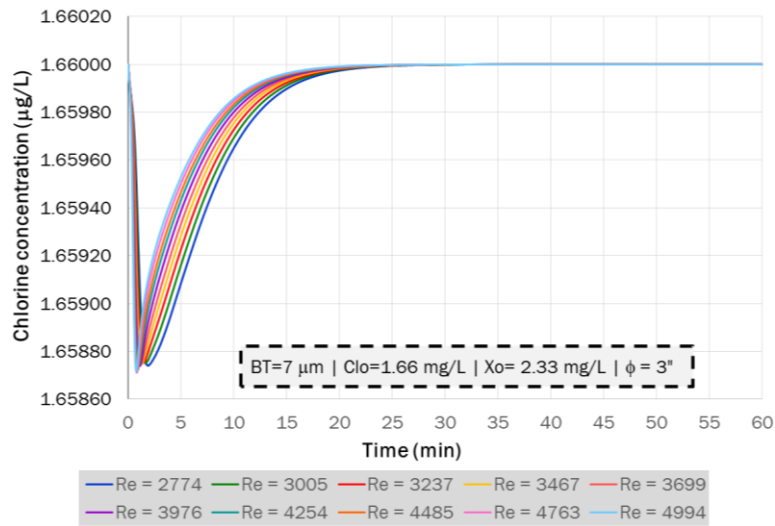


(b)

Figure 5-24. Average DCAN concentration at the pipe outlet for several Re – Transitional flow (a) BT = 7 µm (b) BT = 102 µm

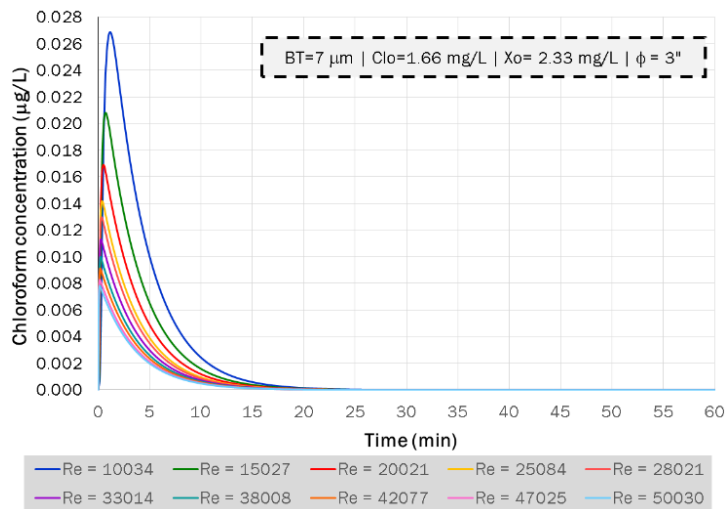


(a)

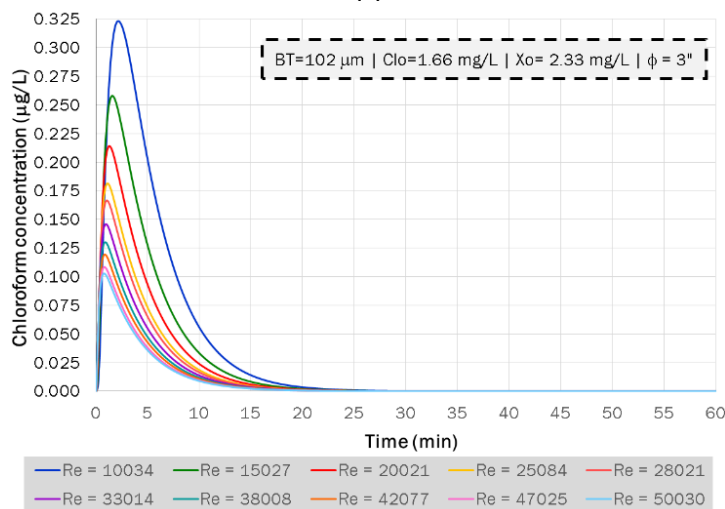


(b)

Figure 5-25. Average chlorine concentration at the pipe outlet for several Re – Transitional flow (a) BT = 7 μm (b) BT = 102 μm

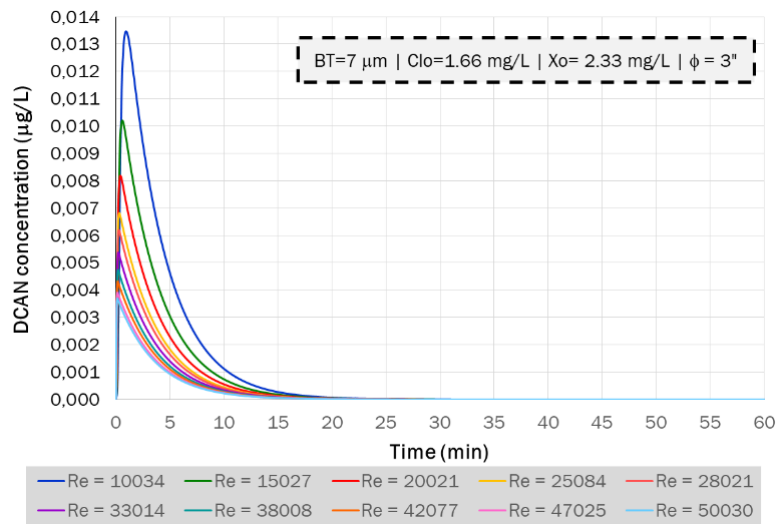


(a)

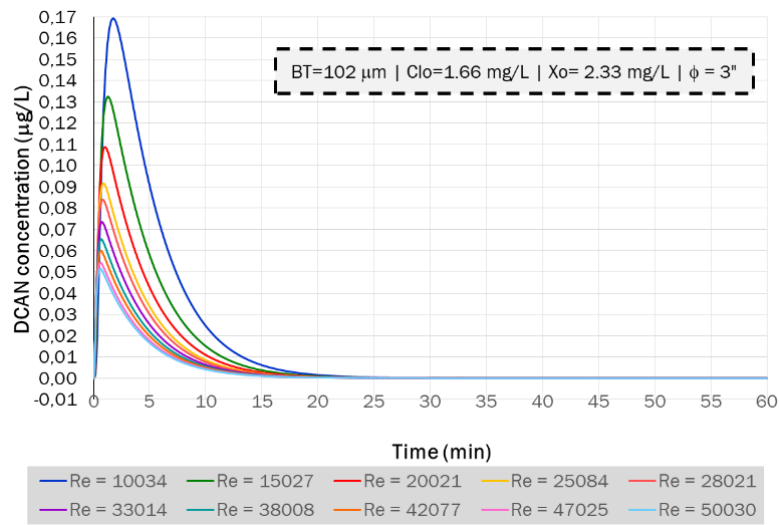


(b)

Figure 5-26. Average chloroform concentration at the pipe outlet for several Re – Turbulent flow (a) BT = 7 μm (b) BT = 102 μm

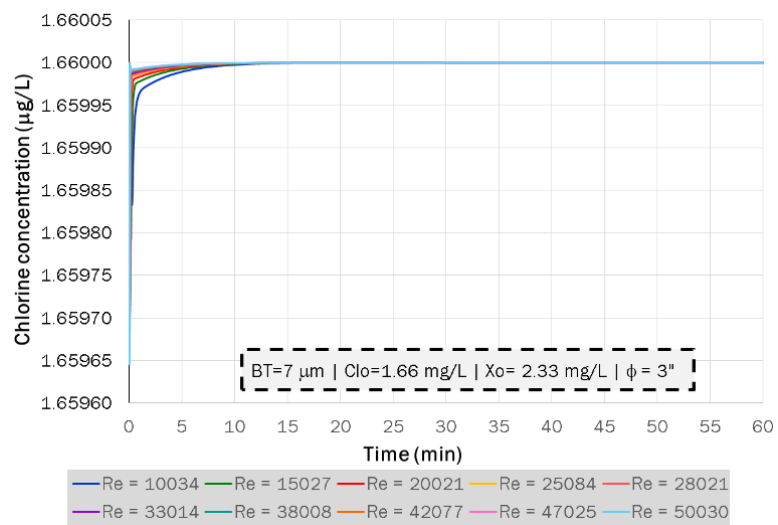


(a)



(b)

Figure 5-27. Average DCAN concentration at the pipe outlet for several Re – Turbulent flow (a) BT = 7 µm (b) BT = 102 µm



(a)

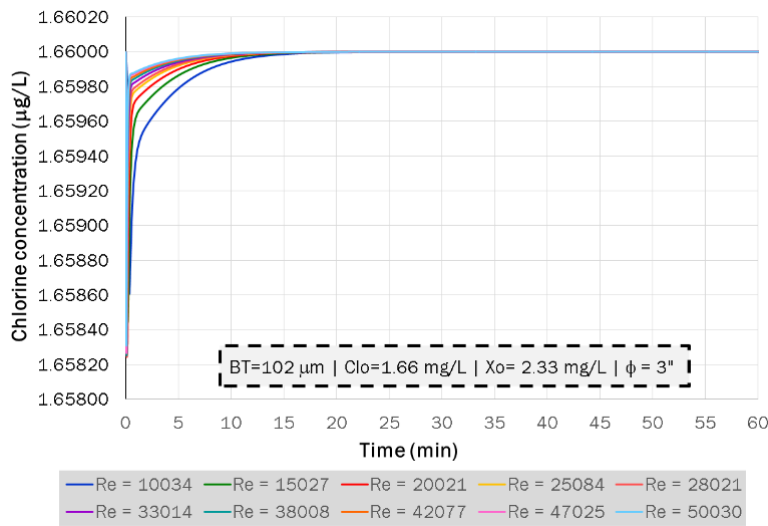


Figure 5-28. Average chlorine concentration at the pipe outlet for several Re – Turbulent flow (a) BT = 7 μm (b) BT = 102 μm

As it is expected, DBP concentrations were decreasing as Re increased, due to dilution effect caused by the increase of the flow rate (Figure 5-23, Figure 5-24, Figure 5-26, and Figure 5-27). Chlorine demand increased with higher Re, which is probably associated with faster mass transport towards the biofilm (Figure 5-25 and Figure 5-28). This is also observed in the shape of the concentration curves. Minimum chlorine concentrations occurred faster as Re increases. Figure 5-23, Figure 5-24, Figure 5-26, and Figure 5-27 also allows observing the influence of increase of Re on mass transport of DBPs. Curves of chloroform and DCAN concentrations are slightly closer to the vertical axis of the plots and are narrower as Re rises, which apparently reflects the faster evacuation of both DBP species from the pipe, when convective transport became more important in relation to diffusion transport. For instance, for BT=102 μm , DCAN concentration of 0.05 $\mu\text{g/L}$ is obtained at t=15 min for Re=2774, while the same concentration is found at t=11 min for Re=4994.

Finally, concentrations of both DBP species were higher for BT=102 μm in comparison with BT=7 μm , as expected when more biomass is available to react with chlorine. This is in agreement with the structure of the model, since higher biofilm thickness represents higher biomass available for reaction with chlorine, when the pipe is continuously fed with disinfectant. However, this has not been tested yet by experimental studies, to the author's knowledge. Published research studied other variables influencing the DBP formation from biomass disinfection such as pH, temperature, reaction time, disinfectant dose, pipe material, bacteria species, and type of biomass organic matter; then concentration of DBP precursors were maintained constant during the experiments

(Fang et al., 2010a; Fang et al., 2010b; Wang et al., 2012c; Pu et al., 2013; Wang et al., 2013a; Wang et al., 2013b). On the other hand, the current model did not consider the protective role of EPS for cells against disinfection. Such protective role consists on increased chlorine demand by reaction with EPS and dissolved organic matter, and more compact structure at the bottom of the biofilm. This could reduce the availability of disinfectant in the deeper layers and cells located in this region are able to survive (Xue et al., 2012; Xue et al., 2013).

In this line, DBP risk assessment associated to biomass disinfection must be analysed carefully, since the simplifications of the current model may lead to overestimation of the risk, considering that the model presented here simulate the DBP formation potentials. Avoiding EPS protective role leads to complete oxidation of cells by chlorine; this means that biofilm would not exist in real scale DWDNs, since disinfectant would oxidize every cell produced. However, this is not true; biofilms do grow in drinking water pipes and are more diverse than bacterial communities in bulk water, as discussed in Chapter 3. The current model used reaction terms associated to EPS according to experiments carried out by Chen and Stewart (1996), who used agarose as surrogate of EPS produced by *P. aeruginosa*. However, biofilms in DWDNs are heterogeneous and EPS may be diverse as well (Lemus Pérez and Rodríguez Susa, 2017). Then, chlorine demand exerted by EPS may be different than the calculated by Chen and Stewart (1996). It is important to highlight that factors F_x and F_E corresponds to experimental tests carried out with extracted and suspended intracellular and extracellular organic matter from algae, by separate (Fang et al., 2010b); this differed from the real physical configurations of biofilms. To the author's knowledge, work by Wang et al. (2013a) is the only published study which includes DBP formation from biofilm chlorination, under the natural conditions (i.e., biofilm growing attached to a surface).

Despite of this, thicker biofilms, either related to higher cell density or EPS concentration, may increase both microbial and chemical risks. This means that increased biomass is available for reaction with the disinfectant and major bulk water concentrations of DBPs may be expected. Additionally, the secreted EPS protect the cells against the action of the disinfectant, then allowing them to grow and reproduce. If pathogenic microorganisms were present in biofilms, these can survive within this habitat and be released to bulk water if the proper hydraulics conditions were present. Then, they could reach the consumers, which represents an important microbial risk depending on the pathogen dose, level of exposure and susceptibility of the consumer. Water operators must pay special attention to dead-end branches, where slow flow is frequent (Abokifa et al., 2016b), since thicker biofilms may be present there due to limited transport of nutrients (Picioreanu et al., 1998b; Jayatilake et al., 2017). Therefore, it is necessary to design and apply

a plan for O&M of DWDNs, which includes cleaning of pipes, flushing dead-end sections, and opportune replacement of old pipelines.

5.3.3.2 Mass transport

In order to examine transport of dissolved substances in more detail, \bar{Sh} and \bar{k}_f for chloroform, DCAN and chlorine were analysed. Results are presented in Figure 5-29, Figure 5-30, and Figure 5-31, respectively, for transitional flow. For turbulent flow, \bar{Sh} and \bar{k}_f for chloroform, DCAN and chlorine are shown in Figure 5-32, Figure 5-33, and Figure 5-34. The behaviour of both parameters is the same for the three dissolved substances analysed here, for both flow regimes: \bar{Sh} and \bar{k}_f increases as Re rises.

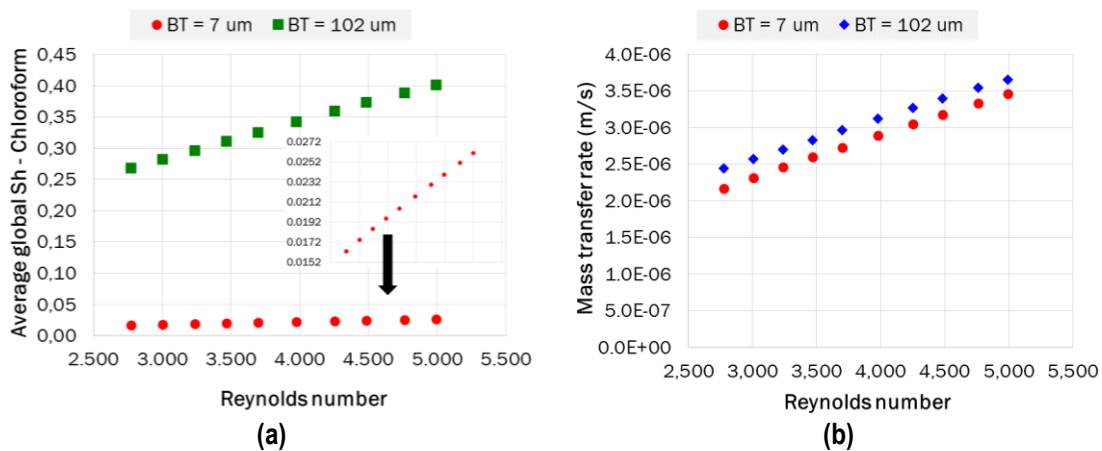


Figure 5-29. \bar{Sh} (a) and mass transfer rate (b) of chloroform for several Re – Transitional flow

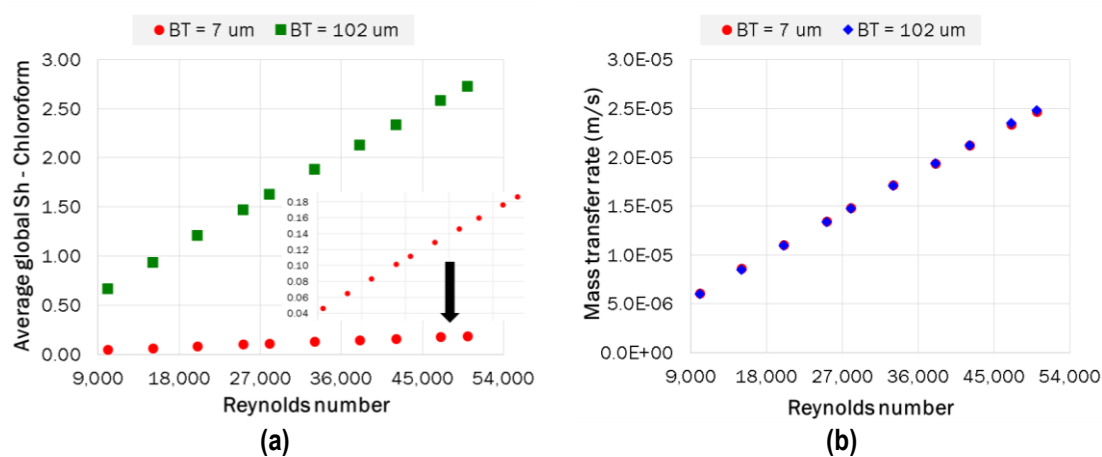


Figure 5-30. \bar{Sh} (a) and mass transfer rate (b) of chloroform for several Re – Turbulent flow

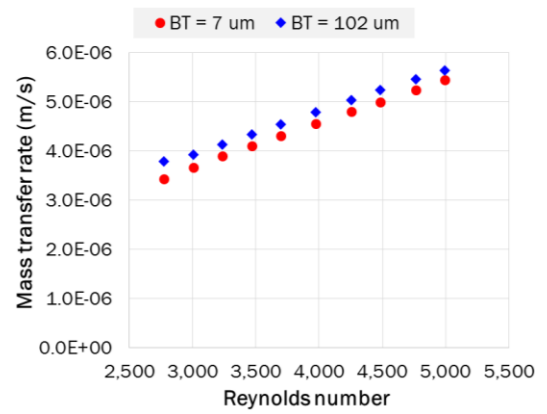
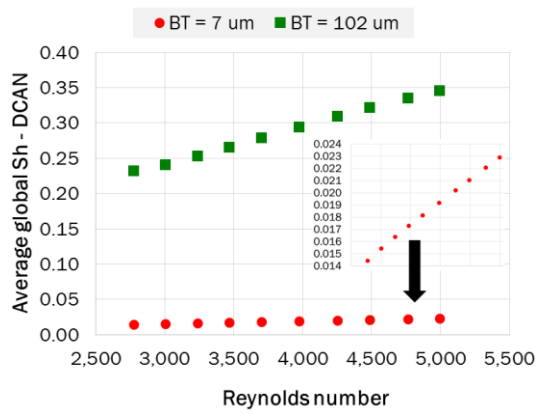


Figure 5-31. \bar{Sh} (a) and mass transfer rate (b) of DCAN for several Re – Transitional flow

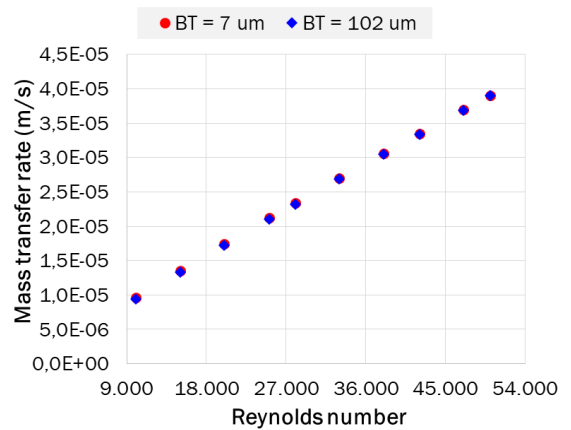
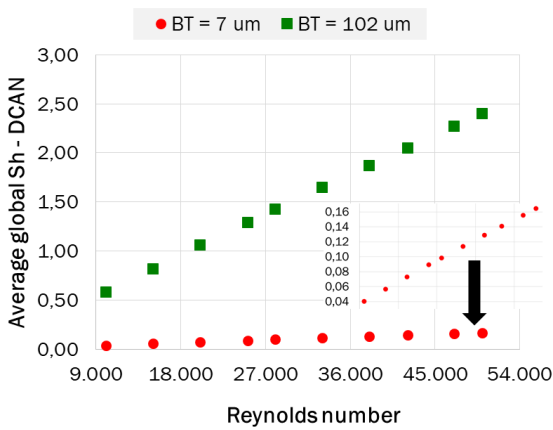


Figure 5-32. \bar{Sh} (a) and mass transfer rate (b) of DCAN for several Re – Turbulent flow

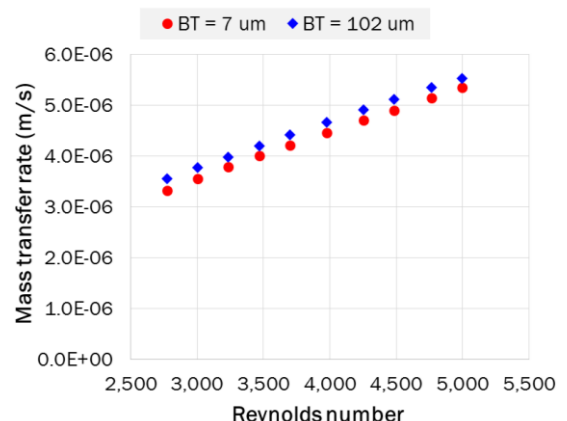
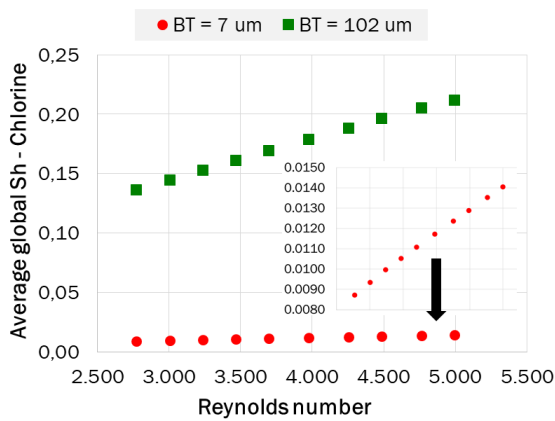


Figure 5-33. \bar{Sh} (a) and mass transfer rate (b) of chlorine for several Re – Transitional flow

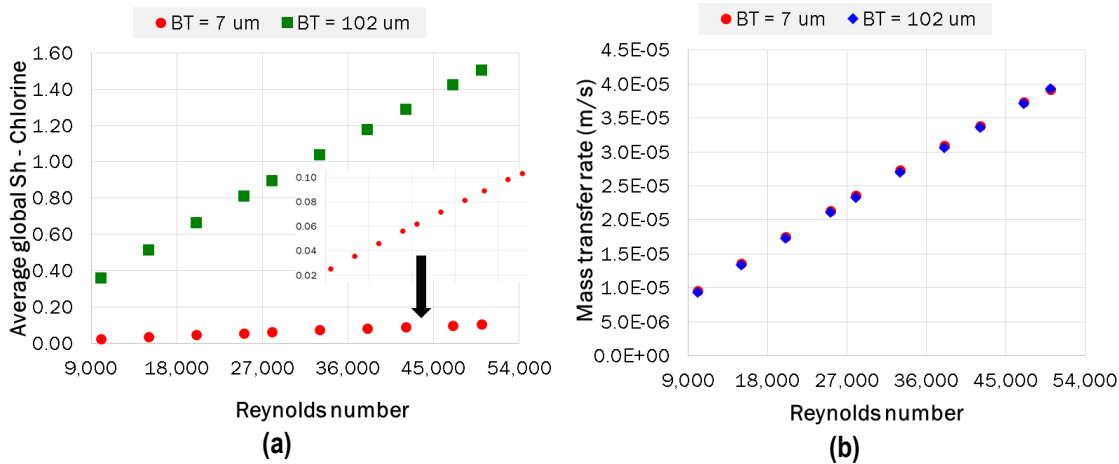


Figure 5-34. \bar{Sh} (a) and mass transfer rate (b) of chlorine for several Re – Turbulent flow

Particularly, \bar{Sh} was notably higher for BT=102 μm than for BT=7 μm (Figures 5-29a – 5-34a), which is logic since the parameter BT was included in the numerator of Equation (2-9) as the characteristic length. This also corresponds to the nature of the model, considering that higher biofilm thickness included more biomass available for reaction with chlorine, then chlorine demand and transport of chlorine and DBPs increased through the biofilm surface boundary.

Simulated results suggest that the difference among BT was compensated in the calculation of \bar{k}_f (Equation (2-11)). Therefore, the difference between \bar{k}_f for both BT values and for the three dissolved substances was significantly reduced, and such difference reduced even more when Re increased (Figures 5-29b – 5-34b). For turbulent flow, \bar{k}_f was similar for both BT values analysed here. Percentage of difference of \bar{k}_f for chlorine and DBPs reduced from 7-12% for Re=2774 to 0.05-0.5% for Re=50,030. Simulated values of \bar{k}_f were in the order of 10^{-6} - 10^{-5} m/s and always exhibited an increasing pattern. These results are not surprising since higher velocities (i.e., higher Re) correlates with thinner boundary layers, then higher \bar{Sh} and \bar{k}_f could be obtained (IWA Task Group on Biofilm Modeling et al., 2006; Taherzadeh et al., 2012).

Another important result of this study is the behaviour of \bar{Sh} . As explained in Section 2.3.2.2, several empirical correlations have been proposed for \bar{Sh} under laminar and turbulent flow, which represents a polynomial relationship with Re and Sc. The behaviour of \bar{Sh} found with the current model was far from such approach. The relationship between \bar{Sh} and Re was clearly linear, which may be related to the assumption of a flat biofilm surface. It is known that irregular biofilm surface results in non-uniform boundary layer thickness, then different values of \bar{Sh} and \bar{k}_f can be obtained along each point of the biofilm surface (Picioreanu et al., 1998b). Taherzadeh et al. (2012) also

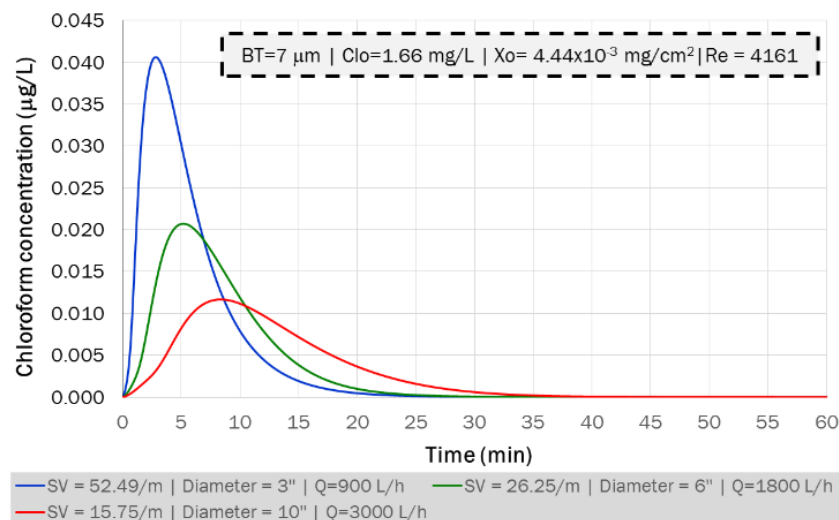
found a linear relationship between \bar{Sh} and Re for a single cell with a moving tail, under laminar flow conditions (Re up to 150).

5.3.4 Influence of S/V ratio on DBP transport

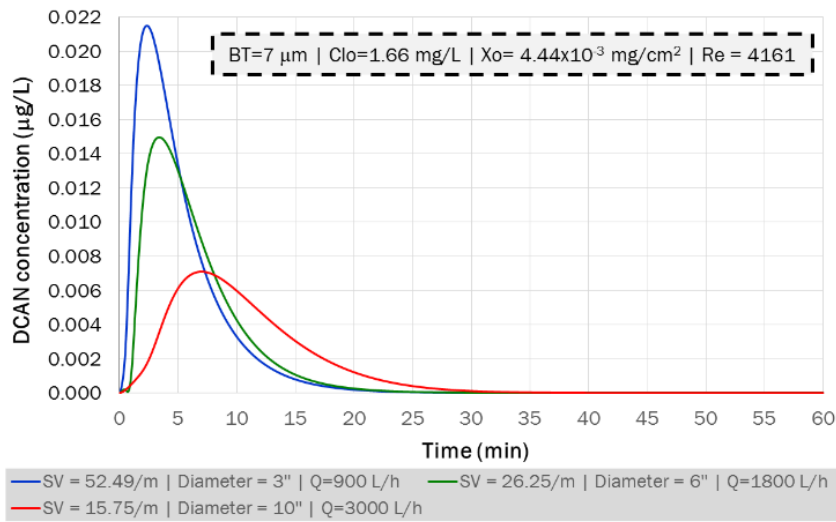
5.3.4.1 Different flow rates and equal Re

Results from Chapter 3 explained how S/V ratio influenced the DBP formation under stagnation conditions. A similar analysis is included here for chloroform and DCAN, under transitional flow, and three different pipe diameters (3, 6, and 10 inches), keeping the same Re in each pipe. Figure 5-35 presents the average concentrations of chloroform and DCAN at the pipe outlet. Figure 5-36 shows the average concentrations of chlorine at the pipe outlet. Figure 5-37 shows \bar{Sh} for the three dissolved substances simulated. As expected, higher concentrations of chloroform and DCAN and higher chlorine demand were found in smaller pipe diameters.

For transitional flow, maximal concentration of chloroform increased from $1.17 \times 10^{-2} \mu\text{g/L}$ for $\phi=10''$ to $4.06 \times 10^{-2} \mu\text{g/L}$ for $\phi=3''$ (Figure 5-35a). Minimal chlorine decreased from 1.65997 mg/L for $\phi=10''$ to $1.65988 \mu\text{g/L}$ for $\phi=3''$ (Figure 5-35b). The increased DBP concentrations found in smaller diameters is in agreement with the findings of other researchers in relation to the increase of chlorine demand when pipe diameter decreases (Lu et al., 1999; Buamah et al., 2014; Lee et al., 2014). This is related to interactions bulk-wall become more significant in smaller pipe diameters.



(a)



(b)

Figure 5-35. Average chloroform (a) and DCAN (b) concentrations at the pipe outlet for several pipe diameters – Transitional flow

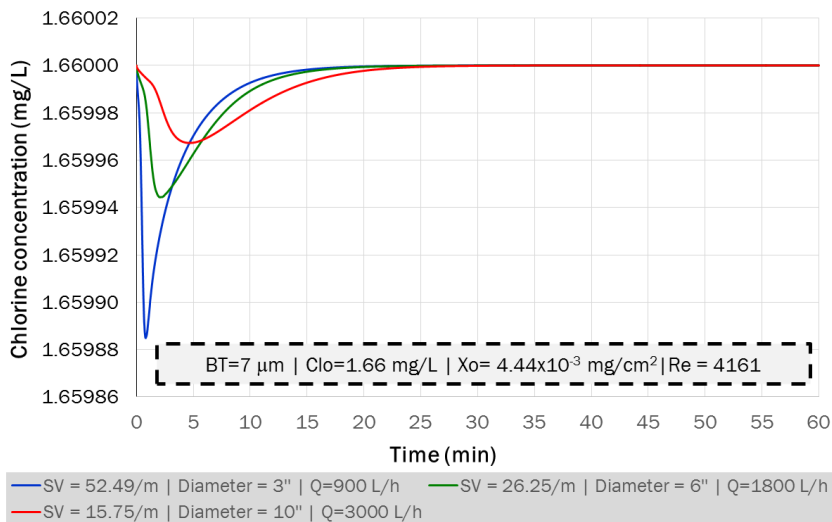


Figure 5-36. Average chlorine concentrations at the pipe outlet for several pipe diameters – Transitional flow

Similarly, mass transport increased in smaller pipe diameters, which is reflected in the shape of concentration curves, since curves are narrower and closer to the vertical axis, which suggests that substances were leaving the pipe faster (Figure 5-35). \bar{Sh} could have also implied faster mass transport in smaller pipes. For transitional flow, \bar{Sh} of chloroform increased from 0.0059 for $\phi=10''$ to 0.0226 for $\phi=3''$ (Figure 5-37a). \bar{Sh} of DCAN increased from 0.0052 for $\phi=10''$ to 0.0199 for $\phi=3''$ (Figure 5-37a). \bar{Sh} of chlorine increased from 0.0028 for $\phi=10''$ to 0.0121 for $\phi=3''$ (Figure 5-37b).

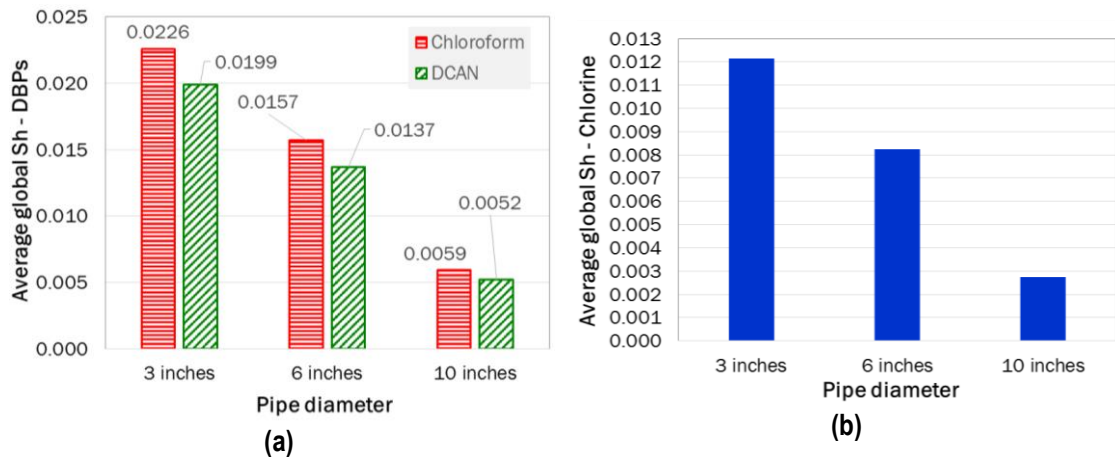
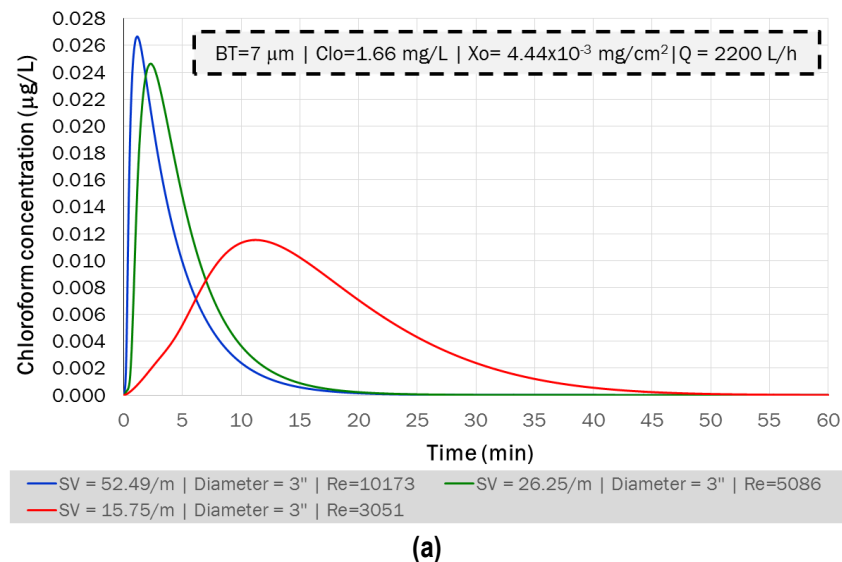
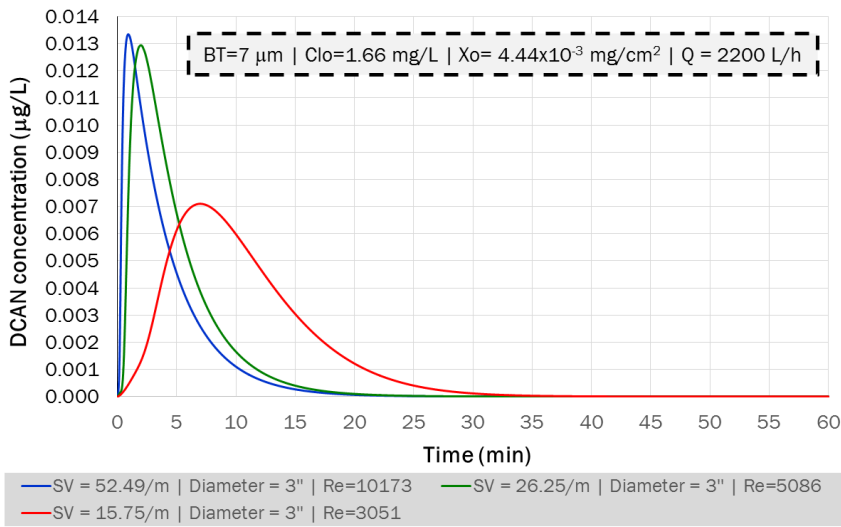


Figure 5-37. Average \bar{Sh} for DBPs (a) and Chlorine (b) for several pipe diameters – Transitional flow

5.3.4.2 Equal flow rates and different Re

A similar analysis to the previous one is included here for chloroform and DCAN, under transitional and turbulent flow, by keeping the same flow rates and different Re in each pipe of diameters 3, 6 and 10 inches. Figure 5-38 presents the average concentrations of chloroform and DCAN at the pipe outlet. Figure 5-39 shows the average concentrations of chlorine at the pipe outlet. Figure 5-40 shows \bar{Sh} for the three dissolved substances simulated. As expected, higher concentrations of chloroform and DCAN and higher chlorine demand were found in smaller pipe diameters.





(b)

Figure 5-38. Average chloroform (a) and DCAN (b) concentrations at the pipe outlet for several pipe diameters – Turbulent flow

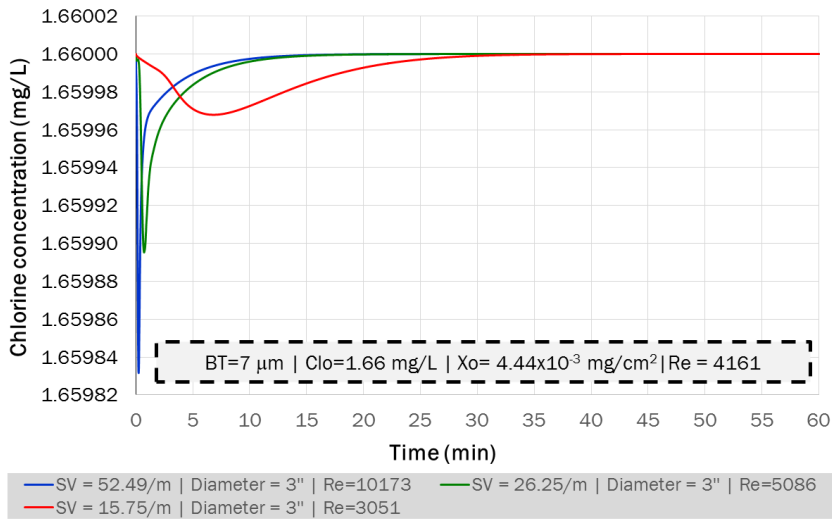


Figure 5-39. Average chlorine concentrations at the pipe outlet for several pipe diameters – Turbulent flow

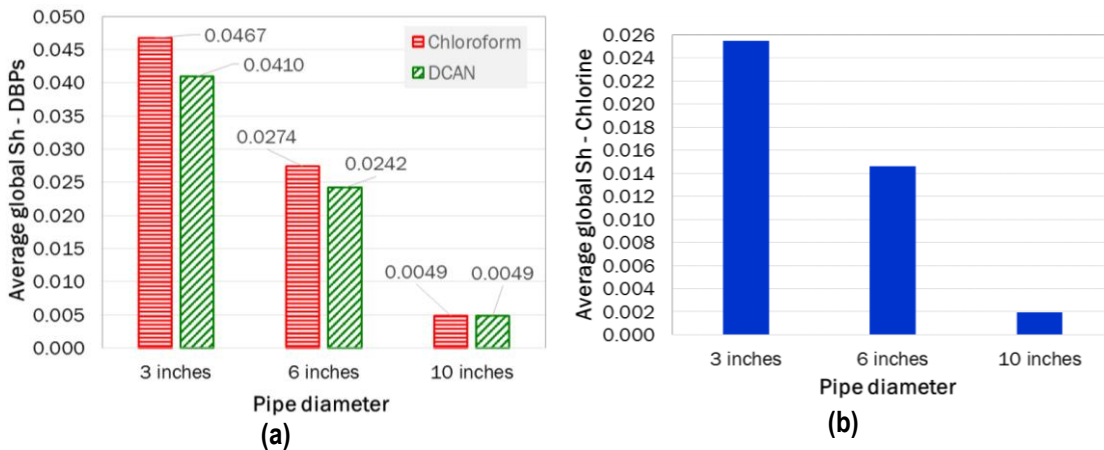


Figure 5-40. Average \bar{Sh} for DBPs (a) and Chlorine (b) for several pipe diameters – Turbulent flow

5.3.5 DBP formation under several conditions of drinking water quality

5.3.5.1 *Transitional flow*

Two scenarios of drinking water quality were selected to test the DBP formation under those conditions. The least critical scenario corresponded to the lower bound of the range for parameters BT, Clo, and X_o (Table 5-22). The most critical scenario corresponded to the upper bound of the range for parameters BT, Clo, and X_o (Table 5-22). Range of chlorine concentration was defined by the minimal and maximal values found in the field work developed in Cali's DWDN (Chapter 3). Figure 5-41 presents the chloroform and DCAN concentrations at the pipe outlet and Table 5-22 includes \bar{S}_h and \bar{k}_f for the three dissolved substances analysed here for transitional flow. As it is expected, DBP concentrations were higher under the most critical conditions in relation to the lowest BT, Clo, and X_o. While least critical scenario exhibited maximal concentrations of 0.0037 µg/L of chloroform (Figure 5-41a) and 0.0020 µg/L of DCAN (Figure 5-41b), the most critical scenario resulted in maximal concentrations of 0.58 µg/L (Figure 5-41a) of chloroform and 0.34 µg/L of DCAN (Figure 5-41b).

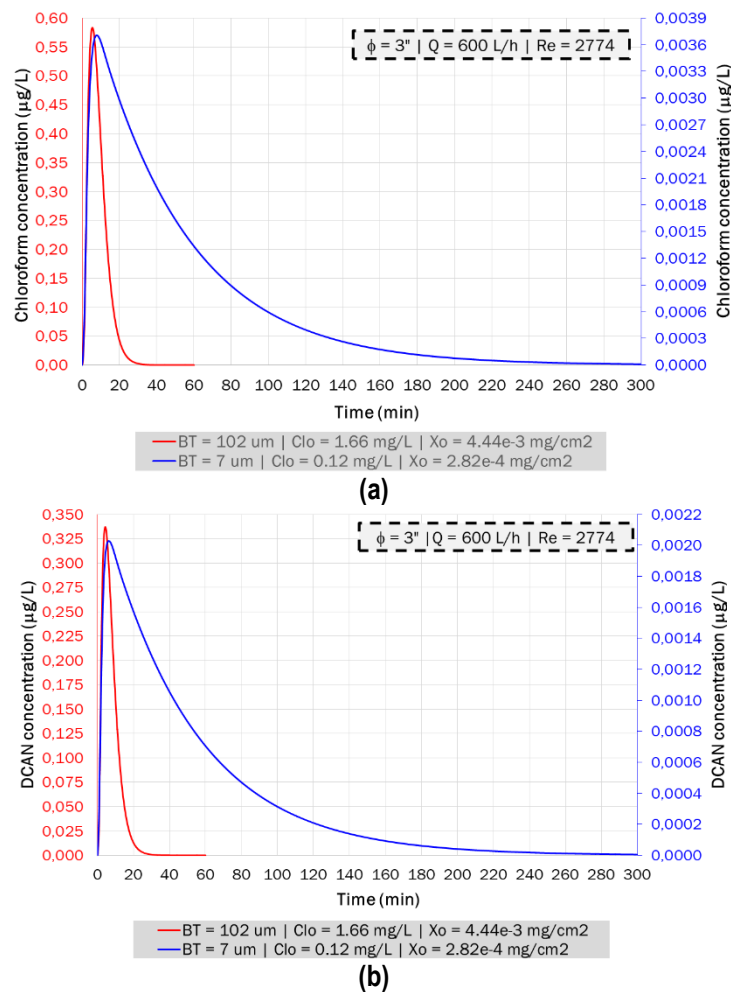


Figure 5-41. Average concentrations of (a) chloroform and (b) DCAN at the pipe outlet for two scenarios of drinking water quality – Transitional flow

On the other hand, the shape of concentration curves showed that mass transport of DBP is different in both scenarios. Both substances left the pipe in five hours under the least critical conditions, while both substances left the pipe in only one hour under the most critical conditions, due to gradient concentrations as explained below. Faster mass transport under the most critical conditions of water quality was evidenced by values of $\bar{S}h$ included in Table 5-22. $\bar{S}h$ of chloroform, DCAN, and chlorine increased around 171% under the most critical conditions in relation to the least critical conditions.

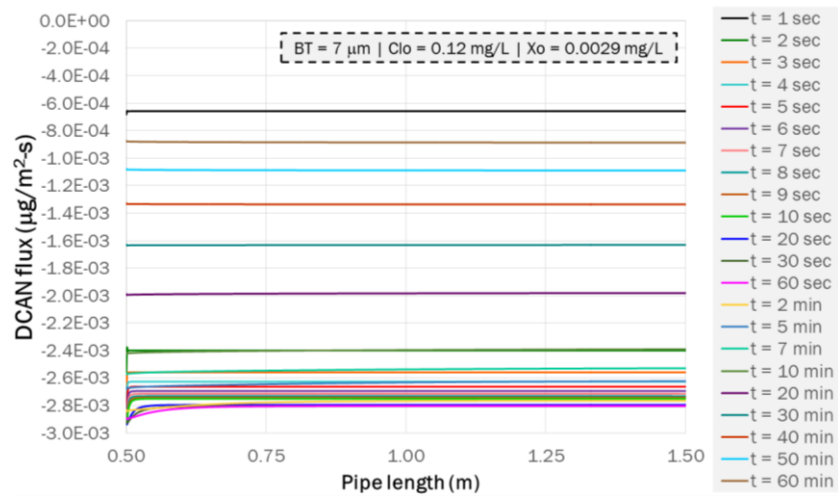
Table 5-22. $\bar{S}h$ and \bar{k}_f for dissolved substances for two scenarios of drinking water quality – Transitional flow

Scenario	$\bar{S}h$ - Chloroform	$\bar{S}h$ - DCAN	$\bar{S}h$ - Chlorine
Least critical scenario: BT = 7 μm Clo = 0.12 mg/L $X_o = 2.82 \times 10^{-4}$ mg/cm ²	0.0212	0.0178	0.0109
Most critical scenario: BT = 102 μm Clo = 1.66 mg/L $X_o = 4.44 \times 10^{-3}$ mg/cm ²	0.2680	0.2326	0.1396
Scenario	Mass transfer (m/s) - Chloroform	Mass transfer (m/s) - DCAN	Mass transfer (m/s) - Chlorine
Least critical scenario: BT = 7 μm Clo = 0.12 mg/L $X_o = 2.82 \times 10^{-4}$ mg/cm ²	2.81×10^{-6}	4.23×10^{-6}	4.10×10^{-6}
Most critical scenario: BT = 102 μm Clo = 1.66 mg/L $X_o = 4.44 \times 10^{-3}$ mg/cm ²	2.44×10^{-6}	3.79×10^{-6}	3.64×10^{-6}

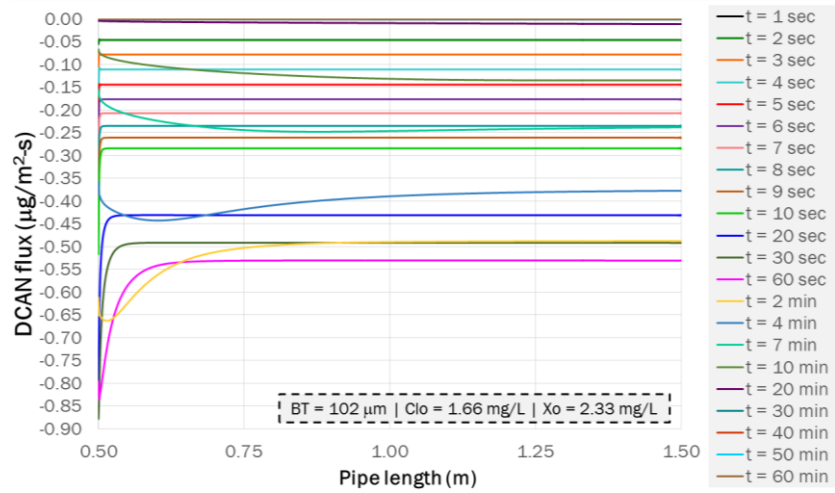
In contrast, despite of $\bar{S}h$ is directly proportional to the biofilm thickness and flux at the biofilm surface (Equation (2-9)), \bar{k}_f resulted higher under the least critical conditions in relation to the most critical conditions, for the three dissolved substances simulated (Table 5-22). For instance, flux of DCAN was in the order of 10^{-3} - 10^{-4} $\mu\text{g}/\text{m}^2\text{-s}$ under the least critical conditions, while such flux was in the order of 10^{-1} $\mu\text{g}/\text{m}^2\text{-s}$ under the most critical conditions (Figure 5-42). The same pattern applies for flux of chlorine; values of magnitude order of 10^{-6} – 10^{-5} mg/m²-s resulted under the least critical conditions, in comparison to values of magnitude order of 10^{-2} – 10^{-3} mg/m²-s under the most critical conditions (Figure 5-43). Then, $\bar{S}h$ was lower when concentrations of chlorine and DBPs were lower, which may indicates that diffusive transport is predominant over convective transport at the biofilm surface under those conditions.

On the other hand, calculation of \bar{k}_f (Equation (2-11)) is inversely proportional to the characteristic length (BT here), then \bar{k}_f resulted lower for BT=102 μm in relation to BT=7 μm . Higher mass transfer rate at biofilm surface occurred in the least critical scenario due to smaller BT, which is related to faster consumption of biomass. This was also confirmed by the time when DCAN left the biofilm and reached very low concentrations in this domain ($\cong 10^{-9}$ mol/m³); DCAN evacuated the

biofilm domain at $t=60$ min under the most critical conditions, while DCAN left the biofilm domain at $t=7$ min under the least critical conditions.

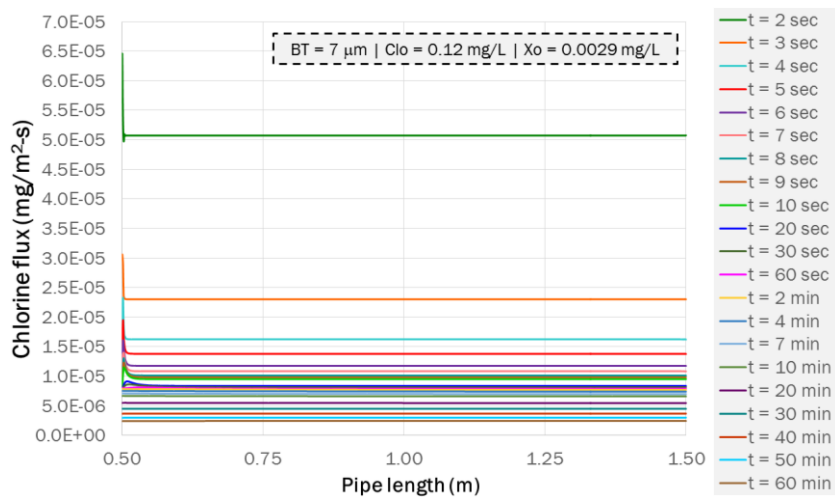


(a)

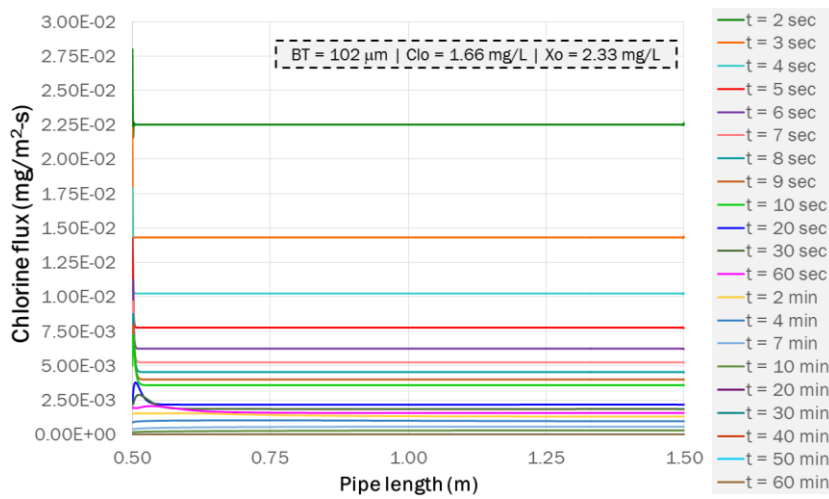


(b)

Figure 5-42. Flux of DCAN at the biofilm surface for two scenarios of drinking water quality (a) Least critical scenario (b) Most critical scenario



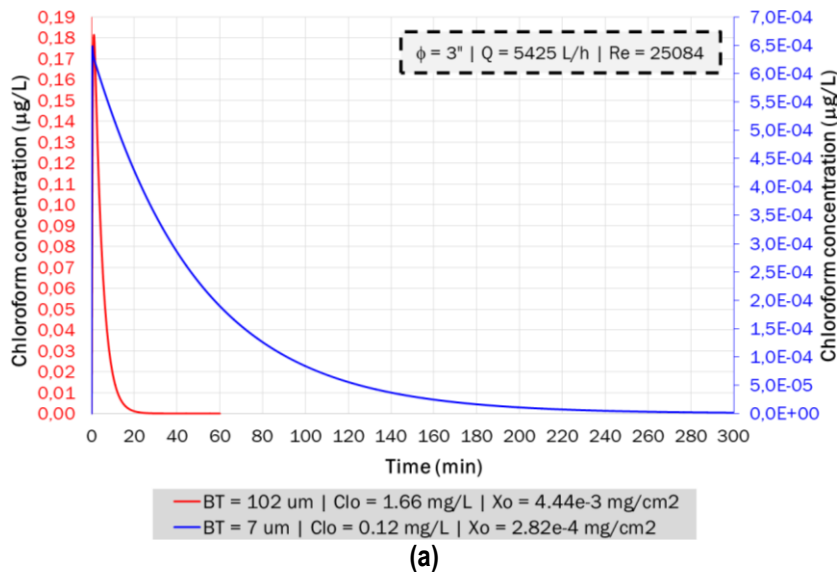
(a)

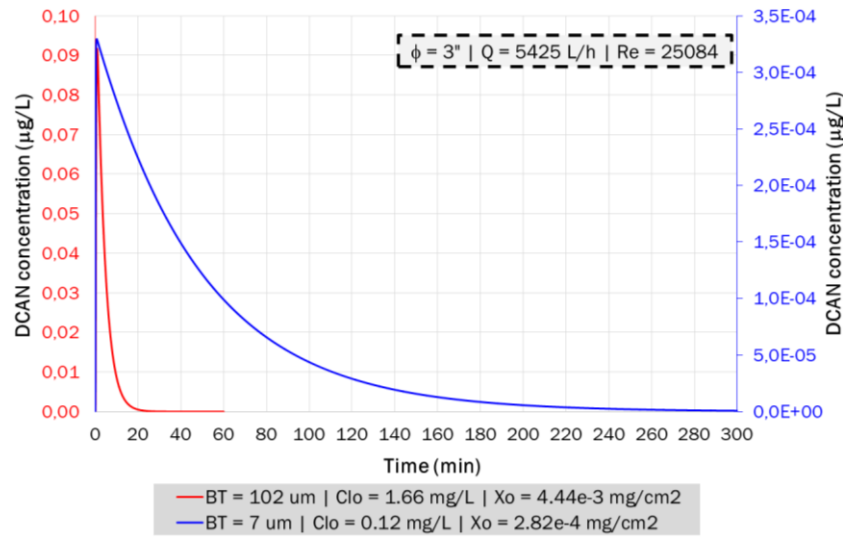


(b)
Figure 5-43. Flux of chlorine at the biofilm surface for two scenarios of drinking water quality – Transitional flow (a) Least critical scenario (b) Most critical scenario

5.3.5.2 Turbulent flow

Average concentrations of chloroform and DCAN at the pipe outlet are observed in Figure 5-44, for the least and most critical scenario regarding water quality parameters. Similarly to transitional flow, simulations for turbulent flow indicate that concentrations of both DBP species were higher for the most critical scenario in comparison to the least critical scenario, which is related to more biomass available for reaction with chlorine when biofilm thickness is higher.





(b)
Figure 5-44. Average concentrations of (a) chloroform and (b) DCAN at the pipe outlet for two scenarios of drinking water quality – Turbulent flow

Table 5-23 shows the \bar{Sh} and \bar{k}_f for DBP species and chlorine corresponding to turbulent flow. Similar to transitional flow, \bar{Sh} was higher for the most critical conditions, which is related to the higher biofilm thickness, as explained previously and suggests that convection effects increases when higher concentrations are present in bulk water. This was also observed when comparing the time required for DBPs to evacuate the pipe: one and five hours for the most and least critical conditions, respectively. In relation to \bar{k}_f , mass transfer also resulted slightly lower for higher BT (most critical scenario), due to calculation of this parameter is inversely proportional to BT (Equation (2-11)). This is reflecting that lower biomass is consumed faster, as explained in the previous section.

Table 5-23. \bar{Sh} and \bar{k}_f for dissolved substances for two scenarios of drinking water quality – Turbulent flow

Scenario	\bar{Sh} - Chloroform	\bar{Sh} - DCAN	\bar{Sh} - Chlorine
Least critical scenario: BT = 7 μm Clo = 0.12 mg/L $X_o = 2.82 \times 10^{-4}$ mg/cm ²	0.1027	0.0901	0.0566
Most critical scenario: BT = 102 μm Clo = 1.66 mg/L $X_o = 4.44 \times 10^{-3}$ mg/cm ²	1.4733	1.2929	0.8107
Scenario	Mass transfer (m/s) - Chloroform	Mass transfer (m/s) - DCAN	Mass transfer (m/s) - Chlorine
Least critical scenario: BT = 7 μm Clo = 0.12 mg/L $X_o = 2.82 \times 10^{-4}$ mg/cm ²	1.36×10^{-5}	2.14×10^{-5}	2.15×10^{-5}
Most critical scenario: BT = 102 μm Clo = 1.66 mg/L $X_o = 4.44 \times 10^{-3}$ mg/cm ²	1.34×10^{-5}	2.10×10^{-5}	2.11×10^{-5}

5.3.6 Discussion

The current 2D model presented here predicted the formation potentials of chloroform and DCAN from biofilm chlorination in a drinking water pipe of length equal to 1 m. The simulations were undertaken for several scenarios in order to evaluate the influence of flow regime, Re , S/V ratio, and drinking water quality on DBP formation and mass transport. In terms of absolute concentrations, some extrapolations can be made with regards to UK and Colombian standards for chloroform (100 $\mu\text{g/L}$ and 200 $\mu\text{g/L}$, respectively) (UK Parliament, 2000; Ministerio de la Protección Social and Ministerio de Ambiente Vivienda y Desarrollo Territorial, 2007) and WHO guideline for DCAN (20 $\mu\text{g/L}$) (WHO, 2017). According to the maximum concentrations presented in the Section 5.3.5, for transitional flow, DCAN concentrations might be higher than 20 $\mu\text{g/L}$ for pipelines length of 9.85 Km and 0.06 Km, if the least and most critical conditions uniformly prevailed along the pipes, respectively. In the case of chloroform, lengths of 27 Km and 54 Km would be necessary to exceed the UK (100 $\mu\text{g/L}$) and Colombian (200 $\mu\text{g/L}$) regulation, respectively (UK Parliament, 2000; Ministerio de la Protección Social and Ministerio de Ambiente Vivienda y Desarrollo Territorial, 2007), if the least critical conditions prevailed along the pipes. For the most critical conditions, 0.17 Km and 0.34 Km would be required to surpass the regulations mentioned previously, respectively.

In the case of turbulent flow, DCAN concentrations might be higher than 20 $\mu\text{g/L}$ for pipelines length of 60.79 Km and 0.22 Km, if the least and most critical conditions uniformly prevailed along the pipes, respectively. In the case of chloroform, lengths of 154 Km and 309 Km would be necessary to exceed the UK (100 $\mu\text{g/L}$) and Colombian (200 $\mu\text{g/L}$) regulation, respectively (UK Parliament, 2000; Ministerio de la Protección Social and Ministerio de Ambiente Vivienda y Desarrollo Territorial, 2007), if the least critical conditions prevailed along the pipes. For the most critical conditions, 0.55 Km and 1.10 Km would be required to surpass the regulations mentioned previously, respectively.

This simple analysis suggests that the higher risk is related to DCAN under transitional flow (lower velocities). As explained in Chapters 2 and 4, the experimental evidence on cells indicates that toxicity of nitrogenous DBPs is higher in comparison to carbonaceous DBPs (Muellner et al., 2007). The most clear epidemiological evidence in relation to THMs, but not conclusive, is related to bladder cancer (Hrudey et al., 2015b). Therefore, for higher biomass content and chlorine residuals, the potential risk may be present even in small DWDNs, specially is small pipes. For bigger water systems, even low biomass content and chlorine residuals may also represent potential health risks. However, it is important to highlight that DCAN is an unstable DBP since it is degraded depending on the pH and chlorine concentration. DCAN degrades in the absence of chlorine above

pH 7 and below pH 6.5. In the presence of free chlorine, DCAN degradation can be much faster from a pH of about 6–8.5 under low to moderate chlorine residuals (Reckhow et al., 2001). Therefore, higher risk may be present in building premises and in the portion of the network supplying directly the consumers (smaller pipes), since less opportunities may occur for changing the physico-chemical conditions of drinking water, then reducing the probability of degradation of DCAN.

On the other hand, there is mass transport. The present results showed that mass transport is faster for turbulent flow, higher Re , smaller pipe diameters, and higher Clo , higher BT , and higher Xo together. Thus, a balance between control of acute and chronic risk must be considered by water operators. Slow mass transfer favour the reduction of DBP concentrations, since chlorine is slowly penetrating the biofilm thickness and DBP formed within it are being slowly transported to the bulk. However, this slow mass transport may also favour the growth of microorganisms living within the biofilm, even pathogenic microbes. If there was enough contact time between biomass and chlorine, the disinfectant can be completely depleted and DBP concentrations can reach the maximum potentials. Absence of chlorine would also favour the biofilm regrowth. As mentioned in Chapter 3, the best approach for water operators is to minimize the biofilm formation, which can host pathogenic microorganisms and may be significant DBP precursors. A deeper analysis of the health implications of biofilm presence in drinking water pipes is presented in Chapter 6.

5.3.7 Sensitivity analysis

Sensitivity analysis was carried out based on the Morris method adapted by Menberg et al. (2016) and calculations were performed using the MATLAB toolbox developed by Pianosi et al. (2015). The influence of 12 parameters was evaluated for response variables \bar{Sh} for chlorine, \bar{Sh} for DCAN, average of average concentrations of DCAN at the pipe outlet, and median of average concentrations of DCAN at the pipe outlet.

5.3.7.1 \bar{Sh} - chlorine

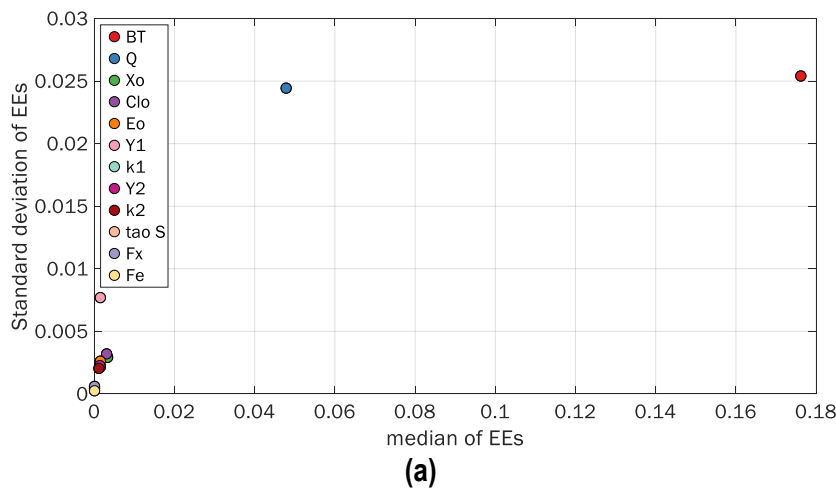
Table 5-24 shows the median and standard deviation of EE for each parameter assessed. Parameters were sorted in descendent order according to the level of influence; i.e., from highest to lowest median of EE. Figure 5-45 shows the points corresponding to both values of EE from Table 5-24 (a) and the area covered by each parameter according to the lower and upper bounds of median and standard deviation of EE (b). Then, the most influencing parameters on \bar{Sh} - chlorine were biofilm thickness and flow rate, which is a logical result since the Sherwood number is a

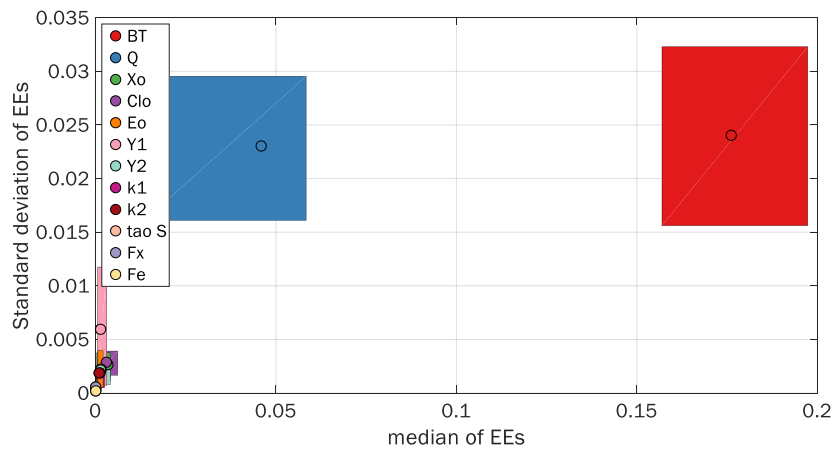
measure of the diffusion and convective transport at the biofilm surface. The influence of the remaining parameters was very low; they are located near to the origin in Figure 5-45a.

Table 5-24. Median and standard deviation of EEs on response variable \bar{S}_h - Chlorine

Parameter	Median of EE	Standard deviation of EE	Parameter	Median of EE	Standard deviation of EE
BT	0.173	0.024	Y_2	0.001	0.002
Q	0.046	0.023	k_1	0.001	0.002
X_o	0.003	0.003	k_2	0.001	0.002
Cl _o	0.003	0.003	τ_s	0.000	0.000
E _o	0.001	0.002	F _x	0.000	0.001
Y_1	0.001	0.006	F _E	0.000	0.000

Convective transport depends on the hydrodynamics of the bulk flow, which is directly linked to the flow rate. Additionally, calculation of \bar{S}_h (Equation (2-9)) includes the characteristic length assumed here as the biofilm thickness. This parameter is more influencing than flow rate; Figure 5-45b shows that standard variation of EEs for biofilm thickness presented more variation in comparison to its median value, while the median of EEs for flow rate varied more in comparison to its standard variation. Therefore, flow calculation is important in modelling, then it is necessary to appropriate define the turbulence model and flow rate.





(b)

Figure 5-45. EEs on response variable \bar{S}_h - Chlorine (a) Median vs Standard deviation (b) Median vs Standard deviation including upper and lower bounds

5.3.7.2 \bar{S}_h - DCAN

Similarly to \bar{S}_h of chlorine, Table 5-25 shows the median and standard deviation of EE for each parameter assessed for \bar{S}_h of DCAN. Figure 5-46 shows the points intersecting the median and standard deviation of EEs (a) and the area covered by each parameter according to the lower and upper bounds of median and standard deviation of EEs (b). These results allowed identifying that the most influencing parameters were biofilm thickness, followed by τ_s , and Q (Table 5-25). As explained in the previous section, BT and Q are influencing \bar{S}_h of DCAN because the calculation of Sherwood number (Equation (2-9)) includes the biofilm thickness as the characteristic length and it is a measure of the diffusive and convective transport at the biofilm surface. In addition and as described in Section 5.2.8, the effective diffusion coefficient within the biofilm is an important parameter for determining the mass transport of DBPs at the biofilm surface because this model included only diffusive transport within the biofilm. Then, the gradient concentration at this region is determined by the diffusion of the dissolved substances within the biofilm.

Table 5-25. Median and standard deviation of EEs on response variable \bar{S}_h - DCAN

Parameter	Median of EE	Standard deviation of EE	Parameter	Median of EE	Standard deviation of EE
BT	0.343	0.307	Xo	0.004	0.010
τ_s	0.229	0.881	k ₁	0.003	0.015
Q	0.074	0.144	k ₂	0.003	0.004
Clo	0.008	0.011	Eo	0.002	0.001
Y ₁	0.005	0.021	Fx	0.001	0.002
Y ₂	0.005	0.004	F _E	0.000	0.002

As it is observed in Figure 5-46a, the influence of other parameters assessed is very low since they are located near to the origin of the plot. While BT is the most influencing parameter on $\bar{S}h$ of DCAN, τ_s presented the highest variation in both median and standard deviation of EEs. This represent that this parameter must be carefully defined in case of the interest is mainly on the study of the mass transport of DBPs at the biofilm surface.

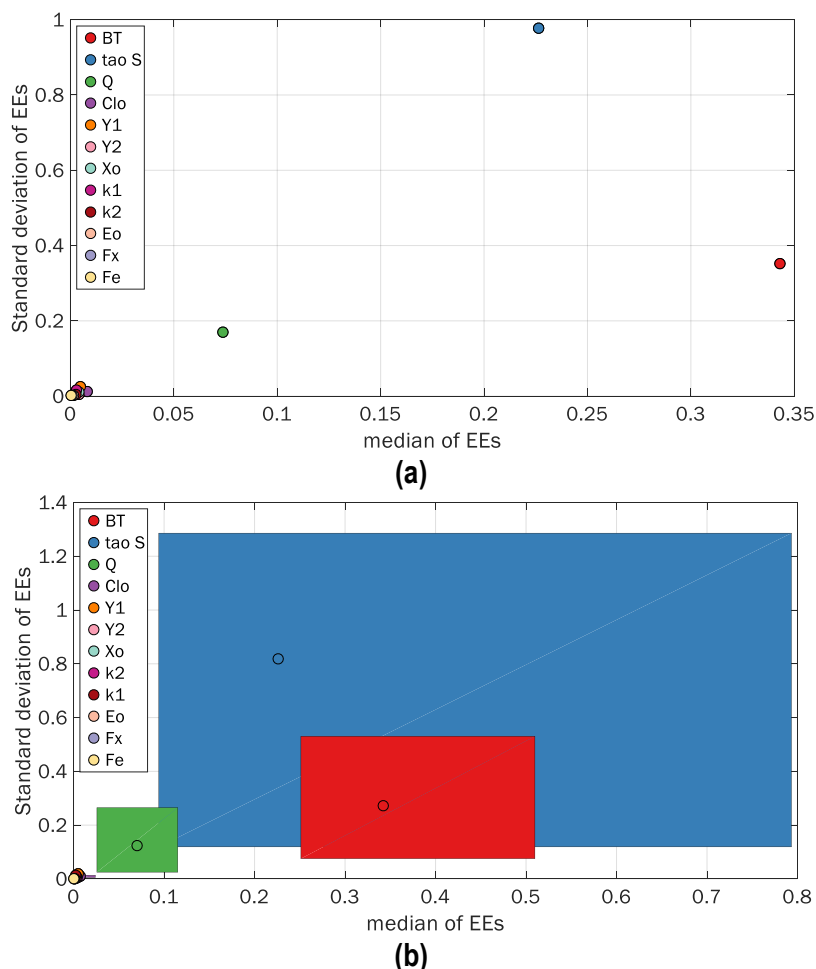


Figure 5-46. EEs on response variable $\bar{S}h$ - DCAN (a) Median vs Standard deviation (b) Median vs Standard deviation including upper and lower bounds

5.3.7.3 Average DCAN

Table 5-26 presents the list of parameters sorted according to the level of influence over the response variable average DCAN. Figure 5-47 shows the points corresponding to both values of EE from Table 5-26 (a) and the area covered by each parameter according to the lower and upper bounds of median and standard deviation of EE (b). For the average DCAN at the pipe outlet, the most influencing parameters were Xo, BT and Fx. This is related to the effect caused by the maximal concentrations on the average DCAN. When higher values of these three parameters are present together, more DBPs are formed. Then, average concentrations are higher.

Table 5-26. Median and standard deviation of EEs on response variable average DCAN

Parameter	Median of EE	Standard deviation of EE	Parameter	Median of EE	Standard deviation of EE
Xo	0.170	0.122	Q	0.048	0.076
BT	0.136	0.264	Y ₂	0.040	0.105
Fx	0.092	0.284	Clo	0.005	0.189
Y ₁	0.075	0.109	τ _s	0.000	0.001
F _E	0.061	0.076	k ₁	0.000	0.046
Eo	0.055	0.078	k ₂	0.000	0.074

In contrast to the Sherwood number, other parameters such as yield coefficients Y₁ and Y₂, Eo, and Q are also influencing the average DCAN at the pipe outlet but in less degree than the other three parameters mentioned previously (Figure 5-47a). Parameters k₁, k₂, and τ_s have no influence on the average DCAN at the pipe outlet (Figure 5-47a). Xo was the most influencing parameter but variation of average and standard variation of EEs is low compared to the parameters BT and Fx. Particularly BT exhibited higher variation of the median of EEs, while Fx exhibited higher variation of the standard variation of EEs (Figure 5-47b).

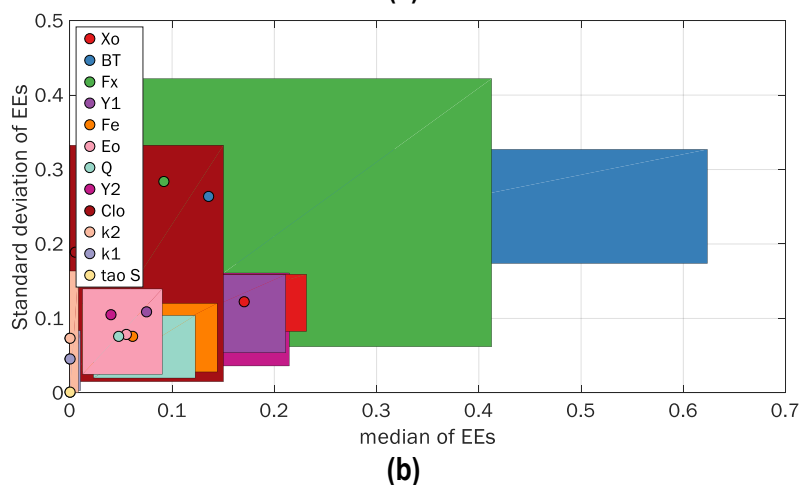
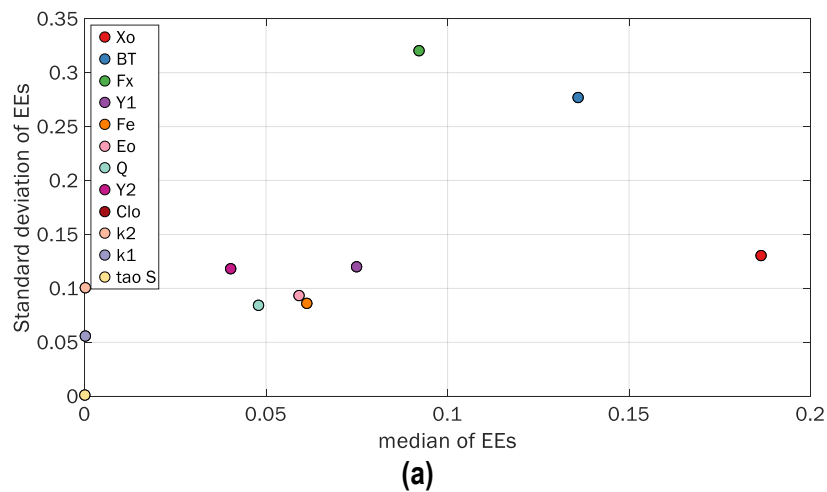


Figure 5-47. EEs on response variable average DCAN (a) Median vs Standard deviation (b) Median vs Standard deviation including upper and lower bounds

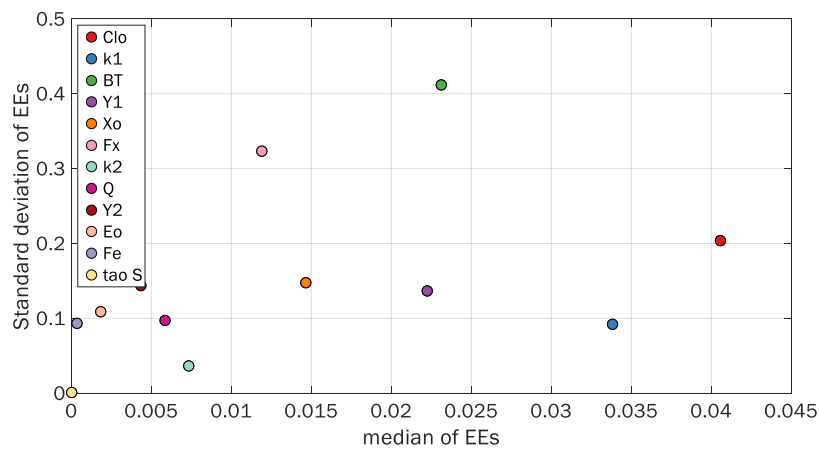
5.3.7.4 Median DCAN

Table 5-27 presents the list of parameters sorted on descending order of influence over the response variable median DCAN. Figure 5-48 presents the intersection points of median and standard deviation of EEs for the same response variable and the area covered by the upper and lower bounds or such values. For the case of the median DCAN at the pipe outlet, the most influencing parameter is C_{lo} , followed by k_1 , BT, Y_1 , X_o , and F_x . This represents that all the parameters involved in the reaction with cells are the most influencing ones over the median of DCAN at the pipe outlet. This means that the influence over the median DCAN is distributed among more parameters, which is the result of eliminating the effect of outliers over the measures of central tendency as the median value. The parameters associated to EPS (i.e E_o and F_E) and τ_s have little or no influence on the median DCAN.

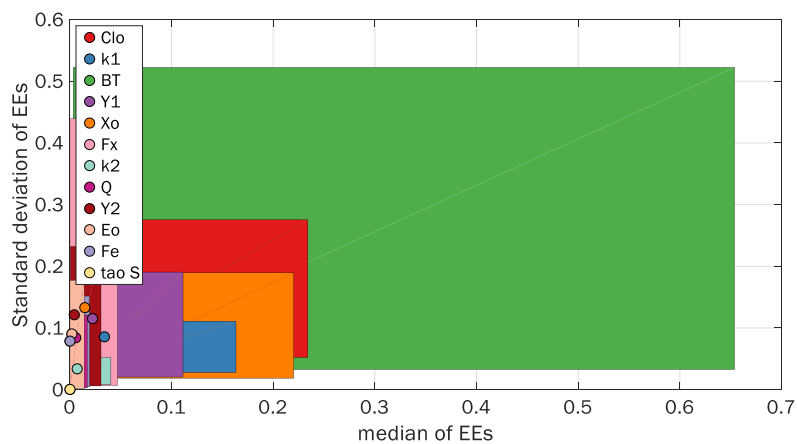
Table 5-27. Median and standard deviation of EEs on response variable median DCAN

Parameter	Median of EE	Standard deviation of EE	Parameter	Median of EE	Standard deviation of EE
C_{lo}	0.039	0.185	k_2	0.007	0.033
k_1	0.034	0.086	Q	0.006	0.084
BT	0.023	0.371	Y_2	0.004	0.121
Y_1	0.022	0.115	E_o	0.002	0.090
X_o	0.015	0.133	τ_s	0.000	0.000
F_x	0.012	0.269	F_E	0.000	0.079

The spread of parameters influencing the median DCAN is more clear in Figure 5-48a. While BT is the third parameter most influencing the median DCAN, its variation of median and standard deviation of EEs is higher than the other two parameters ranked in the two first places. Since higher BT represent more biomass available for reaction with chlorine and further transformation into DBPs, it is logical to find that variations on this parameter led to variations on the median concentrations of DCAN at the pipe outlet.



(a)



(b)

Figure 5-48. EEs on response variable median DCAN (a) Median vs Standard deviation (b) Median vs Standard deviation including upper and lower bounds

5.3.7.5 Summary

Table 5-28 presents the ranking of the parameters included in the sensitivity analysis according to their influence on response variables. In general, BT resulted the most important parameter for the characterization of the mass transport of DBPs through the biofilm surface and their concentrations in bulk water. Other important parameters are Xo, Clo, Y₁, Q, and k₁. Parameters related to EPS (E_o, k₂, F_E, Y₂) exhibited medium and low influence on the response variables. This may be related to the current model assumed that cells contributed more to DBP concentrations, EPS and cells were completely mixed within the biofilm and the protective role of EPS to cells against disinfection was not considered. Refinement of the model should include this feature of EPS to model how chlorine reacts first with it, then reducing its availability for disinfection in the deeper layers of the biofilm. Q is globally representing medium influence of response variables, but especially important for the mass transport through the biofilm surface; similarly, τ_s is also very important for this.

Experimental calculation of τ_s involves the development of micro-sensors to measure concentrations of the target DBPs within the biofilm.

Table 5-28. Ranking of parameters according to their influence on response variables

Parameter	Parameter ranking			
	Sh – Chlorine	Sh – DCAN	Average DCAN	Median DCAN
BT	1	1	2	3
Q	2	3	7	8
Xo	3	7	1	5
Clo	4	4	9	1
Eo	5	10	6	10
Y ₁	6	5	4	4
Y ₂	7	6	8	9
k ₁	8	8	11	2
k ₂	9	9	12	7
τ_s	10	2	10	11
Fx	11	11	3	6
Fe	12	12	5	12

As previously mentioned and discussed in Chapter 3, more efforts must be made in order to improve laboratory techniques to properly monitor microbiological parameters of biofilm such as thickness and cell density in real scale DWDNs. This will contribute to improve the estimation of DBP formation potentials from biofilm chlorination in water pipes and increase the availability of data for further calculations of microbial risks related to biofilms. Data of flow rates and chlorine concentrations are available from historic records of the water utilities or can be directly measured in the DWDN.

5.4 MODEL APPLICATIONS AND LIMITATIONS

The 2D model developed here presents several features that contribute to new knowledge in the field of biofilm–DBP modelling in drinking water. This model was formulated for prediction of formation potentials of two DBP species (chloroform and DCAN), under transitional and turbulent flow, which are the flow regimes commonly found in drinking water pipes. The flow field was calculated and the turbulent model SST was selected to solve the flow near to the pipe wall. This allowed calculating the local and global Sh at the biofilm surface boundary; then, mass transport rates were also available for the scenarios considered in this study.

Mass transport characterization is important in the current model since the interest of researchers on biomass (cells and EPS) as DBP precursors is increasing from the point of view of experimental

works (Hong et al., 2008; Fang et al., 2010a; Fang et al., 2010b; Wang et al., 2012c; Pu et al., 2013; Wang et al., 2013a; Wang et al., 2013b; Lemus Pérez and Rodríguez Susa, 2017). Therefore, this model can be used to compare to and explain experimental data obtained under hydrodynamic conditions. Experimental studies for mass transport in biofilms have been developed for substrate consumption such as glucose and oxygen (Zhang and Bishop, 1994; Guimerà et al., 2016). The researchers have made attempts to represent such process by engineered correlations among Sh, Re, and Sc. The current model showed that Sh for the substances chloroform, DCAN, and chlorine is linearly correlated with Re for a flat biofilm, in the range 2,774-50,030. To the author's knowledge, this is the first study reporting such analysis for these substances.

Coupling the flow field to the transport of dissolved substances by CFD is a computationally expensive task. Therefore, the current model included several simplifications such as flat biofilm, no biofilm growth in order to only simulate DBP formation potentials, and flow in steady state. It is known that biofilms can have irregular surfaces as a result of their internal morphology, depending on the substrate concentration (Picioleanu et al., 1998b). The dynamics between residual disinfectant and planktonic cells and biofilms in drinking water pipes is characterized by depletion of the disinfectant by reaction with biomass and other inorganic and organic substances. During this process, microorganisms are inactivated; once disinfectant is low, bacteria regrowth occurs.

Abokifa et al. (2016a) included this dynamics in their 1D model, under transitional flow, and found that THM contribution from biomass occurs in pulses. While microorganism inactivation were taking place, chlorine was decaying and THMs were increasing until reaching a plateau in the curve. When bacteria regrowth occurred, the same previous pattern was repeated, increasing the absolute THM concentration from biomass chlorination (Abokifa et al., 2016a). Furthermore, flow in water pipes varies according to changes on customer demand or due to operative procedures such as closing valves or intermittent supply (NRCNA, 2006). Therefore, steady state would not be the predominant hydraulic condition. Variation of flow leads to changes on shear stress and biofilm detachment can occur.

The current model is also limited by the absence of experimental data to compare to. Previous experimental studies were carried out under static conditions or laminar flow regime. However, this model can help to design new experiments on DBP formation in drinking water pipes under transitional and turbulent flow. In addition, the sensitivity analysis of the model was carried out by using the method with the lowest computational cost (Morris method) and by evaluating the method only once. This represented 33 days to complete the sensitivity analysis. The methodology applied by Menberg et al. (2016) included 10 evaluations of the model with the Morris method. The high

computational cost of CFD models limited the application of more thorough sensitivity analysis methods and this may represent that parameter influence was not properly ranked. However, the results of the sensitivity analysis presented here agreed with the variables involved in the equations included in the model. Furthermore, this analysis offered a general idea of the parameters which must be determined with more accuracy and frequency in real scale DWDNs to be used as inputs of the current model.

As hardware, software and more efficient numerical models are developed, more characteristics of the real biofilm and flow in drinking water pipes can be included in future modelling studies. In the meantime, the current model is an appropriate tool to evaluate the factors that influence the DBP formation potentials resulting in certain initial characteristics of the biofilm, which can be relative easy to measure. As mentioned in Chapter 4, some improvements on microscopy techniques must be done to measure biofilm thickness from real scale DWDNs. On the other hand, the water industry must do more efforts to incorporate biofilm research results into routine O&M of DWDNs. In this line, an effective and close relationship academy, water industry and regulatory agencies must be promoted.

5.5 CONCLUSIONS

This chapter presented the development of a model, in two dimensions, for predicting the formation potentials of chloroform and DCAN, under bulk flow.

- Biofilms should be actively acknowledged as DBPs precursors. This may lead to improve the prediction of DBPs in distribution networks. Improved models of DBP formation coupled with validated hydraulic models in water networks may help to improve the assessment of chronic risks in drinking water.
- Turbulence model SST is appropriate to solve the flow in the whole domain, especially near to the pipe wall, where wall reactions take place. This model is also solver independent as shown through solution in both COMSOL 5.2a and Ansys Fluent 16.0.
- The concentrations of chloroform and DCAN are mainly dependent of water quality parameters such as initial chlorine concentration, initial cell concentration, and biofilm thickness. Higher values of such parameters can lead to higher concentrations of both DBP species.
- Pipe diameter was also an important parameter influencing the DBP concentrations. Such concentrations were higher with small pipe diameter such as 3 inches in relation to 10 inches.

- Faster mass transport at the biofilm surface was found for higher Re , being faster for turbulent flow, followed by transitional and laminar. Similarly, faster mass transport may occur in smaller pipe diameter, and with higher initial concentrations of chlorine and cells and higher biofilm thickness.
- Mass transfer rates of magnitude order of $10^{-6} - 10^{-5} \text{ mg/m}^2\text{-s}$ were found for chloroform and DCAN under transitional and turbulent flow regime.
- A linear relationship between Re and Sh was found with the simulations run by the model developed in this study.
- From the point of view of microbiological risk, slow flow represents the most critical condition to properly disinfect biofilms and control bacteria growth within them. Similarly, chemical risk may be also high due to lower flow rates led to higher concentrations of DBPs, despite of the reduced mass transfer.
- Field and laboratory assessment of the biofilm properties must be focused primarily on biofilm thickness and cell density. Reaction rates and yield coefficients can still rely on published data in the scientific literature but further experimental studies may refine those results by using other types of disinfectant, multispecies biofilm, and environmental temperature.
- Water operators must pay especial attention to control the chronic risk associated with DBPs and human health in the smaller pipes of the DWDNs, where lower flow rates can be present, then major interactions bulk-biofilm are expected and more DBPs can be formed. Furthermore, for those portions of the networks are immediately close to the customers, then the formed DBPs will enter the plumbing systems and may increase their concentration under stagnation conditions, which prevail within the building facilities.

6 GENERAL DISCUSSION, IMPLICATIONS AND APPLICATIONS

6.1 GENERAL DISCUSSION

The current research project analysed the impact of the presence of biofilms in DWDNs by two approaches: microbial and chemical risk, with major emphasis on the last one, due to the growing research interest on biomass as DBP precursors. Figure 6-1 shows how the dual role of biofilms was studied in the current research project. Such impact was studied by a fieldwork carried out in a full scale DWDN located in a tropical-weather country. Such fieldwork allowed identifying the predominant bacterial communities in biofilm and bulk water habitat, in nine points of the DWDN. Correlations between biotic parameters and engineered factors were determined and relationships between bacterial communities and THMs were also explored. Following the field study, two models were developed as tools to predict the formation potentials of chloroform and DCAN from chlorination of biofilms in drinking water pipes. Such models allowed determination of the concentrations of such DBPs under stagnation and hydrodynamic conditions, according to biofilm characteristics, pipe diameter, water quality, and hydraulic conditions.

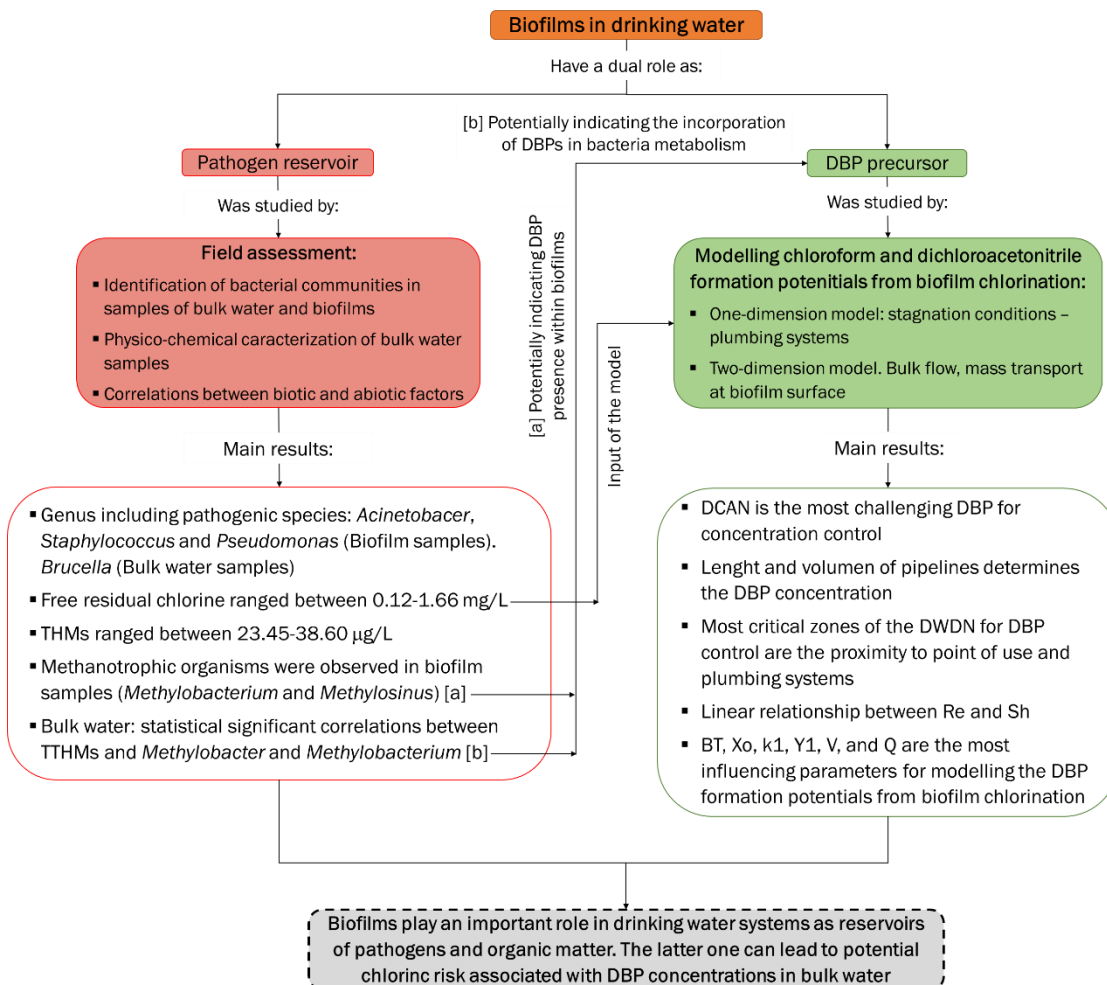


Figure 6-1. Dual role of biofilms studied in the current research project

As can be observed in Figure 6-1, by the field assessment in a tropical-weather DWDN, correlations between TTHMs and methanotrophs in bulk water samples and the presence of these organisms in biofilm samples may confirm the interrelations between microorganisms and chemical substances such as DBPs in real scale DWDNs. Concentrations of free residual chlorine measured in the Cali's distribution network were used as inputs of the several scenarios simulated with the two models developed in the current research project. In this line, Figure 6-2 presents other parameters to be considered in further field assessments of biofilms, in order to collect more field data to be used as inputs of models of disinfectant decay and DBP formation including biomass contribution. Parameters to be considered in future field works should include biofilm thickness, chlorine and DBP concentrations, flow rate, pipe diameter, cell density, EPS concentration and identification of microbial communities. This will contribute to improve definition and validation of hydraulic and water quality models focused on analysis of balance between microbial and chemical risk in drinking water systems.

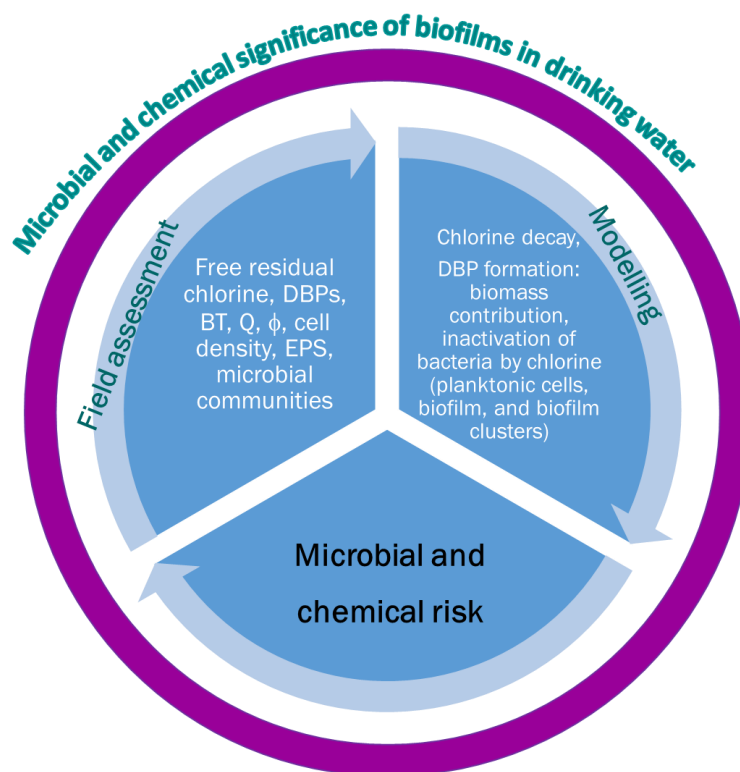


Figure 6-2. Two approaches to study the microbial and chemical significance of biofilms in drinking water

Biofilms in drinking water have been mainly studied for research purposes, especially due to its capacity to host pathogens. These organisms can be released to the bulk, reach the consumers, and cause infection if the biofilm is detached and disinfectant is insufficient or unable to inactivate them. In plumbing systems, opportunistic pathogens (e.g., *Legionella spp.*, *Mycobacterium spp.*,

Pseudomonas aeruginosa) generate special concerns due to they find the perfect conditions there for survival and growth. Opportunistic pathogens are disinfectant resistant, biofilm formers, and able to grow within amoeba, under oligotrophic conditions and low oxygen levels (Falkinham et al., 2015). Additional to the ingestion exposure route, opportunistic pathogens can also be inhaled from aerosols formed during showering. These pathogens affect to individuals with predisposal conditions such as advance age (older than 70 years), cancer or immunodeficiency (Falkinham et al., 2015). Therefore, special attention must be paid to safety of drinking water supplied particularly in medical institutions and care homes.

On the other hand, investigation on biomass as DBP precursors has been continuously developed in the last decade. Researchers have been interested on quantifying, by laboratory tests, the contribution of algae, EPS, planktonic cells of single species, both heterogeneous and homogeneous biofilms, detached clusters biofilms, and biomolecules to the formation of carbonaceous and nitrogenous DBPs, by both chlorination and chloramination (Hong et al., 2008; Fang et al., 2010a; Fang et al., 2010b; Wang et al., 2012c; Pu et al., 2013; Wang et al., 2013a; Wang et al., 2013b; Lemus Pérez and Rodríguez Susa, 2017). According to this, a recent study focused on modelling the formation of THMs in a DWDN, for turbulent flow regime, included the contribution of fixed and suspended biomass (Abokifa et al., 2016a). The researchers estimated that biomass contributed with around maximum 12% of the total THM concentrations simulated (Abokifa et al., 2016a).

According to Lee and Schwab (2005), DWDNs from developing countries are characterized for several failures such as low or absence of residual disinfectant, low water pressure, intermittent service, and high rate of leaks; poor basic sanitation is also a common situation in such countries. Everything together represents that a big portion of the population of these countries are exposed to microbial risks by water consumption (Lee and Schwab, 2005). As described in Chapter 3, the DWDN of the city of Cali presents all the failures mentioned previously, in certain portions of the network and during specific times. A special feature of this network, which has been reported frequently in communication media, is the intermittent supply due to the contamination of the water source. In addition, the ageing infrastructure (30.4% of the pipelines are made of asbestos) and the hydraulic changes cause a high rate of leaks (81/100 Km for year 2013)¹⁷. High rate of leaks represents that service must be frequently interrupted in the affected region to repair the leak, then disturbing the hydraulics of the circuit. According to USEPA's guidelines (USEPA, 2002c) and during the field work, it was also observed that the new piece of pipe installed did not contain any

¹⁷ EMCALI EICE ESP, 2014, personal communication, 10th December

protection against contamination and it is unknown if this was disinfected prior to installation. Neither disinfection nor flushing prior to putting the pipe into service was confirmed. Repair staff neither take any preventive procedure to protect themselves to avoid passing contamination to the pipelines. The affected portion of the network was not flushed either prior to reinitiate water supply.

Thus, it is clear that several processes are simultaneously occurring in Cali's DWDN that may threaten the microbial drinking water quality delivered to the consumers. With regards to chemical risk, DBP concentrations were in average 31.76 $\mu\text{g/L}$, which is below the UK and Colombian standards (100 and 200 $\mu\text{g/L}$, respectively) (UK Parliament, 2000; Ministerio de la Protección Social and Ministerio de Ambiente Vivienda y Desarrollo Territorial, 2007). In this line, the models developed here showed that the more risky situation is under stagnant conditions, particularly in plumbing premises, where DBP exposure occurs. Similarly, other studies have also established that households are exposed to microbial risk in the building facilities (Falkinham et al., 2015; Ji et al., 2015; Ji et al., 2017). Under no flow situation, chlorine may decay by reaction with pipe walls, then DBPs are formed and transported to bulk water, and bacteria regrowth occurs in both bulk water and biofilm. After a period of stagnation, householders use stagnant water and can be exposed, by mainly ingestion or inhalation, to DBPs and bacteria.

Under turbulent flow situation, it is clear that the major chemical risk associated to DBPs is in smaller pipes, i.e., those around the point of use, where bulk-wall interactions are more important, and flow rates are lower, then dissolved substances as DBPs are more concentrated. Furthermore, mass transfer is enhanced when Re is higher. Under the same Re , low chlorine concentrations led to reduced mass transfer, and DBP formation and transport is reduced. However, low disinfectant residuals also poses a microbial risk, because low mass transfer at the biofilm surface reduces the penetration of the biofilm by chlorine and, consequently, the inactivation of potential pathogenic microorganisms may decrease.

Disinfectant resistance by bacteria, protection by biofilm of microorganisms, DBP formation by biofilm chlorination, and disinfectant decay occur in real scale DWDNs. Then, exclusively relying on disinfection for biofilm control with focus on pathogen control is not sufficient. In this line, it is necessary to establish a trade-off between the microbial and chemical risk and minimize the biofilm formation to guarantee the delivery of safe water to the consumers, which is the final goal of water utilities, as it has been established by Hrudehy and collaborators (Hrudehy, 2009; Hrudehy and Charrois, 2012). In order to present the practical implications of both approaches, the next sections include the discussion of the microbial risk associated with bacteria identified in the field assessment, the

chemical risk analysed with the mathematical models, their implications on O&M of DWDNs, and the applicability of this research.

6.2 BACTERIAL COMMUNITIES AND PUBLIC HEALTH

Potential pathogenic bacteria were identified in several bulk and biofilm samples in Cali's DWDN. Due to such identification was based on DNA sequencing of a low number of base pairs, it can only be established the presence of the bacteria to genus level. The establishment of species and pathogenic strains and their viability must be done by other microbiological techniques such as quantitative and real-time PCR, staining-microscopy methods, measurement of ATP, and incorporation of bromodeoxyuridine, microautoradiography combined with FISH (Douterelo et al., 2014a). Due to the limitations of this study, it is not possible to calculate quantitative microbiological risk assessment. However, the results presented here are crossed with the map risks determined by Pérez-Vidal et al. (2012) for the same DWDN.

The city of Cali is administratively divided into 22 communes, which are groups of neighbourhoods that share similar socio-economic conditions. Pérez-Vidal et al. (2012) generated maps of hydraulic, physical and water quality integrity, according to criteria such as minimal pressure, number of leakages in aqueduct, number of leakages in sewage, number of leakages in household connections, percentage of material in the DWDN, historical records of water quality, and water quality complaints. The map risk was the result of the weighed combination of previous maps and population density.

Table 6-1 presents the sampling points and communes where DNA of potential pathogenic bacteria was identified and the respective risk classification obtained by Pérez-Vidal et al. (2012). The crossed information presented in Table 6-1 shows that sampling points where pathogenic bacteria were identified are located in the areas of high and very high risk. This is not a coincidence, since samples were collected during leak repair activities and map risk was created using the number of leaks in the aqueduct. Pérez-Vidal et al. (2012) assigned the highest weight to this criterion together with minimal pressure in the map of physical and hydraulic integrity (30% each). Similarly, this type of integrity had the highest weight together with water quality (40% each). Finding pathogenic bacteria in those communes represents that choosing the criterion number of leakage in a DWDN is reasoning, due to the loss of physical integrity during repair activities promotes the introduction of external contaminants to the system. This is probably the cause of the presence of bacteria listed in Table 6-1.

Table 6-1. Potential pathogenic bacteria identified in Cali's DWDN and their corresponding risk area defined by Pérez-Vidal et al. (2012)

Bacteria genus / Habitat	Sampling points	Commune	Commune risk classification according to risk maps
<i>Acinetobacter</i> Biofilm	Point 8	4	Very high risk
<i>Brucella</i> Bulk water	Point 1	4	Very high risk
	Point 2	8	Very high risk
	Point 4	7	High risk
	Point 6	8	Very high risk
<i>Mycobacterium</i> Bulk water	Point 1	4	Very high risk
<i>Staphylococcus</i> Biofilm	Point 6	8	Very high risk
	Point 8	4	Very high risk
	Point 9	7	High risk
<i>Pseudomonas</i> Biofilm	Point 3	10	High risk
	Point 5	4	Very high risk
	Point 8	17	High risk

Acinetobacter, *Staphylococcus* and *Pseudomonas* are biofilm formers, opportunistic pathogens, have been identified in infected patients and are able to colonize medical devices (Heilmann et al., 1996; Stover et al., 2000; Carr et al., 2003). Therefore, it is important that medical institutions and care homes incorporate additional remediation measures to avoid potential interaction between opportunistic pathogen and immune compromised patients. In order to reduce opportunistic pathogens in this type of institutions, Falkinham et al. (2015) recommended to increase the temperature of hot water and avoid its recirculation; clean and disinfect shower heads; replace shower heads with large hole; install single unit hot water systems to reduce the travel time of hot water; remove aerators from taps and faucets; carry out building wide disinfection; reduce aerosols by filter entrapment; and install microbial filtration devices in specific locations. It is important to mention that these organisms may be present in other regions of Cali's DWDN, which may be transported from one point to others during hydraulic changes.

To the author's knowledge, this is the first study reporting *Brucella* in a DWDN. This genus was the predominant group in Point 1. *Brucella* comprises 11 species, ten of them are associated with human infections (Scholz et al., 2010; Xavier et al., 2010) and the hosts of these pathogenic bacteria are commonly mammals (Eisenberg et al., 2012). Human brucellosis is considered as a life-threatening debilitating disease and sources of infection include inhalation of contaminated dust or aerosols, ingestion of contaminated milk and unpasteurized dairy products, and exposure of mucosa or skin abrasions to fluids and tissues from aborted fetuses of infected animals or carcass (Xavier et al., 2010). Despite of there is not conclusive evidence on microbial risk in the studied DWDN, the results presented here indicate that water managers should adopt improved O&M

measures to prevent deterioration of drinking water quality delivered to the consumers. Furthermore, another study should be carried out to confirm the presence of potential pathogenic bacteria belonging to the genus identified in this project.

6.3 DBPS AND PUBLIC HEALTH

DBP formation is a very complex process occurring in drinking water systems because many factors participate in it. Factors include type and dose of disinfectant, type and amount of precursors, pH, temperature, residence time, and presence of bromide. This complexity is reflected on the identification of around 600 DBPs, classified into 26 groups, but only four groups are currently subject of regulation or recommendation of health-based thresholds (Richardson et al., 2007). Certainly, the presence of disinfectant in drinking water is the main driver of DBP formation. Non-disinfected systems do not deal with this problem, but this occurs in cities, where water sources such as groundwater are properly preserved. Supply systems from Netherlands, Switzerland and Germany do not rely on residual disinfectants, but do on advanced treatment processes, improved physical integrity of the distribution system, and careful management of distribution system operations (Rosario-Ortiz et al., 2016).

When the water sources are contaminated, water utilities must rely on disinfection to inactivate pathogenic microorganisms in raw water and protect the distributed water from further contamination. Since the discovery of THMs in 1974, great amount of research has been conducted and regulations around the world have been designed to protect the consumers from chemical risk associated with DBPs. In this line, water operators have faced the dilemma about either maintaining disinfectant residuals in the water network or minimize the DBP formation. When disinfection cannot be evaded, chemical safety of drinking water is supported by the regulation, then water utilities focuses on reducing the DBP precursors. It is clear then that regulation of DBPs have promoted the improvement of drinking water quality by advancement on treatment processes and better practices of O&M of DWDNs (Humpage, 2012).

The previous analysis is the ideal approach in the context of the uncertainty of the association between mutagenic, carcinogenic and teratogenic effects on human health. According to Hrudey and Charrois (2012); Hrudey et al. (2015b), the epidemiological evidence is not yet conclusive to directly associate the most abundant and regulated DBPs such as THMs and HAAs with such negative health impacts. To date, the study developed by Cantor et al. (2010) has provided the strongest indication of potential association between bladder cancer and THMs in drinking water

(Hrudey et al., 2015b). However, the relationship between DBPs and negative health outcomes is still an open question. While the answers to this question arrive, it is necessary to put in proper perspective the management and control of DBPs in drinking water. In this line and according to the aim of this project, it is necessary to assume the biofilm risk as a trade-off and assimilate the biofilms as DBP precursors and potential reservoirs of pathogens.

In this context, the models developed in this project represent a tool to improve the prediction of DBP concentrations in plumbing systems and DWDNs, under both stagnation and hydrodynamic conditions. Proper prediction of DBPs would help to improve the assessment exposure, which is a key component on epidemiological studies related to these substances. The hydrodynamic model also contributes to understand the mass transfer of dissolved substances like chlorine and DBPs at the biofilm surface, then scenarios where more or less chlorine is desirable in certain areas of the network can be identified, in order to find the balance between bacteria and DBP control.

Consolidated results of both 1D and 2D models are included in Table 6-2 and Table 6-3, respectively. These results evidence that the most critical conditions in relation to DBP concentrations are under stagnation conditions, followed by transitional and turbulent flow. Diffusion is the predominant mass transport mechanism when there is not flow. For contact time of 11 hours, which can normally occur even in single building premises, all the biomass and chlorine are available for reacting, and formed DBPs are transported to the bulk water and diluted in small volumes.

Table 6-2. Main results of 1D model of potential of DBP formation from biofilm chlorination

Initial conditions (Contact time = 11 hours, $\phi = \frac{1}{2}$ inches)			Potential DBP concentrations
BT (μm)	Clo (mg/L)	Xo (mg/L)	
7	0.12 and 1.66	0.89	Chloroform = 6.98 $\mu\text{g/L}$ DCAN = 3.43 $\mu\text{g/L}$
		13.98	Chloroform = 31.62 $\mu\text{g/L}$ DCAN = 13.16 $\mu\text{g/L}$
102	0.12	0.89	Chloroform = 89.29 $\mu\text{g/L}$ DCAN = 44.30 $\mu\text{g/L}$
		13.98	Chloroform = 146.25 $\mu\text{g/L}$ DCAN = 61.42 $\mu\text{g/L}$
	1.66	0.89	Chloroform = 117.40 $\mu\text{g/L}$ DCAN = 58.26 $\mu\text{g/L}$
		13.98	Chloroform = 195.94 $\mu\text{g/L}$ DCAN = 466.20 $\mu\text{g/L}$
Initial conditions			Potential DBP concentrations
ϕ (inches)	Xo (mg/L)	BT and Clo	
$\frac{1}{2}$ - 9	0.89 – 0.05	7 μm 0.12 mg/L	Chloroform: 6.91 – 0.30 $\mu\text{g/L}$

			DCAN: 3.39 - 0.16 µg/L
	13.98 – 0.78	102 µm 1.66 mg/L	Chloroform: 466.20 – 6.55 µg/L
			DCAN: 195.94 – 3.27 µg/L

Table 6-3. Main results of 2D model of potential of DBP formation from biofilm chlorination

Initial conditions (Contact time = 1 hour, Pipe length = 1 m)						Potential DBP concentrations (maximal value)	\bar{Sh} - DBPs	Mass transfer (m/s)
BT (μm)	Clo (mg/L)	Xo (mg/cm ²)	ϕ (inches)	Re	Other			
7	1.66	4.44×10^{-3}	3	1200 4161 25084	Flow regime: Laminar, transitional and turbulent flow	Chloroform Laminar: 4.06×10^{-2} $\mu\text{g/L}$ Transitional: 3.46×10^{-2} $\mu\text{g/L}$ Turbulent: 1.42×10^{-2} $\mu\text{g/L}$ DCAN Laminar: 2.16×10^{-2} $\mu\text{g/L}$ Transitional: 1.97×10^{-2} $\mu\text{g/L}$ Turbulent: 6.82×10^{-3} $\mu\text{g/L}$	Chloroform Laminar: 0.0085 Transitional: 0.0226 Turbulent: 0.1016 DCAN Laminar: 0.0054 Transitional: 0.0023 Turbulent: 0.0895	Chloroform Laminar: 1.13×10^{-6} Transitional: 5.34×10^{-6} Turbulent: 2.14×10^{-5} DCAN Laminar: 1.28×10^{-6} Transitional: 5.44×10^{-6} Turbulent: 2.12×10^{-5}
7	1.66	4.44×10^{-3}	3	2774 - 4994	Transitional flow	Chloroform = $4.72 \times 10^{-2} - 3.76 \times 10^{-2}$ $\mu\text{g/L}$ DCAN = $2.55 \times 10^{-2} - 1.97 \times 10^{-2}$ $\mu\text{g/L}$	Chloroform: 0.0163 – 0.0174 DCAN: 0.0144 – 0.0229	Chloroform: $2.16 \times 10^{-6} - 3.46 \times 10^{-6}$ DCAN: $3.43 \times 10^{-6} - 5.44 \times 10^{-6}$
102	1.66	4.44×10^{-3}				Chloroform = 0.58 – 0.47 $\mu\text{g/L}$ DCAN = 0.34 – 0.25 $\mu\text{g/L}$	Chloroform: 0.2680 – 0.4012 DCAN: 0.2326 – 0.3462	Chloroform: $2.44 \times 10^{-6} - 3.65 \times 10^{-6}$ DCAN: $3.79 \times 10^{-6} - 5.63 \times 10^{-6}$
7	1.66	4.44×10^{-3}	3	10034 - 50030	Turbulent flow	Chloroform = $7.83 \times 10^{-3} - 2.68 \times 10^{-2}$ $\mu\text{g/L}$ DCAN = $3.70 \times 10^{-3} - 1.35 \times 10^{-2}$ $\mu\text{g/L}$	Chloroform: 0.0462 – 0.1863 DCAN: 0.0405 – 0.1646	Chloroform: $6.13 \times 10^{-6} - 2.47 \times 10^{-5}$ DCAN: $9.61 \times 10^{-6} - 3.90 \times 10^{-5}$
102	1.66	4.44×10^{-3}				Chloroform = 0.10 – 0.32 $\mu\text{g/L}$ DCAN = $5.15 \times 10^{-2} - 0.17$ $\mu\text{g/L}$	Chloroform: 0.6654 – 2.7275 DCAN: 0.5792 – 2.3994	Chloroform: $6.06 \times 10^{-6} - 2.48 \times 10^{-5}$ DCAN: $9.43 \times 10^{-6} - 3.90 \times 10^{-5}$
7	1.66	4.44×10^{-3}	3	4161	$SV = 52.5 \text{ m}^{-1}$	Chloroform = 4.06×10^{-2} $\mu\text{g/L}$ DCAN = 2.15×10^{-2} $\mu\text{g/L}$	Chloroform = 0.0226 DCAN = 0.0199	Chloroform = 2.99×10^{-6} DCAN = 4.71×10^{-6}
7	1.66	4.44×10^{-3}	6		$SV = 26.3 \text{ m}^{-1}$	Chloroform = 2.07×10^{-2} $\mu\text{g/L}$ DCAN = 1.50×10^{-2} $\mu\text{g/L}$	Chloroform = 0.0120 DCAN = 0.0137	Chloroform = 1.59×10^{-6} DCAN = 3.24×10^{-6}

Initial conditions (Contact time = 1 hour, Pipe length = 1 m)						Potential DBP concentrations (maximal value)	\bar{Sh} - DBPs	Mass transfer (m/s)
BT (μm)	Clo (mg/L)	Xo (mg/cm ²)	ϕ (inches)	Re	Other			
7	1.66	4.44×10^{-3}	10		$SN = 15.8 \text{ m}^{-1}$	Chloroform = $1.17 \times 10^{-2} \mu\text{g/L}$ DCAN = $7.10 \times 10^{-3} \mu\text{g/L}$	Chloroform = 0.0059 DCAN = 0.0052	Chloroform = 7.84×10^{-7} DCAN = 1.24×10^{-6}
7	1.66	4.44×10^{-3}	3	10173	$SN = 52.5 \text{ m}^{-1}$	Chloroform = $2.67 \times 10^{-2} \mu\text{g/L}$ DCAN = $1.33 \times 10^{-2} \mu\text{g/L}$	Chloroform = 0.0467 DCAN = 0.0410	Chloroform = 6.20×10^{-6} DCAN = 9.72×10^{-6}
7	1.66	4.44×10^{-3}	6	5086	$SN = 26.3 \text{ m}^{-1}$	Chloroform = $2.46 \times 10^{-2} \mu\text{g/L}$ DCAN = $1.29 \times 10^{-2} \mu\text{g/L}$	Chloroform = 0.0274 DCAN = 0.0242	Chloroform = 3.63×10^{-6} DCAN = 5.74×10^{-6}
7	1.66	4.44×10^{-3}	10	3051	$SN = 15.8 \text{ m}^{-1}$	Chloroform = $1.15 \times 10^{-2} \mu\text{g/L}$ DCAN = $7.10 \times 10^{-3} \mu\text{g/L}$	Chloroform = 0.0049 DCAN = 0.0049	Chloroform = 6.44×10^{-7} DCAN = 1.15×10^{-6}
7	0.12	2.82×10^{-4}	3	2774	Transitional flow	Chloroform = $3.71 \times 10^{-3} \mu\text{g/L}$ DCAN = $2.03 \times 10^{-3} \mu\text{g/L}$	Chloroform: 0.0211 DCAN: 0.0178	Chloroform: 2.81×10^{-6} DCAN: 4.23×10^{-6}
102	1.66	4.44×10^{-3}				Chloroform = 0.58 $\mu\text{g/L}$ DCAN = 0.34 $\mu\text{g/L}$	Chloroform: 0.2680 DCAN: 0.2326	Chloroform: 2.44×10^{-6} DCAN: 3.79×10^{-6}
7	0.12	2.82×10^{-4}	3	25084	Turbulent flow	Chloroform = $6.48 \times 10^{-4} \mu\text{g/L}$ DCAN = $3.29 \times 10^{-4} \mu\text{g/L}$	Chloroform: 0.1027 DCAN: 0.0901	Chloroform: 1.36×10^{-5} DCAN: 2.14×10^{-5}
102	1.66	4.44×10^{-3}				Chloroform = 0.18 $\mu\text{g/L}$ DCAN = $9.17 \times 10^{-2} \mu\text{g/L}$	Chloroform: 1.4733 DCAN: 1.2929	Chloroform: 1.34×10^{-5} DCAN: 2.10×10^{-5}

The major concern in building facilities is that formed DBPs are ready to be consumed once the householders use again drinking water. Therefore, consumers may be exposed to high concentrations of DBPs by either ingestion or inhalation, after a period of stagnation. On the contrary, the quantification and impact of DBPs formed under transitional and turbulent flow regime depends on the pipeline length, flow rate and pipe diameter. The results of the 2D model allow inferring that the major risk can be in small pipes due to the high S/V ratio and lower flow rates. Such pipes can be those in the proximity to the consumers; then exposure probability to such DBPs by customers may increase. Subnetworks installed within residential neighbourhoods are also prone to stagnation conditions overnight; then the DBP concentrations would increase, as explained for 1D model results.

With regards to mass transport, mass transfer is faster when Re is higher and pipe diameter smaller. Decreasing chlorine concentrations in bulk water reduces the mass transport of this disinfectant and DBP formed at the biofilm surface. This is an important outcome of the model because it allows assessing the balance between microbial and chemical risk. Low concentrations of chlorine leads to slow penetration of the biofilm thickness and slow formation of DBPs, which are transported to the bulk water and leave the pipe slower than when high chlorine concentrations are present. From the point of view of chemical risk, this would be a desirable condition; however, slow penetration of the biofilm thickness also represents that potential pathogens are not being inactivated. The 2D model and further improvements can be useful to evaluate when it is necessary to increase disinfectant concentrations to inactivate microorganisms and when it must be reduced to minimise DBP exposure to customers. Such improvements may be achieved by further availability of microbial characteristics of biofilm in full scale DWDNs; important variables are biofilm thickness, cell density, and EPS concentration. Measuring DBP concentrations within biofilms by micro-sensors is also a crucial step for model validation.

The aforementioned leads to recommend close collaboration between water industry and research laboratories to improve the analytical and microbiological techniques that promote better monitoring of biofilm roles as both pathogen hosts and DBP precursors. Combined data from models and field assessments in DWDNs should lead to improve O&M if they are properly interpreted to protect drinking water quality. Additionally, including wall contribution of DBPs to bulk water concentrations may also improve the performance of current DBP models for DWDNs.

6.4 IMPLICATIONS

6.4.1 Implications for water quality in Cali's DWDN in the context of extreme weather events

According to IPCC (2014), one of the clear consequences of climate change is the increase in frequency and severity of a variety of extreme weather events, including heavy rainfall, floods and droughts. Similarly, the overall frequency in climate phenomena such as El Niño and La Niña is expected to increase under global warming (Cai et al., 2014; Cai et al., 2015). Additionally, climate change is projected to increase water scarcity in urban areas, and rural areas are expected to experience major impacts on water availability and supply (IPCC, 2014). To cope with the urban risks associated with water supply, IPCC (2014) includes adaptation options such as changes to network infrastructure as well as demand-side management to ensure sufficient water supplies and qualities; and increased capacities to manage reduced freshwater availability, and flood risk reduction. For the present times, IPCC (2014) have calculated water supply-associated urban risk as medium, medium-very high risk with potential to reduce to medium for the near term (2030-2040), medium-very high and medium risk for the long term (2080-2100), under the scenarios of 2 °C and 4 °C of increase of global temperature, respectively.

In this line, Cann et al. (2012) documented 87 and 304 waterborne outbreaks from medical and meteorological databases and the global electronic reporting system ProMED, respectively. Such waterborne outbreaks were commonly preceded by extreme weather events such heavy rainfall and flooding. The most common pathogens reported in these outbreaks were *Vibrio spp.* and *Leptospira spp.* The events were often the result of contamination of the drinking water system (Cann et al., 2012). According to data from medical and meteorological databases, most of the *Vibrio*-associated outbreaks occurred in Asia, followed by Africa and South America and most of the *Leptospira*-associated outbreaks took place in North America or Asia. Causes of contamination of the drinking water system included failure to cope by the WTP after the extreme weather events, failure or inability to cope by sewage systems, and resulting in contamination of drinking water. In developed countries, route of infection was mainly through the DWDNs. In developing countries, the main cause was contamination of the water supply.

The information collected from ProMED by Cann et al. (2012) evidenced that the majority of events were in Africa, followed by Asia and North America. The likely causes of the waterborne outbreaks were contamination of water, shortage of clean drinking water, poor sanitation and hygiene following the extreme weather event. In conclusion, less developed countries are more vulnerable to the consequences of extreme weather events (Cann et al., 2012; Rataj et al., 2016). However,

developed countries are also susceptible to suffer the negative effects of these events. In both cases, upgrading the drinking water supply systems, changing water use patterns, explore new water sources are some adaptation measures, which can be implemented by water utilities and planners (WHO, 2017).

Additionally to the increased frequency of extreme weather events due to climate change, which will affect water supply, global warming per se is also expected to change the surface water quality, consequently affecting the performance of WTPs. Global warming refers to the increase of environment temperature. Temperature is the main factor affecting almost all physico-chemical equilibriums and biological reactions (dissolution, solubilisation, complexation, degradation, evaporation, etc.) (Delpla et al., 2009). Therefore, the impacts of climate change on water quality parameters include increase of temperature, reduction of dissolved oxygen; rise of DOC, alkalinity, and pH; enhancement of nitrogen mineralisation; release of nitrogen, phosphorus, and carbon from soil to water bodies; loss of dilution capacity of water bodies during droughts; rise of organic and inorganic pollutants; spread of waterborne pathogens and cyanobacteria blooms (Delpla et al., 2009).

Delpla et al. (2009) established that such changes on surface water quality due to climate change impact the drinking water quality produced by WTP due to the increase of stable DBP concentrations, as a consequence of higher concentrations of precursors such as DOC, algae, and biomass in general. It is expected to have moderate impact for unstable DBPs such as DCAN and 1,1-DCP since they decompose with higher temperatures and HAAs are biodegradable. On the other hand, spread or waterborne pathogens challenge the operation of WTPs, since disinfection must be maintained in the treatment train and more efforts must be done on removal of DBP precursors to minimize DBP concentrations in the DWDNs.

However, Colombian DWDNs may be poorly operated and maintained, even in centralised systems such as in Cali. Unfortunately, this is a common situation in developing countries due to limited resources (Lee and Schwab, 2005). One of the causes of deficiencies in DWDNs of developing countries is the leakages. In the year 2013, Cali's DWDN reported 81 leakages per 100 Km¹⁸. In addition, Cali's water utility loses 53% of the DW produced; in order to reduce loss of water, it is required to replace around 1200 Km of the oldest pipelines, corresponding to pipe materials CI and asbestos, which represent 40% of the total network length¹⁹. Additionally, the two main WTPs of

¹⁸ EMCALI EICE ESP, 2014, personal communication, 10th December

¹⁹ Rojas Ramírez, 2017, personal communication, 10th July. E-mail: jurojas@emcali.com.co

the city of Cali suspended their operation during events of water source contamination in a range of 1-13 times in the period 2009-2016²⁰. The high number of leakage repairs and water supply interruptions due to deterioration of raw water quality lead to unstable hydraulic conditions in the DWDN, which can promote the uncontrolled release of biofilm, sediments, loose deposits, and other biological material. These elements can reach the customers and may represent complaints due to poor aesthetic conditions or, even worse, public health risks if pathogens were present.

One of the most common recommendations to adapt to climate change, especially during extreme weather events, is to adjust chlorine doses in the WTPs and maintain residual chlorine in the network. Such recommendation obeys to the concern of acute risk due to the potential presence of pathogens, with the subsequent negative impacts on public health, which can be worse in developing countries with low adaptation and response capacity. From the results presented in this research project, it is advisable that modelling tools be used to evaluate the trade-off between microbial and chemical risk in drinking water pipes. In the meantime, DBP research should focus on providing conclusive evidence on which specific DBP species produce negative health outcomes, in which degree, which minimal concentrations, and what type of diseases. It is also advisable that O&M of DWDNs consider the bio-stability approach to preserve the drinking water quality to the customers.

6.4.2 Implications for O&M activities in DWDN

Bacteriological composition of drinking water biofilms have been mainly studied because of the protective effects offered to pathogens against disinfectants; such pathogens can be released to bulk water if hydraulic changes occur. Experimental studies have shown that biomass can act as DBP precursors. Prevention and removal of biofilms must be a key concern for water utilities; flushing water pipes has been proved as a suitable technique to remove material attached to internal pipe surfaces but it is inefficient to completely detach biofilms (Abe et al., 2012; Douterelo et al., 2013; Fish et al. 2016). Advanced water treatment processes such as membrane filtration has been proved successful in highest reduction of number of microorganisms in biofilms collected at the inlet of a DWDN (Shaw et al., 2014). However, a recent study argues that is impossible to prevent biofilm accumulation but high flow variation could be used to promote young biofilms, which are more vulnerable to disinfection (Fish et al., 2017).

²⁰ Events counted until September 2016

In the case of this studied network, avoiding uncontrolled biofilm detachment and contamination of bulk water is particularly difficult, as it exhibits specific O&M challenges associated with emptying of the network due to the interruption of operation of the WTPs, pumping operation, closing/opening valves during leakages repairs and pipelines and accessories replacement. This may lead to favour the formation of young biofilms, however it is important to consider that the biofilm detachment may occur in an uncontrolled way, then biofilm clusters containing potential pathogens may reach the customers.

Samples collected in this study potentially contained pathogenic and opportunistic bacteria but, whether they were metabolically active or not, is unknown since DNA was used to characterise the samples. However, these results can motivate the application of proper practices of O&M of the DWDN in order to avoid uncontrolled biofilm detachment and contamination of bulk water. Furthermore, CI pipes represent 10% of the total length of the pipelines and asbestos 30%; and 2,400 leakages were repaired in 2013²¹. These O&M activities cause uncontrolled and partial removal of sediments and biological material and allow the entrance of external particles, which all together could be promoting microbial growth in the network. Future plans for pipeline replacements should avoid the use of metal and cement pipes and instead promote the use of pipe materials with more stable bio-chemical and physical conditions. It is also advisable to maintain stable hydraulic conditions to avoid biofilm detachment; controlled cleaning procedures of pipes such as flushing should be carried out to reduce the amount of nutrients available for microorganisms in bulk water and biofilms and avoid alterations of the organoleptic conditions of DW for the consumers. Special attention must be put in dead-end zones to flush stagnant water to reduce microorganism regrowth and DBP formation. More importantly, the efforts carried out in protecting water sources and improving water treatment could be useless if suitable O&M practices are not applied in the DWDNs in order to preserve the safety of drinking water delivered to the customers.

6.5 APPLICABILITY OF THE CURRENT RESEARCH PROJECT

Despite of the research evidence in relation to microbial and chemical risk associated to the presence of biofilms in drinking water pipes, there is not knowledge to date about introduction of biofilm monitoring in O&M of DWDNs by water utilities. In this line, the tools and results of the current research project become relevant with regards to the supply of new information of the

²¹ EMCALI EICE ESP, 2014, personal communication, 10th December

bacterial communities that may be present in the studied full scale DWDN, and their relationship with engineered factors and water quality characteristics. In addition, the models developed here are relatively easy to use and implement, especially for stagnation conditions, if the appropriate knowledge, trained staff, and software and hardware requirements are available. In this line, more efforts must be done in order to transfer the practical knowledge to the water industry and strengthen their capacity to apply such knowledge, especially in the context of developing countries, where economical limitations exist and are more vulnerable to the impacts of climate change. The author suggests applying the results of this research project to inform better practices of O&M of Cali's DWDN, improve prediction of DBPs in DWDN, assess the balance between microbial and chemical risk, and make more progress on DBP exposure assessment in epidemiological studies.

7 KEY FINDINGS, CONCLUSION AND FUTURE RESEARCH

7.1 GENERAL CONCLUSION

Biofilms play an important role in DWDNs as pathogen reservoirs and DBP precursors. Additionally, diverse bacterial communities exist in this habitat. Such communities can lead to diverse physico-chemical and biological processes in this type of engineered systems, by the influence of pipe materials, hydraulic factors, and drinking water characteristics. One of such processes is the formation of DBPs by reactions between biofilm matrix and disinfectants. Then, mathematical models developed in the current research project represent a progress to analyse the chemical and microbiological risks in drinking water pipes. The models are also useful for prediction of DBP formation potentials, designing laboratory experiments, and the evaluation of regulation compliance scenarios. Special attention must be put on large DWDNs in order to control the DBP formation in the sectors where small pipes and low flow rates or stagnation conditions are frequent.

7.2 KEY FINDINGS

This research potentially informs to water engineers and managers on the impact of the presence of biofilms in drinking water pipes. The following key findings correspond to the objectives formulated in the current research project.

7.2.1 Bacterial communities in a tropical-climate DWDN

The field study enabled analysis of the bacterial communities in the DWDN of the city of Cali, and the following are the key findings:

- Biofilm samples were more diverse in relation to bulk water samples.
- *Proteobacteria* phyla was also the predominant group in all the samples collected in the tropical-weather DWDN.
- Genus bacteria associated with soil, surface water, pathogenicity-related, and methyl radicals like THMs were identified in both habitats.
- Significant correlations were found between TTHM concentrations and RA of methanotrophs in bulk water.

7.2.2 Relationships between abiotic and biotic parameters in a tropical-weather DWDN

The field study enabled the identification of relationships between biotic, physico-chemical, and engineered factors determined in the DWDN of the city of Cali, and the following are the key findings:

- Pipe age, pipe material, water age, free chlorine, pH and temperature were associated with microbiological parameters indicating that these are key to the composition of bacterial communities.
- Pipe material influences the microbial ecology of DWDNs. *Desulfovibrio* was identified exclusively in the cast iron pipe.

7.2.3 DBP formation potentials from biofilm chlorination under stagnation conditions

The development and analysis of the one-dimensional model enabled the study of the parameters influencing the formation of chloroform and DCAN under stagnation conditions. The key findings are the following:

- High stagnation times and S/V ratios favour DBP formation. Therefore, plumbing systems, which have these characteristics, may be more likely at risk. However, this study did not obtain direct evidence for this type of system.
- Plumbing systems can favour the DBP formation from disinfection of biofilms due to the high stagnation times and S/V ratios.
- Concentrations of DBP and DCAN may exceed the UK and Colombian regulated thresholds, under certain conditions of water quality and biofilm properties.
- Pipe diameters as small as ½ inches may lead to DBP concentrations higher than the regulated or guidance values. Increasing the diameter to ¾ inches can significantly reduce the concentrations, even to values under such thresholds. Such reduction are around 51% and 36% for chloroform and DCAN, respectively.
- DCAN is the more challenging substance in terms of guidance following, compared to chloroform, because of its potential higher toxicity, which originated a lower reference value: 20 µg/L.

7.2.4 DBP formation potentials from biofilm chlorination under hydrodynamic conditions

The development and analysis of the two-dimensional model enabled the study of the parameters influencing the formation of chloroform and DCAN under bulk flow. The key findings are the following:

- Higher chlorine concentration, biofilm thickness, cell density, and smaller pipe diameter led to higher concentrations of DBPs.
- Faster mass transport at the biofilm surface was found for higher Re , smaller pipe diameter, higher initial concentrations of chlorine and cells, and higher biofilm thickness.
- A linear relationship was identified between Re and Sh .
- Compliance of chloroform and DCAN regulations is linked to the length of the water network the pipe diameter, and flow regime. Higher chemical risk may occur in long networks, smaller pipes and lower flow rates related to transitional flow.

7.2.5 Practical recommendations on biofilm and disinfection by-products control in drinking water networks

The practical recommendations below are the result of the analysis and discussion of the results included in Chapters 3, 4, and 5.

- To adapt the water industry to climate change from the management, technical, and infrastructure points of view.
- To develop and implement the Water Safety Plans for water supply systems, which considers that O&M and these systems should be based in risk management, from the catchment to the tap.
- To keep fluent communication between treatment and distribution departments in water utilities in order to coordinate activities, optimize resources and make decisions together. This could improve the service provided to customers in terms of drinking water quality and service continuity.
- To upgrade the treatment processes for minimization of organic matter, nutrients and biomass in treated water in order to reduce the biofilm growth and DBP formation in the DWDNs.
- In order to control both microbial and chemical risks in the DWDNs, it is necessary to design and apply an integral plan of O&M of DWDNs. Such plan must include replacement of ageing pipelines, flushing pipes, cleaning storage tanks, reduction of water age, maintaining positive pressures, and guaranteeing continuous water supply.

- To avoid metal and cement materials in new pipelines. Bio-stability concept should be considered when pipe materials are being chosen for drinking water supply.
- To use predictive tools to analyse the balance between microbial and chemical risks in the DWDNs and improve DBP estimation and exposure assessment in DWDNs. Biofilm contribution to DBP concentrations in bulk water must be included in such tools.
- To promote closer relationship among academy, water industry and regulatory agencies in order to improve communication, transfer knowledge and impact of water quality research in the water industry.

7.3 FUTURE RESEARCH

- A long-term study to characterize pathogenic microorganisms by molecular methods, in both bulk water and biofilms, in Cali's DWDN. Techniques such as q-PCR and microscopy should be applied to identify the presence and viability of pathogenic bacteria. Biofilms should be grown in coupons installed directly in the network in order to monitor several points of the network, without affecting the normal operation of it (Douterelo et al., 2014a). This is important because previous study and the current one have identified a potential risk due to the high leak rate this network presents. Furthermore, the DNA of potential pathogenic bacteria was found in either biofilm or bulk water sampled in Cali's DWDN.
- To identify the limiting-nutrient for bacterial regrowth in Cali's DWDN. This would help to water managers to define the goal of future plans for upgrading the WTPs in Cali's supply system.
- To continue investigation on laboratory techniques to improve measuring DBPs and monitoring biofilms. Better microscopy techniques are needed to properly measure thickness of biofilms found in real scale DWDNs. Moreover, to develop micro-sensors are required to measure DBP concentrations at different depths within biofilms. Improved laboratory analytical capacities are fundamental for the progress of research on DBPs and biofilms in drinking water supply.
- To assess the high flow variation in DWDNs on the detachment of biofilms, and to evaluate the impact of detached biofilm clusters on the transport and fate of pathogens and DBP formation. Loss of hydraulic integrity may increase in the future due to more frequent interruption of normal operation of the DWDNs. Therefore, recurrent hydraulic changes may lead the detachment of biofilm clusters, which can react with free chlorine and increase the DBP concentrations. Furthermore, clusters mobilization may also favour the biofilm colonization of clean pipe walls and transport pathogens to the water point of use.

- To include the contribution of DBP formation in DWDNs as concentration pulses, lasting the same time than bacterial regrowth takes place. This would allow the indirect incorporation of biofilm growth simultaneously with DBP formation from disinfectant-biomass interactions, with potential reduction of computational cost.

8 REFERENCES

- Abe, Y. et al. 2012. Cohesiveness and hydrodynamic properties of young drinking water biofilms. *Water Research*. **46**(4), pp.1155-1166.
- Abokifa, A.A. et al. 2016a. Investigating the role of biofilms in trihalomethane formation in water distribution systems with a multicomponent model. *Water Research*. **104**, pp.208-219.
- Abokifa, A.A. et al. 2016b. Water quality modeling in the dead end sections of drinking water distribution networks. *Water Research*. **89**, pp.107-117.
- Abraham, J.P. et al. 2009. Heat transfer in all pipe flow regimes: laminar, transitional/intermittent, and turbulent. *International Journal of Heat and Mass Transfer*. **52**(3), pp.557-563.
- Adin, A. et al. 1991. Trihalomethane formation in chlorinated drinking water: A kinetic model. *Water Research*. **25**(7), pp.797-805.
- Ahmadi, M. et al. 2013. Failures analysis of water distribution network during 2006-2008 in Ahvaz, Iran. *Journal of Advances in Environmental Health Research*. [Online]. **1**(2), pp.129-137. Available from: http://jaehr.muk.ac.ir/index.php/jaehr/article/view/article_40134_004e6287758dbc4a925c4feadf4b9522.pdf
- Al-Jasser, A.O. 2007. Chlorine decay in drinking-water transmission and distribution systems: Pipe service age effect. *Water Research*. **41**(2), pp.387-396.
- Al-Omari, A. et al. 2004. Modeling trihalomethane formation for Jabal Amman water supply in Jordan. *Environmental Modeling & Assessment*. **9**(4), p245.
- Antoun, E.N. et al. 1999. Unidirectional flushing: A powerful tool. *American Water Works Association Journal*. **91**(7), pp.62-71.
- Arboleda, V.J. 2000. *Teoría y Práctica de la Purificación del Agua*. Bogotá: Mc Graw Hill.
- Babaei, A.A. et al. 2015. Trihalomethanes formation in Iranian water supply systems: predicting and modeling. *Journal of Water and Health*. **13**(3), pp.859-869.
- Badar, M. et al. 2015. Removal of cyanobacterial toxins from drinking water sources by aluminium sulphate treatment. *Brazilian Journal of Biological Sciences*. [Online]. **2**(3), pp. 135-145. Available from: <http://revista.rebibio.net/v2n3/v02n03a14.html>
- Barbeau, B. et al. 2005. Dead-end flushing of a distribution system: Short and long-term effects on water quality. *Journal of Water Supply: Research and Technology - Aqua*. **54**(6), p371.
- Barrett, S.E. et al. 2000. Natural Organic Matter and Disinfection By-Products: Characterization and Control in Drinking Water—An Overview. *Natural Organic Matter and Disinfection By-Products*. American Chemical Society, pp.2-14.
- Bautista-de los Santos, Q.M. et al. 2016. The impact of sampling, PCR, and sequencing replication on discerning changes in drinking water bacterial community over diurnal time-scales. *Water Research*. [Online]. **90**, pp.216-224. [Accessed 3/1/]. Available from: <http://www.sciencedirect.com/science/article/pii/S0043135415304048>

- Berry, D. et al. 2006. Microbial ecology of drinking water distribution systems. *Current Opinion in Biotechnology*. **17**(3), pp.297-302.
- Betancourt, W.Q. and Rose, J.B. 2004. Drinking water treatment processes for removal of *Cryptosporidium* and *Giardia*. *Veterinary Parasitology*. **126**(1–2), pp.219-234.
- Bond, T. et al. 2014. Examining the interrelationship between DOC, bromide and chlorine dose on DBP formation in drinking water — A case study. *Science of The Total Environment*. **470–471**(0), pp.469-479.
- Boyalla, R.L. 2004. *Formation and modeling of disinfection by-products in Newfoundland communities*. Master of Engineering thesis, Memorial University of Newfoundland.
- Brettar, I. and Höfle, M.G. 2008. Molecular assessment of bacterial pathogens - a contribution to drinking water safety. *Current Opinion in Biotechnology*. **19**(3), pp.274-280.
- Buamah, R. et al. 2014. Modelling the chlorine decay process in a distribution network using a pilot system. *Water Practice & Technology*. **9**(4), pp.534-550.
- Bull, R.J. et al. 2011. Potential carcinogenic hazards of non-regulated disinfection by-products: Haloquinones, halo-cyclopentene and cyclohexene derivatives, N-halamines, halonitriles, and heterocyclic amines. *Toxicology*. **286**(1–3), pp.1-19.
- Buse, H.Y. et al. 2013. Eukaryotic diversity in premise drinking water using 18S rDNA sequencing: implications for health risks. *Environmental Science and Pollution Research*. **20**(9), pp.6351-6366.
- Buzatu, D. et al. 2007. Diffusion Coefficients for the Ternary System Water + Chloroform + Acetic Acid at 25 °C. *Journal of Solution Chemistry*. **36**(11), pp.1373-1384.
- Cai, W. et al. 2014. Increasing frequency of extreme El Nino events due to greenhouse warming. *Nature Clim. Change*. **4**(2), pp.111-116.
- Cai, W. et al. 2015. Increased frequency of extreme La Nina events under greenhouse warming. *Nature Clim. Change*. **5**(2), pp.132-137.
- Cann, K.F. et al. 2012. Extreme water-related weather events and waterborne disease. *Epidemiology and Infection*. **141**(4), pp.671-686.
- Cantor, K.P. et al. 2010. Polymorphisms in GSTT1, GSTZ1, and CYP2E1, disinfection by-products, and risk of bladder cancer in Spain. *Environmental Health Perspectives*. **118**(11), pp.1545-1550.
- Canuto, C. et al. 2007. *Spectral Methods. Evolution to Complex Geometries and Applications to Fluid Dynamics*. New York: Springer-Verlag Berlin Heidelberg.
- Caporaso, J.G. et al. 2011. Global patterns of 16S rRNA diversity at a depth of millions of sequences per sample. *Proceedings of the National Academy of Sciences*. **108**(Supplement 1), pp.4516-4522.
- Carr, E.L. et al. 2003. Seven novel species of *Acinetobacter* isolated from activated sludge. *International Journal of Systematic and Evolutionary Microbiology*. **53**(4), pp.953-963.
- CCC, C.d.C.d.C. et al. 2016. *Cali cómo vamos. Informe de Calidad de Vida en Cali 2015*. Santiago de Cali.

- CCWater, C.C.f.W. 2013. *Research into customer perceptions of leakage: Report*. London.
- Celmer, D. et al. 2008. Impact of shear force on the biofilm structure and performance of a membrane biofilm reactor for tertiary hydrogen-driven denitrification of municipal wastewater. *Water Research*. **42**(12), pp.3057-3065.
- Charisiadis, P. et al. 2015. Spatial and seasonal variability of tap water disinfection by-products within distribution pipe networks. *Science of The Total Environment*. **506–507**, pp.26-35.
- Checinska, A. et al. 2015. Bacillus and Other Spore-Forming Genera: Variations in Responses and Mechanisms for Survival. *Annual Review of Food Science and Technology*. **6**(1), pp.351-369.
- Chen, B. and Westerhoff, P. 2010. Predicting disinfection by-product formation potential in water. *Water Research*. **44**(13), pp.3755-3762.
- Chen, X. and Stewart, P.S. 1996. Chlorine Penetration into Artificial Biofilm Is Limited by a Reaction–Diffusion Interaction. *Environmental Science & Technology*. **30**(6), pp.2078-2083.
- Chowdhury, S. 2016. Effects of plumbing systems on human exposure to disinfection byproducts in water: a case study. *Journal of Water and Health*. **14**(3), p489.
- Chowdhury, S. and Champagne, P. 2008. An investigation on parameters for modeling THMs formation. *Global NEST Journal*. [Online]. **10**(1). [Accessed 10th June 2016]. Available from: http://journal.gnest.org/sites/default/files/Journal%20Papers/80-91_518_Chowdhury_10-1.pdf
- Chowdhury, S. et al. 2007. Fuzzy risk-based decision-making approach for selection of drinking water disinfectants. *Journal of Water Supply: Research and Technology - Aqua*. **56**(2), pp.75-93.
- Chowdhury, S. et al. 2009. Models for predicting disinfection byproduct (DBP) formation in drinking waters: A chronological review. *Science of The Total Environment*. **407**(14), pp.4189-4206.
- Clarelli, F. et al. 2013. A fluid dynamics model of the growth of phototrophic biofilms. *Journal of Mathematical Biology*. **66**(7), pp.1387-1408.
- Clark, R.M. 1998. Chlorine Demand and TTHM Formation Kinetics: A Second-Order Model. *Journal of Environmental Engineering*. **124**(1), pp.16-24.
- Clark, R.M. 2015. The USEPA's distribution system water quality modelling program: a historical perspective. *Water and Environment Journal*. **29**(3), pp.320-330.
- Clark, R.M. and Sivaganesan, M. 1998. Predicting chlorine residuals and formation of TTHMs in drinking water. *Journal Environmental Engineering*. **124**(12), pp.1203-1210.
- Clark, R.M. et al. 2001. Predicting the Formation of Chlorinated and Brominated By-Products. *Journal of Environmental Engineering*. **127**(6), pp.493-501.
- Clarke, K.R. and Warwick, R.M. 2001. *Change in Marine Communities: An Approach to Statistical Analysis and Interpretation*. 2nd ed. Plymouth, UK: PRIMER-E.
- Codony, F. et al. 2005. Role of discontinuous chlorination on microbial production by drinking water biofilms. *Water Research*. **39**(9), pp.1896-1906.

- Cogan, N. 2010. An Extension of the Boundary Integral Method Applied to Periodic Disinfection of a Dynamic Biofilm. *SIAM Journal on Applied Mathematics*. **70**(7), pp.2281-2307.
- Cogan, N.G. 2006. Effects of persister formation on bacterial response to dosing. *Journal of Theoretical Biology*. **238**(3), pp.694-703.
- Cogan, N.G. 2008. Two-Fluid Model of Biofilm Disinfection. *Bulletin of Mathematical Biology*. **70**(3), pp.800-819.
- Cogan, N.G. 2011. Computational exploration of disinfection of bacterial biofilms in partially blocked channels. *International Journal for Numerical Methods in Biomedical Engineering*. **27**(12), pp.1982-1995.
- COMSOL. 2012. *COMSOL Multiphysics User's Guide Version 4.3*. p.1292. Available from: <http://people.ee.ethz.ch/~fieldcom/pps-comsol/documents/User%20Guide/COMSOLMultiphysicsUsersGuide.pdf>
- COMSOL. 2013. *CFD Module User's Guide Version 4.4*. p.654. Available from: [https://lost-contact.mit.edu/afs/pdc.kth.se/roots/ilse/v0.7/pdc/vol/comsol/4.4.248/doc/pdf/CFD Module/CFDModuleUsersGuide.pdf](https://lost-contact.mit.edu/afs/pdc.kth.se/roots/ilse/v0.7/pdc/vol/comsol/4.4.248/doc/pdf/CFD%20Module/CFDModuleUsersGuide.pdf)
- COMSOL. 2017. *What Is Mass Transfer?* [Online]. [Accessed 3rd May]. Available from: <https://www.comsol.it/multiphysics/what-is-mass-transfer>
- Coroneo, M. et al. 2014. Biofilm growth: A multi-scale and coupled fluid-structure interaction and mass transport approach. *Biotechnology and Bioengineering*. **111**(7), pp.1385-1395.
- Costerton, J.W. et al. 1995. Microbial biofilms. *Annual review of microbiology*. **49**, pp.711-745.
- Cumsille, P. et al. 2014. A novel model for biofilm growth and its resolution by using the hybrid immersed interface-level set method. *Computers & Mathematics with Applications*. **67**(1), pp.34-51.
- D'Acunto, B. and Frunzo, L. 2011. Qualitative analysis and simulations of a free boundary problem for multispecies biofilm models. *Mathematical and Computer Modelling*. **53**(9), pp.1596-1606.
- D'Acunto, B. et al. 2015. Modeling multispecies biofilms including new bacterial species invasion. *Mathematical Biosciences*. **259**, pp.20-26.
- DANE. 2017. *Proyecciones de población*. [Online]. [Accessed 24th April]. Available from: www.dane.gov.co
- Dearmont, D. et al. 1998. Costs of water treatment due to diminished water quality: A case study in Texas. *Water Resources Research*. **34**(4), pp.849-853.
- Dechatiwongse, P. 2015. *A Study of the Growth and Hydrogen Production of Cyanothecce sp. ATCC 51142*. Doctor of Philosophy thesis, Imperial College London.
- Deen, W.M. 1998. *Analysis of Transport Phenomena*. New York: Oxford University Press.
- Delpia, I. et al. 2009. Impacts of climate change on surface water quality in relation to drinking water production. *Environment International*. **35**(8), pp.1225-1233.

- DeSantis, T.Z. et al. 2006. Greengenes, a Chimera-Checked 16S rRNA Gene Database and Workbench Compatible with ARB. *Applied and Environmental Microbiology*. [Online]. **72**(7), pp.5069-5072.
- Di Cristo, C. et al. 2013. Modelling trihalomethanes formation in water supply systems. *Environmental Technology*. **34**(1), pp.61-70.
- Di Nardo, A. et al. 2013. Water Network Protection from Intentional Contamination by Sectorization. *Water Resources Management*. **27**(6), pp.1837-1850.
- Di Piazza, I. and Ciofalo, M. 2010. Numerical prediction of turbulent flow and heat transfer in helically coiled pipes. *International Journal of Thermal Sciences*. **49**(4), pp.653-663.
- Dippong, T. et al. 2016. Mathematical modeling of the variation in water quality along the network of water supply of Satu Mare municipality, Romania. *Studia Universitatis Babes-Bolyai, Chemia*. **61**.
- Doederer, K. et al. 2014. Factors affecting the formation of disinfection by-products during chlorination and chloramination of secondary effluent for the production of high quality recycled water. *Water Research*. **48**(0), pp.218-228.
- Douterelo, I. et al. 2014a. Methodological approaches for studying the microbial ecology of drinking water distribution systems. *Water Research*. **65**(0), pp.134-156.
- Douterelo, I. et al. 2014b. The bacteriological composition of biomass recovered by flushing an operational drinking water distribution system. *Water Research*. **54**, pp.100-114.
- Douterelo, I. et al. 2014c. Bacterial community dynamics during the early stages of biofilm formation in a chlorinated experimental drinking water distribution system: implications for drinking water discoloration. *Journal of Applied Microbiology*. **117**(1), pp.286-301.
- Douterelo, I. et al. 2013. Influence of hydraulic regimes on bacterial community structure and composition in an experimental drinking water distribution system. *Water Research*. **47**(2), pp.503-516.
- Duddu, R. et al. 2008. A combined extended finite element and level set method for biofilm growth. *International Journal for Numerical Methods in Engineering*. **74**(5), pp.848-870.
- Duddu, R. et al. 2009. A Two-Dimensional Continuum Model of Biofilm Growth Incorporating Fluid Flow and Shear Stress Based Detachment. *Biotechnology and Bioengineering*. **103**(1), pp.92-104.
- Eaton, A.D. et al. 2005. *Standard Methods for the Examination of Water and Wastewater 21st edition*. 21st edition ed. Baltimore: American Public Health Association.
- Eberl, H.J. and Demaret, L. 2007. A finite difference scheme for a degenerated diffusion equation arising in microbial ecology. *Electronic Journal of Differential Equations*. [Online]. **15**, pp.77–95. [Accessed 4th June 2014]. Available from: <http://www.mat.ub.edu/EMIS/journals/EJDE/Monographs/Monographs/Volumes/conf-proc/15/e1/erbel.pdf>
- Eberl, H.J. and Efendiev, M.A. 2003. A transient density-dependent diffusion-reaction model for the limitation of antibiotic penetration in biofilms. *Electronic Journal of Differential Equations*. **10**, pp.123-142.

- Eberl, H.J. et al. 2001. A New Deterministic Spatio-Temporal Continuum Model for Biofilm Development. *Journal of Theoretical Medicine*. **3**(3).
- Eberl, H.J. et al. 2000. A three-dimensional numerical study on the correlation of spatial structure, hydrodynamic conditions, and mass transfer and conversion in biofilms. *Chemical Engineering Science*. **55**(24), pp.6209-6222.
- Eberl, H.J. and Sudarsan, R. 2008. Exposure of biofilms to slow flow fields: The convective contribution to growth and disinfection. *Journal of Theoretical Biology*. **253**(4), pp.788-807.
- Eisenberg, T. et al. 2012. Isolation of Potentially Novel Brucella spp. from Frogs. *American Society for Microbiology*. **78**(10), pp. 3753–3755.
- El-Chakhtoura, J. et al. 2015. Dynamics of bacterial communities before and after distribution in a full-scale drinking water network. *Water Research*. **74**(0), pp.180-190.
- Elshorbagy, W.E. et al. 2000. Simulation of THM species in water distribution systems. *Water Research*. **34**(13), pp.3431-3439.
- EMCALI EICE ESP. 2016. *Informe de Gestión*. Cali.
- Environment Agency. 2010. *The Microbiology of Drinking Water (2010) - Part 2 - Practices and procedures for sampling*. Available from: https://www.gov.uk/government/uploads/system/uploads/attachment_data/file/316769/MoDW-2-232.pdf
- Council Directive 98/83/EC of 3 November 1998 on the quality of water intended for human consumption 1998.
- European Union. 2015. 2015. *COMMISSION DIRECTIVE (EU) 2015/1787 of 6 October 2015 amending Annexes II and III to Council Directive 98/83/EC on the quality of water intended for human consumption*.
- Falkinham, O.J. et al. 2015. Opportunistic Premise Plumbing Pathogens: Increasingly Important Pathogens in Drinking Water. *Pathogens*. **4**(2).
- Fan, Y. 2012. *Chlorination of toxic cyanobacterial cells and their associated toxins*. Maîtrise ès Sciences Appliquées thesis, Université de Montréal.
- Fang, F. et al. 2014. Characteristics of extracellular polymeric substances of phototrophic biofilms at different aquatic habitats. *Carbohydrate Polymers*. **106**(0), pp.1-6.
- Fang, J. et al. 2010a. Formation of carbonaceous and nitrogenous disinfection by-products from the chlorination of *Microcystis aeruginosa*. *Water Research*. **44**(6), pp.1934-1940.
- Fang, J. et al. 2010b. Characterization of algal organic matter and formation of DBPs from chlor(am)ination. *Water Research*. **44**(20), pp.5897-5906.
- Farley, M. 2015. Water leakage trends for 2015: the changing face of water loss management. *Water21*. **February**(1), pp.36-38.
- Fish, K. et al. 2012. The structure and stability of drinking water biofilms. In: *WDSA 2012: 14th Water Distribution Systems Analysis Conference, 24-27 September 2012, Adelaide, South Australia*. Barton, A.C.T.; Engineers Australia, pp.455-467.

- Fish, K. et al. 2017. Biofilm structures (EPS and bacterial communities) in drinking water distribution systems are conditioned by hydraulics and influence discolouration. *Science of The Total Environment*. **593–594**, pp.571-580.
- Fish, K.E. et al. 2015. Characterisation of the Physical Composition and Microbial Community Structure of Biofilms within a Model Full-Scale Drinking Water Distribution System. *PLoS ONE*. **10(2)**, pe0115824.
- Fish, K.E. et al. 2016. Characterising and understanding the impact of microbial biofilms and the extracellular polymeric substance (EPS) matrix in drinking water distribution systems. *Environmental Science: Water Research & Technology*.
- Flemming, H.-C. et al. 2002. Contamination potential of biofilms in water distribution systems. *Water Science and Technology: Water Supply*. **2(1)**, pp.271-280.
- Flemming, H.C. and Wingender, J. 2010. The biofilm matrix. *Nature Reviews Microbiology*. [Online]. **8(9)**, pp.623-633. [Accessed 18 January 2014]. Available from: <http://www.nature.com/nrmicro/journal/v8/n9/abs/nrmicro2415.html>
- Frei, W. 2013. Which Turbulence Model Should I Choose for My CFD Application? [Online]. Available from: <https://www.comsol.com/blogs/which-turbulence-model-should-choose-cfd-application/>
- Gagnon, G.A. et al. 2005. Disinfectant efficacy of chlorite and chlorine dioxide in drinking water biofilms. *Water Research*. **39(9)**, pp.1809-1817.
- Gallego, V. et al. 2005. *Methylobacterium isbiliense* sp. nov., isolated from the drinking water system of Sevilla, Spain. *International Journal of Systematic and Evolutionary Microbiology*. **55(6)**, pp.2333-2337.
- Gamito, S. 2010. Caution is needed when applying Margalef diversity index. *Ecological Indicators*. **10(2)**, pp.550-551.
- Gang, D.D. et al. 2002. Using chlorine demand to predict TTHM and HAA9 formation. *American Water Works Association Journal*. **94(10)**, pp.76-86.
- Garcia-Villanova, R.J. et al. 1997a. Formation, evolution and modeling of trihalomethanes in the drinking water of a town: I. At the municipal treatment utilities. *Water Research*. **31(6)**, pp.1299-1308.
- Garcia-Villanova, R.J. et al. 1997b. Formation, evolution and modeling of trihalomethanes in the drinking water of a town: II. In the distribution system. *Water Research*. **31(6)**, pp.1405-1413.
- Garcia Sanchez, D. et al. 2014. Application of sensitivity analysis in building energy simulations: Combining first- and second-order elementary effects methods. *Energy and Buildings*. **68, Part C**, pp.741-750.
- Ghosh, P. et al. 2013. Modeling cell-death patterning during biofilm formation. *Physical Biology*. **10(6)**, p066006.
- Golfinopoulos, S.K. and Arhonditsis, G.B. 2002a. Multiple regression models: A methodology for evaluating trihalomethane concentrations in drinking water from raw water characteristics. *Chemosphere*. **47(9)**, pp.1007-1018.

- Golfonopoulos, S.K. and Arhonditsis, G.B. 2002b. Quantitative assessment of trihalomethane formation using simulations of reaction kinetics. *Water Research*. **36**(11), pp.2856-2868.
- Golfonopoulos, S.K. et al. 1998. Use of a multiple regression model for predicting trihalomethane formation. *Water Research*. **32**(9), pp.2821-2829.
- Gomez-Alvarez, V. et al. 2012. Metagenomic Analyses of Drinking Water Receiving Different Disinfection Treatments. *Applied and Environmental Microbiology*. [Online]. **78**(17), pp.6095–6102. Available from: <http://aem.asm.org/content/early/2012/06/17/AEM.01018-12.short#cite-by>
- Gordon, G. and Tachiyashiki, S. 1991. Kinetics and mechanism of formation of chlorate ion from the hypochlorous acid/chlorite ion reaction at pH 6-10. *Environmental Science & Technology*. **25**(3), pp.468-474.
- Grayman, W.M. et al. 2009. Effects of Redesign of Water Systems for Security and Water Quality Factors. In: *World Environmental and Water Resources Congress 2009, Kansas City, Missouri*.
- Guimerà, X. et al. 2016. Dynamic characterization of external and internal mass transport in heterotrophic biofilms from microsensors measurements. *Water Research*. **102**, pp.551-560.
- Hallam, N.B. et al. 2002. The decay of chlorine associated with the pipe wall in water distribution systems. *Water Research*. **36**(14), pp.3479-3488.
- Hammes, F. et al. 2010. Assessing biological stability of drinking water without disinfectant residuals in a full-scale water supply system. *Journal of Water Supply: Research and Technology—AQUA*. **59**(1), pp.31–40.
- Harrington, G.W. et al. 1992. Developing a Computer Model to Simulate DBP Formation During Water Treatment. *American Water Works Association Journal*. **84**(11), pp.78-87.
- Heilmann, C. et al. 1996. Molecular basis of intercellular adhesion in the biofilm-forming *Staphylococcus epidermidis*. *Molecular Microbiology*. **20**(5), pp.1083-1091.
- Henne, K. et al. 2012. Analysis of Structure and Composition of Bacterial Core Communities in Mature Drinking Water Biofilms and Bulk Water of a Citywide Network in Germany. *Applied and Environmental Microbiology*. **78**(10), pp.3530-3538.
- Henne, K. et al. 2013. Seasonal dynamics of bacterial community structure and composition in cold and hot drinking water derived from surface water reservoirs. *Water Research*. **47**(15), pp.5614-5630.
- Heydorn, A. et al. 2000. Quantification of biofilm structures by the novel computer program comstat. *Microbiology*. **146**(10), pp.2395-2407.
- Holinger, E.P. et al. 2014. Molecular analysis of point-of-use municipal drinking water microbiology. *Water Research*. **49**(0), pp.225-235.
- Hong, H.C. et al. 2007. Modeling of trihalomethane (THM) formation via chlorination of the water from Dongjiang River (source water for Hong Kong's drinking water). *Science of The Total Environment*. **385**(1–3), pp.48-54.

- Hong, H.C. et al. 2008. Yield of trihalomethanes and haloacetic acids upon chlorinating algal cells, and its prediction via algal cellular biochemical composition. *Water Research*. **42**(20), pp.4941-4948.
- Hozalski, M.R. et al. 2008. Degradation of Halogenated Disinfection Byproducts in Water Distribution Systems. *Disinfection By-Products in Drinking Water*. American Chemical Society, pp.334-348.
- Hrudey, S.E. 2009. Chlorination disinfection by-products, public health risk tradeoffs and me. *Water Research*. **43**(8), pp.2057-2092.
- Hrudey, S.E. et al. 2015a. Evaluating Evidence for Association of Human Bladder Cancer with Drinking-Water Chlorination Disinfection By-Products. *Journal of Toxicology and Environmental Health, Part B*. **18**(5), pp.213-241.
- Hrudey, S.E. et al. 2015b. *Evidence for Association of Human Bladder Cancer With Chlorination Disinfection By-Products*. USA: Water Research Foundation and American Water Works Association.
- Hrudey, S.E. and Charrois, W.A. 2012. Concluding thoughts on DBPs, water quality and public health risks. In: Hrudey, S.E. and Charrois, W.A. eds. *Disinfection by-products and human health*. London, UK: IWA Publishing, p.304.
- Huang, H. et al. 2012. Dichloroacetonitrile and Dichloroacetamide Can Form Independently during Chlorination and Chloramination of Drinking Waters, Model Organic Matters, and Wastewater Effluents. *Environmental Science & Technology*. **46**(19), pp.10624-10631.
- Huixian, Z. et al. 1997. Formation of POX and NPOX with chlorination of fulvic acid in water: Empirical models. *Water Research*. **31**(6), pp.1536-1541.
- Humpage, A.R. 2012. Mutagen X: The evolving story of an extremely potent mutagen, its toxicology and human health risk assessment. In: Hrudey, S.E. and Charrois, W.A. eds. *Disinfection by-products and human health*. London, UK: IWA Publishing, p.304.
- Hutton, G. and Varughese, M. 2016. *The Costs of Meeting the 2030 Sustainable Development Goal Targets on Drinking Water, Sanitation, and Hygiene. Summary Report*. Water and Sanitation Program and World Bank Group.
- IARC. 1999. *Monographs on the Evaluation of Carcinogenic Risks to Humans. Some Chemicals that Cause Tumours of the Kidney or Urinary Bladder in Rodents and Some Other Substances*.
- Ibarluzea, J.M. et al. 1994. Trihalomethanes in water supplies in the San Sebastian area, Spain. *Bulletin of Environmental Contamination and Toxicology*. **52**(3), pp.411-418.
- IDEAM. 2017. *Tiempo y Clima*. [Online]. [Accessed 24th April]. Available from: <http://www.ideam.gov.co/web/tiempo-y-clima/clima>
- IPCC. 2014. *Climate Change 2014 : Synthesis Report. Contribution of Working Groups I, II and III to the Fifth Assessment Report of the Intergovernmental Panel on Climate Change*. Geneva, Switzerland: IPCC.
- Itoh, T. et al. 2011. Aciditerrimonas ferrireducens gen. nov., sp. nov., an iron-reducing thermoacidophilic actinobacterium isolated from a solfataric field. *International Journal of Systematic and Evolutionary Microbiology*. **61**(6), pp.1281-1285.

- IWA Task Group on Biofilm Modeling et al. 2006. *Mathematical Modeling of Biofilms*. London, UK: IWA Publishing.
- Jakubowska, N. and Szeląg-Wasielewska, E. 2015. Toxic Picoplanktonic Cyanobacteria—Review. *Marine Drugs*. **13**(3), pp.1497-1518.
- Jayakumar, J.S. et al. 2008. Experimental and CFD estimation of heat transfer in helically coiled heat exchangers. *Chemical Engineering Research and Design*. **86**(3), pp.221-232.
- Jayathilake, P.G. et al. 2017. A mechanistic Individual-based Model of microbial communities. *PLOS ONE*. **12**(8), pe0181965.
- Ji, P. et al. 2015. Impact of Water Chemistry, Pipe Material and Stagnation on the Building Plumbing Microbiome. *PLOS ONE*. **10**(10), pe0141087.
- Ji, P. et al. 2017. Impact of water heater temperature setting and water use frequency on the building plumbing microbiome. *ISME J*. **11**(6), pp.1318-1330.
- Kalmbach, S. et al. 1997. Dynamics of biofilm formation in drinking water: phylogenetic affiliation and metabolic potential of single cells assessed by formazan reduction and in situ hybridization. *FEMS Microbiology Ecology*. **22**(4), pp.265-279.
- Karanfil, T. et al. 2008. Recent Advances in Disinfection By-Product Formation, Occurrence, Control, Health Effects, and Regulations. *Disinfection By-Products in Drinking Water*. American Chemical Society, pp.2-19.
- Kelly, J.J. et al. 2014. Temporal Variations in the Abundance and Composition of Biofilm Communities Colonizing Drinking Water Distribution Pipes. *PLoS ONE*. [Online]. **9**(5), pep98542. Available from: <http://www.plosone.org/article/info%3Adoi%2F10.1371%2Fjournal.pone.0098542>
- Kettler, A.J. and Goulter, I.C. 1985. An analysis of pipe breakage in urban water distribution networks. *Canadian Journal of Civil Engineering*. **12**(2), pp.286-293.
- Khan, S.J. et al. 2015. Extreme weather events: Should drinking water quality management systems adapt to changing risk profiles? *Water Research*. **85**, pp.124-136.
- Kiénié, L. et al. 1998. Relative importance of the phenomena responsible for chlorine decay in drinking water distribution systems. *Water Science and Technology*. **38**(6), pp.219-227.
- Kim, D.-j. et al. 2012. Relation of microbial biomass to counting units for *Pseudomonas aeruginosa*. *African Journal of Microbiology Research*. **6**(21), pp.620-4622.
- Kirmeyer, G.J. et al. 2001. Practical guidelines for maintaining distribution system water quality. *American Water Works Association Journal*. **93**(7), pp.62-73.
- Kommedal, R. et al. 2001. Modelling production of extracellular polymeric substances in a *Pseudomonas aeruginosa* chemostat culture. *Water Science and Technology*. **43**(6), p129.
- Korn, C. et al. 2002. Development of chlorine dioxide-related by-product models for drinking water treatment. *Water Research*. **36**(1), pp.330-342.

- Kristiana, I. et al. 2012. Research overview, regulatory history and current worldwide status of DBP regulations and guidelines. In: Hrudey, S.E. and Charrois, W.A. eds. *Disinfection by-products and human health*. London, UK: IWA Publishing, p.304.
- Kumpel, E. and Nelson, K.L. 2016. Intermittent Water Supply: Prevalence, Practice, and Microbial Water Quality. *Environmental Science & Technology*. **50**(2), pp.542-553.
- Kundukad, B. et al. 2016. Mechanical properties of the superficial biofilm layer determine the architecture of biofilms. *Soft matter*. **12**(26), pp.5718-5726.
- Långmark, J. et al. 2005. Biofilms in an urban water distribution system: measurement of biofilm biomass, pathogens and pathogen persistence within the Greater Stockholm area, Sweden. *Water Science and Technology*. **52**(8), p181.
- Lau, H.Y. and Ashbolt, N.J. 2009. The role of biofilms and protozoa in Legionella pathogenesis: implications for drinking water. *Journal of Applied Microbiology*. **107**(2), pp.368-378.
- Lechevallier, M.W. and Seidler, R.J. 1980. Staphylococcus aureus in Rural Drinking Water. [Online]. **30**(40), pp.739-742. [Accessed 1st June 2016]. Available from: <http://aem.asm.org/content/39/4/739.full.pdf>
- Lee, E.J. and Schwab, K.J. 2005. Deficiencies in drinking water distribution systems in developing countries. *Journal of Water and Health*. **3**(2), p109.
- Lee, H.D. et al. 2014. A study on evaluation of the pipe wall decay constants of residual chlorine and affecting factors in reclaimed water supply system. *Desalination and Water Treatment*. **53**(9), pp.2378-2387.
- Lehtola, M.J. et al. 2006. The effects of changing water flow velocity on the formation of biofilms and water quality in pilot distribution system consisting of copper or polyethylene pipes. *Water Research*. **40**(11), pp.2151-2160.
- Lehtola, M.J. et al. 2004. Removal of soft deposits from the distribution system improves the drinking water quality. *Water Research*. **38**(3), pp.601-610.
- Leisinger, T. et al. 1994. Microbes, enzymes and genes involved in dichloromethane utilization. *Biodegradation*. **5**(3-4), pp.237-248.
- Lekkas, T.D. and Nikolaou, A.D. 2004. Development of predictive models for the formation of trihalomethanes and haloacetic acids during chlorination of bromide ion rich water. *Water Quality Research Journal of Canada*. **39**(2), pp.149-159.
- Lemus Pérez, M.F. and Rodríguez Susa, M. 2017. Exopolymeric substances from drinking water biofilms: Dynamics of production and relation with disinfection by products. *Water Research*. **116**, pp.304-315.
- Levenspiel, O. 1999. *Chemical reaction engineering*. Third edition ed. NJ, USA: John Wiley & Sons.
- Liang, L. and Singer, P.C. 2003. Factors Influencing the Formation and Relative Distribution of Haloacetic Acids and Trihalomethanes in Drinking Water. *Environmental Science & Technology*. **37**(13), pp.2920-2928.

- Lin, C.K. et al. 2003. The characteristics of the bacterial community structure and population dynamics for phosphorus removal in SBR activated sludge processes. *Water Research*. **37**(12), pp.2944-2952.
- Lindley, B. et al. 2012. Multicomponent hydrodynamic model for heterogeneous biofilms: Two-dimensional numerical simulations of growth and interaction with flows. *Physical Review E*. **85**(3), p031908.
- Lipponen, M.T.T. et al. 2002. Occurrence of nitrifying bacteria and nitrification in Finnish drinking water distribution systems. *Water Research*. **36**(17), pp.4319-4329.
- Liu, G. et al. 2014. Pyrosequencing Reveals Bacterial Communities in Unchlorinated Drinking Water Distribution System: An Integral Study of Bulk Water, Suspended Solids, Loose Deposits, and Pipe Wall Biofilm. *Environmental Science & Technology*. **48**(10), pp.5467-5476.
- Liu, G. et al. 2013. A comparison of additional treatment processes to limit particle accumulation and microbial growth during drinking water distribution. *Water Research*. **47**(8), pp.2719-2728.
- Liu, Y. et al. 2017. Formation of disinfection byproducts from accumulated soluble products of oleaginous microalga after chlorination. *Frontiers of Environmental Science & Engineering*. **11**(6), p1.
- Loucks, D.P. and van Beek, E. 2005. *Water resources systems Planning and management*. Turin: UNESCO.
- Lu, W. et al. 1999. Chlorine demand of biofilms in water distribution systems. *Water Research*. **33**(3), pp.827-835.
- Lührig, K. et al. 2015. Bacterial Community Analysis of Drinking Water Biofilms in Southern Sweden. *Microbes and Environments*. **30**(1), pp.99-107.
- Macías-Díaz, J.E. 2015. Positive computational modelling of the dynamics of active and inert biomass with extracellular polymeric substances. *Journal of Difference Equations and Applications*. **21**(4), pp.319-335.
- Mahapatra, A. et al. 2015. Study of Biofilm in Bacteria from Water Pipelines. *Journal of Clinical and Diagnostic Research : JCDR*. **9**(3), pp.DC09-DC11.
- Manuel, C.M. et al. 2007. Dynamics of drinking water biofilm in flow/non-flow conditions. *Water Research*. **41**(3), pp.551-562.
- Manuel, C.M. et al. 2009. Unsteady state flow and stagnation in distribution systems affect the biological stability of drinking water. *Biofouling*. **26**(2), pp.129-139.
- Marra, V. 2013. On Solvers: Multigrid Methods. [Online]. Available from: <https://uk.comsol.com/blogs/on-solvers-multigrid-methods/>
- Martiny, A.C. et al. 2005. Identification of Bacteria in Biofilm and Bulk Water Samples from a Nonchlorinated Model Drinking Water Distribution System: Detection of a Large Nitrite-Oxidizing Population Associated with *Nitrospira* spp. *Applied and Environmental Microbiology*. **71**(12), pp.8611–8617.
- McGuire, M.J. et al. 2002. *Information Collection Rule Data Analysis*. Denver, CO.

- McMurdie, P.J. and Holmes, S. 2014. Waste Not, Want Not: Why Rarefying Microbiome Data Is Inadmissible. *PLOS Computational Biology*. **10**(4), pe1003531.
- McNeill, L.S. and Edwards, M. 2002. The Importance of Temperature in Assessing Iron Pipe Corrosion in Water Distribution Systems. *Environmental Monitoring and Assessment*. **77**(3), pp.229-242.
- Menberg, K. et al. 2016. Sensitivity analysis methods for building energy models: Comparing computational costs and extractable information. *Energy and Buildings*. **133**, pp.433-445.
- Mi, Z. et al. 2015. Impact of disinfection on drinking water biofilm bacterial community. *Journal of Environmental Sciences*. **37**, pp.200-205.
- Miettinen, I.T. et al. 1997. Phosphorus and Bacterial Growth in Drinking Water. *Applied and Environmental Microbiology*. **63**(8), pp.3242–3245.
- Milot, J. et al. 2000. Modeling the susceptibility of drinking water utilities to form high concentrations of trihalomethanes. *Journal of Environmental Management*. **60**(2), pp.155-171.
- Ministerio de la Protección Social. 2007. 2007. *Decreto 1575 de 2007: Por el cual se establece el Sistema para la Protección y Control de la Calidad del Agua para Consumo Humano*.
- Ministerio de la Protección Social and Ministerio de Ambiente Vivienda y Desarrollo Territorial. 2007. 2007. *Resolución número 2115: Por medio de la cual se señalan características, instrumentos básicos y frecuencias del sistema de control y vigilancia para la calidad del agua para consumo humano*.
- Montoya-Pachongo, C. et al. 2016. Effects of water inlet configuration in a service reservoir applying CFD modelling. *Revista Ingeniería e Investigación*. **36**(1), pp.31-40.
- Montoya, C. et al. 2012. Evaluación de las condiciones de mezcla y su influencia sobre el cloro residual en tanques de compensación de un sistema de distribución de agua potable. *Revista Ingeniería y Ciencia*. **8**(5), pp.9-30.
- Montoya, C. et al. 2011. Efecto del incremento en la turbiedad del agua cruda sobre la eficiencia de procesos convencionales de potabilización. *Revista EIA*. **8**(16), pp.137-148.
- Montoya, C. et al. 2009. Propuesta metodológica para localización de estaciones de monitoreo de calidad de agua en redes de distribución utilizando sistemas de información geográfica. *Revista Facultad de Ingeniería de la Universidad de Antioquia*. **2**(49), pp.129-140.
- Morris, M.D. 1991. Factorial Sampling Plans for Preliminary Computational Experiments. *Technometrics*. **33**(2), pp.161-174.
- Morrow, C.M. and Minear, R.A. 1987. Use of regression models to link raw water characteristics to trihalomethane concentrations in drinking water. *Water Research*. **21**(1), pp.41-48.
- Muellner, M.G. et al. 2007. Haloacetonitriles vs. Regulated Haloacetic Acids: Are Nitrogen-Containing DBPs More Toxic? *Environmental Science & Technology*. **41**(2), pp.645-651.
- Mukundan, R. and Van Dreaseon, R. 2014. Predicting Trihalomethanes in the New York City Water Supply. *Journal of Environmental Quality*. **43**(2), pp.611-616.

- Nescerecka, A. et al. 2014. Biological Instability in a Chlorinated Drinking Water Distribution Network. *PLoS ONE*. **9**(5), pe96354.
- Nieuwenhuijsen, M.J. et al. 2000. Chlorination disinfection byproducts in water and their association with adverse reproductive outcomes: a review. *Occupational and Environmental Medicine*. **57**(2), pp.73-85.
- Nikolaou, A.D. et al. 2004. Kinetics of the formation and decomposition of chlorination by-products in surface waters. *Chemical Engineering Journal*. **100**(1-3), pp.139-148.
- Nokes, C.J. et al. 1999. Modelling the formation of brominated trihalomethanes in chlorinated drinking waters. *Water Research*. **33**(17), pp.3557-3568.
- NRCNA, N.R.C.o.t.N.A. 2006. *Drinking Water Distribution Systems: Assessing and Reducing Risks*. [Online]. Washington D.C: National Research Council of the National Academies. [Accessed 7 January 2013]. Available from: http://www.kysq.org/docs/DWDS_NAS.pdf
- Ocampo-Duque, W. et al. 2013. Water quality analysis in rivers with non-parametric probability distributions and fuzzy inference systems: Application to the Cauca River, Colombia. *Environment International*. **52**, pp.17-28.
- Park, S. et al. 1991. Batch cultivation of *Methylosinus trichosporium* OB3b. I: Production of soluble methane monooxygenase. *Biotechnology and Bioengineering*. **38**(4), pp.423-433.
- Parvez, S. et al. 2011. Temporal variability in trihalomethane and haloacetic acid concentrations in Massachusetts public drinking water systems. *Environmental Research*. **111**(4), pp.499-509.
- Patel, R.N. et al. 1982. Microbial Oxidation of Hydrocarbons: Properties of a Soluble Methane Monooxygenase from a Facultative Methane-Utilizing Organism, *Methylobacterium* sp. Strain CRL-26. *Applied and Environmental Microbiology*. **44**(5), pp.1130-1137.
- Peng, C.-Y. et al. 2010. Characterization of elemental and structural composition of corrosion scales and deposits formed in drinking water distribution systems. *Water Research*. **44**(15), pp.4570-4580.
- Perelman, B.L. and Ostfeld, A. 2013. Operation of remote mobile sensors for security of drinking water distribution systems. *Water Research*. **47**(13), pp.4217-4226.
- Pérez-Vidal, A. et al. 2012. Identificación y priorización de peligros como herramientas de la gestión del riesgo en sistemas de distribución de agua potable. *Ingeniería y Universidad*. **16**(2), pp.449-469.
- Peyton, B.M. 1996. Effects of shear stress and substrate loading rate on *Pseudomonas aeruginosa* biofilm thickness and density. *Water Research*. **30**(1), pp.29-36.
- Pianosi, F. et al. 2015. A Matlab toolbox for Global Sensitivity Analysis. *Environmental Modelling & Software*. **70**, pp.80-85.
- Picioreanu, C. et al. 1998a. A new combined differential-discrete cellular automaton approach for biofilm modeling: application for growth in gel beads. *Biotechnology and bioengineering*. **57**(6), pp.718-731.
- Picioreanu, C. et al. 1998b. Mathematical Modeling of Biofilm Structure with a Hybrid Differential-Discrete Cellular Automaton Approach. *Biotechnology and Bioengineering*. **58**(1), pp.101-116.

- Piciooreanu, C. et al. 2000a. Effect of diffusive and convective substrate transport on biofilm structure formation: A two-dimensional modeling study. *Biotechnology and Bioengineering*. **69**(5), pp.504-515.
- Piciooreanu, C. et al. 2000b. A theoretical study on the effect of surface roughness on mass transport and transformation in biofilms. *Biotechnology and Bioengineering*. **68**(4), pp.355-369.
- Plewa, M.J. et al. 2008. Comparative Mammalian Cell Toxicity of N-DBPs and C-DBPs. *Disinfection By-Products in Drinking Water*. American Chemical Society, pp.36-50.
- Poling, E.B. et al. 2007. Physical and Chemical Data. In: Perry, R.H. and Perry, J.H. eds. *Perry's chemical engineers' handbook*. New York: Mc Graw Hill, pp.2-456.
- Prest, E. et al. 2016. Biological stability of drinking water: controlling factors, methods and challenges. *Frontiers in Microbiology*. **7**.
- Propato, M. and Uber, J.G. 2004. Vulnerability of Water Distribution Systems to Pathogen Intrusion: How Effective Is a Disinfectant Residual? *Environmental Science & Technology*. **38**(13), pp.3713-3722.
- Pu, Y. et al. 2013. Formation of THMs and HANs during bromination of *Microcystis aeruginosa*. *Journal of Environmental Sciences*. **25**(9), pp.1795-1799.
- Rainey, F.A. et al. 2005. Extensive Diversity of Ionizing-Radiation-Resistant Bacteria Recovered from Sonoran Desert Soil and Description of Nine New Species of the Genus *Deinococcus* Obtained from a Single Soil Sample. *Applied and Environmental Microbiology*. **71**(9), pp.5225-5235.
- Raseman, W.J. et al. 2017. Emerging investigators series: a critical review of decision support systems for water treatment: making the case for incorporating climate change and climate extremes. *Environmental Science: Water Research & Technology*. **3**(1), pp.18-36.
- Rataj, E. et al. 2016. Extreme weather events in developing countries and related injuries and mental health disorders - a systematic review. *BMC Public Health*. **16**(1), p1020.
- Rathbun, R.E. 1996a. Regression equations for disinfection by-products for the Mississippi, Ohio and Missouri rivers. *Science of The Total Environment*. **191**(3), pp.235-244.
- Rathbun, R.E. 1996b. Speciation of trihalomethane mixtures for the Mississippi, Missouri, and Ohio Rivers. *Science of The Total Environment*. **180**(2), pp.125-135.
- Reckhow, D.A. et al. 2001. Formation and degradation of dichloroacetonitrile in drinking waters. *Journal of Water Supply: Research and Technology - Aqua*. **50**(1), p1.
- Ren, H. et al. 2015. Pyrosequencing analysis of bacterial communities in biofilms from different pipe materials in a city drinking water distribution system of East China. *Applied Microbiology and Biotechnology*. **99**(24), pp.10713-10724.
- Revetta, R.P. et al. 2016. Changes in bacterial composition of biofilm in a metropolitan drinking water distribution system. *Journal of Applied Microbiology*. pp.n/a-n/a.
- Revetta, R.P. et al. 2011. 16S rRNA Gene Sequence Analysis of Drinking Water Using RNA and DNA Extracts as Targets for Clone Library Development. *Current Microbiology*. **63**(1), pp.50-59.

- Richardson, S.D. et al. 2007. Occurrence, genotoxicity, and carcinogenicity of regulated and emerging disinfection by-products in drinking water: A review and roadmap for research. *Mutation Research/Reviews in Mutation Research*. **636**(1–3), pp.178-242.
- Roccaro, P. et al. 2013. Modeling bromide effects on yields and speciation of dihaloacetonitriles formed in chlorinated drinking water. *Water Research*. **47**(16), pp.5995-6006.
- Rodrigues, P.M.S.M. et al. 2007. Factorial analysis of the trihalomethanes formation in water disinfection using chlorine. *Analytica Chimica Acta*. **595**(1–2), pp.266-274.
- Rodriguez, M.J. and Sérodes, J.-B. 2001. Spatial and temporal evolution of trihalomethanes in three water distribution systems. *Water Research*. **35**(6), pp.1572-1586.
- Rodriguez, M.J. et al. 2000. Estimation of water utility compliance with trihalomethane regulations using a modelling approach. *Journal of Water Supply: Research and Technology - Aqua*. **49**(2), p57.
- Roeder, R.S. et al. 2010. Long-term effects of disinfectants on the community composition of drinking water biofilms. *International Journal of Hygiene and Environmental Health*. **213**(3), pp.183-189.
- Rojas, A. et al. 2001. Synergism between *Phyllobacterium* sp. (N₂-fixer) and *Bacillus licheniformis* (P-solubilizer), both from a semiarid mangrove rhizosphere. *FEMS Microbiology Ecology*. **35**(2), pp.181-187.
- Rondon, M.R. et al. 2000. Cloning the Soil Metagenome: a Strategy for Accessing the Genetic and Functional Diversity of Uncultured Microorganisms. *Applied and Environmental Microbiology*. **66**(6), pp.2541-2547.
- Rook, J.J. 1974. Formation of haloforms during chlorination of natural water. *Water Treatment and Examination*. **23**(1), pp.234-243.
- Rosario-Ortiz, F. et al. 2016. How do you like your tap water? *Science*. **351**(6276), p912.
- Rossmann, L. et al. 1994. Modeling Chlorine Residuals in Drinking-Water Distribution Systems. *Journal of Environmental Engineering*. **120**(4), pp.803-820.
- RSPH, R.S.f.P.H. et al. 2017. *Principles of Water Supply Hygiene*.
- Saltelli, A. et al. 2004. *Sensitivity Analysis in Practice*. Chichester, England: Wiley.
- Sanger, F. et al. 1977. DNA sequencing with chain-terminating inhibitors. *Proceedings of the National Academy of Sciences*. **74**(12), pp.5463-5467.
- Scarpino, P.V. et al. 1972. A comparative study of the inactivation of viruses in water by chlorine. *Water Research*. **6**(8), pp.959-965.
- Scholz, H.C. et al. 2010. *Brucella inopinata* sp. nov., isolated from a breast implant infection. *International Journal of Systematic and Evolutionary Microbiology*. **60**(4), pp.801-808.
- Semerjian, L. et al. 2009. Modeling the formation of trihalomethanes in drinking waters of Lebanon. *Environmental Monitoring and Assessment*. **149**(1), pp.429-436.

- Sepkoski, J.J. 1988. Alpha, beta, or gamma: where does all the diversity go? *Paleobiology*. **14**(3), pp.221-234.
- Sérodès, J.-B. et al. 2003. Occurrence of THMs and HAAs in experimental chlorinated waters of the Quebec City area (Canada). *Chemosphere*. **51**(4), pp.253-263.
- Shaw, J.L.A. et al. 2014. Assessing the impact of water treatment on bacterial biofilms in drinking water distribution systems using high-throughput DNA sequencing. *Chemosphere*. **117**, pp.185-192.
- Shen, Y. et al. 2016. Response of Simulated Drinking Water Biofilm Mechanical and Structural Properties to Long-Term Disinfectant Exposure. *Environmental Science & Technology*. **50**(4), pp.1779-1787.
- Siddiqui, M. and Amy, G. 1994. Empirically and Theoretically-Based Models for Predicting Brominated Ozonated By-Products. *Ozone: Science & Engineering*. **16**(2), pp.157-178.
- Simões, C.L. and Simões, M. 2013. Biofilms in drinking water: problems and solutions. *The Royal Society of Chemistry*. (3), p14.
- Simões, C.L. et al. 2007. Biofilm Interactions between Distinct Bacterial Genera Isolated from Drinking Water. *Applied and Environmental Microbiology*. **73**(19), pp.6192–6200.
- Simões, C.L. et al. 2010. Influence of the Diversity of Bacterial Isolates from Drinking Water on Resistance of Biofilms to Disinfection. *Applied and Environmental Microbiology*. **76**(19), pp.6673–6679.
- Sohn, J. et al. 2004. Disinfectant decay and disinfection by-products formation model development: chlorination and ozonation by-products. *Water Research*. **38**(10), pp.2461-2478.
- Song, F. et al. 2015. Effects of Material Properties on Bacterial Adhesion and Biofilm Formation. *Journal of Dental Research*. **94**(8), pp.1027-1034.
- Song, R. et al. 1996. Empirical modeling of bromate formation during ozonation of bromide-containing waters. *Water Research*. **30**(5), pp.1161-1168.
- Srivastava, S. and Bhargava, A. 2015. Biofilms and human health. *Biotechnology Letters*. **38**(1), pp.1-22.
- Stevens, M. et al. 2004. Risk management for distribution systems. In: Ainsworth, R. ed. *Safe Piped Water* Padstow: IWA Publishing, pp.121-138.
- Stewart, P.S. 1994. Biofilm Accumulation Model That Predicts Antibiotic Resistance of *Pseudomonas aeruginosa* Biofilms. *Antimicrobial Agents and Chemotherapy*. **38**(5), pp.1052-1058.
- Stewart, P.S. and Raquepas, J.B. 1995. Implications of reaction-diffusion theory for the disinfection of microbial biofilms by reactive antimicrobial agents. *Chemical Engineering Science*. **50**(19), pp.3099-3104.
- Stover, C.K. et al. 2000. Complete genome sequence of *Pseudomonas aeruginosa* PAO1, an opportunistic pathogen. *Nature*. **406**(6799), pp.959-964.

- SUI, S.Ú.d.I.d.S.P. 2017. *Servicio de Acueducto*. [Online]. [Accessed 24th April]. Available from: www.sui.gov.co
- Sun, H. et al. 2014. Bacterial community of biofilms developed under different water supply conditions in a distribution system. *Science of The Total Environment*. **472**(0), pp.99-107.
- Sung, W. et al. 2000. Modeling DBP formation. *American Water Works Association Journal*. **92**(5), pp.53-63.
- Superintendencia de Servicios Públicos. 2006. 2006. *Por la cual se establece la obligación de reportar información por los prestadores de los servicios públicos de acueducto, alcantarillado y aseo, a través del Sistema Unico de Información, para el cálculo de los indicadores de riesgo de primer nivel de la Resolución CRA 315 de 11 de febrero de 2005*.
- Superintendencia de Servicios Públicos Domiciliarios. 2013. *Informe Sectorial de los Servicios Públicos Domiciliarios de Acueducto, Alcantarillado y Aseo - 2012 Grandes Prestadores*. Bogotá D.C.
- Taherzadeh, D. et al. 2012. Mass Transfer Enhancement in Moving Biofilm Structures. *Biophysical Journal*. **102**(7), pp.1483-1492.
- Thakre, S.S. and Joshi, J.B. 2000. CFD modeling of heat transfer in turbulent pipe flows. *AIChE Journal*. **46**(9), pp.1798-1812.
- The British Geographer. 2017. *The climate of tropical regions*. [Online]. [Accessed 13th September]. Available from: <http://thebritishgeographer.weebly.com/the-climate-of-tropical-regions.html>
- Theron, J. and Cloete, T.E. 2000. Molecular Techniques for Determining Microbial Diversity and Community Structure in Natural Environments. *Critical Reviews in Microbiology*. **26**(1), pp.37-57.
- Tierra, G. et al. 2015. Multicomponent model of deformation and detachment of a biofilm under fluid flow. *Journal of The Royal Society Interface*. **12**(106).
- Toroz, I. and Uyak, V. 2005. Seasonal variations of trihalomethanes (THMs) in water distribution networks of Istanbul City. *Desalination*. **176**(1), pp.127-141.
- Tosun, I. 2007. *Modeling in Transport Phenomena*. Second ed. The Netherlands: Elsevier.
- TravelChinaGuide. 2017. *Shaoxing Weather*. [Online]. [Accessed 28th April]. Available from: <https://www.travelchinaguide.com/cityguides/zhejiang/shaoxing/weather/>
- Tsuneda, S. et al. 2003. Extracellular polymeric substances responsible for bacterial adhesion onto solid surface. *FEMS Microbiology Letters*. **223**(2), pp.287-292.
- Tung, H.-h. and Xie, Y.F. 2009. Association between haloacetic acid degradation and heterotrophic bacteria in water distribution systems. *Water Research*. **43**(4), pp.971-978.
- Tyrovola, K. and Diamadopoulos, E. 2005. Bromate formation during ozonation of groundwater in coastal areas in Greece. *Desalination*. **176**(1), pp.201-209.
- UK Parliament. 2000. 2000. *The Water Supply (Water Quality) Regulations 2000*.

- United Nations. 2015. *Sustainable Development Goal 6*. [Online]. [Accessed 30th March 2017]. Available from: <https://sustainabledevelopment.un.org/sdg6>
- Universidad de los Andes, D.d.I.C.y.A.C.d.I.e.A.y.A. 2010. 2010. *Reglamento Técnico del Sector de Agua Potable y Saneamiento Básico: Título B*. Bogotá D.C.
- Urano, K. et al. 1983. Empirical rate equation for trihalomethane formation with chlorination of humic substances in water. *Water Research*. **17**(12), pp.1797-1802.
- USEPA. 1998. 1998. *National primary drinking water regulations: Disinfectants and Disinfection Byproducts*.
- USEPA. 2000. *Chloroform*. [Online]. [Accessed 11th July]. Available from: <https://www3.epa.gov/airtoxics/hlthef/chlorofo.html>
- USEPA. 2002a. *Effects of Water Age on Distribution System Water Quality*. Washington DC.
- USEPA. 2002b. *Finished Water Storage Facilities*. Washington DC.
- USEPA. 2002c. *New or Repaired Water Mains*. Washington DC.
- USEPA. 2006. 2006. *National primary drinking water regulations: stage 2 disinfectants and disinfection by products rule: final rule*.
- USEPA. 2008. *EPANET multi-species extension. User's manual*.
- USEPA. 2016a. *IRIS (Integrated Risk Information System). The Integrated Risk Information System online database*. [Online]. [Accessed 13th June 2016]. Available from: <https://www.epa.gov/iris>
- USEPA. 2016b. *Quick guide to drinking water sample collection*. Golden, CO. Available from: https://www.epa.gov/sites/production/files/2015-11/documents/drinking_water_sample_collection.pdf
- Uyak, V. and Toroz, I. 2007. Investigation of bromide ion effects on disinfection by-products formation and speciation in an Istanbul water supply. *Journal of Hazardous Materials*. **149**(2), pp.445-451.
- Uyak, V. et al. 2005. Monitoring and modeling of trihalomethanes (THMs) for a water treatment plant in Istanbul. *Desalination*. **176**(1), pp.91-101.
- Vannecke, T.P.W. et al. 2015. Considering microbial and aggregate heterogeneity in biofilm reactor models: how far do we need to go? *Water Science and Technology*. **72**(10), pp.1692-1699.
- Vasconcelos, J.J. et al. 1997. Kinetics of chlorine decay. *American Water Works Association Journal*. **89**(7), p54.
- Villanueva, C.M. et al. 2007. Bladder Cancer and Exposure to Water Disinfection By-Products through Ingestion, Bathing, Showering, and Swimming in Pools. *American Journal of Epidemiology*. **165**(2), pp.148-156.
- Vreeburg, I.J.H.G. and Boxall, D.J.B. 2007. Discolouration in potable water distribution systems: A review. *Water Research*. **41**(3), pp.519-529.

- Vreeburg, J.H.G. et al. 2008. How Effective Is Flushing of Cast Iron Pipes? In: Van Zyl, J.E., et al., eds. *10th Annual Water Distribution Systems Analysis Conference WDSA 2008, August 17-20, 2008, Kruger National Park, South Africa*. American Society of Civil Engineers, pp.559-570.
- Wang, D. et al. 2011. Biodeterioration of asbestos cement (AC) pipe in drinking water distribution systems. *International Biodeterioration & Biodegradation*. **65**(6), pp.810-817.
- Wang, H. et al. 2012a. Effects of disinfectant and biofilm on the corrosion of cast iron pipes in a reclaimed water distribution system. *Water Research*. **46**(4), pp.1070-1078.
- Wang, H. et al. 2014. Effect of Disinfectant, Water Age, and Pipe Materials on Bacterial and Eukaryotic Community Structure in Drinking Water Biofilm. *Environmental Science & Technology*. **48**(3), pp.1426-1435.
- Wang, J.-J. et al. 2013a. Disinfection byproduct formation from chlorination of pure bacterial cells and pipeline biofilms. *Water Research*. **47**(8), pp.2701-2709.
- Wang, Q. and Zhang, T. 2010a. Review of mathematical models for biofilms. *Solid State Communications*. **150**(21–22), pp.1009-1022.
- Wang, Z.-P. and Zhang, T. 2010b. Characterization of soluble microbial products (SMP) under stressful conditions. *Water Research*. **44**(18), pp.5499-5509.
- Wang, Z. et al. 2013b. Relative Contribution of Biomolecules in Bacterial Extracellular Polymeric Substances to Disinfection Byproduct Formation. *Environmental Science & Technology*. **47**(17), pp.9764-9773.
- Wang, Z. et al. 2012b. The role of extracellular polymeric substances on the sorption of natural organic matter. *Water Research*. **46**(4), pp.1052-1060.
- Wang, Z. et al. 2012c. Influence of Bacterial Extracellular Polymeric Substances on the Formation of Carbonaceous and Nitrogenous Disinfection Byproducts. *Environmental Science & Technology*. **46**(20), pp.11361-11369.
- Water Research Foundation. 2014. *Water Quality Impacts of Extreme Weather-Related Events [Project #4324]*.
- Wei, J. et al. 2010. Spatial and temporal evaluations of disinfection by-products in drinking water distribution systems in Beijing, China. *Science of The Total Environment*. **408**(20), pp.4600-4606.
- Weinberg, H.S. 2009. Modern approaches to the analysis of disinfection by-products in drinking water. *Philosophical Transactions of the Royal Society of London A: Mathematical, Physical and Engineering Sciences*. **367**(1904), pp.4097-4118.
- Weishaar, J.L. et al. 2003. Evaluation of Specific Ultraviolet Absorbance as an Indicator of the Chemical Composition and Reactivity of Dissolved Organic Carbon. *Environmental Science & Technology*. **37**(20), pp.4702-4708.
- Wen, G. et al. 2014. Using coagulation to restrict microbial re-growth in tap water by phosphate limitation in water treatment. *Journal of Hazardous Materials*. **280**(0), pp.348-355.
- Westerhoff, P. et al. 2000. Applying DBP models to full-scale plants. *American Water Works Association Journal*. **92**(3), pp.89-102.

- Westrin, B.A. and Axelsson, A. 1991. Diffusion in gels containing immobilized cells: A critical review. *Biotechnology and Bioengineering*. **38**(5), pp.439-446.
- Wheeler, Q.D. 2008. Introductory toward the New Taxonomy. In: Wheeler, Q.D. ed. *The New Taxonomy*. London: CRC Press.
- Whiley, H. et al. 2015. Opportunistic Pathogens Mycobacterium Avium Complex (MAC) and Legionella spp. Colonise Model Shower. *Pathogens*. **4**(3).
- Whittaker, R.H. 1975. *Communities and Ecosystems*. New York: MacMillan.
- WHO, W.H.O. 2004. *Concise International Chemical Assessment Document 58: Chloroform, WHO, W.H.O.*, [Exhibition catalogue]. Geneva, Switzerland.
- WHO, W.H.O. 2005. *Water Safety Plans. Managing drinking-water quality from catchment to consumer*. [Online]. Switzerland: WHO. Available from: http://www.who.int/water_sanitation_health/dwq/wsp170805.pdf
- WHO, W.H.O. 2008. *Guidelines for drinking-water quality: incorporating 1st and 2nd addenda, Vol.1, Recommendations. – 3rd ed.* [Online]. 3rd ed. Geneva: WHO Press. [Accessed 28th July 2014]. Available from: http://www.who.int/water_sanitation_health/dwq/gdwq3rev/en/
- WHO, W.H.O. 2017. *Guidelines for drinking-water quality. 4th Editon. Incorporating the 1st addendum*. [Online]. 4th ed. Geneva: WHO Press. [Accessed 20th February 2017]. Available from: <http://apps.who.int/iris/bitstream/10665/254637/1/9789241549950-eng.pdf?ua=1>
- Williams, K.P. et al. 2010. Phylogeny of Gammaproteobacteria. *Journal of Bacteriology*. [Online]. **192**(9), pp.2305–2314. Available from: <http://jb.asm.org/content/192/9/2305.short>
- Wingender, J. and Flemming, H.-C. 2011. Biofilms in drinking water and their role as reservoir for pathogens. *International Journal of Hygiene and Environmental Health*. **214**(6), pp.417-423.
- Wingender, J. and Flemming, H.C. 2004. Contamination potential of drinking water distribution network biofilms. *Water Science and Technology*. **49**(11-12), p277.
- Wolmarans, E. et al. 2005. Significance of bacteria associated with invertebrates in drinking water distribution networks. *Water Science and Technology*. **52**(8), p171.
- Wright, J.M. et al. 2017. Disinfection By-Product Exposures and the Risk of Specific Cardiac Birth Defects. *Environmental Health Perspectives*. **125**(2), pp.269-277.
- Wright, R. et al. 2014. Adaptive water distribution networks with dynamically reconfigurable topology. *Journal of Hydroinformatics*. **16**(6), p1280.
- Xavier, J.B. et al. 2005a. A framework for multidimensional modelling of activity and structure of multispecies biofilms. *Environmental Microbiology*. **7**(8), pp.1085-1103.
- Xavier, J.d.B. et al. 2005b. A general description of detachment for multidimensional modelling of biofilms. *Biotechnology and Bioengineering*. **91**(6), pp.651-669.
- Xavier, M.N. et al. 2010. Pathogenesis of Brucella spp. *The Open Veterinary Science Journal*. **4**, pp. 109-118

- Xie, P. et al. 2013. Comparison of Permanganate Preoxidation and Preozonation on Algae Containing Water: Cell Integrity, Characteristics, and Chlorinated Disinfection Byproduct Formation. *Environmental Science & Technology*. **47**(24), pp.14051-14061.
- Xue, Z. et al. 2013. Pseudomonas aeruginosa inactivation mechanism is affected by capsular extracellular polymeric substances reactivity with chlorine and monochloramine. **83**(1), pp.101-111.
- Xue, Z. et al. 2014. Selective Reactivity of Monochloramine with Extracellular Matrix Components Affects the Disinfection of Biofilm and Detached Clusters. *Environmental Science & Technology*. **48**(7), pp.3832-3839.
- Xue, Z. et al. 2012. Multiple Roles of Extracellular Polymeric Substances on Resistance of Biofilm and Detached Clusters. *Environmental Science & Technology*. **46**(24), pp.13212-13219.
- Xue, Z. and Seo, Y. 2013. Impact of Chlorine Disinfection on Redistribution of Cell Clusters from Biofilms. *Environmental Science & Technology*. **47**(3), pp.1365-1372.
- Yang, X. et al. 2010. Nitrogenous disinfection byproducts formation and nitrogen origin exploration during chloramination of nitrogenous organic compounds. *Water Research*. **44**(9), pp.2691-2702.
- Yoon, J.-H. et al. 2005. Proposal of the genus *Thermoactinomyces* sensu stricto and three new genera, *Laceyella*, *Thermoflavimicrobium* and *Seinonella*, on the basis of phenotypic, phylogenetic and chemotaxonomic analyses. *International Journal of Systematic and Evolutionary Microbiology*. **55**(1), pp.395-400.
- Yorkshire Water. 2013. *Our Blueprint for Yorkshire. The right outcome for Yorkshire. Our Wholesale Water Business Plan*. Yorkshire Water.
- Zhang, C. et al. 2017. Effect of pipe materials on chlorine decay, trihalomethanes formation, and bacterial communities in pilot-scale water distribution systems. *International Journal of Environmental Science and Technology*. **14**(1), pp.85-94.
- Zhang, P. et al. 2009. Biodegradation of Haloacetic Acids by Bacterial Isolates and Enrichment Cultures from Drinking Water Systems. *Environmental Science & Technology*. **43**(9), pp.3169-3175.
- Zhang, T. 2012. Modeling of Biocide Action Against Biofilm. *Bulletin of Mathematical Biology*. **74**(6), pp.1427-1447.
- Zhang, T. et al. 2008. Phase-Field Models for Biofilms II. 2-D Numerical Simulations of Biofilm-Flow Interaction. *Communications in Computational Physics*. **4**(1), pp.72-101.
- Zhang, T.C. and Bishop, P.L. 1994. Experimental determination of the dissolved oxygen boundary layer and mass transfer resistance near the fluid-biofilm interface. *Water Science and Technology*. **30**(11), pp.47-58.
- Zhao, J. et al. 2016. Modeling antimicrobial tolerance and treatment of heterogeneous biofilms. *Mathematical Biosciences*. **282**, pp.1-15.

Appendix 9-A. Water age map

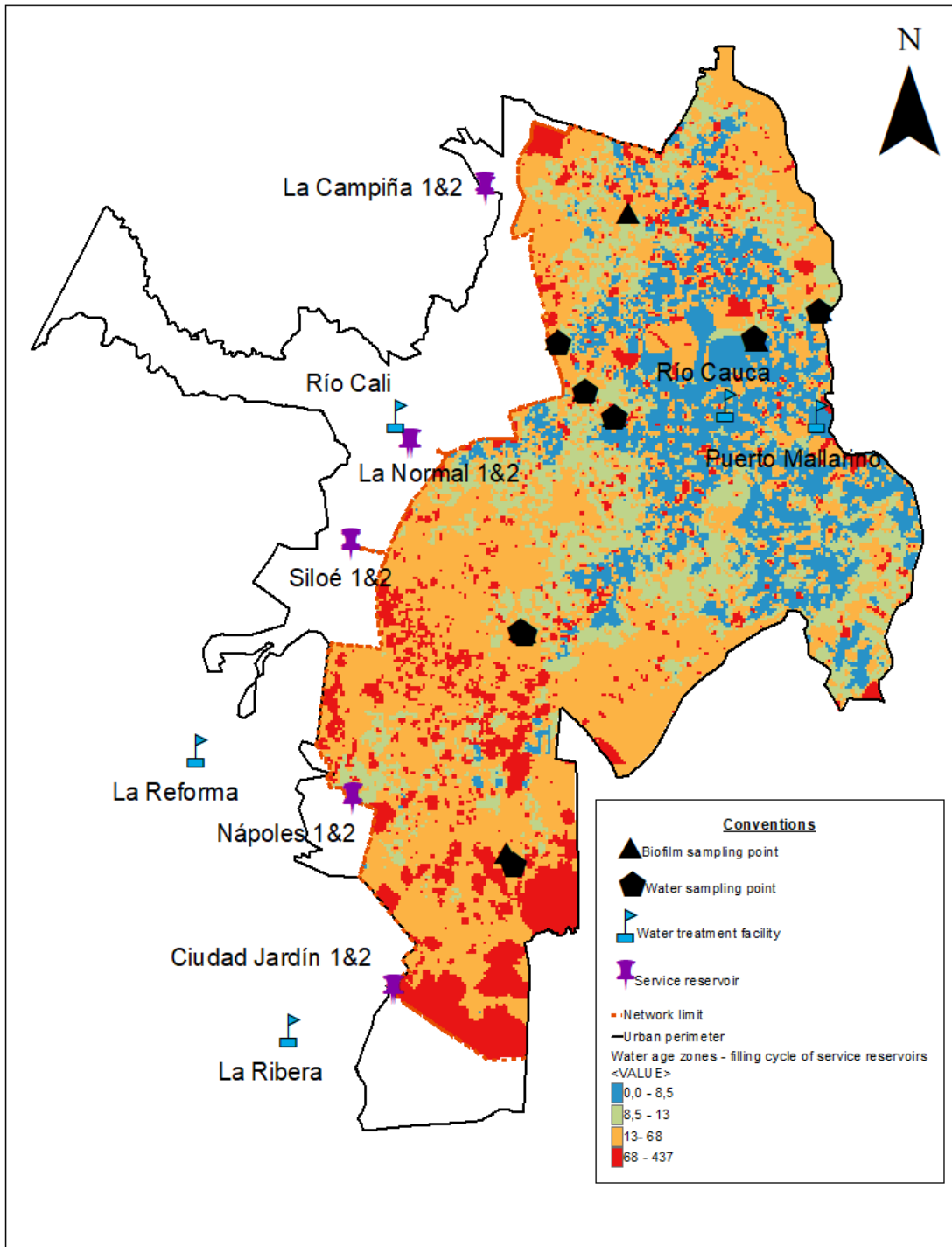


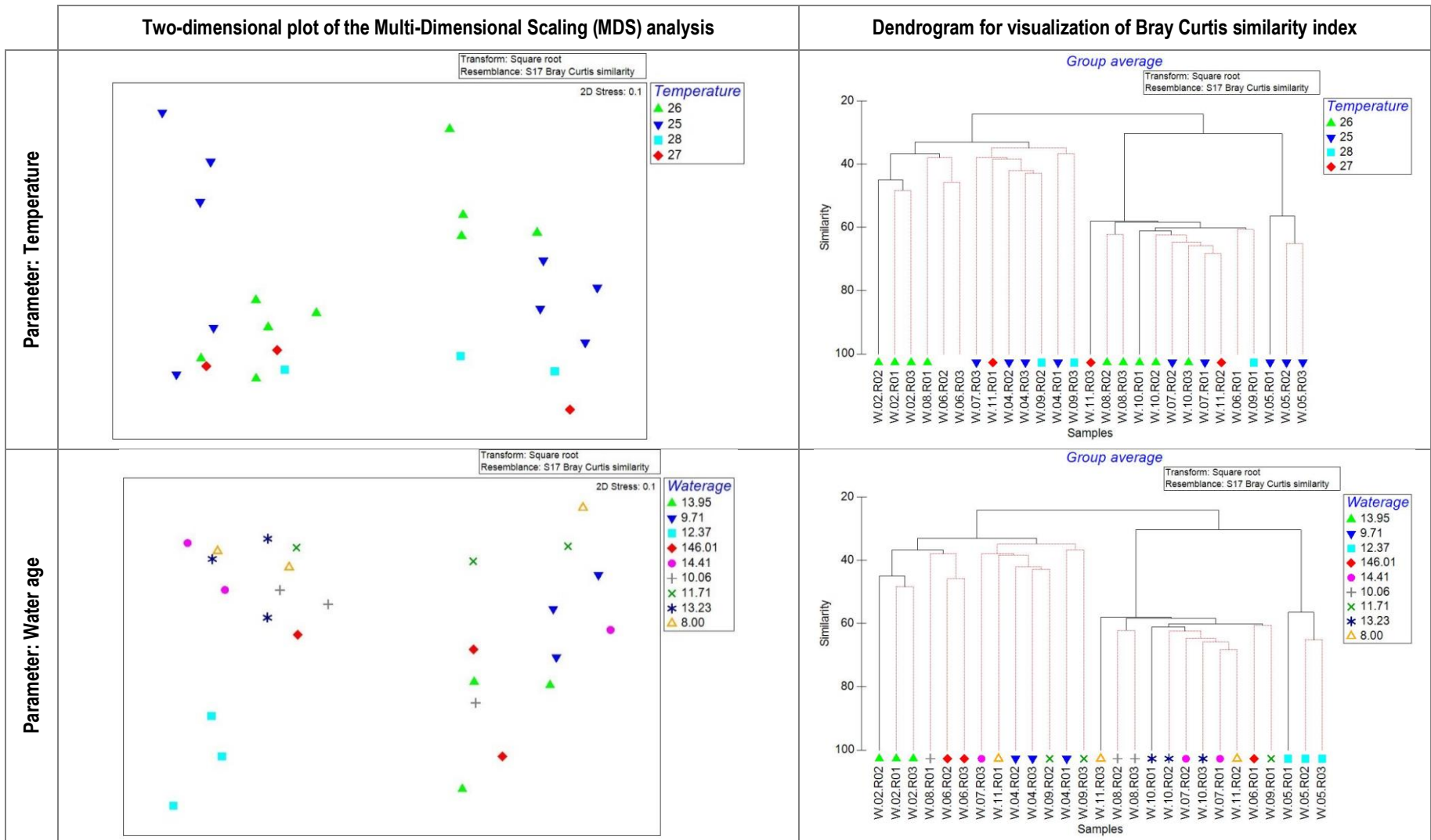
Figure 9-1. Water age for subnetwork 4 at the DWDN of the city of Cali - Colombia

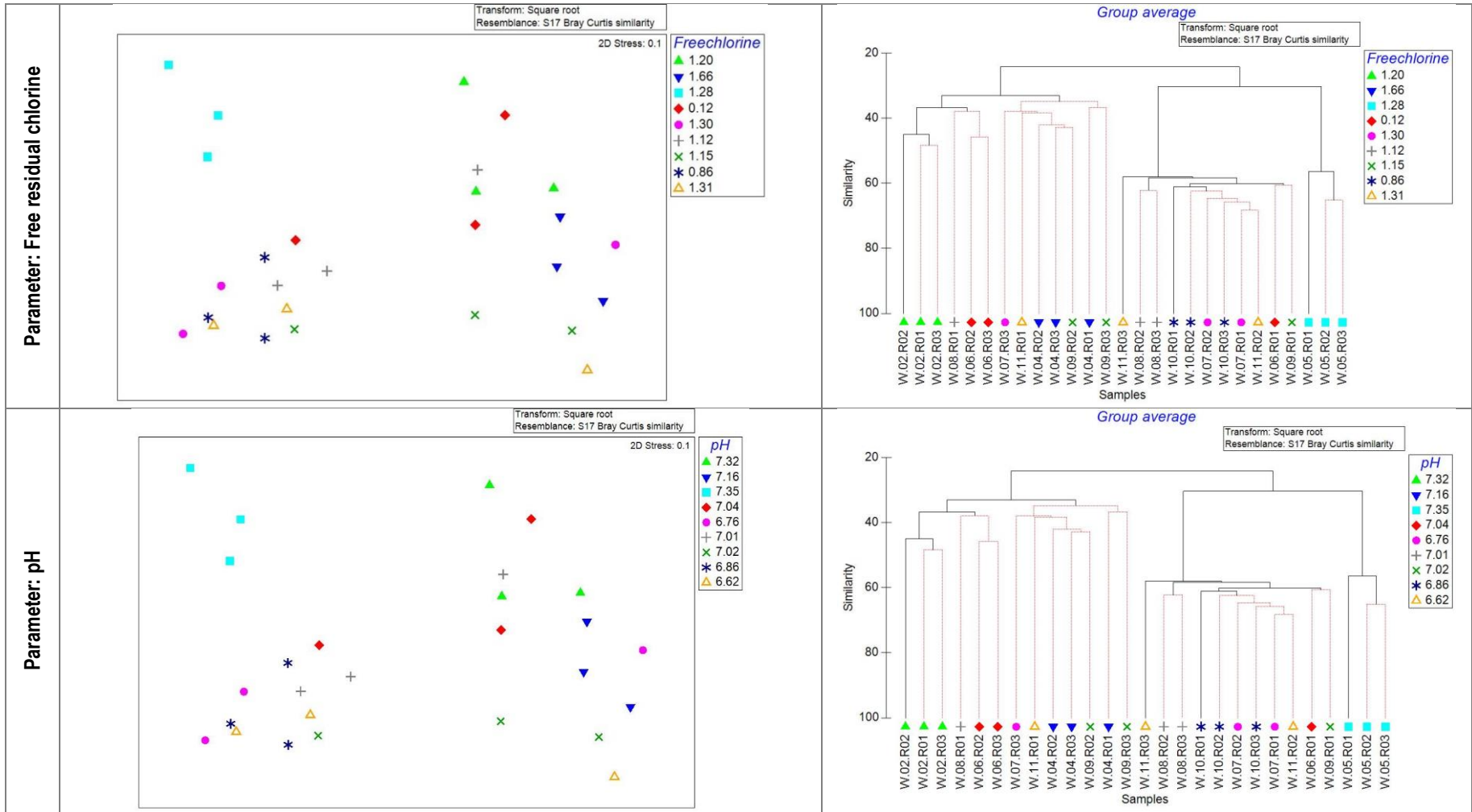
Appendix 9-B. Normality tests of correlated parameters

Table B-1. Normality tests for water and biofilm parameters

Variable	Significance Shapiro-Wilk test	Classification
Temperature	0.001	Data do not have normal distribution
pH	0.053	Data have normal distribution
Free residual chlorine	0.318	Data have normal distribution
Total chlorine	0.189	Data have normal distribution
Total trihalomethanes	0.930	Data have normal distribution
TOC in biofilms	0.000	Data do not have normal distribution
Water age (water sampling point)	0.000	Data do not have normal distribution
Water age (biofilm sampling point)	0.754	Data have normal distribution
Pipe age	0.315	Data have normal distribution
Pipe diameter	0.000	Data do not have normal distribution
Dry biomass per surface area (minimal values)	0.014	Data have normal distribution
Dry biomass per surface area (median values)	0.180	Data have normal distribution
Dry biomass per surface area (maximal values)	0.000	Data do not have normal distribution
Unit dry biomass (all the values)	0.000	Data do not have normal distribution
Margalef richness index (biofilm)	0.001	Data do not have normal distribution
Shannon diversity index (biofilm)	0.008	Data do not have normal distribution
Margalef richness index (water)	0.310	Data have normal distribution
Shannon diversity index (water)	0.313	Data have normal distribution

Appendix 9-C. Two-dimensional plots of the Multi-Dimensional Scaling (MDS) analysis and dendrograms for visualization of Bray Curtis similarity index





Chapter 9. Appendices

Disinfection by-product formation from biofilm chlorination in drinking water pipes
Carolina Montoya Pachongo. School of Civil Engineering

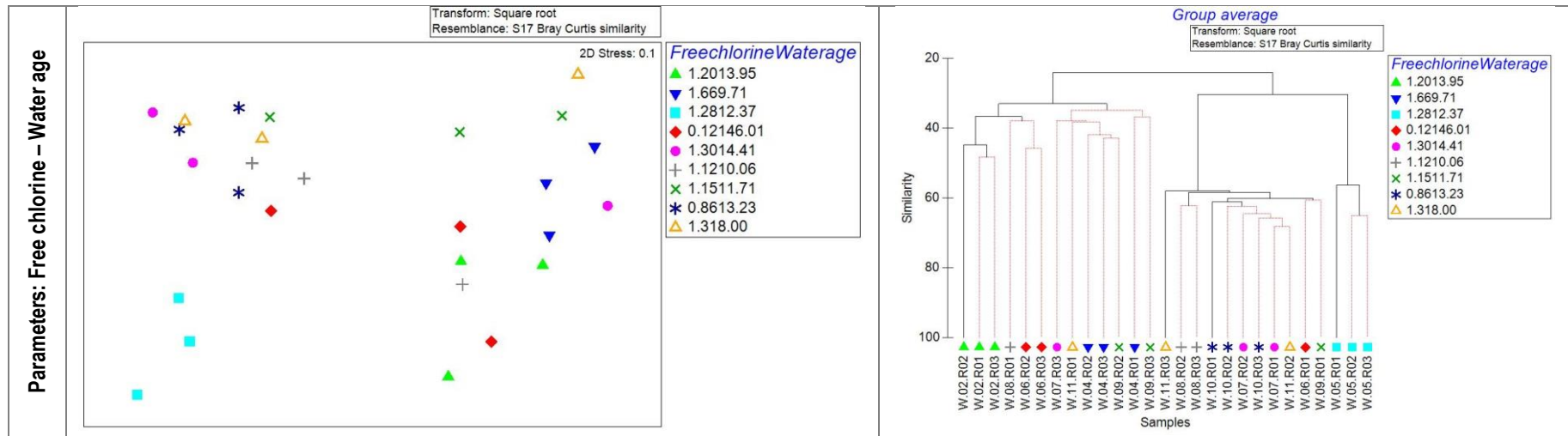
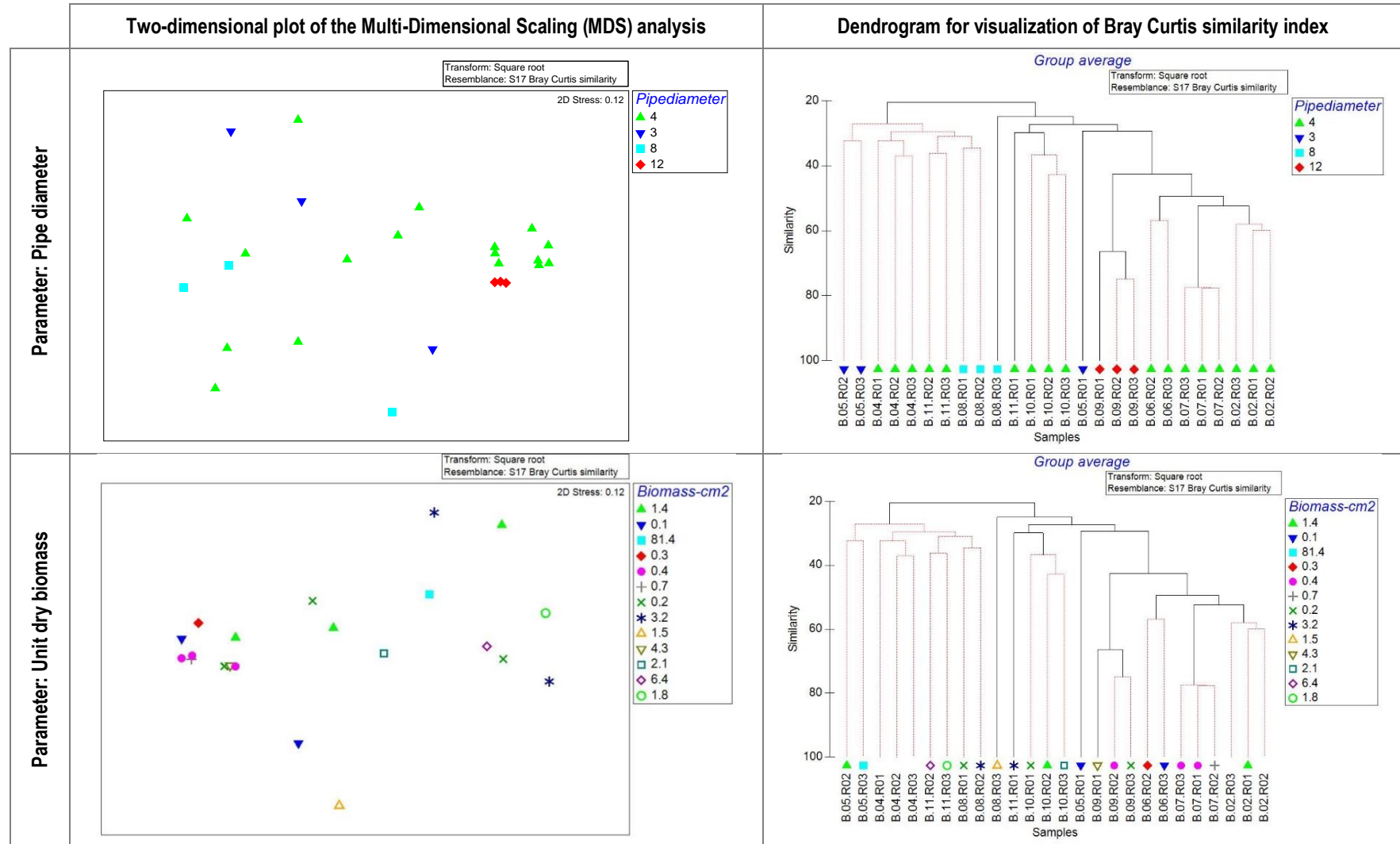
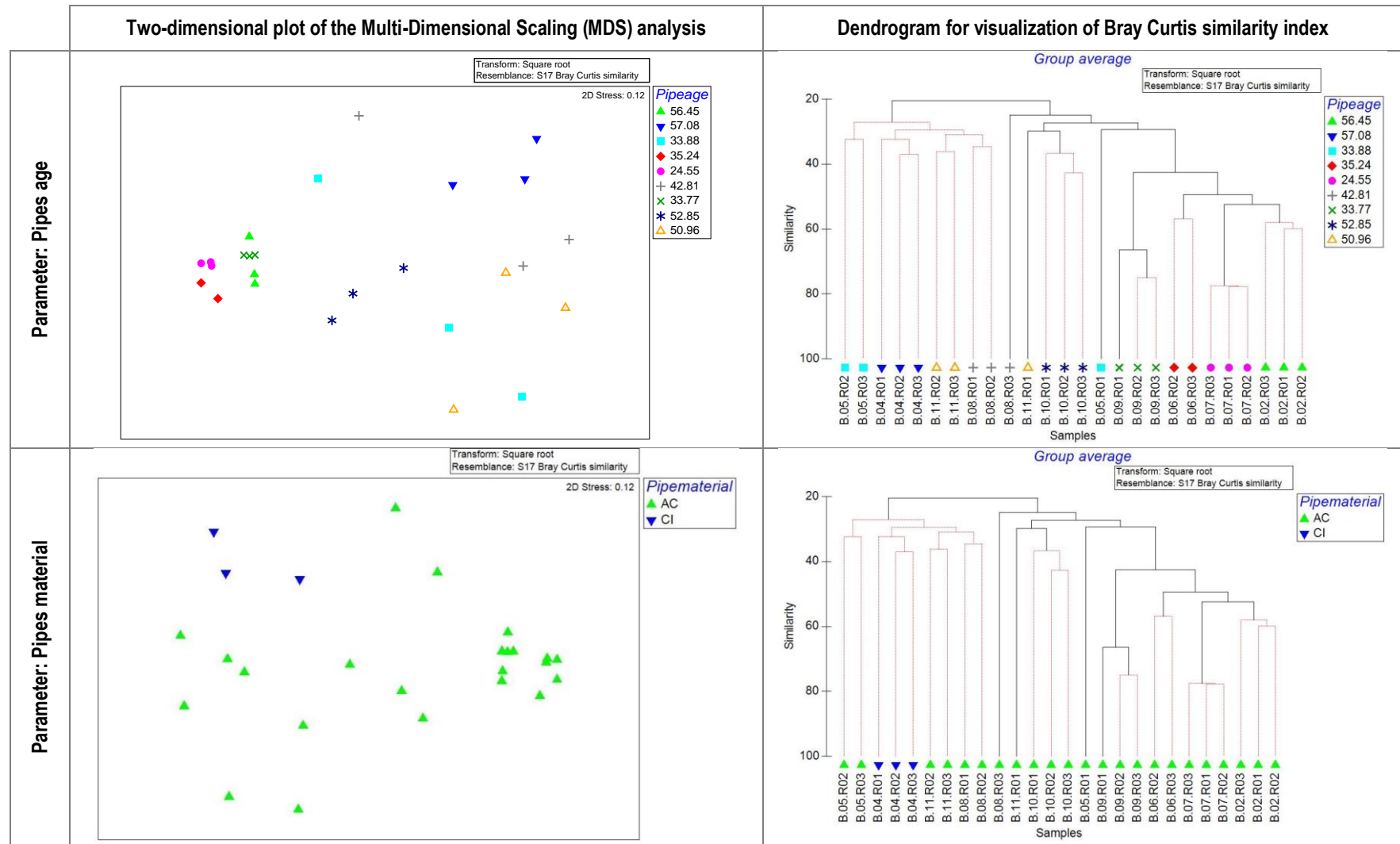


Figure 9-2. Bray Curtis similarities of the relative abundance percentage of species in biofilm samples – Water species



Chapter 9. Appendices

Disinfection by-product formation from biofilm chlorination in drinking water pipes
Carolina Montoya Pachongo. School of Civil Engineering



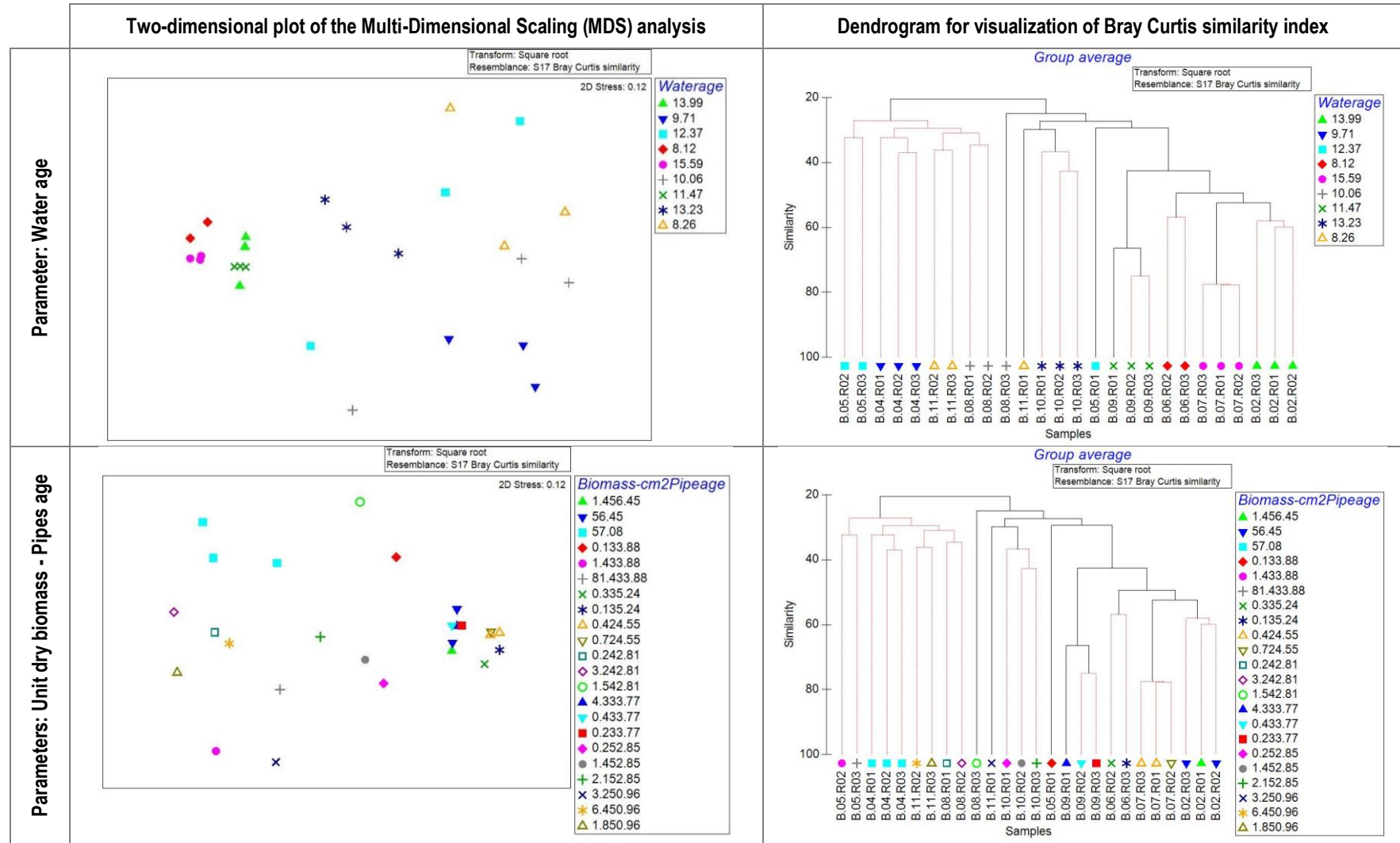
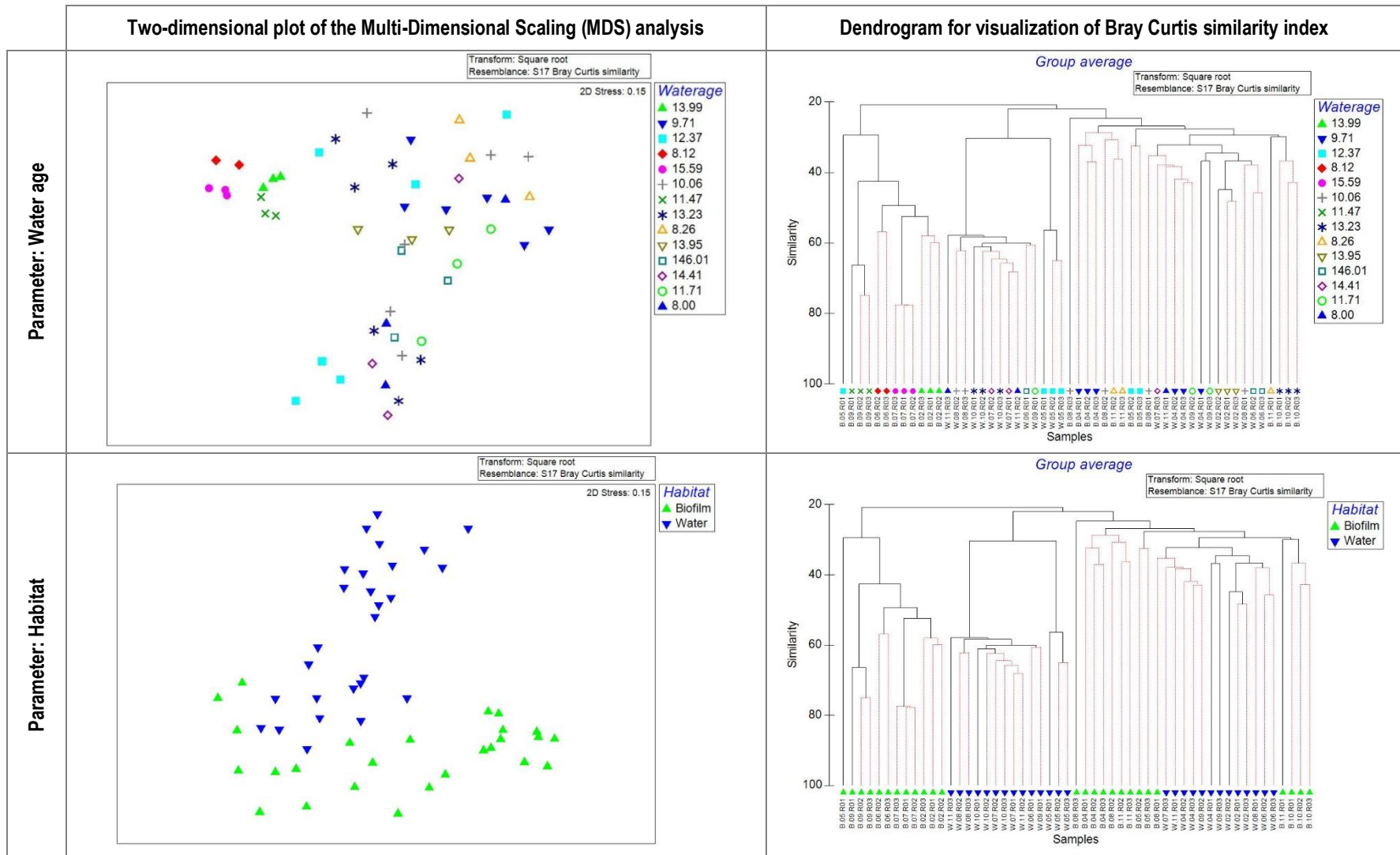


Figure 9-3. Bray Curtis similarities of the relative abundance percentage of species in biofilm samples – Biofilm species



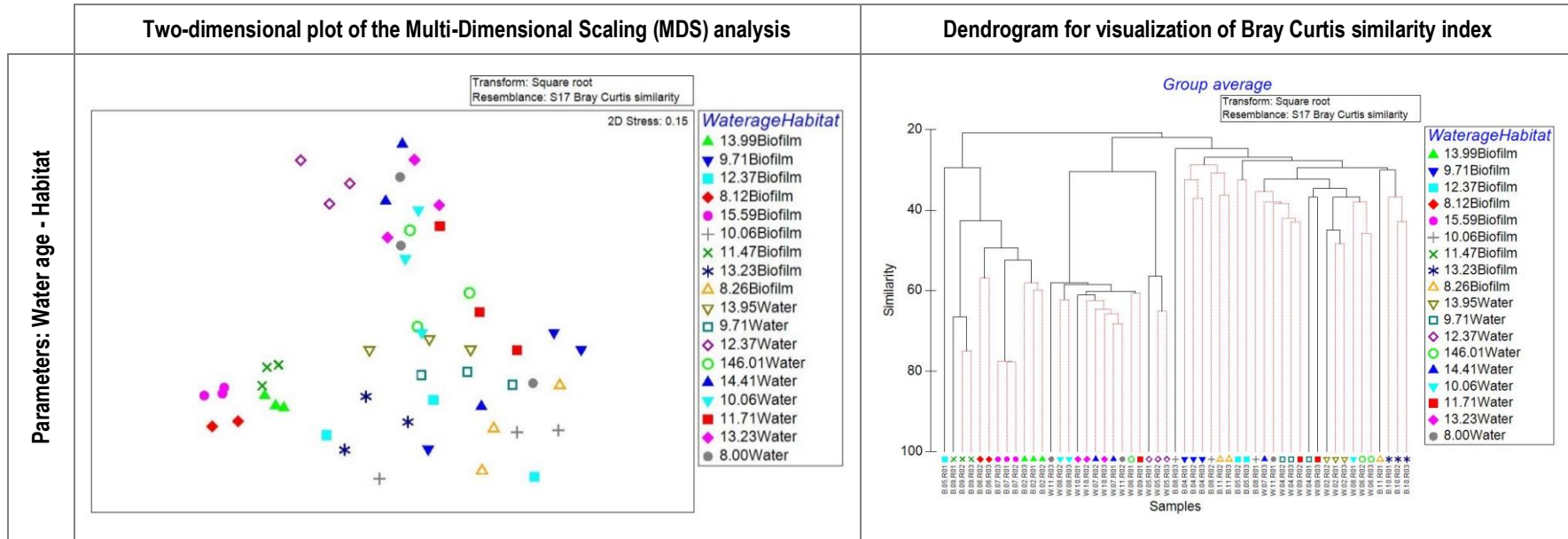


Figure 9-4. Bray Curtis similarities of the relative abundance percentage of species in biofilm samples – Water and biofilm species together